Dissertation

Scanning Tunneling Microscopy Investigations of the Ordered Thins Films of Squaraine Dye Molecules on HOPG

Submitted by
Michele E. Stawasz
Department of Chemistry

In partial fulfillment of the requirements
for the Degree of Doctor of Philosophy

Colorado State University
Fort Collins, CO
Fall 2002

COLORADO STATE UNIVERSITY

January 4, 2002

WE HEREBY RECOMMEND THAT THE DISSERTATION PREPARED UNDER OUR SUPERVISION BY MICHELE E. STAWASZ ENTITLED: SCANNING TUNNELING MICROSCOPY INVESTIGATIONS OF THE ORDERED THINS FILMS OF SQUARAINE DYE MOLECULES ON HOPG, BE ACCEPTED AS FULFILLING IN PART REQUIREMENTS FOR THE DEGREE OF DOCTOR OF PHILOSOPHY.

Committee on Graduate Work

Alan Van Orden

Nancy Levinger

Peter Dorhout

Stuart Field

Advisor – Bruce Parkinson

Department Head

Abstract of Dissertation

Scanning Tunneling Microscopy Investigations of the Ordered Thins Films of Squaraine Dye Molecules on HOPG

Squaraines are organic dye molecules with a symmetrical donor-acceptor-donor (DAD) structure that allows them to undergo intra- and intermolecular donor-acceptor charge transfer. These donor-acceptor interactions drive squaraines to form ordered aggregates in both solution and in the solid state. In addition squaraines absorb very strongly in the red region of the visible spectrum. As a result of these characteristics, squaraines are used in industry as thin film photoconductors in laser printers and photocopiers. The orientation and aggregate state of the molecules within these films has been shown to effect device efficiency. Furthermore, the orientation of molecules at the film-substrate interface has been known to affect the order of the rest of the film. Thus, the interfacial ordering of squaraines is of importance to efficient device design.

This Dissertation describes the use of scanning tunneling microscopy (STM) to investigate the adsorption and 2D ordering of ultrathin films of squaraines deposited from phenyloctane solution onto the (0001) surface of highly oriented pyrolytic graphite (HOPG). A total of 11 squaraine molecules, varying in their dialkylamino tail length (CH_3 to $C_{18}H_{37}$), symmetry (equal or unequal tail length), and phenyl ring substituent (OH or H), were investigated. We found that, regardless of structural variation, squaraines are highly surface active, forming monolayer and multiple layer structures (up to four layers) consisting of ordered domains (tens of nm to microns in diameter). Two general

types of aggregate structure were observed, herringbone and row, although many polymorphs of these two types were observed (oftentimes for a single molecule). Shorter-tailed squaraines tended to exhibit herringbone structures whereas only row structures were exhibited by longer-tailed squaraines. Determination of the type of structure exhibited appeared to depend upon a delicate balance of chromophore-chromophore DA interactions, tail-tail interactions, and tail-HOPG interaction. It was found that hydroxylated and non-hydroxylated molecules exhibited the same structures, suggesting that intermolecular hydrogen bonding was not a factor in the determination of adsorbate aggregate structure. Changing the symmetry, by employing different tail lengths within the same molecule, showed that the adsorbate structure was determined by the longer of the tails, with the shorter tails providing little or no influence. Interaction of the tails with the HOPG caused squaraines with longer tail lengths (≥ 12 carbons) to exhibit an orientational relationship to the HOPG lattice whereas shorter-tailed squaraines showed no distinct relationship to the HOPG lattice.

Michele Stawasz
Department of Chemistry
Colorado State University
Fort Collins, CO 80523

Fall 2002

ACKNOWLEDGEMENTS

I would like to thank the following people for their roles in my graduate career:

I sincerely thank my advisor, Professor Bruce Parkinson, for his support and mentorship in my (many) projects. His vast knowledge continuously inspires me to never stop learning.

My fellow Parkinson group members, both past and present, for their comradery and their roles in teaching me new things and new ways of thinking.

Professor Nancy Levinger, for always believing in me and for helping me to believe in myself.

The Scorchers and the Atomic Forces for so many great games and so many cherished friendships.

To Jon Lorenz, for his unwavering friendship, companionship and loving support through both the good times in graduate school and the frustrating ones.

Finally, thank you to my family for their love and support, especially my parents, who have always believed in me and always been there for me. I hope that I can repay you someday.

Table of Contents

List of Tables

List of Figures

CHAPTER ONE

Introduction

STM and its Capabilities

Since its invention by Binnig and Rohrer two decades ago,[1,2] the scanning tunneling microscope (STM) has become an essential and versatile tool for the localized study of the topography of surfaces on the microscopic and nanoscopic scale. STM's superiority lies in its ability to image samples under virtually all experimental conditions with atomic resolution. Initial STM studies investigated bare metal and semiconductor surfaces under extremely clean, ultrahigh vacuum (UHV) conditions.[3-5] With the aid of improved instrumentation and theoretical methods, STM studies can now be routinely carried out not only in UHV, but in ambient air, in liquids (both conducting and insulating), in electrochemical environments, and over a wide temperature range. STM has been used to determine the local surface structure of crystalline and amorphous conducting and semiconducting solids, either "clean" or with adsorbate layers. Adsorbates range from simple adatoms to multiple ring aromatic molecules, phsyisorbed or chemisorbed, and can be conducting, semiconducting, or insulating. Due to the rise of STM to a well-known and now relatively commonplace technique, well-reviewed in the literature, its construction and theoretical considerations will not be presented in detail in this dissertation.

Organized Molecular Adsorption

The study of molecular adsorption and self-assembly, especially of physisorbed molecules, on crystalline conducting or semiconducting substrates has become one of the forefront areas of STM study in recent years. Particularly, the growing fields of nanoscale molecular engineering and thin film device engineering provide ample justification for its popularity. In both of these fields, the controlled assembly of molecules, either in distinct patterns and arrays or in stable, well-ordered layers, is essential to proper device functioning. In order to achieve the routine production of these arrays or films, the fundamental issues at the heart of the controlled adsorption and ordering of molecules on surfaces must be identified and understood. They can be simplified into three: (1) the nature of the forces governing the molecular organization on the surface, (2) the roles of the adsorbate-adsorbate interactions relative to the adsorbate-substrate interactions in driving and stabilizing the molecular order, and (3) the role of substrate structure and roughness. Understanding and controlling these factors can lead to the more efficient design of devices utilizing molecular thin films or nanostructures, thus ushering in a new generation of organic/metal or organic/semiconductor devices.

Careful design of the STM experiment by systematic variation of the molecular functionality and geometry, as well as substrate symmetry, lattice constant and smoothness, can lead to elucidation of these fundamental issues. One of the most extensively-studied groups of these molecules is the long-chain alkanes. The collective knowledge about this system has been gained from the

work of several research teams, making the factors that control its ordered adsorption well understood. In addition, the systematic investigation of this adsorbate system can be used as a model for the investigation of the 2D ordering of other molecular systems. A brief overview of the STM studies that contributed most significantly to the understanding of the influences of intermolecular interaction on this adsorbate system, as well as the conclusions that can be made as a result of these studies, will be presented in this introductory chapter.

Alkanes- Nature of the Interactions Governing Ordered Adsorption

The study of long-chain alkanes began with dotriacontane ($C_{32}H_{66}$) adsorbed onto the basal plane surface of highly oriented pyrolytic graphite (HOPG) from iso-octane solution.[6] It was found that these molecules form highly ordered arrays of molecules on the HOPG surface. Molecular lamella were observed consisting of straightened-out dotriacontane molecules lying side-by-side in an all-trans conformation with their long axes forming a 90° angle to the edge of the lamella (see Figure 1.1 for a STM image and Figure 1.2 for a schematic). The 4.5 ± 0.5 Å intermolecular spacing of molecules within the same lamella was evidence that the molecules were adsorbed commensurately[‡] on the HOPG lattice. This was expected due to the structural similarity in the all-trans structure (C-C bond length and angles) of dotriacontane to the zigzagging carbon chain backbone of the HOPG surface (along $[1\bar{1}00]$ and symmetry-equivalent

‡ The concept of commensuration and the other modes of epitaxial growth for physisorbed molecular systems is explained in detail in Appendix A.

vectors). In addition, domains of ordered lamella followed the HOPG crystallographic directions, and intersected at 120° angles, further signs of commensurate ordering. It was proposed that the adsorbed alkane molecules lie with their carbon backbone parallel to the HOPG surface such that their methylene carbons are situated above the centers of the hexagons of the HOPG lattice. The weak van der Waals interaction arising from this commensuration

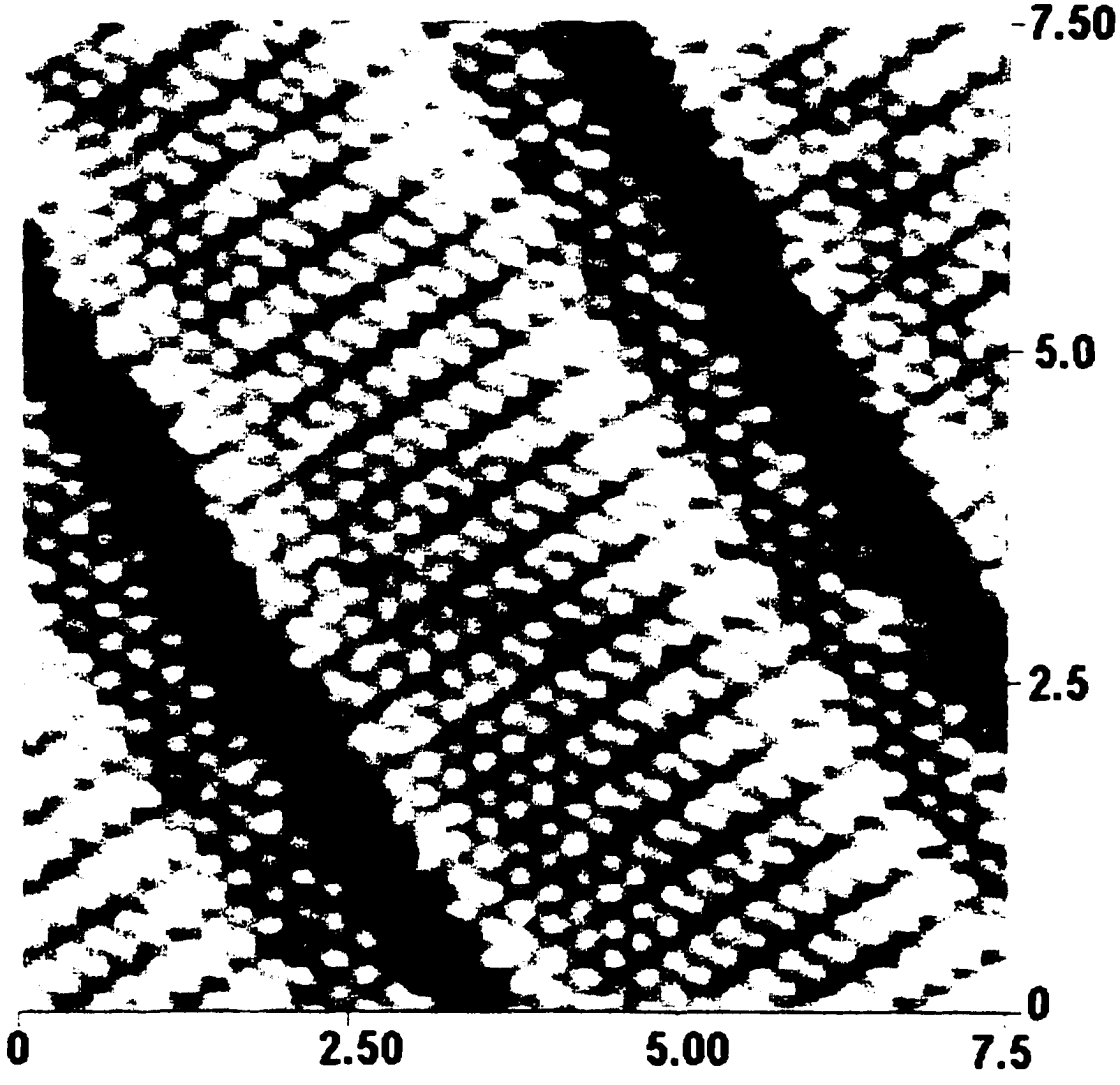

Figure 1.1: 7.5 x 7.5 nm STM image of $C_{35}H_{72}$ adsorbed on HOPG. Reproduced from Claypool et al.[9]

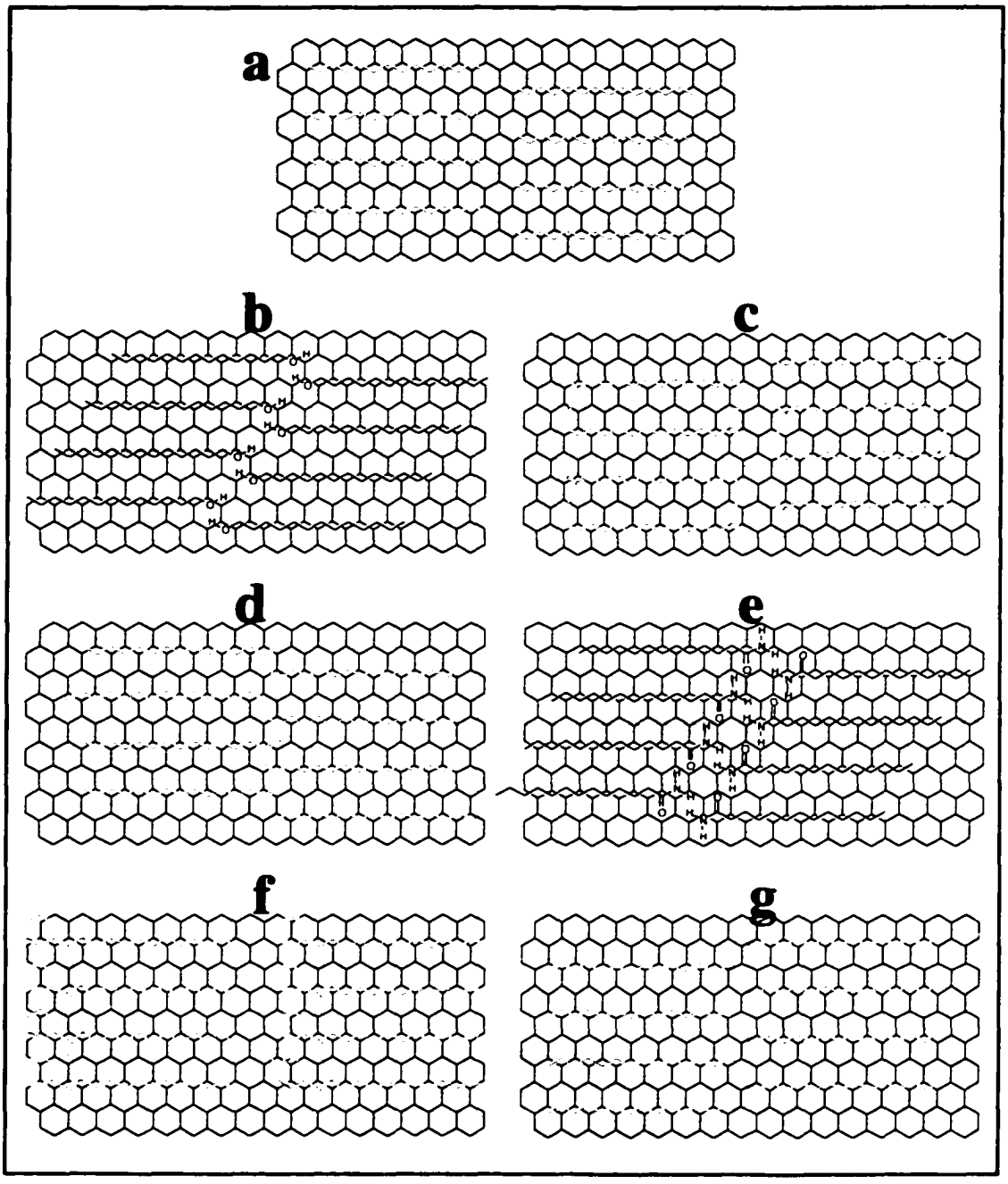

Figure 1.2: Schematics of the 2D ordered adsorption of n-alkanes and several alkane derivatives on HOPG. Molecular systems shown in red exhibit a 90° angle of the molecular long axis to the edge of the lamella.

has been estimated to be ~1.5 kcal/mole/CH_2[7] from heats of adsorption studies and ~1.7 kcal/mole/CH_2 from molecular dynamics.[8] At this 4-5 Å intermolecular distance, weak van der Waals interactions likewise exist between adjacent molecules within the same lamella (~1 to 2 kcal/mole/CH_2).[10] Following the publication of this initial work, STM studies of alkanes of various chain lengths ($C_{17}H_{36}$ to $C_{50}H_{102}$) were then undertaken. It was found that similar commensurate structures were formed by all the alkanes regardless of length. As a result of these initial studies, it can be confidently proposed that the nature of the forces governing the ordered adsorption of long chain alkanes on HOPG is van der Waals, both in adsorbate-adsorbate interaction and in adsorbate-substrate. It is not possible from these studies alone, however, to determine whether the alkane adsorption and ordering is driven by the registry between the carbon lattices of adsorbate and substrate,[7] or by a 2D crystallization of the adsorbate on a flat surface, independent of the substrate lattice.[11]

Influence of the Substrate

Several characteristics of the substrate may influence the 2D ordered adsorption of molecules by altering the relative strength of substrate-adsorbate interactions: the symmetry of the substrate, its lattice constant, the type of intermolecular interaction between the substrate and adsorbate molecules (van der Waals/covalent), and the possibility of commensurism between the substrate and adsorbate lattices. It is clear that in order to determine the relative importance of the adsorbate-adsorbate vs adsorbate-substrate interactions in driving the ordering of long-chain alkanes on HOPG, the experiment described

above must be performed on additional substrates. The first STM studies of long-chain alkanes on substrates other than HOPG were the adsorption of dotriacontane on $MoSe_2$.[12] $MoSe_2$ is a transition metal dichalcogenide composed of a hexagonally-packed molybdenum atom layer sandwiched between two hexagonally-packed selenium layers. Like HOPG, these Se/Mo/Se sandwiched layers are held together by attractive van der Waals interactions. When cleaved, a nearly-atomicallly smooth surface of hexagonally-oriented selenium atoms is exposed. Thus, there should not be significant topographical or symmetry-related effects on the alkane 2D structures, since the $MoSe_2$ surface is smooth, like that of HOPG, and has similar symmetry. As with HOPG, van der Waals interactions are expected to be the predominant intermolecular force between alkane adsorbates and a $MoSe_2$ surface. Thus, the adsorbate-substrate interactions for ordered $C_{32}H_{66}$ on $MoSe_2$ should remain approximately the same as on HOPG. Since the fortuitous matching of the HOPG lattice distance and angles with the bond distances and angles of all-trans geometry normal alkanes appears to be the main adsorbate-substrate interaction consideration, the differing lattice constant of $MoSe_2$ should play a significant role in the 2D adsorption of $C_{32}H_{66}$. The lattice constant between the selenium atoms in $MoSe_2$ is 3.29 Å as opposed to the 2.46 Å distance between every other atom along the zigzagging carbon backbone of HOPG.

STM images of dotriacontane on $MoSe_2$ reveal that ordered layers can form even when there is a mismatch between molecular and lattice parameters.[12] Like on HOPG, lamella of all-trans molecules are observed. These lamella

exhibit the same inter- and intra-lamellar distances as on HOPG, despite the differing lattice constant and polarizability of $MoSe_2$. Thus, the inter-adsorbate distance does not simply scale with substrate lattice constant. However, the molecules *were* observed to order with their long axes parallel to one of the $MoSe_2$ lattice axes. Additionally, the orientation of the long axes of the alkanes to the edge of the lamella was measured to be ~60° rather than the 90° orientation observed on HOPG. Molecular modeling has shown that this 60° angle corresponds a minimum energy configuration on the $MoSe_2$ lattice.[13] This calculation, in combination with the lamellar orientation to the substrate crystallographic axes supports the proposition that the 2D structure of dotriacontane on $MoSe_2$ is coincident. An unambiguous relationship could not be supported or refuted with the obtained STM images, however. An alternative hypothesis, based upon the assumption that the 2D ordered structures of $C_{32}H_{66}$ on $MoSe_2$ are incommensurate, is that adsorbate-adsorbate van der Waals interactions dominate the adsorption and the only requirement for an adsorbate to attain 2D order is that the substrate be flat.

These hypotheses were tested through the STM investigation of the ordered adsorption of a long-chain alkane ($C_{36}H_{74}$) on β-Nb_3I_8.[14] If the only requirement for the ordered adsorption of long-chain alkanes is an atomically flat substrate, then a surface with z-axis variation should cause a significant change in its 2D order. β-Nb_3I_8 has a structure where a sheet of niobium atoms is sandwiched between two iodine sheets. In the niobium sheet, the niobium atoms form triangular Nb_3 clusters, each niobium atom of which is in a distorted

octahedral environment. In the iodine sheets, iodine ions positioned over the triangle's centers are displaced out of the halide plane. Thus the basal plane of the crystal has hexagonally-packed iodine ions protruding ~1.2 Å above the rest of the iodine surface at a periodicity of 7.6 Å. Conversely, the non-protruding iodine areas can be thought of as "grooves" in the surface which are oriented at 60° with respect to one another. Thus, β-Nb_3I_8 has similar symmetry to that of HOPG, but it is not atomically smooth. Additionally, its lattice constant is 7.60 Å, significantly larger than that for HOPG. Dotriacontane does produce ordered 2D structures on β-Nb_3I_8, however, its packing is very different than seen on any of the aforementioned substrates. The STM images produced consisted of a hexagonal array of bright features with a 3.8 nm separation distance between nearest neighbors. This has been interpreted as a molecule lying in each of the grooves with the end of the carbon chain protruding up out of the groove.[14] With this geometry the adsorbate layer attains a commensurate structure on the β-Nb_3I_8 surface, however, at the expense of optimal interaction between neighboring alkanes.

When the results of the adsorption of $C_{36}H_{74}$ on β-Nb_3I_8 are compared to the adsorption studies of $C_{32}H_{66}$ on flat hexagonal surfaces, a theme of epitaxy appears. On all three substrates, alkane adsorbates achieve some degree of epitaxy with the substrate lattice. On HOPG and $MoSe_2$, $C_{32}H_{66}$ is able to maintain optimal intra-lamellar inter-adsorbate distances (~4.8 Å) while attaining commensuration or coincidence. As seen in the studies on $MoSe_2$, however, some interadsorbate interaction is sacrificed to attain some degree of epitaxy.

The change in the molecular angle to the edge of the lamella from 90° (HOPG) to 60° ($MoSe_2$), thereby reducing the overall interaction between adjacent molecules in the same lamella, is evidence that even on flat substrates adsorbate-adsobate interactions can be sacrificed for an alkane overlayer to be commensurate or coincident. In the extreme case of β-Nb_3I_8, with its protruding ions and large lattice constant, adsorbate-adsorbate interactions are essentially sacrificed altogether as the alkane overlayer attains commensuration. Thus, it appears that flat substrate or not, epitaxial growth drives the 2D adsorbed structures of long-chain alkanes on crystalline surfaces.

The effect of substrate roughness on the stability of adsorbed long-chain alkanes has not been probed. Such a study would be important and easily accomplished, however. It is well known that circular, single-layer deep pits can be formed in the basal plane of HOPG in a controlled fashion with surface densities in the range of 1 to 25 μm^{-2}.[15-18] Heating HOPG in the presence of O_2 at ~650 °C causes carbon oxidation and subsequent removal from pre-existing point defects. The diameters of the pits (5 nm to 500 nm) can be controlled by varying the heating temperature and time. Multiple layer pits can be formed on lower-grade HOPG (ZYC, for example), which has a higher density of crystal defects. By varying the size of the pits and monitoring the adsorption that occurs *within* the pits, the critical size of flat surface that is necessary for the formation of ordered nuclei can be determined. This approach has already been successfully utilized for the ordered adsorption of n-alkyl-cyanobiphenyls on HOPG.[19]

Alkane Derivatives- Influence of Adsorbate-Adsorbate Intermolecular Interactions

Examples of the systematic study of adsorbate-substrate interactions via STM for the adsorbate system of long-chain alkanes have been presented. Returning to the issue of adsorbate-adsorbate interactions and their influence on the observed 2D structure, the nature and strength of these interactions can likewise be probed by systematic variation of the *adsorbate* molecular structure. For example, by adding functionality to the terminal carbon, the linearity of the alkane molecule can be preserved while the adsorbate-adsorbate interactions are tweaked. The first STM investigation to probe changes in the adsorbate-adsorbate interactions of long-chain alkanes on graphite due to the introduction of a terminal functionality was published in 1991 by J.P. Rabe.[20] In this study the effects of two variations in terminal functionality were probed with several alcohols ($C_{18}H_{37}OH$, $C_{24}H_{49}OH$, $C_{30}H_{61}OH$) and acids ($C_{17}H_{35}COOH$, $C_{19}H_{39}COOH$, $C_{23}H_{47}COOH$). The alcohols all formed lamella of parallel-packed molecules similar to those formed by alkanes (see Figure 1.2b): the same ~4.8 Å distance between parallel molecules within the same lamella characteristic for alkane adsorption on HOPG was likewise observed, and the alcohols were found to be commensurate with the HOPG surface. Alcohols, specifically, orient such that the OH groups of neighboring molecules in adjacent lamella face one another. Unlike $C_{32}H_{66}$ and the other long-chain alkanes on HOPG, however, the long axes of the alcohols form a 60° rather than 90° angle to the edge of the lamella. This was explained to be due to hydrogen bonding between alcohols in adjacent lamella (see Figure 1.2b).[21] Although the 60° offset between molecules

in a lamella reduces the total van der Waals interactions between adjacent molecules, the stabilization gained from hydrogen-bonding must exceed the loss in van der Waals interactions. Despite this change in orientation, commensuration with the HOPG lattice was still attained. The acids also formed commensurate lamellar structures with a 4.8 Å intermolecular distance, however, their molecular angle to the lamella direction was 90°, like that found in alkanes (see Figure 1.2c). Additionally, the acid groups were found to alternate direction with every molecule down the length of the lamella (i.e. every other molecule had the acid on the same side of the lamella). This is caused by repulsive interactions between COOH groups of adjacent molecules within the same lamella. However, like with the alcohol adsorbates, the COOH groups of neighboring molecules in adjacent lamella face one another, allowing the formation of two hydrogen bonds per pair of COOHs. Thus, through the terminal susbstitution of alcohol or acid functionality onto a carbon chain, the 2D ordered adsorption on HOPG was altered by the new intermolecular interactions that arise between these functionalities. At the same time, however, commensuration with the HOPG substrate was maintained.

The effects of many other terminal functional groups, including thiols, amides, analides, and a number of halides, on the ordered adsorption of long-chain alkanes have been probed with STM (see Table 1.1). Substitution of one functional group for another similar group can probe the effects of subtle changes in structure on the molecular packing and orientation. For example, the substitution of an alcohol for a terminal thiol can probe how an electronically

Substituted Alkanes‡ Studied via STM

Terminal Functionality:*

- Alcohols
- Acids
- Thiols
- Amides
- Anilides
- Halides

Internal Functionality:

- Alkenes
- Ethers
- Sulfides
- Disulfides
- Amines

Functionality at both terminii:

- Diols
- Halogenated alcohols
- Halogenated acids
- Halogenated amides

Geometry-altering functionality:

- Alkynes
- Secondary alcohols
- Secondary halides
- Dialkyl amines
- Dialkyl benzenes
- Cyclic alkanes

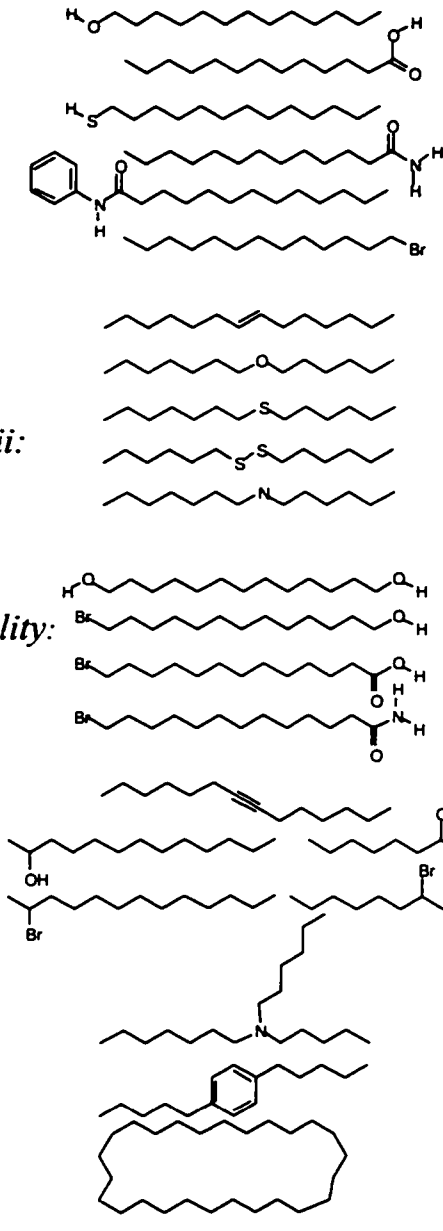

Table 1.1: Systematic variation in long-chain alkane structure for the purpose of probing the intermolecular forces driving and stabilizing 2D orgainzation of adsorbed long-chain alkanes on the basal plane surface of HOPG, as studied by STM. Chain lengths shown here are generic. Asterisks (*) denote groups which have been described in detail in this chapter. ‡ Not an exhaustive list.

similar, but larger atom can affect the 2D structure. A thiol sulfur should have the capability of forming hydrogen-bonded systems similar to that exhibited by a hydroxyl group, but its larger covalent radius (1.04 Å[22] compared to 0.74 Å for oxygen[23]) may affect the close-packing of the adsorbates. In fact, the STM investigation of $C_{22}H_{45}SH$ on HOPG showed that alkylthiols order in lamella on the HOPG surface with a 4.8 Å molecular spacing (same as alcohols and alkanes), but with a 90° orientation angle of the long molecular axis to the lamella (see Figure 1.2d).[23,24] Additionally, it was found that the SH group of a molecule in one lamella did not necessarily face the SH group of the molecule in the adjacent lamella (sometimes it did and sometimes it did not). This was proposed to indicate that the relatively weak hydrogen bonding between the SH groups may not dominate the stabilization of these molecules on the HOPG surface as much as the H-bonding in alcohol monolayers.[23,24]

Amides and anilides also have H-bonding capabilities. STM studies of these molecules show remarkably different 2D structures on HOPG. Alkyl amides produce structures similar to that of acids, in which H-bonding exists between the amide groups of molecules in adjacent lamella (see Figure 1.2e). Two N-H···O H-bonds are possible between pairs of molecules in adjacent lamella. However, because the orientation of the long axis of the molecule to the edge of the lamella is ~65° for alkyl amides, N-H···O H-bonding is also possible between amide groups of adjacent molecules in the same lamella. As a result, the position of the amide groups do not alternate down a lamella. The 90° orientation of the alkyl acid molecules to the edge of the lamella does not

accommodate a suitable angle for O-H···O H-bonds between acid groups of adjacent molecules in the same lamella. As a result, repulsion between adjacent acid groups is not stabilized and a head-tail orientation is maintained down the length of the molecular lamella. Alkyl *anilides* form a 90° lamella structure in which a head-tail packing was maintained across adjacent lamella, whereas down the length of a single lamella heads orient on one side and tails on the other side of the lamella (see Figure 1.2f). In this system the bulky anilide group hinders any hydrogen bonding between adjacent molecules. As a result molecules in adjacent lamella did not orient in a head-to-head fashion. Alkyl *halides* (Cl, Br, F, I) have been found to order similarly to alkanes, with a 90° orientation of the molecular long axis to the edge of the lamella and an ~4.8 Å intra-lamellar inter-adsorbate distance (see Figure 1.2g). Head-to-head/tail-to-tail orientation both down the length of a lamella and across adjacent lamella was observed.[9,23,25,26] Thus, an attractive halide-halide interaction, due to the polarizable nature of these atoms, caused the molecules to orient with the halide atoms towards one another.

Several further variations in the structure of long-chain alkanes can be systematically investigated to probe how adsorbate-adsorbate interactions affect 2D ordered structures (see Table 1.1). So far, only functional variations at one termina of the chain have been presented. Substitution at internal positions can give insight into the importance of chain-chain interactions on the 2D structure. Alkenes,[9] ethers,[9] sulfides,[9] disulfides,[9,27] and amines[9] have all been investigated

on HOPG. Substitutions at both termini (alkane diols,[9] halogenated alcohols,[9] halogenated acids,[28] halogenated amides[26]) have likewise been investigated. Substitutions that alter the geometry of the molecule (alkynes,[9] secondary alcohols[29,30] and halides,[30] dialkylamines,[31] dialkyl benzenes[20] and cyclic alkanes[32]) have likewise provided insight into how adsorbate-adsorbate interactions can be altered and the subsequent effect of their alteration on 2D order.

The Alkane System- What Has Been Learned

Through the investigations outlined here a substantial amount of knowledge has been gained about the ordered adsorption of long-chain alkanes and their derivatives. The general findings will be briefly iterated here. It has been determined that long-chain alkanes tend to form commensurate or coincident structures on flat and nearly flat crystalline surfaces. In the absence of topographical restrictions, commensuration with the substrate lattice tends to allow adsorbate-adsorbate intermolecular interactions to remain very similar to that found in the bulk 3D alkane structures (lamellar packing with intra-lamellar adsorbate-adsorbate distances of ~4.8 Å). Angles of molecular long axes to the lamella direction are a result of the balance between epitaxy requirements and parallel alkane-alkane van der Waals forces. Terminal functionality gives rise to new intermolecular interactions between adsorbate molecules, but tend not to disrupt commensuration. Functionality within the alkane chain can cause geometrical changes in the molecular structure which affect the 2D order, but do not disrupt commensuration. Functionalities on both ends of the molecule

introduce new intermolecular interactions that influence 2D structure, but do not disrupt commensuration.

The Functional Variation of Squaraines

Squaraines are a class of organic dye molecules, so named because of their "square" central four-membered ring. See Figure 1.3 for a general structure of squaraine. Squaraines have a symmetrical donor-acceptor-donor (D-A-D) structure such that electron density is donated from the electron-rich anilino and squaric oxygen moieties to the electron-poor central ring. This intramolecular charge transfer is associated with an optical transition at ~680 nm. When aggregated, squaraines undergo intermolecular donor-acceptor charge transfer (D-A CT). The optical transition for this transfer is at ~800 nm. Extinction coefficients for squaraines can be greater than 10^5 $M^{-1}cm^{-1}$. As a monomer in solution, many squaraines show sharp and intense absorption in the visible region, with λ_{max} ranging from 620 to ~670 nm, depending on the substituent in the phenyl ring and the substituent at the nitrogen atom.[33] In the microcrystalline solid-state, squaraines tend to form extended parallel stacks with electron-rich amino groups aligned over the electron-deficient 4-membered rings.[34-40]

Due to these strong intermolecular D-A CT intermolecular interactions, the solid state absorption is very broad, from 550 to 900 nm.[35,41] The combination of these two characteristics, (1) intense visible to near-IR absorption and (2) facile charge transfer, have made squaraines very attractive for several applications in industry, particularly as xerographic and laser printer photoreceptors,[35,42-44] in

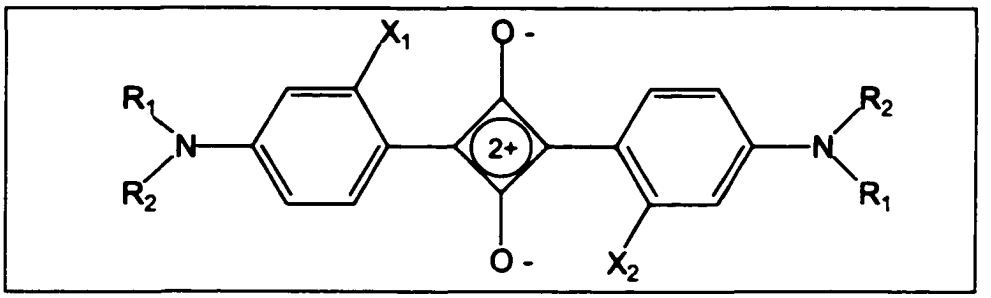

Figure 1.3: General structure of a squaraine molecule.

Abbreviation	X Substituent	R_1	R_2
1-1 OHSQ	OH	CH_3	CH_3
4-4 OHSQ	OH	C_4H_9	C_4H_9
8-8 OHSQ	OH	C_8H_{17}	C_8H_{17}
12-12 OHSQ	OH	$C_{12}H_{25}$	$C_{12}H_{25}$
2-18 OHSQ	OH	C_2H_{37}	$C_{18}H_{37}$
3-3 HSQ	H	C_3H_7	C_3H_7
4-4 HSQ	H	C_4H_9	C_4H_9
8-8 HSQ	H	C_8H_{17}	C_8H_{17}
18-18 HSQ	H	$C_{18}H_{37}$	$C_{18}H_{37}$
1-6 HSQ	H	CH_3	C_6H_{13}
1-8 HSQ	H	CH_3	C_8H_{17}

Table 1.2: List of squaraines studied via STM.

which squaraines are incorporated into thin films. In both of these applications the ability of the dye molecules to (1) form excitons when exposed to visible or near-IR light, (2) allow the excitons to dissociate in an electric field, and (3) transfer these charges through numerous molecular layers is vital to the proper

and efficient functioning of these devices. These properties are directly influenced by the orientation and relative distances of adjacent molecules within the molecular film.[45] In particular, the interfacial region between a substrate and the bulk of the organic thin film is often crucial to the performance of devices incorporating molecular thin films. The interfacial layer may control the rate of carrier transport between the film and the substrate as well as template the bulk structure of the thin film. It is therefore important to understand the orientations of molecules at interfaces to subsequently control the performance of the devices and to understand basic molecule-substrate interactions. Therefore, understanding the mechanism of molecular alignment on a surface is critical to proper and reproducible photoconductor manufacturing.

Squaraines, in particular, were chosen for the work described herein as a result of their relevance to another area of research undertaken in the Parkinson group. The Parkinson group has long had an interest in the conversion of solar energy into electrical energy through the use of wide-bandgap semiconductors (~2 eV and above) that are "sensitized" to a wider range of solar wavelengths than that allowed through their direct optical excitation through the use of an adsorbed layer of dye molecules.[46-49] The most popular and successful of these devices to date is the Grätzel cell, which utilizes a film of nanocrystalline TiO_2 (3.2 eV bandgap), upon which ruthenium-based dye (N3) molecules are covalently bound to the surface.[50] Squaraines have been shown to sensitize

nanocrystalline TiO_2[51-54] and single crystal [‡]SnS_2.[55] As a result of this capability, squaraines were of general interest to our group. When it was discovered that squaraines self-assemble into highly ordered structures at the liquid/solid interface,[56] understanding the factors which controlled its organized adsorption became a goal.

As described earlier in the review of substituted alkane investigations, functional group variation of a system of molecular adsorbates can elucidate the adsorbate-adsobate interactions in an adsorbed structure and can aid in determining their relative influence on the 2D structures produced on flat, relatively inert substrates. This dissertation describes the STM investigation of the effect of structural, geometrical, and functional group variation on the ordered adsorption of squaraine molecules on the HOPG basal plane surface. HOPG was chosen as the substrate because of its nearly atomically-flat, relatively inert surface which can be easily renewed (as well as its relatively low cost). In addition, HOPG was not expected to exert significant influence on the adsorbed structures produced by squaraines, as their aforementioned strong intermolecular donor-acceptor interactions were expected to dominate. Thus, the 2D adsorbed structures produced on HOPG were expected to be similar to that found in the bulk squaraine, and the effects of squaraine variation could be more directly probed. It was not the goal of this work to determine the effect of specific substrates on the 2D structures of adsorbed squaraines, however.

---

‡ SnS_2 was attempted to be used as a substrate for the STM investigation of the ordered adsorption of squaraines. It was found that SnS_2 etches too severely (electric field induced) in non-vacuum conditions to allow the nucleation of ordered squaraine structures.

At least five molecular parameters may be varied in the bis(dialkylamino-X-phenyl)squaraine molecule (Figure 1.3) to investigate the nature of the forces governing their molecular organization on the surface: (1) the length of the alkyl tails ($R_1 = R_2$) , (2) the symmetry of the molecule in terms of the lengths of its tails ($R_1 \neq R_2$) , (3) the identity of the phenyl ring substituent (X), (4) the symmetry of the molecule in terms of its ring substituent ($X_1 \neq X_2$), and (5) the position of the X substituent (non-H) on the phenyl ring. In the work comprising this dissertation, four of these five variations were probed within a set of eleven molecules. They are shown in Table 1.2 and consist of two series: (1) molecules with hydroxyl groups as the X_1 and X_2 substituents at the C2 positions on the phenyl rings, designated OHSQs; and (2) those with a simple proton, designated HSQs. Within these two series, the length of the R_1 and R_2 alkyl tails are varied from very short tails (CH_3) to relatively long tails ($C_{18}H_{37}$). In addition, the symmetry of the molecule is changed with unequal lengths of R_1 and R_2 alkyl tails. Thus, the effects of the variation in phenyl substituent, alkyl tail length, molecular geometry, and molecular symmetry on the ordered adsorption of these molecules on the HOPG surface were investigated with the STM. Specifically, the results obtained by the STM investigation of the ordered adsorption of the hydroxylated series of squaraines, including one less-symmetric molecule are presented in Chapter 3; Chapter 4 presents the results of the investigation of five of the six non-hydroxylated molecules, including two less-symmetric molecules; Chapter 5 presents the results for the sixth non-hydroxylated squaraine, which proved to be a particularly rich adsorbate system, deserving of a chapter unto

itself. Naturally, it was not possible to conduct all of the variations necessary to create a clear picture of squaraine ordered adsorption. Chapter 6 proposes extensions of the experiments presented in the previous chapters, as well as new experiments that would contribute to the knowledge gained thus far on the ordered adsorption of squaraines. Chapter 7 summarizes and concludes this work.

At this point it should be noted that a convention for the abbreviation of these functionally-varied squaraine molecules was developed and used in this thesis. The abbreviations, shown in Table 1.2, are of the formula R_1-R_2 XSQ. R_1 and R_2, as shown in the structure in Figure 1.3, stand for the two pairs of alkyl tails. Since X_1 and X_2 are equal in these series, X stands for the substituents at the C2 position of both the phenyl groups. Thus, the abbreviation 2-18 OHSQ corresponds to a hydroxylated squaraine with $R_1 = C_2H_5$ and $R = C_{18}H_{37}$. This abbreviation convention appears throughout this dissertation.

Chapter One References

(1) Binnig, G.; Rohrer, H., *Helv. Phys. Acta* **1982**, *55*, 726-735.
(2) Binnig, G.; Rohrer, H.; Gerber, C.; Weibel, E., *Appl. Phys. Lett.* **1982**, *40*, 178-180.
(3) Binnig, G.; Rohrer, H.; Gerber, C.; Weibel, E., *Phys. Rev. Lett.* **1982**, *49*, 57-60.
(4) Scheel, H. J.; Binnig, G.; Rohrer, H., *J. Crystal Growth* **1982**, *60*, 199-202.
(5) Binnig, G.; Rohrer, H.; Gerber, C.; Weibel, E., *Surface Science* **1983**, *131*, L379-L384.
(6) McGonigal, G. C.; Bernhardt, R. H.; Thomson, D. J., *Appl. Phys. Lett.* **1990**, *57*, 28-30.
(7) Groszek, A. J., *Proc. Roy. Soc. Lond. A.* **1970**, *314*, 473-498.
(8) Hentschke, R.; Schurmann, B. L.; Rabe, J. P., *J. Chem. Phys.* **1992**, *96*, 6213-6221.
(9) Claypool, C. L.; Faglioni, F.; III, W. A. G.; Gray, H. B.; Lewis, N. S.; Marcus, R. A., *J. Phys. Chem. B* **1997**, *101*, 5978-5995.
(10) Segerman, E., *Acta Crystallographica* **1965**, *19*, 789-796.
(11) Findenegg, G. H.; Liphard, M., *Carbon* **1987**, *25*, 119-128.
(12) Cincotti, S.; Rabe, J. P., *Appl. Phys. Lett.* **1993**, *62*, 3531-3533.
(13) Cincotti, S.; Burda, J.; Hentschke, R.; Rabe, J. P., *Phys. Rev. E* **1995**, *51*, 2090-2098.
(14) Magonov, S. N.; Wawkuschewski, A.; Cantow, H.-J.; Liang, W.; Whangbo, M.-H., *Appl. Phys. A* **1994**, *59*, 119-133.
(15) Ubbelohde, A. R.; Lewis, F. A. *Graphite and Its Crystal Compounds*; Clarendon Press: Oxford, 1960, pp 176.
(16) Evans, E. L.; Griffiths, R. J. M.; Thomas, J. M., *Science* **1971**, *171*, 174-175.
(17) Chang, H.; Bard, A. J., *J. Am. Chem. Soc.* **1990**, *112*, 4598-4599.
(18) Chu, X.; Schmidt, L. D., *Carbon* **1991**, *29*, 1251-1255.
(19) Patrick, D. L.; Cee, V. J.; T.P. Beebe, J., *J. Phys. Chem.* **1996**, *100*, 8478-8481.
(20) Rabe, J. P.; Buchholtz, S., *Science* **1991**, *253*, 424-427.
(21) Venkataraman, B.; Breen, J. J.; Flynn, G. W., *J. Phys. Chem.* **1995**, *99*, 6608-6619.
(22) Cartmell, E.; Fowles, G. W. A. *Valency and Molecular Structure;* 3rd ed.; D. Van Nostrand Co.: Princeton, NJ, 1966.
(23) Venkataraman, B.; Flynn, G. W.; Folkers, J. P.; Whitesides, G. M., *J. Phys. Chem.* **1995**, *99*, 8684-8689.
(24) Cyr, D. M.; Venkataraman, B.; Flynn, G. W., *Chem. Mater.* **1996**, *8*, 1600-1615.
(25) Cyr, D.; Venkataraman, B.; Flynn, G. W.; Black, A.; Whitesides, G. M., *J. Phys. Chem.* **1996**, *100*, 13747-13759.
(26) Giancarlo, L. C.; Fang, H.; Rubin, S. M.; Bront, A. A.; Flynn, G. W., *J. Phys. Chem. B* **1998**, *102*, 10255-10263.

(27) Rabe, J. P.; Buchholz, S.; Askadskaya, L., *Synthetic Metals* **1993**, *54*, 339-349.
(28) Fang, H.; Giancarlo, L. C.; Flynn, G. W., *J. Phys. Chem. B* **1999**, *103*, 5712-5715.
(29) LePoulennec, C.; Cousty, J.; Xie, Z. X.; Mioskowski, C., *Surf. Sci.* **2000**, *448*, 93-100.
(30) Claypool, C.; Faglioni, F.; Matzger, A. J.; III, W. A. G.; Lewis, N. S., *J. Phys. Chem. B* **1999**, *103*, 9690-9699.
(31) Gorman, C. B.; Touzov, I.; Miller, R., *Langmuir* **1998**, *14*, 3052-3061.
(32) Wawkuschewski, A.; Cantow, H.-J.; Magonov, S. N., *Langmuir* **1993**, *9*, 2778-2781.
(33) Law, K. Y., *J. Phys. Chem.* **1987**, *91*, 5184-5193.
(34) Farnum, D. G.; Neuman, M. A.; Suggs, W. T., *J. Cryst. Mol. Struct.* **1974**, *4*, 199-212.
(35) Wingard, R. E., *IEEE Trans. Ind. Appl.* **1982**, 1251-1254.
(36) Tristani-Kendra, M.; Eckhardt, C. J.; Bernstein, J.; Goldstein, E., *Chem. Phys. Lett.* **1983**, *98*, 57-61.
(37) Bernstein, J.; Goldstein, E., *Mol. Cryst. Liq. Cryst.* **1988**, *164*, 213-229.
(38) Dirk, C. W.; Herndon, W. C.; Cervantes-Lee, F.; Selnau, H.; Martinez, S.; Kalmegham, P.; Tan, A.; Campos, G.; Velez, M.; Zyss, J.; Ledoux, I.; Cheng, L., *JACS* **1995**, *117*, 2214-2225.
(39) Ashwell, G. J.; Bahra, G. S.; Brown, C. R.; Hamilton, D. G.; Kennard, C. H. L.; Lynch, D. E., *J. Mater. Chem.* **1996**, *6*, 23-26.
(40) Hamilton, D. G.; Lynch, D. E.; Smith, G., *Aust. J. Chem.* **1996**, *49*, 1339-1343.
(41) Law, K. Y.; Facci, J. S.; Bailey, F. C.; Yanus, J. F., *J. Imaging Sci.* **1990**, *34*, 31-38.
(42) Tam, A. C.; Balanson, R. D., *IBM J. Res. Dev.* **1982**, *26*, 186.
(43) Tam, A. C., *App. Phys. Lett.* **1980**, *37*, 978-981.
(44) Melz, R. J.; Champ, R. B.; Chang, L. S.; Chiou, C.; Keller, G. S.; Liclican, L. C.; Neiman, R. B.; Shattuck, M. D.; Weiche, W. J., *Photogr. Sci. Eng.* **1977**, *21*, 73-78.
(45) Law, K. Y., *J. Phys. Chem.* **1988**, *92*, 4226-4231.
(46) Spitler, M.; Parkinson, B. A., *Langmuir* **1986**, *2*, 549-553.
(47) Parkinson, B. A., *Langmuir* **1988**, *4*, 967-976.
(48) Parkinson, B. A.; Spitler, M. T., *Electrochimica Acta* **1992**, *37*, 943-948.
(49) Fillinger, A.; Parkinson, B. A., *J. Electrochem. Soc.* **1999**, *146*, 4559-4564.
(50) O'Regan, B.; Gratzel, M., *Nature* **1991**, *353*, 737-740.
(51) Kamat, P. V.; Hotchandani, S.; Lind, M. d.; George, M. V., *J. Chem. Soc. Faraday Trans.* **1993**, *89*, 2397-2402.
(52) Hotchandani, S.; Das, S.; Thomas, K. G.; George, M. V.; Kamat, P. V., *Res. Chem. Intermed.* **1994**, *20*, 927-938.
(53) Liu, D.; Kamat, P. V.; Thomas, K. G.; Das, S.; George, M. V., *J. Chem. Phys.* **1997**, *106*, 6404-6411.

(54) Wang, C.; Liu, C.; Wang, W.; Shen, T., *J. Photochem. & Photobiol. A* **1997**, *109*, 159-164.
(55) Takeda, N.; Parkinson, B. A., *Electrochimica Acta* **2000**, *45*, 4559-4564.
(56) Sampson, D. L. Ph.D. Thesis, Colorado State University, 1997.

CHAPTER TWO

Experimental Methods

Squaraine solutions

Squaraines were obtained in the form of purified (recrystallized) microcrystalline powder that ranged in color from aquamarine blue to shimmery green to violet. Bis(4-dimethylamino-2-hydroxyphenyl)squaraine (1-1 OHSQ) was provided by Dr. Gregg Haggquist of Lexmark, International. Bis(4-dibutylamino-2-hydroxyphenyl)squaraine (4-4 OHSQ), bis(4-dioctylamino-2-hydroxyphenyl)squaraine (8-8 OHSQ), and bis(4-didodecylamino-2-hydoxyphenyl)squaraine (12-12 OHSQ) were obtained from Dr. P.M. Kazmaeir of the Xerox Research Centre of Canada. Bis(4-ethylstearylamino-2-hydroxyphenyl)squaraine (2-18 OHSQ) was purchased from Nippon Kankoh-Shikiso Kenkyusho. Bis(4-dimethylamino-phenyl)squaraine (1-1 HSQ) was purchased from Aldrich and susbequently recrystallized in dichloromethane. Bis(4-dipropylamino-phenyl)squaraine (3-3 HSQ), bis(4-dibutylamino-phenyl)squaraine (4-4 HSQ), bis(4-dioctylamino-phenyl)squaraine (8-8 HSQ), bis(4-distearylamino-phenyl)squaraine (18-18 HSQ), and bis(4-methyloctylamino-phenyl)squaraine (1-8 HSQ) were obtained from Marina Stanescu of the Whitten group at the University of Rochester and used with no further purification. Bis(4-methylhexylamino-phenyl)squaraine (1-6 HSQ) was obtained from the Ashwell group at Cranfield University in the United Kingdom.

Solutions of OHSQs or HSQs were prepared in concentrations of approximately 10^{-4} to 10^{-6} M in phenyloctane (Aldrich). Solutions were sonicated ~10 minutes before use to ensure that the squaraine microcrystallites were dissolved. 1-1OHSQ, 1-1HSQ, 4-4OHSQ, 4-4HSQ, 2-18OHSQ, and 18-18HSQ did not dissolve well in phenyloctane. The solubility limit of these molecules in phenyloctane was not determined. At concentrations as low as ~1 × 10^{-6} M, even after ~20 minutes of sonication, these squaraines remained as a fine dispersion in phenyloctane. These solutions were used as-is in their finely-dispersed form following sonication. Microfiltration was found to be unnecessary, as no large aggregates were ever observed in the STM images, thus the dispersed form did not interfere with STM imaging. Sonicated solutions were allowed to return to room temperature before use. Samples were prepared by applying a (~1μL) drop of squaraine solution using a simple Pasteur pipette onto a freshly cleaved piece of highly ordered pyrolytic graphite (HOPG). Experiments were performed with solutions in either the low concentration range (low 10^{-5} to low 10^{-6}) or the high range (high 10^{-4} to high 10^{-5}) to observe differences in nucleation.

Scanning Tunneling Microscopy

Experiments were performed with a Digital Instruments Nanoscope III STM under ambient conditions (room temperature, ambient air). Vibration isolation was provided by a bungee system enclosed in an environmental chamber. STM tips were cut to a sharp point mechanically from (80:20) Platinum/Iridium 0.2mm diameter wire (Alpha Aesar) using DuraSharp 1300

stainless steel scissors (average success rate of 1 in 3 cut tips). Other scissors, including other DuraSharps, were found to have lower success rates. Mechanical cutting to produce a sufficiently sharp tip was accomplished using the following procedure: an ~1.5 cm long piece of PtIr wire was tightly gripped at a position within the bottom third of the wire with sturdy non-ridged tweezers in the weak hand. The DuraSharp scissors were held in the dominant hand. The top ~1/5 of the wire was placed at the intersection of the shears. As the shears were quickly closed, they were pushed away from the body. This action caused the wire to be pulled or drawn into a thinner apex as it was cut. The scanning electron micrograph in Figure 2.1 shows the shape of a typical PtIr tip (proven to be capable of atomic resolution) produced by this method. The sharpness of the tip was evaluated by scanning the freshly-cleaved bare piece of HOPG just before solution deposition. Achievement of atomic resolution of the HOPG lattice at a 10 nm scan size (200 mV bias, 800 pA setpoint, 3.0 gains, 20-30 Hz scan rate, and 1.0 nm z-range) and sharp images at a 500 nm size assured that the tip was suitably sharp for molecular imaging of squaraines. If atomic resolution was not achieved, the application of a 2.0-5.0V (sample positive) voltage pulse (~0.5 s) could sometimes "condition" the tip, thereby allowing atomic resolution.[1-4] Sometimes several such pulses were necessary to achieve atomic resolution of the HOPG lattice. Conversely, sometimes the pulsing only succeeded in destroying the sharpness of the tip. When pulsing the tip did not improve its resolution, it was re-cut and reinstalled to again image HOPG. This procedure was repeated until atomic resolution and noise-free images of the HOPG

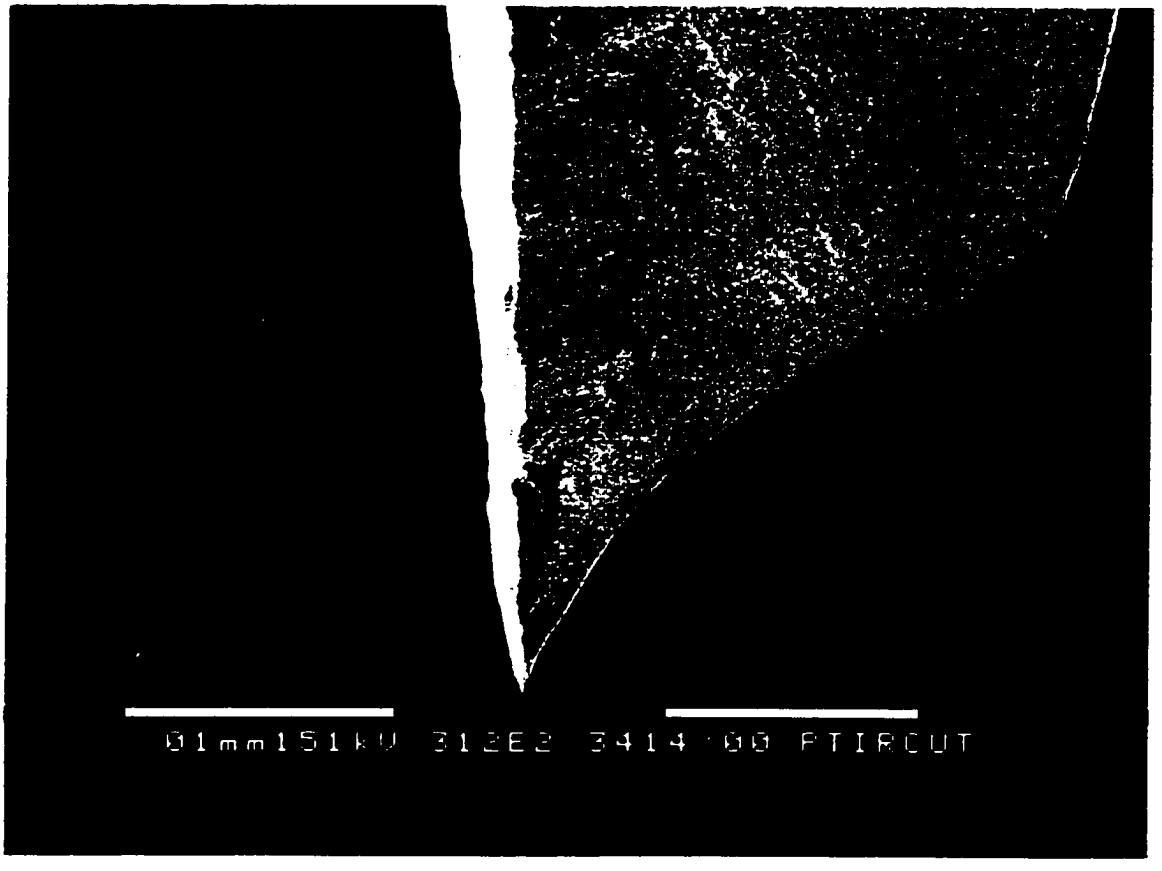

Figure 2.1: Thermionic emission SEM micrograph showing the shape of a mechanically-cut PtIr STM tip. Note the tiny protrusion at the apex. This is most likely a result of the "pulling" action.

substrate could be obtained. When the tip was ensured to be sufficiently sharp, a drop of solution was deposited on the HOPG surface and the tip was immersed into the layer of solution. Solution layer thickness was estimated to be several hundred microns. Tunneling occurred at the liquid-solid interface within seconds of solution deposition. Typical tunneling parameters for the observation of squaraines were –2.0 V to –0.8 V (sample negative) and 30 to 45 pA with the STM operating in constant current mode. Hydroxylated squaraine molecules (except 1-1 OHSQ) tended to image better at higher biases (-1.6 to –2.0 V) whereas non-hydroxylated squaraine images tended to be too noisy at these higher biases, requiring them to be imaged from –0.8 to –1.4 V. Excessive noise present even at "noise-alleviating" tunneling conditions (lower bias) was generally due to the squaraine concentration being too high. In this case, the addition of a drop of phenyloctane diminished the noise.

After a series of squaraine images were obtained, the tunneling gap resistance was lowered in order to characterize the HOPG surface in the exact same spot. The resolution of the HOPG surface after lowering the gap resistance tended to be very poor, presumably due to contamination of the tip by displaced molecules. As a result, the tip often had to be withdrawn and re-engaged in the same general area to characterize the HOPG lattice constant and directions. The vertical motion of tip withdrawal and re-engagement appeared to clean to tip of these molecules. Because the grain size of the polycrystalline HOPG was typically hundreds of microns, it was assumed that the HOPG imaged after re-engagement was within the same grain as the squaraine

overlayer previously imaged. Thus the two (overlayer and HOPG) lattices could be compared to determine relative orientations. Images of each squaraine system were obtained with different Pt/Ir tips and several different solutions to test for reproducibility and ensure that data was free of tip and sample artifacts.

Experimental Difficulties

Problems were sometimes encountered in the course of an experiment, even when the procedure above was followed faithfully. The most common difficulty experienced was the failure to observe an ordered monolayer or nuclei even when the scanning conditions were good (flat surface, low noise, atomic resolution of substrate). There are two possible reasons why this might occur: (1) the tip shape is poor for imaging molecules, or (2) no ordered adsorption has occurred. When imaging conditions are good and no ordered absorption is observed at SQ imaging parameters at large scan sizes, it is usually an adsorption/ordering problem and not a tip problem. In these cases, adsorption of squaraine molecules may well have occurred, but in a disordered state where molecular motion is too rapid for molecules to be resolved by STM. This may occur when there are not enough squaraine molecules on the surface to nucleate ordered domains. To overcome this difficulty, the following procedure was developed. It was followed in order, step by step, until ordered adsorption was apparent in the STM image.

1. Withdraw the tip. Deposit more solution right on top of the solution already there (do not re-cleave or wipe off first deposition). Re-engage

with SQ parameters at large scan sizes (500 nm – 1 μm) and a slow rate (1 - 2 Hz).

2. Scan HOPG (200 mV, 800 pA) at small scan sizes (10 nm) and high rates (~20 – 30 Hz) for a few minutes. Withdraw and re-engage with SQ parameters at a large scan size (500 nm – 1 μm) and slow rate (1 - 2 Hz).
3. Apply a brief (~0.5 s) voltage pulse (2 - 4 V sample positive).
4. Withdraw. Wipe squaraine solution from the HOPG surface (rub HOPG with Kimwipe). Re-cleave with Scotch tape and check tip by scanning with HOPG parameters at small scan sizes. Withdraw the tip and deposit a new drop of solution. Engage with SQ parameters at a large scan size and slow rate.
5. Make a more concentrated squaraine/phenyloctane solution and begin again with (1).

When the above procedure was not successful in achieving images of ordered adsorption, it was assumed that the problem was one of tip shape. A second procedure was followed:

1. Apply a brief (~0.5 s) voltage pulse (2 - 5 V sample positive).[1-3]
2. Re-cut tip.
3. Repeat (1) and (2) until able to resolve HOPG at small scan sizes and scan without noise at larger scans (500 nm to 2 μm).

Eventually, these procedures always led to success for obtaining images of the ordered adsorption of squaraines. Sometimes images were obtained several

hours after the initial commencement of the experiment. The bottom line in achieving success in these experiments was having patience, being persistent, and not giving up.

Data Collection

Images at all scan sizes, regardless of content, were always obtained (when possible) in pairs of sequential "up" and "down" images (see Figure 2.2). As the tip rasters back and forth in the x-direction of the square STM scan (referred to as the "fast-scan axis"), it also slowly moves in the y-direction (the "slow-scan axis"). After the completion of a single square scan, the direction of the "slow-scanning" automatically reverses. Thus, if the tip begins a scan at the top of the square area and finishes at the bottom, it is referred to as a "down" scan, and vice versa for an "up" scan. Pairs of "up" and "down" scans unambiguously show whether sample drift is occurring. In addition, the direction of the drift can be inferred from the differences between the "up" and "down" scans. For example, if the features in an image appear to be compressed in the y-direction during a "down" scan and elongated in an "up" scan, then the direction of drift can be inferred to be parallel to the slow scan axis, moving "up". Likewise, if the position of the features appears to drift across the image from left to right when comparing a pair of "up" and "down" images of the same area, it can be inferred that the sample is drifting parallel to the "fast-scan axis" moving right. These are simplified examples. Most drift occurred simultaneously in both the x and y directions. Drift tended to subside over the period of an hour of

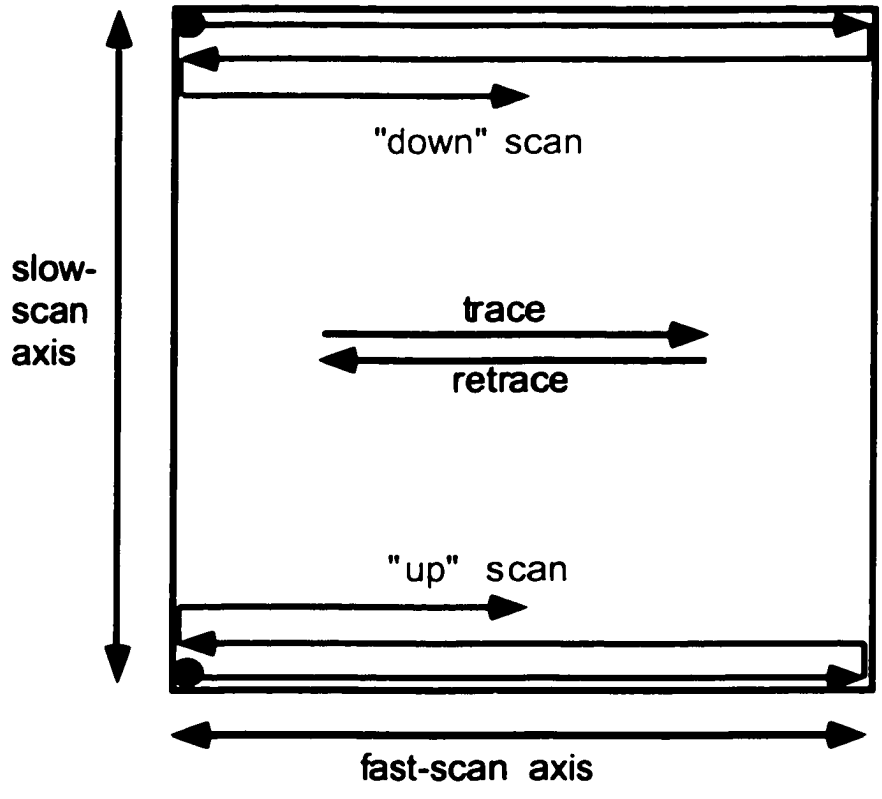

Figure 2.2: Schematic of a square STM scan for the purpose of defining the terms "fast-" and "slow-scan" axes, "up" (blue) and "down" (red) scans, and "trace" and "retrace". The red and blue dots signify the beginning of an "up" and "down" scan, respectively.

scanning. The extent of drift varied from experiment to experiment, with some experiments experiencing imperceptible drift even at the onset of the experiment.

Data was collected for as long as images of stable ordered molecular layers could be obtained. This ranged from a few hours to in excess of a day. When a single solution deposition no longer yielded stable molecular images, the sample was removed, the HOPG re-cleaved, the sample solution re-sonicated, and finally re-deposited on the fresh HOPG surface to allow another imaging session.

Image Analysis

Before STM images can be presented, or useful information can be obtained from them, they must be normalized by a "flattening" routine provided in the Nanoscope software package. This process is necessary because of the gradual, line-by-line nature in which STM images are produced. During image acquisition, a color value is assigned to every height value represented within each line. The assignment of each line occurs independently of the others. As a result, a given color value is not necessarily assigned to the same height value in all of the lines within an image. Flattening is a normalization procedure which attributes a given color scale value to the same height throughout the entire image.

Further processing of the images was performed only in cases of distracting noise, such as horizontal streaks. Images of HSQs tended to be noisier than those of OHSQs, and further processing was sometimes performed to remove or reduce this noise without affecting the features in the image. This

noise was always parallel to the fast-scan axis, and thus was easily recognizable as a vertical stripe in the center of the frequency spectrum of the image. It could easily be removed from the frequency spectrum without affecting the other image features. A reverse fast-Fourier transform then restored the image to real space without the horizontal noise. Fourier transform filtering was not used in the vast majority of images presented in this dissertation.

Distances between features within an image are determined by cross-sectional analysis. Basically, a line is drawn on the image that passes through two points of interest. This line is then converted into a cross-section. Distances, as well as differences in apparent height, between any two designated points on that line can be determined. In determining the widths of features containing straight edges, such as molecular rows, the cross-section feature was used in conjunction with an "averaging" option. In the example of the determination of the width of a molecular row, a cross-section line is drawn through the row, perpendicular to the edge of the row. The user then designates the length of row that they want to include in the calculation of average width. The software then sums the cross-sections along the included length of row and divides by the number of cross-sections within that length. An average cross section for the designated length of row used in the calculation is presented by the software. Distances and differences in apparent heights between any two points on that average cross–section can then be determined. Points were placed at the FWHM positions of the features when determining lateral distances between features in an image. Unit cell distances for a particular 2D molecular

polymorph were determined by taking the mean and standard deviation of hundreds of such cross-sectional measurements obtained from scores of high resolution images.

Angles were determined using the software "top view", "angle" function. In this software routine, vectors oriented parallel to the features of interest can be drawn over the image. The calculated angle between the two vectors is then displayed. Unfortunately, there was no way to obtain an average angle for designated features within an image by software routines. As a result, individual angles within scores of images were measured and tabulated, ultimately being expressed by their mean and standard deviation.

It is important to mention that when analyzing images for intermolecular distances and unit cell parameters by the methods just described, it was imperative that drift, if present, was recognized. This could be accomplished by comparing data obtained from several high resolution images of the same scanned area taken in both "up" and "down" directions. When considering images for unit cell or intermolecular angles or distances, those exhibiting drift > a few angstroms were avoided. This exclusion was possible because ~90 % of the experiments conducted acquired high resolution images meeting this requirement.

Analysis of the STM images to yield unit cells and other distances of interest (such as the observed lengths of the chromophore region of the molecule, the distances between adjacent chromophores in the same row, the angle between the long axis of the chromophore to the edge of its molecular row,

etc) was tedious and time-consuming, taking far more time than that to acquire the images.

Calibration

As mentioned above, images of the HOPG lattice were always obtained within the same general area as the molecular images. The measured lattice distances of the HOPG surface within these images were then used to calibrate the distances measured for the adsorbate lattice.

Molecular Modeling

Modeling of the proposed structures of ordered adsorbate squaraines was performed to aid in their visualization. They were not performed to determine possible minimum energy structures or to calculate energies, however. This visualization modeling was done with the Computer-Assisted Chemistry molecular modeling program (CAChe, Inc.).

References

(1) Smith, D. P. E.; Horber, H.; Gerber, C.; Binng, G., *Science* **1989**, *245*, R43-R45.

(2) Stabel, A.; Herwig, P.; Mullen, K.; Rabe, J. P., *Angew. Chem. Int. Ed. Engl.* **1995**, *34*, 1609-1611.

(3) Stevens, F.; Dyer, D. J.; Walba, D. M., *J. Vac. Sci. Technol. B* **1996**, *14*, 38-41.

(4) Sampson, D. L. Ph.D. Thesis, Colorado State University, 1997.

CHAPTER THREE

STM Investigation of the Ordered Structures of Dialkylamino Hydroxylated Squaraines Adsorbed on HOPG

Published: M. E. Stawasz, D. L. Sampson and B. A. Parkinson, *Langmuir* **2000**, *16*, 2326-2342.

Abstract

Squaraine dyes form aggregates in solution and in the solid state. We have found that bis(4-dialkylamino-2-hydroxyphenyl)squaraines form two-dimensional (2D) ordered layers when adsorbed onto HOPG from phenyloctane and from liquid crystalline solvents. We investigated with scanning tunneling microscopy the 2D structures of the adsorbed phases of five bis(4-dialkylamino-2-hydroxyphenyl) squaraines (both symmetric and asymmetric) and mixtures of these squaraines. Differences in the stability of the 2D structures and molecular packing are observed when the alkyl tail length and symmetry are varied. A transition in 2D structure from a herringbone packing to lamellar packing occurs between the tail lengths of 4 carbons and 8 carbons. Many of the compounds form a number of 2D polytypes on HOPG. Multilayers of squaraine molecules were observed for most of the studied molecules. Squaraines with tail lengths of 12 carbons exhibited a tendency towards registry with the HOPG substrate whereas all other squaraine compounds investigated showed a lack of molecule-substrate registry. Domain sizes of the investigated molecules varied from tens of nanometers to a micron.

Introduction

Since the invention of scanning tunneling microscopy (STM), a number of different organic molecular systems that form two-dimensional ordered arrays on solid surfaces have been studied. These systems can be roughly divided into three basic types distinguished from each other by the relative strengths of their molecule-molecule and molecule-substrate interactions. The first type, represented by alkanes and alkane derivatives on HOPG exhibits only weak van der Waals molecule-molecule interactions.[1-18] Although there are molecule-molecule interactions, the two dimensional organization of molecules within this type of molecular system is primarily driven by interaction between the adsorbed molecules and the substrate. Changing the lattice spacing of the substrate changes the relationship of the molecules within the adsorbate layer.

The second group shows a relatively balanced influence of intermolecular interactions within the adsorbed layer and between the adsorbed molecules and the substrate. This system is best exemplified by liquid crystals.[19-34] Molecules that form liquid crystalline phases generally contain a polar head group and an aliphatic tail. Within the adsorbate layer the main intermolecular interactions are dipole-dipole and van der Waals. Between the adsorbate layer and the substrate, the interaction tends to be driven by alkyl tail registry with the substrate lattice. Both the adsorbate-adsorbate and adsorbate-substrate interactions exert an influence on the two-dimensional structure of the adsorbate layer. Thus subtle changes in the substrate lattice constant or molecular structure can result in very different two-dimensional surface structures.[35]

The third system of molecules, which spontaneously form 2D ordered arrays/layers on surfaces, are those in which adsorbate-adsorbate intermolecular interactions dominate the two dimensional structure. Adenine molecules are indicative of this third type of adsorbate system.[36-42] The relatively stronger hydrogen bonding between adjacent molecules controls the molecular packing of adenines and similar molecules in the adsorbed layer. When the lattice spacing of the substrate is changed, the packing order and distance relationship between adjacent adenine molecules within the layer do not change substantially.[37-39,41]

We report a new ordered molecular adsorbate system, squaraine dye molecules (see Table 3.1 for structure), belonging to the third class as described above. Squaraines are dyes so named because of the square central carbon ring.[43] They are highly polarized and symmetric molecules that are able to undergo intermolecular charge transfer in the ground state as well as in the first excited state. In the ground state the anilino moieties act as electron donors (D) while the central C_4O_2 unit acts as the electron acceptor (A), resulting in the squaraine molecule having a donor-acceptor-donor (DAD) internal structure. The DAD structure results in strongly attractive intermolecular interactions between the donor and acceptor moieties of adjacent molecules.[44-48] In addition, its DAD structure makes the squaraine molecule a good charge transfer vehicle, both intramolecularly and intermolecularly. Squaraines are strongly absorbing with extinction coefficients on the order of 3×10^5 $M^{-1}cm^{-1}$ in many solvents.[47] At low concentrations ($<10^{-6}$ M) in solution most squaraines exist as monomers, with λ_{max} varying between 620 and 670 nm, depending on the nitrogen and phenyl

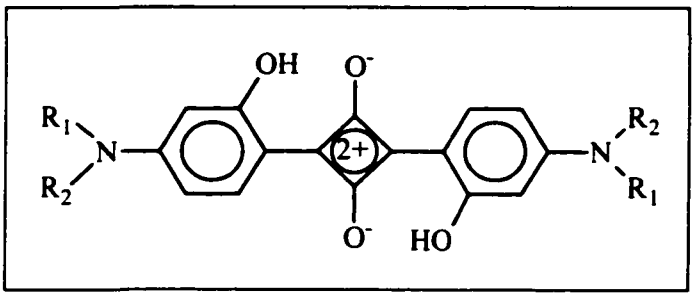

1-1OHSQ	$R_1 = R_2 = C_1H_3$
4-4OHSQ	$R_1 = R_2 = C_4H_9$
8-8OHSQ	$R_1 = R_2 = C_8H_{17}$
12-12OHSQ	$R_1 = R_2 = C_{12}H_{25}$
2-18OHSQ	$R_1 = C_2H_5$; $R_2 = C_{18}H_{37}$

Table 3.1: Structure of a generic hydroxylated squaraine molecule and list of the hydroxylated squaraines studied.

Substituents.[49] At higher concentrations, however, aggregation of squaraines in solution is evident with λ_{max} shifted to the red or blue depending on the aggregate structure. The predominant industrial use for squaraines has been in photoreceptor devices as photogenerating molecules in xerography [50-51] and ablative optical recording,[52-54] although they have also been used for research on organic solar cells.[48,55-57]

The strong intermolecular interactions, resulting in a tendency to aggregate in solution, combined with intermolecular charge transfer make squaraines promising molecular systems for STM study. There is an additional applied justification for studying squaraine structures with STM. It has been shown that the three-dimensional (3D) structure of squaraines affects their ability to generate and transport charge in photoreceptor devices.[45] It has also been shown that n-alkyl substituents disturb the intermolecular CT interaction between the squaraine chromophores due to their steric bulk.[58] STM is useful for imaging the two-dimensional ordered structures of organic molecules on solid substrates.

The goal of this study was to determine the effect of structural differences in the squaraine molecules on the two-dimensional packing structures formed on HOPG surfaces. This systematic variation in structure from short alkane chains to long alkane chains should also lead to a progression in adsorbate structure dominated by molecule-molecule interactions to structures showing a more balanced influence between molecule-molecule interactions and substrate-molecule interactions.

Experimental

Experiments were performed with a Digital Instruments Nanoscope III STM under ambient conditions. Vibration isolation was provided by a bungee system enclosed in an environmental chamber. Three different squaraine molecules were obtained from Dr. P.M. Kazmaeir of the Xerox Research Centre of Canada. They were bis(4-dibutylamino-2-hydroxyphenyl) squaraine (4-4 OHSQ), bis(4-dioctylamino-2-hydroxyphenyl) squaraine (8-8 OHSQ), and bis(4-didodecylamino-2-hydoxyphenyl) squaraine (12-12 OHSQ). Bis(4-ethylstearylamino-2-hydroxyphenyl) squaraine (2-18 OHSQ) was purchased from Nippon Kankoh-Shikiso Kenkyusho and bis(4-dimethylamino-2-hydroxyphenyl) squaraine (1-1 OHSQ) was provided by Dr. Gregg Haggquist of Lexmark. 4'-n-octyl-4-cyanobiphenyl (8CB) was obtained from Aldrich. Table 3.1 shows the structure of the five squaraine molecules studied and the abbreviations used in the rest of this paper. For single component solutions, concentrations of approximately 10^{-4} to 10^{-6} M were prepared in phenyloctane (Aldrich). For binary squaraine solutions, mole per cent ratios of 1:1, 1:10, and 10:1 were prepared. Mixtures of 2-18 OHSQ and 8CB were prepared by dissolving 0.1 to 5% wt/wt 2-18 OHSQ into neat 8CB. Solutions of 1-1 OHSQ were also prepared in dichloromethane (CH_2Cl_2) due to the low solubility of 1-1 OHSQ in phenyloctane. STM tips were cut to a sharp point mechanically from (80:20) Platinum/Iridium 0.2mm diameter wire (Alpha Aesar). Samples were prepared by applying a drop of squaraine solution onto a freshly cleaved piece of highly ordered pyrolytic graphite (HOPG). Tunneling occurred with the tip immersed into the layer of

solution using typical tunneling parameters of –2.0 V to –1.6 V (sample negative) and 40 pA with the STM operating in the constant current mode. In the case of 1-1 OHSQ deposited from CH_2Cl_2 solution, the cleaved HOPG surface was immersed into the solution for two minutes, the solvent was evaporated off, and a drop of phenyloctane was deposited on top of the deposited molecular film. The tip was then immersed into the phenyloctane solution for imaging. After a series of squaraine images were obtained, the tunneling gap resistance was lowered in order to characterize the HOPG surface in the exact same spot. Images were obtained with different tips and several different series of solutions to test for reproducibility and ensure that data was free of tip and sample artifacts. All images presented here have been flattened by software routines.

A range of solution concentrations for which ordered adsorption could be achieved and observed with STM was determined. Solutions with a concentration of 8×10^{-7} M to about 3×10^{-4} M produced monolayers or multilayers of molecules easily imaged with the STM. Less concentrated solutions did not form a monolayer, and hence no molecular order was seen. When solutions more concentrated than about 3×10^{-4}M were used, several layers of ordered molecules form on the surface, but their structure was obscured by the further adsorption of squaraine layers. Amorphous layers are composed of randomly adsorbed squaraine molecules without an ordered packing structure. The application of a short voltage pulse often removed these adsorbed molecules and briefly revealed the ordered squaraine layers. An image produced by this amorphous adsorption can be distinguished from the effects

that are produced using a contaminated tip since individual molecules within amorphous layers could often be resolved, however their orientation within the layer was completely random. Hence tip contamination is not an alternative explanation for the observance of this phenomenon. Often even when solutions within the range of acceptable concentrations (usually 10^{-5} to 10^{-4} M) were used, some amorphous adsorption did occur on top of the ordered multilayers. This small amount of adsorption could be enough to somewhat obscure the order of the layers beneath. When this occurred, a voltage pulse was applied to the surface, revealing the ordered layers.

Results and Discussion

Squaraines were found to be highly surface active molecules even when compared with other well-known 2-D molecular systems. In initial experiments performed by D.L. Sampson,[59] 2-18 OHSQ was dissolved into 4'-n-octyl-4-cyanobiphenyl (8CB) at a ratio of 0.1 to 5.0% wt/wt SQ/CB and deposited onto graphite. Although 8CB molecules were present in great excess, an ordered monolayer consisting solely of squaraine molecules was formed with no evidence of ordered 8CB molecules on the surface. Pure solutions of squaraine (with concentrations within the range described above) formed ordered layers of squaraine that could be observed with STM shortly after deposition. The length of time elapsed between deposition and observation of adsorbed layers with STM ranged from several seconds to tens of minutes, depending on the identity of the squaraine. This time dependence will be explained in following sections. With the exception of 1-1 OHSQ and 2-18 OHSQ, the surfaces tended to show

either no coverage or complete coverage representing a step in the adsorption isotherm that is consistent with strong molecule-molecule interactions.

Squaraine molecules appear in most of our STM images as football-shaped areas of bright contrast measuring 15.0 ± 1.5 Å in length, 2.5 ± 1.5 Å in width, and from 0.7 Å to 1.5 Å in relative height. Images of particularly good resolution show two bright spots within the football shaped region each measuring ~3 Å in length (see Figure 3.1). The length of the football shape corresponds well with the length of the chromophore of the molecule (from the nitrogen at one end of the chromophore to the nitrogen at the other end) with the spots assigned to the phenyl rings. The width of the football corresponds well with the width of a phenyl group, not including the oxygens and hydroxyls. The aromatic chromophore of the squaraine molecule should be imaged as an area of bright contrast since this is where the majority of electron density is located in the molecule. In addition, this moiety is highly polarizable in contrast to the rather insulating alkyl tails. The difference in exhibited contrast between the oxygens (dark) and the nitrogens (bright), is explained by the theory proposed by Claypool et al relating ionization potential to STM contrast.[7] Essentially, atoms with high ionization potentials have a low probability for tunneling (O → dark contrast) whereas atoms with low ionization potentials have a high probability for tunneling (N → bright contrast). The lack of resolution of the alkyl tails of these squaraine molecules with the STM is puzzling in light of the fact that n-alkanes and the tails of cyanobiphenyls have been routinely imaged on graphite

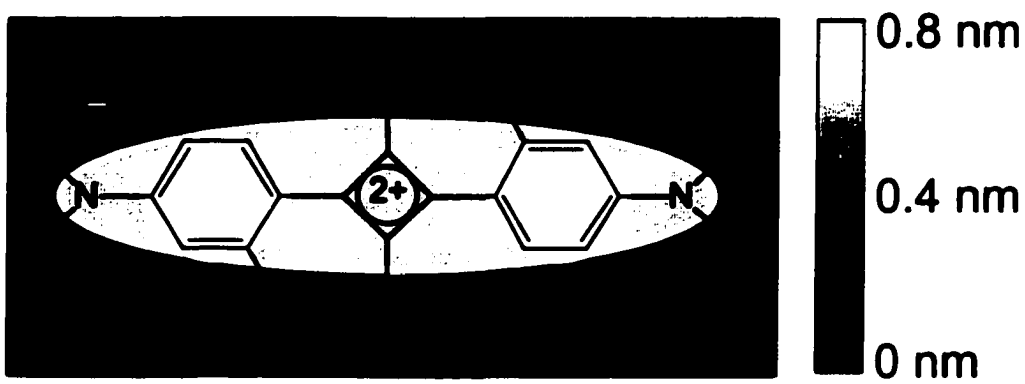

Figure 3.1: Cartoon showing the STM image contrast exhibited by a single squaraine molecule. The chromophore region (from N to N) appears as a bright oval. At high resolution, the phenyl rings appear as bright spots.

surfaces.[1-8,12,13,15-18] The length, width and relative height of the bright football shaped areas correspond well with a model of the molecule lying with chromophore flat on the HOPG surface. Measured relative heights of 1 to 2 Å are typical for π systems adsorbed lying flat on the substrate surface, as measured by STM.[41] Since the alkyl tails are not resolved, packing of the bright chromophores must be examined quantitatively to deduce the orientation of the tails.

Domain and Unit Cell Structure

Ordered layers of squaraines (with the exception of 4-4 OHSQ) were found to be highly stable, and could be imaged continuously over periods of several days. These layers consisted of domains of tens of nanometers to several hundred nanometers in size. The domains within these layers were not stable, however, and tended to grow or contract over time with smaller domains sometimes transforming into larger domains. This process of Ostwald ripening was observed most often and most obviously in samples of 1-1 OHSQ and 2-18 OHSQ. This can be seen in Figure 3.2, which shows a series of images of 2-18 OHSQ on HOPG which capture the process of domain nucleation and growth, and subsequent competition between domains. The shapes of domains exhibited by the squaraine series varied depending on the type of adsorbate structure that each squaraine produced. In general, squaraines that produced herringbone structures formed elliptical or rectangular domains and squaraines that produced row structures formed diamond-shaped, faceted domains. The differences in

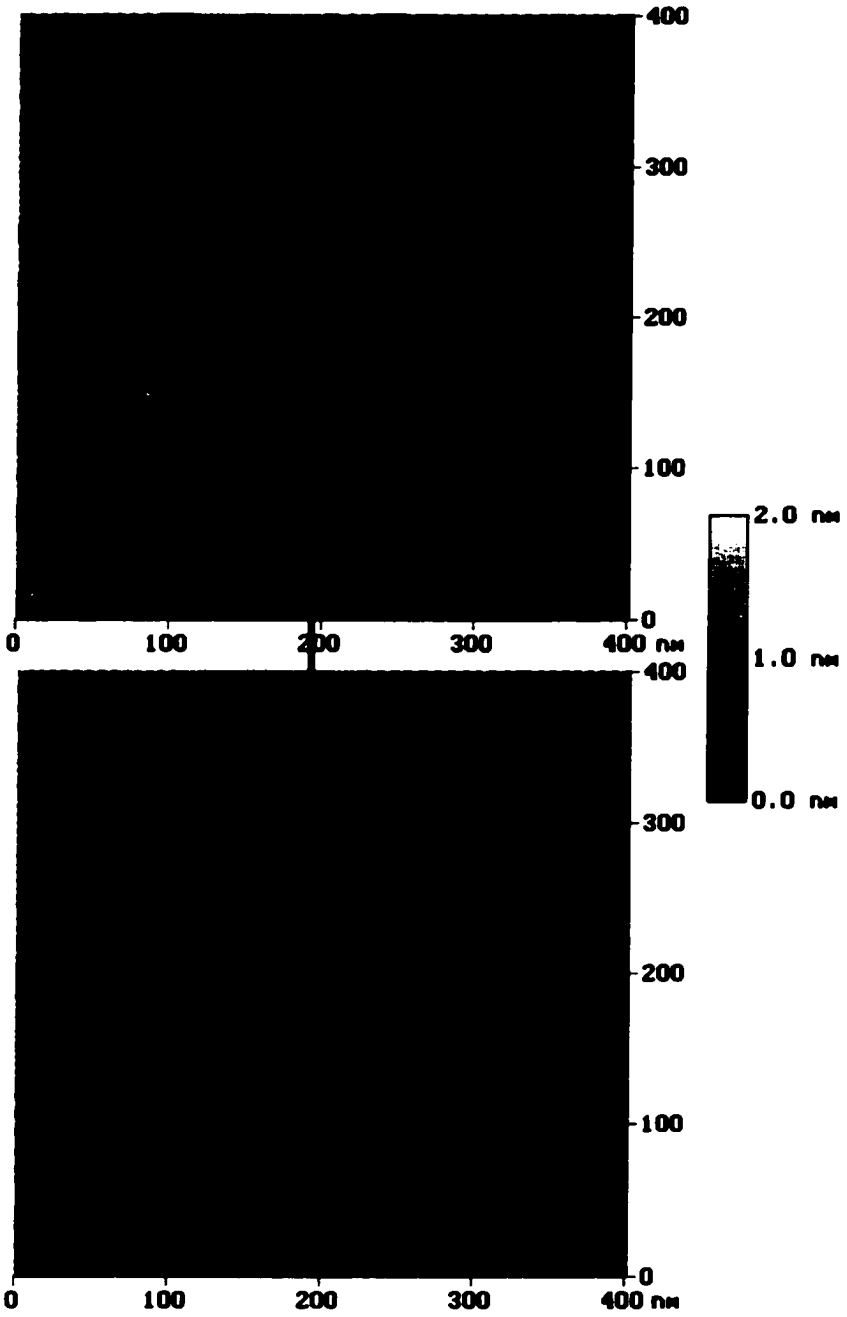

Figure 3.2: Two STM images of 2-18 OHSQ adsorbed on HOPG. Images (A) and (B) are 400 nm x 400 nm scans, taken 15 minutes apart, scan (A) being 5 minutes after deposition. Bare areas of HOPG can be seen in image (A) whereas in image (B) the domains have grown substantially in size and almost fully cover the surface. In addition one domain direction is becoming prominent. This direction does not correlate with the HOPG lattice. The arrow serves as a point of reference, indicating a domain cluster common to both images.

domain stability, sizes, and shapes will be elaborated upon in each of the individual squaraine sections.

1-1 OHSQ

Ordered regions of adsorbed 1-1 OHSQ were the most difficult of the five squaraine systems studied to observe with STM, with images of ordered 1-1 OHSQ layers being obtained only about 10% of the time. The length of the alkyl tail substituents have been shown to effect the charge transfer ability of the molecular aggregates, with aggregates of the longer-tailed squaraines being the least efficient.[45] The higher "conductivity" of aggregates of 1-1 OHSQ may allow charge transfer/tunneling to occur more easily through its non-ordered layers than would occur for non-ordered regions of longer-tailed squaraines. This may explain why 90% of the images obtained with STM of 1-1 OHSQ are of amorphous layers/regions. Thus the amount of data acquired for 1-1 OHSQ is the smallest of the five squaraines studied.

When they are successfully imaged, as shown in Figure 3.3A, it can be seen that 1-1 OHSQ nucleates to form oblong, rounded domains of a few hundred nanometers in length which quickly grow together to cover the entire surface (Figure 3.3B) and frequently continue growing to form multiple layers. Isolated domains were extremely stable to the rastering motion of the tip, but grew and shrank readily over time, presumably due to small temperature fluctuations. At scan sizes larger than 100 nm, it was difficult to distinguish the molecular packing structure of 1-1 OHSQ, since individual molecules appear simply as an approximately 15 Å long and 2.5 Å wide football shape. When scan

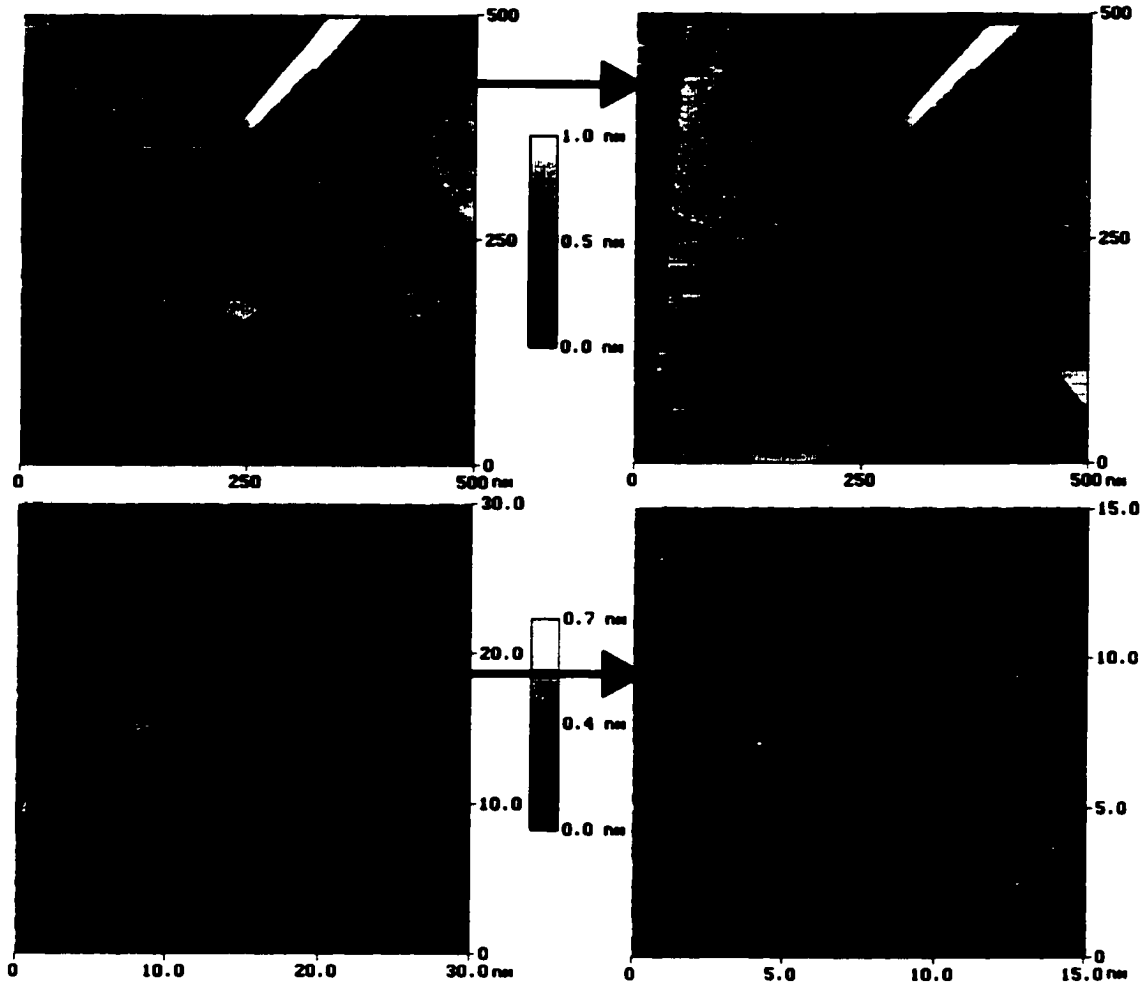

Figure 3.3: STM images of 1-1 OHSQ adsorbed on HOPG. Images (A) and (B) show a timelapsed sequence in which (A) was captured within 5 minutes of deposition and shows nucleation of oblong domains. (B) was captured 3 minutes after (A) and shows not only the growth of domains but also the relatively fast formation of multilayers. The numerous bright lines may be due to the presence of 1-1 OHSQ molecules trapped between the adsorbate layers and the tip which are dragged across the surface by the rastering motion of the tip. Image (C) shows a 30 nm x 30 nm scan in which 3 different types of molecular packing coexist within the same domain. "90° degree herringbone", "Herringbone-row", and "J-like" packing are shown in regions 1, 2, and 3, respectively. A zoomed-in image of "90° degree herringbone" is shown in (C1). Lack of molecular resolution prevents showing similar zoomed-in images of the "Herringbone-row" or "J-like" polymorphs.

sizes were decreased to less than 100 nm it was usually possible to resolve individual molecules within the ordered domains and determine the unit cell and sub-unit cell dimensions. The measured unit cell dimensions, calculated molecular areas, calculated packing densities, and other data for 1-1 OHSQ as well as all five hydroxylated squaraines are listed in Tables 3.2 and 3.3.

As seen in Figure 3.3C, 1-1 OHSQ exhibits at least three polymorphs. The first is a herringbone-like structure in which molecules intersect at 90 ° angles that we will refer to as the 90 ° herringbone (Figure 3.3C region 1). The second and third have been difficult to characterize unambiguously due to a lack of stable, small-scale, molecularly-resolved images of these two polymorphs. However, they can be distinguished from one another in images. The unit cells for these latter two polymorphs have been determined through Fourier analysis and are listed in Table 3.2. The second polymorph appears to be a row/herringbone hybrid, in which adjacent molecules within the same row intersect with each other at 65 ± 5 ° angles. We refer to this polymorph as herringbone-row (Figure 3.3C region 2). The final polymorph appears to be a J-aggregate-like structure in which adjacent rows of molecules are staggered by half a molecular length with respect to one another (Figure 3.3C region 3). We refer to this third polymorph as J-like. Of the three polymorphs, herringbone-row and 90 ° herringbone are observed most often and can coexist within the same domain and reversibly convert between the two forms, thus suggesting that they are of similar energy. The J-like-aggregate is very rarely seen, usually being converted into one of the other two polymorphs, and appears only in very small

Table 3.2

Squaraine	Packing structure	Unit cell α	a ±1.5Å	b ±1.5Å	Packing density (molecules/ nm^2)	Molecular area ($Å^2$)/molecule
1-1OHSQ	90° Herringbone	90±2°	25	25	0.64 ± 0.05	156 ± 13
	Herringbone-row	100±1°	15	8	1.53 ± 0.32	66 ± 13
	J-like	80±3°	19	13	0.81 ± 0.11	124 ± 17
	Row (from CH_2Cl_2)	46±2°	24	9	0.46 ± 0.08	216 ± 38
4-4OHSQ	70° Herringbone	85±3°	19.5	18.5	0.55 ± 0.06	180 ± 20
	90° Herringbone	90±2°	29	29	0.48 ± 0.04	210 ± 15
8-8OHSQ	Row	72±5°	25	8	0.5 ± 0.1	200 ± 39
12-12 OHSQ	Type (1) Row	84±5°	28	7.5	0.48 ± 0.10	210 ± 13
	Type (2) Row	100±5°	30	11.5	0.58 ± 0.08	173 ± 24
2-18 OHSQ	Type (1) Row		*		*	*
	Type (2) Row	90±2°	42± 2	8	*	*
	Type (3) Row		*		*	*
	Type (4) Row		*		*	*
	Type (5) Row		*		*	*
	Type (6) Row		*		*	*
	Type (7) Row		*		*	*

Table 3.2: Unit cell data for the major polymorphs of the five OHSQs studied. Asterisks represent a lack of data due to insufficient molecular STM resolution.

Table 3.3

Squaraine	Ordered structure	Observed Bright row Width (90° to row direction)	Observed Dark row Width (90° to row direction)	Expected Bright row Width (Width of chromophore (N to N))	Expected Dark row Width (Length of alkyl tail)	Angle of molecule to row
1 – 1 OHSQ	90° herringbone Herringbone-row Slipped-J Row (CH_2Cl_2)	NA 9 ± 1Å • 14 ± 1Å	NA 6.5 ± 0.5Å • 10 ± 1Å	NA 15Å • 15Å	NA 1Å • 1Å	NA 56 ± 3° • 47 ± 1.3°
4 – 4 OHSQ	Herringbone	NA	NA	15Å	4 – 4.5Å	NA
8 – 8 OHSQ	Row	14 ± 1.5Å	11 ± 1.5Å	15Å	9.5 – 10Å	68 ± 3°
12 – 12 OHSQ	Type (1) Row Type (2) Row	14 ± 2 Å 18 ± 2Å	13 ± 2Å 11 ± 2Å	15Å	14 – 14.5Å	60 ± 5°
2 – 18 OHSQ	Type (1) Row Type (2) Row Type (3) Row Type (4) Row Type (5) Row Type (6) Row Type (7) Row	18 ± 1Å 22 ± 2Å 23 ± 1Å 23 ± 1Å 26 ± 1Å 26 ± 1Å 30 ± 2Å	21 ± 1Å 20 ± 2Å 16 ± 1Å 24 ± 0.5Å 16 ± 0.5Å 21 ± 0.5Å 14 ± 2Å	15Å	1.5-2.2Å(C_2) 21-22Å (C_{18})	60 ± 5°

Table 3.3: Adsorption and ordering data of the five OHSQs studied. Asterisks represent insufficient data.

areas of a few hundred nm^2. None of the polymorphs observed showed any registry with the surface.

As of yet, the only polymorph that has been imaged with high enough resolution to allow for unambiguous characterization is 90 ° herringbone. As a result, detailed discussion of the structures, intermolecular interactions, and polymorph conversions in the herringbone-row and J-like polymorphs will not be presented. The 90 ° herringbone polymorph will be the focus of the following discussion.

The close proximity of the molecules within the 90 ° herringbone phase (4.5 ± 1.5 Å between adjacent chromophores) presents a confusing case when trying to model the positions of the methyl tails of the 1-1 OHSQ molecules within the molecular packing. Unfortunately, the methyl groups are not resolved in any of the polymorphs, so their positions must be deduced from the orientation and distances between the observed molecular chromophores. The 90 ° orientation of the chromophores and the measured chromophore-to-chromophore distance of only 4.5 Å suggests that the dimethylamino moiety is rotated from the plane of the molecule, despite the loss of conjugation in the π system of the chromophore that this rotation would cause. If the methyl groups were in the same plane as the molecule the distance between bright chromophores would be larger due to the steric repulsion between adjacent molecules (at least 6.5 Å). In addition, methyl groups lying in the same plane as the chromophore might mitigate the interaction between positive and negatively-polarized regions on adjacent molecules. It is this Coulomb interaction between negatively-polarized oxygens and positively-polarized nitrogens that appears

to be the dominant molecule-molecule interaction between chromophores of adjacent 1-1 OHSQ molecules in the 90 ° herringbone polymorph. In addition, this structure appears to have donor-acceptor charge-transfer interactions. The donor moieties of each 90 ° herringbone squaraine molecule are pointed directly towards and are in close proximity to the acceptor moiety of two of the adjacent molecules (one on either side). Conversely, the acceptor moiety of each squaraine molecule is oriented with two donor moieties (one from a molecule on either side) pointed towards and in close proximity to it. The 90 ° orientation of the squaraine molecules to one another may be the result of the dimethylamino groups being oriented almost perpendicularly to the plane of the molecule. As a result all four of the molecules surrounding a single central molecule may orient at right angles to it at close enough proximity (4.5 ± 1.5 Å) to allow donor-acceptor CT interactions to occur. A molecular model showing the orientation of 1-1 OHSQ molecules within the 90 ° herringbone polymorph is shown in Figure 3.4. The large surface area that is unoccupied within the 90 ° herringbone unit cell by squaraine molecules would appear to go against the trend of closest packing of 2D molecular adsorbates. We speculate that there are unimaged water molecules in these spaces that may stabilize the relatively open 90 ° herringbone unit cell structure through water-hydroxyl hydrogen bonding. Other than this speculative hydrogen bonding, donor-acceptor and Coulomb forces appear to be the major molecule-molecule interactions directing packing in the 90° herringbone polymorph of 1-1 OHSQ and, in combination, may compensate for the proposed sterically-induced loss in π conjugation that is caused by amino rotation out of plane.

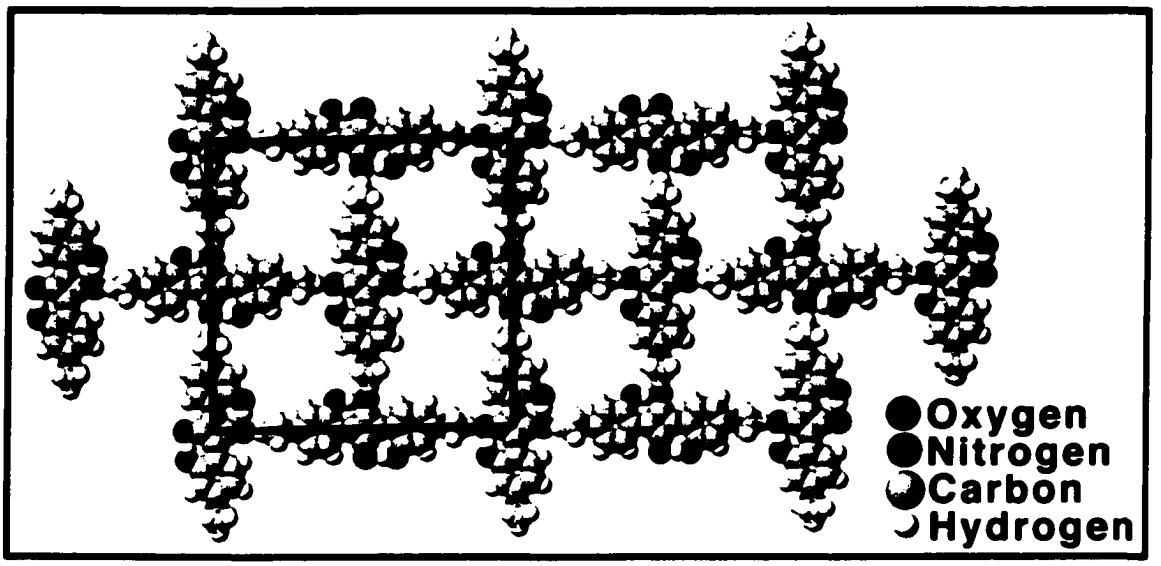

Figure 3.4: Molecular model proposed for the most stable of the three polymorphs exhibited by 1-1 OHSQ when adsorbed onto the HOPG surface from phenyloctane solution, "90° herringbone". This was the only polymorph of 1-1 OHSQ for which high enough resolution STM images were obtained to be able to construct a packing model. The unit cell is represented by a black box.

Additional work on the 1-1 OHSQ system involving deposition from a dichloromethane solution showed that another 2D polymorph exists.[60] Using this method, nucleation and growth events occurred outside of the STM environment. Thus, STM was performed ex-situ in this deposition case. Upon investigation, it was apparent that multiple layers of ordered molecules were formed even when relatively dilute μM solutions were used. Deposited 1-1 OHSQ layers appeared smooth except for step edges and missing molecule defects, which often revealed the presence of multiple layers (Figure 3.5A). At larger scan sizes the domain intersections are barely visible except where erosion has occurred between the domains. A few times small islands of molecules adsorbed on top of the smooth mono or multiple layers were imaged. These islands were 60 – 70 nm in length, 10 – 20 nm in width, and 2 – 3 nm in height. They tended to orient with their long axis at 30° or 60° angles to each another and along crystallographic directions, as can be seen in Figure 3.5B, where some oriented islands are parallel to a graphite step edge. At smaller scan sizes (<300 nm) molecular lamella were observed. Widths of the bright stripes were typically measured to be ~14 Å, a distance which corresponds to the length of the chromophore of the 1-1 OHSQ molecule. The lamellar domains often showed rectangular missing molecule defects. Some experiments, in which multiple layers of 1-1 OHSQ were adsorbed on the graphite surface, exhibited entire missing rows (see Figure 3.5C). These row defects were measured to be one or more layers deep.

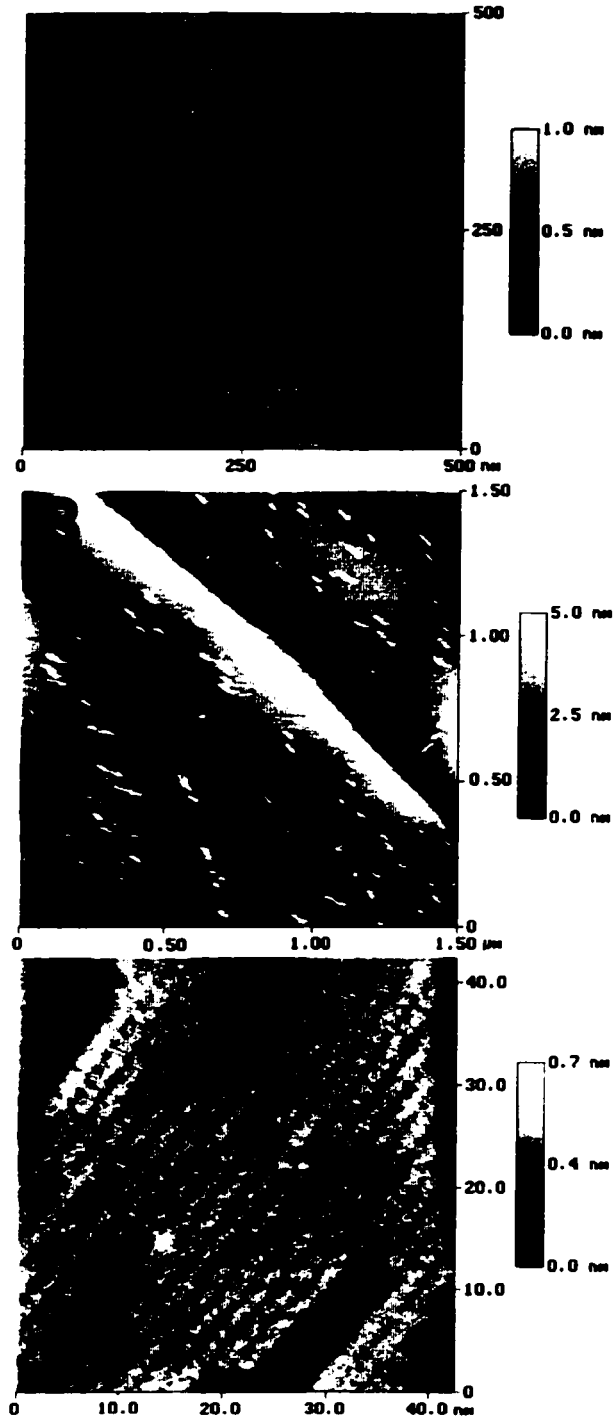

Figure 3.5: Three STM images showing the ordered adsorption of 1-1 OHSQ on HOPG deposited from CH_2Cl_2 solution. Images were taken under a film of phenyloctane. (A) 500 nm x 500 nm STM image showing smooth layers of adsorbed 1-1 OHSQ. Multiple layers are evident at defect sites. (B) 1.5 μm x 1.5 μm scan of 1-1 OHSQ monolayer with additional small islands adsorbed on HOPG. (C) Several missing rows are evident in this 42 nm x 42 nm STM image.

Figure 3.6 (right) shows a 15 nm × 15 nm image of the row structure observed for 1-1 OHSQ on HOPG deposited from dichloromethane solution. The chromophores of the molecules appear as football-like shapes measuring ~14 Å in length. The distance between chromophores within the same row was measured to be ~10 Å, while the distance between chromophores in adjacent rows was ~ 24 Å. The angle of the long axis of the molecule to the direction of the row was measured to be ~47°. Dialkylaminophenyl moieties in squaraines have an electron-donating character while the central four-membered ring has an electron-accepting character.[44] The 47° angle of molecule to the row aligns adjacent molecules within the same row such that their donor and acceptor moieties interact (see the molecular model proposed for this structure at the bottom of Figure 3.6). This structure is similar to the J-like structure observed for 1-1 OHSQ deposited onto HOPG from phenyloctane solutions. Occasionally a smearing of the electron density between two molecules adjacent to one another (in the same row) occurred producing a bright zig-zag pattern within the row (see the left image in Figure 3.6). The coupling of electron densities from two adjacent aminophenyl moieties (represented by the circled area in Figure 3.6) might contribute to this pattern. Unit cell values for both phenyloctane-deposited and dichloromethane-deposited 1-1 OHSQ are shown in Table 3.2.

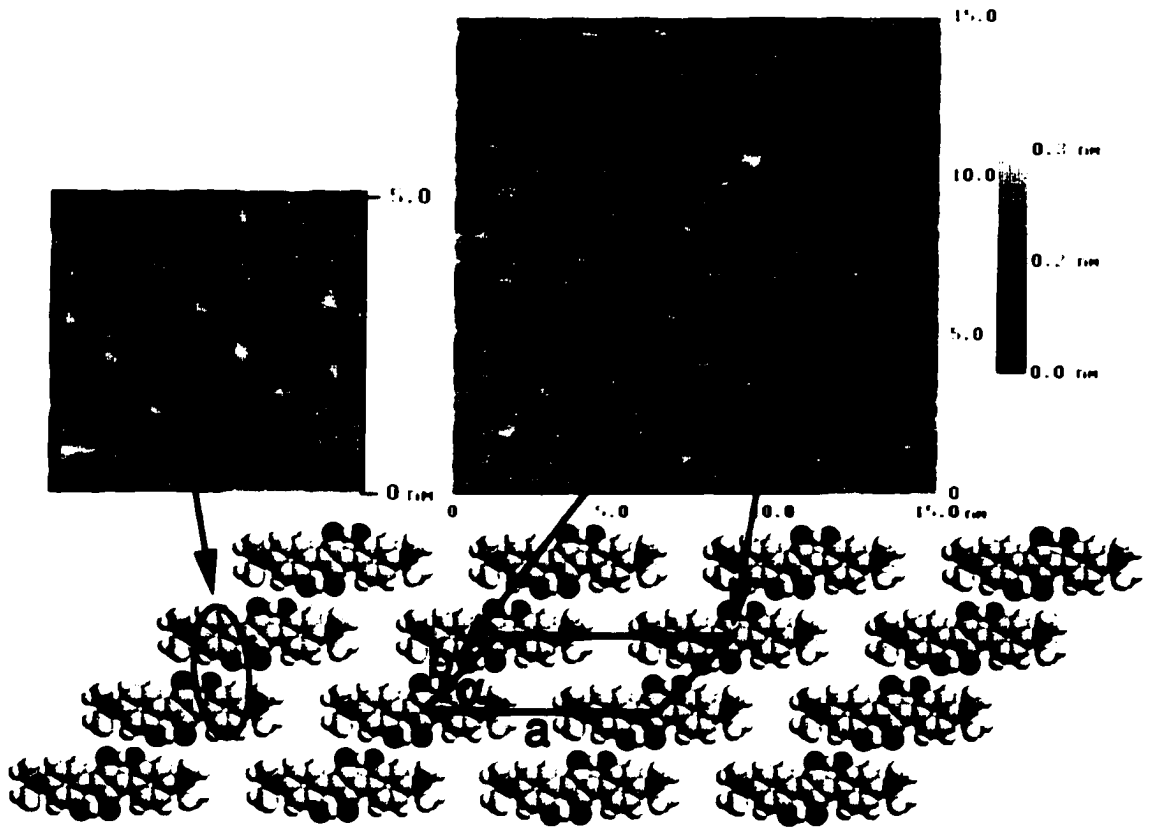

Figure 3.6: 15 nm x 15 nm scan showing the row orientation of 1-1 OHSQ on HOPG adsorbed from CH_2Cl_2 solution. Individual squaraine chromophores are visible as bright football-like shapes. The black box represents the unit cell, which has been enlarged and projected onto the proposed molecular model for comparison. Donor-acceptor interactions between adjacent molecules within the same row appear to be the dominant interaction driving this order. Yellow football shapes overlaid on the model represent coupling of electron density between adjacent molecules within the same row that might lead to the zig-zag structures which are sometimes observed (shown in the insert).

4-4 OHSQ

Molecularly-resolved 4-4 OHSQ adsorbate images were only slightly less difficult to acquire than for 1-1 OHSQ (in phenyloctane solution). Images showing ordered domains of 4-4 OHSQ obtained within the first half-hour of squaraine solution deposition were of poor quality. The adsorbed domains were easily stripped off of the graphite surface and the images were very noisy. Amidst the noise small patches of clearly resolved molecules were observed (~10 nm x 10 nm) in which a herringbone pattern of molecules consisting of bright football-shapes oriented at 90 ± 2 ° to one another could be distinguished. Upon Fourier filtering of these patches, the 90 ° angle was confirmed. It is doubtful that these clearly-resolved patches of molecules were simply domain nuclei that then grew and stabilized. Micron-sized islands composed of a number of smaller domains of ordered molecules with only very slight variations in orientation with respect to other domains were usually evident a few minutes after solution deposition. Zooming in on small areas of the surface to achieve molecular resolution usually resulted in noise that then obscured most of the molecules within the domain except for the aforementioned few clear patches. Furthermore, this small area of clarity within a noisy domain did not stay in one place. The noise became greater or lesser in different areas of the domain over time and thus exposed or obscured various parts of the domain at various times. Due to the excessive noise and poor quality of these images, they will not be presented. However, within minutes of the observance of the 90 ° herringbone phase, the adsorbate domains became clearer. Larger areas of the domains

(~100 nm x 100 nm) now showed molecular resolution, were less susceptible to desorption, and less noisy. Analysis of these more stable images showed that the angle between adjacent molecules within the herringbone pattern changed to 70 ± 3 ° (as seen in Figure 3.7). All further images of 4-4 OHSQ domains showed a 70 ° angle between adjacent molecules until the system became unable to be imaged (~5 hours). This behavior was reproducible from session to session.

Despite this reproducible increase in image clarity, only about one session in ten resolved the individual phenyl rings within each football shape. One imaging session revealed a patch of molecules during the transition from 90 ° to 70 ° that exhibited an 80 ° angle. Due to excessive noise in the images, the few images of this 80 ° phase are not shown here. Lack of clarity in the images also prevented us from obtaining unit cell measurements for this 80 ° phase. Unit cell measurements for the 90 ° and 70 ° herringbone phases, however, are listed in Table 3.2. A metastable 80 ° phase may be an intermediate phase in the 90 ° to 70 ° transition.

The three polymorphs observed for 4-4 OHSQ differ only in the angles between adjacent molecules. The 80 ° and 90 ° structures appeared only briefly at the onset of ordering, with 90 ° converting into 80 ° and 80 ° into the 70 °. The 70 ° polymorph was observed to be the most stable structure. In order for D-A or Coulomb interactions to occur, the nitrogen must be oriented close to the acceptor moiety. This necessitates that the nitrogen be "exposed" to an adjacent molecule. Thus the alkyl tails can either

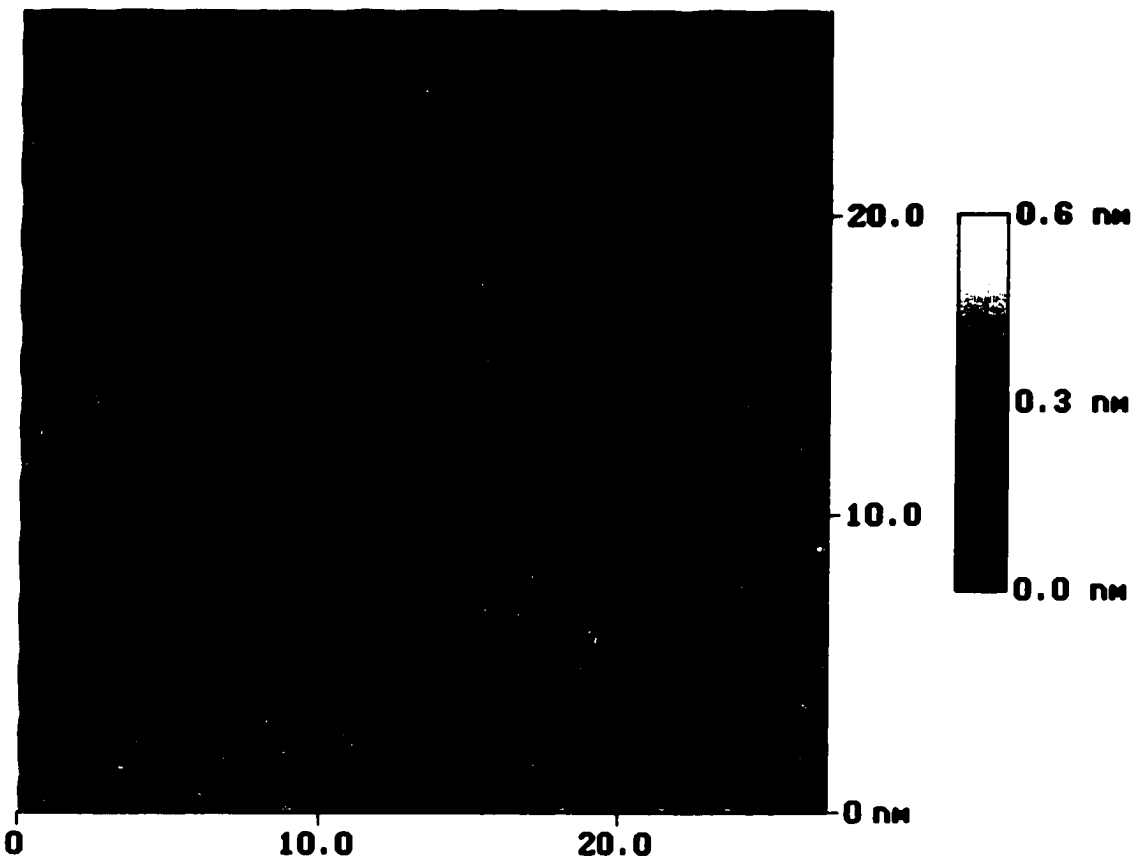

Figure 3.7: 27 nm x 27 nm STM image of the 70° angle herringbone phase of 4-4 OHSQ adsorbed on the HOPG surface. The 90° and 80° angle phase structures were too transient to obtain high quality images. In this image individual phenyl rings are visible within many of the bright squaraine chromophore "footballs".

lie on the graphite surface perpendicular to the long axis of the molecule as modeled in Figure 3.8A, or protrude from the surface into the solvent as modeled in Figure 3.8B. If the tails are oriented perpendicular to the molecule and on the graphite surface, then the optimum packing appears to be when the adsorbed molecules are oriented at 90 ° to one another. This minimizes the distance between nitrogen donor and acceptor, producing a stronger interaction. However, this 90 ° packing quickly transforms into an intermediate 80 ° structure that is too unstable for accurate unit cell measurements.

Our modeling shows that the rotation of molecules from 90 ° to each other to the 70 ° packing structure requires the alkyl tails to desorb from the surface and protrude up into the solvent. This process is sterically hindered if the tails remain on the surface while the molecules rotate from 90 ° to 70 °. The intermediate 80 ° phase may have only alkyl tails from one side of the molecule protruding into the solvent. Neither the 90 ° nor the 90 ° structures show any alignment with the major surface lattice vectors, so commensuration is not an explanation for the stability of one phase with respect to another (refer to Orientation with Respect to HOPG section). One explanation is that the 70 ° phase is more entropically favored due to more degrees of freedom from the freely rotating protruding alkyl tails. There may also be a slightly larger packing density for the 70 ° phase but the quantitative estimates are within the experimental error for both phases (Table 3.2).

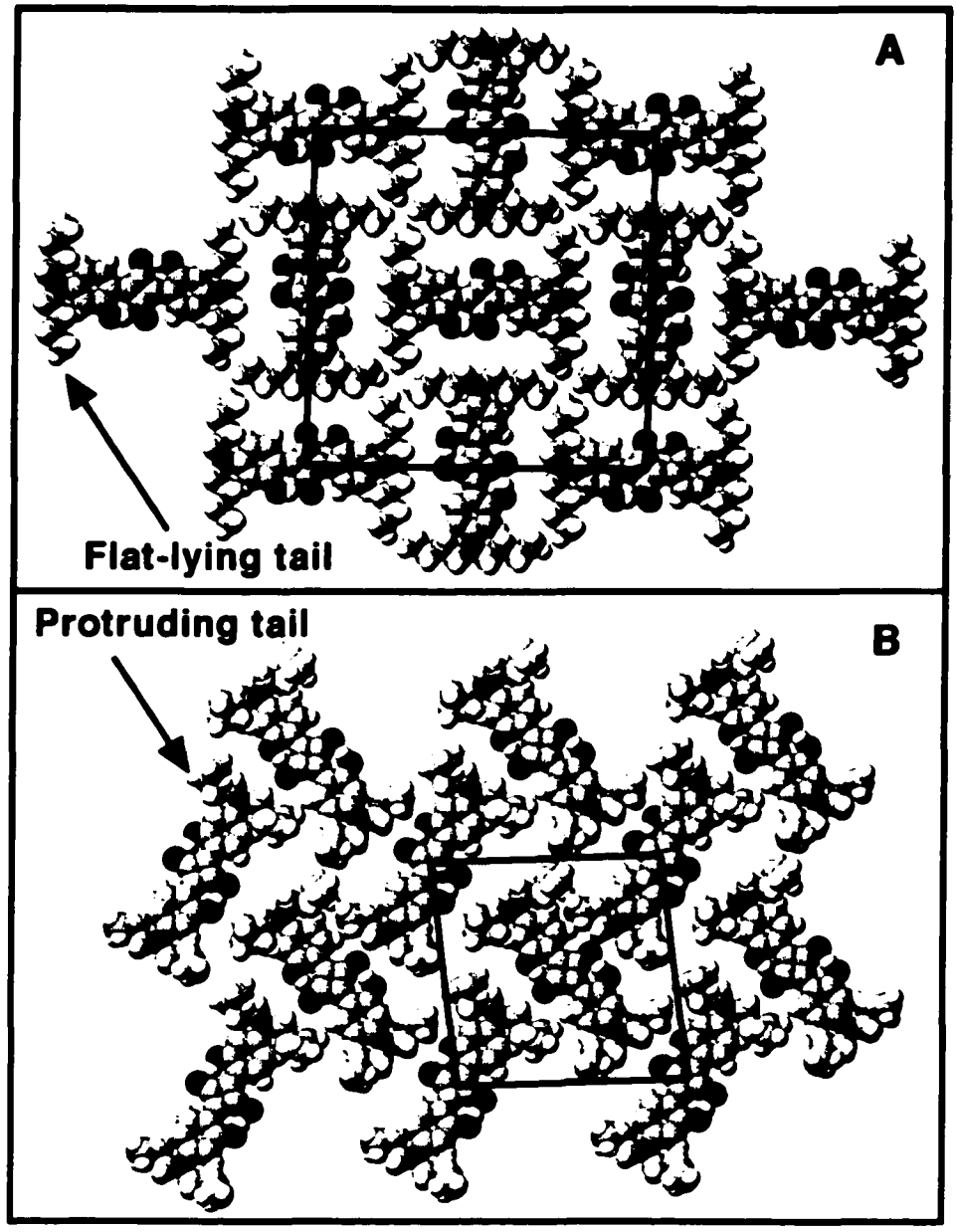

Figure 3.8: Molecular models of two of the three polymorphs exhibited by 4-4 OHSQ on HOPG. Model (A) shows the structure proposed for the initial 4-4 OHSQ polymorph with 90° herringbone packing. All 4 butyl tails of the adsorbed 4-4 OHSQ molecules must lie perpendicular to the long axis of the molecule if they are to lie on the HOPG surface. Model (B) shows the structure proposed for the final polymorph which exhibits a 70° herringbone packing. The butyl tails may still lie perpendicular to the long axis of the molecule, however they must partially desorb (some of the methylene units must protrude up from the surface) in order to adopt the 70°/110° angle of orientation to one another.

8-8 OHSQ

Unlike 1-1 OHSQ and 4-4 OHSQ, 8-8 OHSQ was found to form stable domains of adsorbed molecules that produced clear STM images. Almost immediately upon deposition of the 8-8 OHSQ solution onto the HOPG surface monolayer and sometimes multilayer coverage of ordered domains was observed in the STM images (see Figure 3.9). Unlike the 1-1 OHSQ and 4-4 OHSQ domains, which were of elliptical or square-like shape, domains of 8-8 OHSQ were diamond-like in shape with angular edges, or facets. They were typically about 100 nm in length and about 50 nm in width, and were composed of alternating bright and dark stripes, as can be seen in Figure 3.10A. Domains of ordered 8-8 OHSQ molecules were extremely stable and could be imaged continuously over the course of several days without much change in structure, except for the formation of multiple layers.

At small scan sizes molecular and sub-molecular features of 8-8 OHSQ adsorbate structures could be resolved. The bright stripes, measuring 15 ± 1.5 Å in total width, consisted of a column of bright football shapes stacked in a row. This width is consistent with the length of the squaraine chromophore (from the nitrogen at one end of the molecule to the nitrogen at the other end: 15 Å). About 50 % of the time a pair of bright spots within each football shape could be resolved, an example of which is shown in Figure 3.10B. These spots were assigned to the phenyl rings in the squaraine chromophore. No features could be distinguished within the dark stripes, however, which typically measured 11.0 ± 1.5 Å in width. This distance corresponds well with the length of an octyl tail (~10 Å). The heights measured by STM for the bright stripes relative to the dark stripes (0.8 to 1.5 Å) are relative heights typical for π

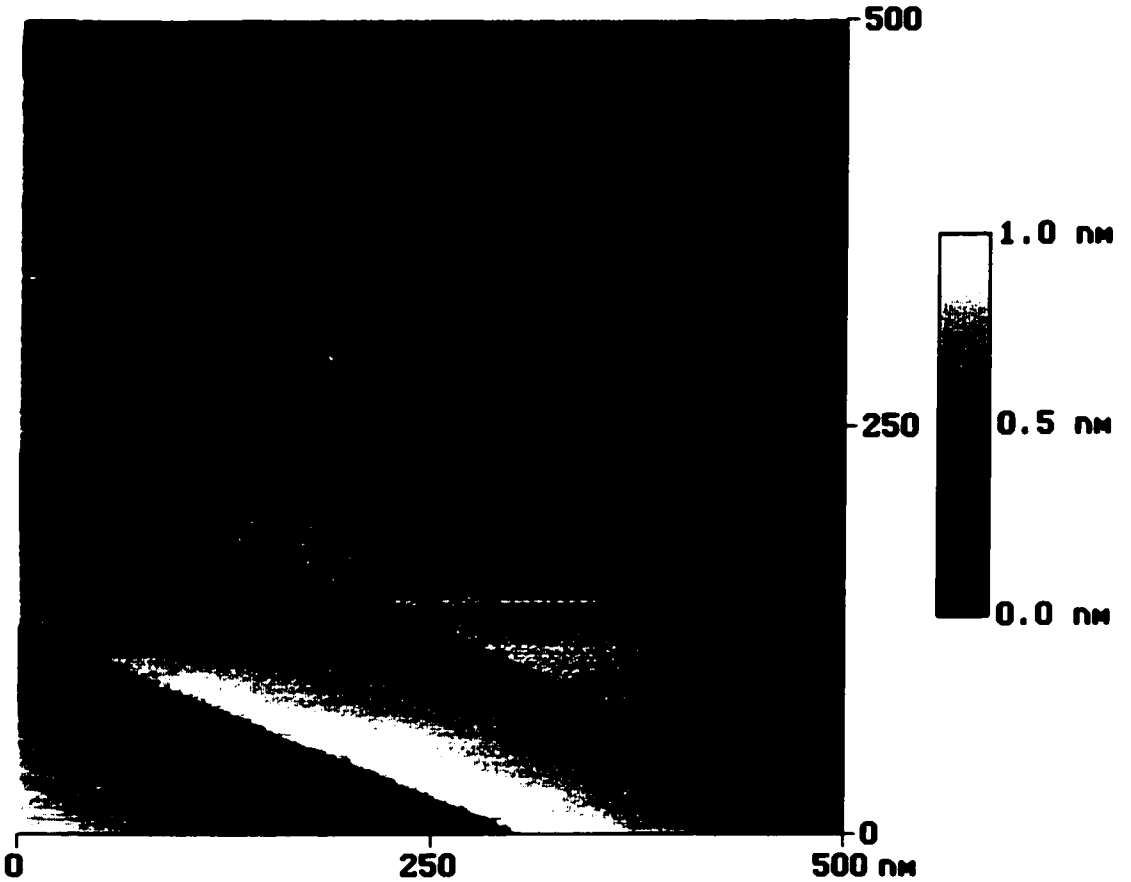

Figure 3.9: 500 nm x 500 nm scan showing multiple layers of adsorbed 8-8OHSQ molecules ordered on HOPG in numerous and relatively small domains of molecular rows.

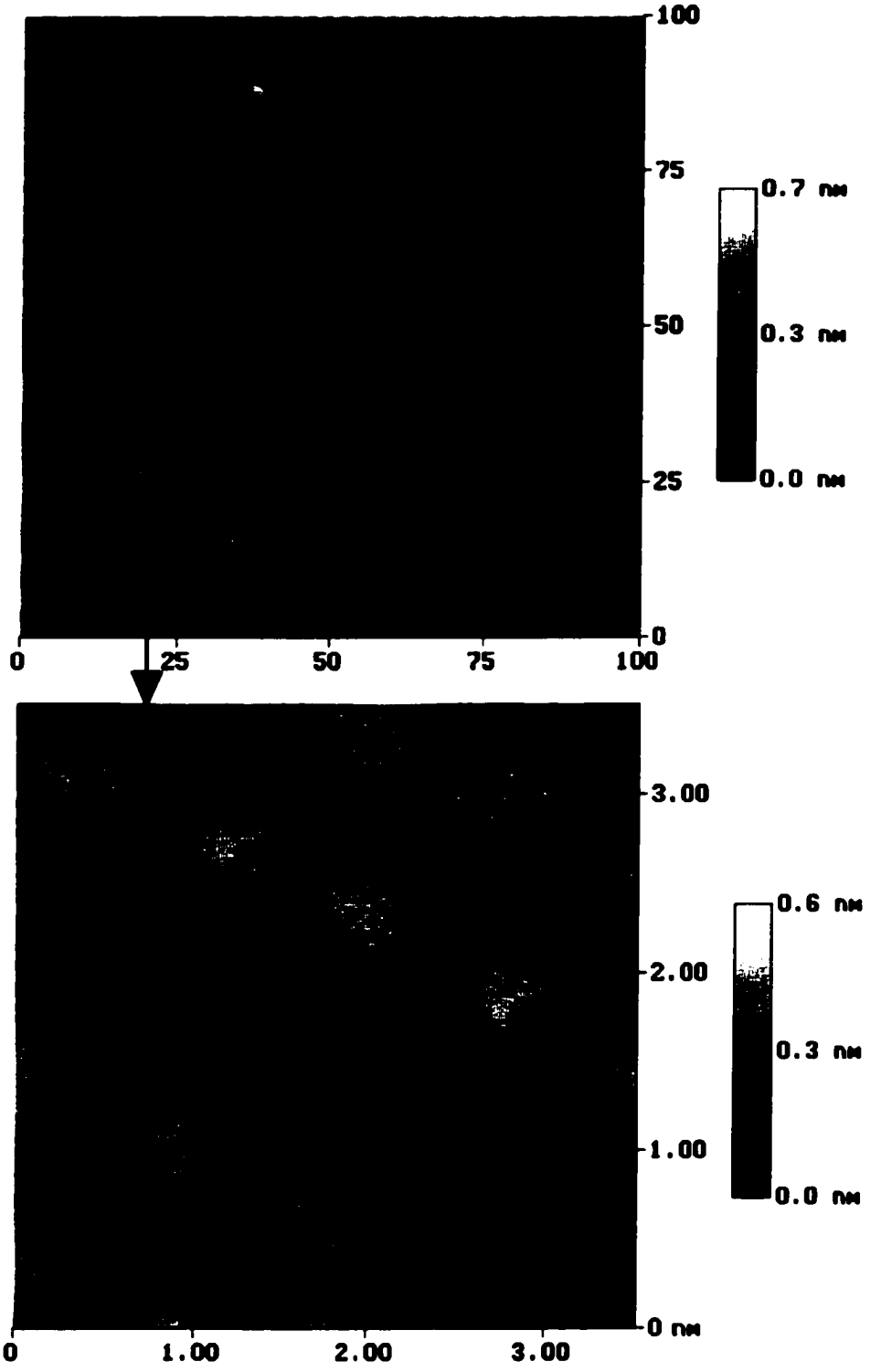

Figure 3.10: (A) 100 nm x 100 nm showing 5 domains of different orientations of 8-8 OHSQ rows. A zoomed-in portion of the top left domain is shown in (B). Individual molecules within the rows are clearly seen as a pair of spots, the spots being the phenyl rings.

systems adsorbed lying flat on the HOPG surface,[41] suggesting that the chromophore of the molecule is likewise lying flat on the HOPG surface. The distance between pairs of bright spots within the same stripe was measured to be 4 ± 1 Å. This relatively close spacing between adjacent squaraine chromophores within the same row requires that only one of the octyl tails of each dialkylamino group can lie flat on the HOPG surface. If both tails lie on the surface a minimum distance of 12 Å between adjacent chromophores within the same row would be needed so that alkyl tails from adjacent molecules would not sterically interfere with each other. This row structure, in which the chromophores of the molecules are widely spaced, is not observed and furthermore would be very unfavorable since there is a well known strong interaction between adjacent chromophores that is not present in this structure. Instead, one tail from each dialkylamino might protrude up from the surface and be solvated by the phenyloctane solvent or it may form a second ordered alkyl layer. Evidence of this kind of three-dimensional adsorbate structure has been reported by Gorman et al in their study of the ordered adsorption of the didecylamino molecule DAPDA.[61] Recognizing the similarity in structure between the DAPDA and the alkyl portions of the squaraine molecules, it is tempting to assign the same molecular conformation to the second tail in both 8-8 OHSQ and DAPDA, since the non-planar functional group is the same for both molecules except for the length of the alkyl tails. For squaraines, however, it appears that protruding alkyl groups are only possible in monolayers or in the case of the topmost ordered layer. When multilayers of squaraine molecules are imaged the relative height of the edge of each layer is 2.5 ± 0.5 Å. Although STM does not measure actual heights, the small magnitude of this

distance (still very close to the typical 1-2 Å relative height measured via STM for planar aromatic molecules lying flat on the HOPG surface) makes it very doubtful that alkyl tails of molecules that are not in the topmost molecular layer should be protruding perpendicularly. In sandwiched layers the remaining two alkyl tails must lie either on top of the planar tail or on top of the chromophore. Remaining alkyl tails lying coplanar with the molecular plane (lying on the HOPG surface if in the first molecular layer) most likely interdigitate such that tails from molecules in adjacent rows lie side by side. Thus, in addition to the molecule-substrate interactions between adsorbed alkyl tails and the HOPG lattice, a new intermolecular interaction is introduced by the formation of rows of molecules: dispersion forces between intercalated alkyl tails.

By measuring the angle between the direction of the bright stripe and the long axis of the bright football shapes within the stripe, it was found that the 8-8 OHSQ molecules within a row are found to orient 68 ± 3 ° to the direction of the row. This angle results in an offset between adjacent molecules of ~ 2.5 ± 0.5 Å, allowing alignment of their respective donor and acceptor moieties. The proposed model of this molecular packing is shown in Figure 3.11. This structure is very similar to the "slipped-stack variant structure" proposed by Law et al for 1-1 OHSQ (non-hydroxylated) solution aggregates.[62] Hence the D-A interaction between adsorbate molecules is preserved in the row structure despite the introduction of dispersion interactions between akyl tails with other alkyl tails and the substrate. A third intermolecular interaction is possible between molecules in a row that are offset by 2.5 Å. This offset combined with the 4 Å distance between adjacent phenyls puts one of

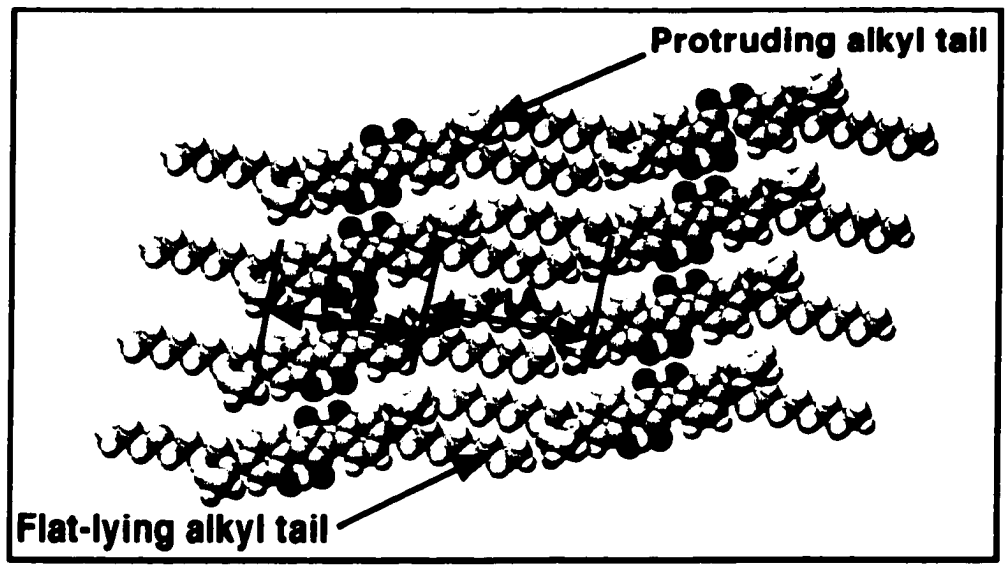

Figure 3.11: Molecular model showing the proposed row packing structure of a monolayer or topmost adsorbed layer of 8-8 OHSQ on HOPG. One tail from each dialkylamino group lies coplanar with the chromophore on the HOPG surface while the other tail protrudes up from the surface into the phenyloctane solvent. Molecular layers of 8-8 OHSQ which are sandwiched between a bottom and topmost layer most likely do not have this structure since the protruding tails would be sterically hindered by the presence of the layer above. Instead these tails may lie atop either the coplanar tails or the chromophore.

the oxygens of the square core within 2 Å of a hydroxyl hydrogen of the neighboring squaraine within the same row. Hence hydrogen bonding may be possible between adjacent squaraines. Whether it is a driving force for the formation of the row structure is uncertain without studying analogous molecules without hydroxyl groups.

12-12 OHSQ

Like 8-8 OHSQ, 12-12 OHSQ molecules adsorb in row structures and order in layers of oriented domains within minutes of solution deposition onto the graphite surface, as can be seen in Figure 3.12A. Unlike 8-8 OHSQ, two different types of 12-12 OHSQ domains were observed defined by their differing stripe widths. Bright stripes in the first domain type were measured to be 14.0 ± 2 Å in width and dark stripes 13 ± 2 Å, whereas in the second domain type bright stripes were measured to be 18 ± 2 Å and dark 11 ± 2 Å. In addition, the second type appeared to be composed of two football shapes across its width (see Figure 3.12B), which when zoomed in upon at scan sizes of ~10 nm x 10 nm often revealed a set of three or four spots (see Figure 3.12C). Again, no features could be distinguished within the dark stripes for either polymorph. With the exception of the widths of the bright and dark stripes and the unit cells, all other parameters measured for the two polymorphs were the same (see Table 3.3). The angle of the long axis of the football shapes to the direction of the row was measured to be 60 ± 5°, while the distance between football shapes within the same row along the length of the row was 4 ± 1 Å for both polymorphs. The height of bright stripes relative to dark was measured to be in the range of 0.8 to 2 Å. In addition, both polymorphs exhibited domains of similar sizes and shapes,

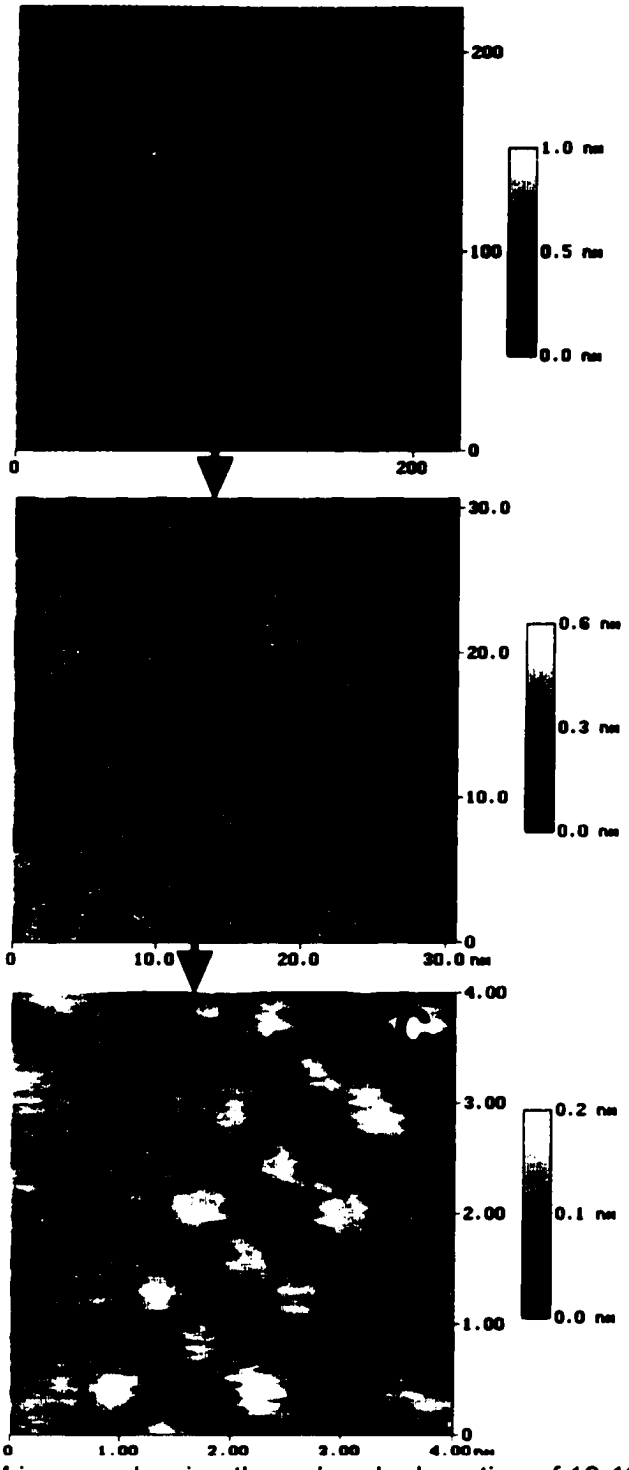

Figure 3.12: Three STM images showing the ordered adsorption of 12-12 OHSQ on HOPG. Each image is a zoomed-in portion of the image above it. Image (B) is a 32 nm x 32 nm scan that appears to show bimolecular rows, the width of each row consisting of 2-3 bright spots which altogether measure 18 ± 2 Å in width. Image (C) is a 4 nm x 4 nm scan that shows one of the rows of 3 bright spots.

ranging from small, diamond like shapes of tens of nm in length and width, to larger less well defined shapes of ~100 nm in length and width. Layers of 12-12 OHSQ containing both polymorphs of domains were found to be stable, generally free of noise, and capable of being imaged continuously over the course of several days.

The widths of the stripes in polymorph type (1) are easily explained based upon the model of the row structure adopted by 8-8 OHSQ when adsorbed on the graphite surface. The bright rows of 14 ± 2 Å width and dark rows of 13 ± 2 Å are consistent with the length of the squaraine chromophore at a 60 ° angle to the row (~12 Å), and with the length of the dodecyl tail (~14 Å). These measurements, as well as that of the 0.8-2 Å relative height, suggest that, like 8-8 OHSQ, molecules of 12-12 OHSQ in the type (1) phase adopt a conformation on the surface in which the chromophore of the molecule and one dodecyl tail from each dialkylamino moiety lies flat on the HOPG surface. The 60 ° angle between the long axis of the chromophore and the direction of the row results in an offset between adjacent molecules within the same row such that donor and acceptor moieties of adjacent molecules are aligned. This is analogous to the structure proposed for 8-8 OHSQ in which molecules align flat on the graphite surface in a J-like aggregate formation with one tail from each dialkylamino group lying on the graphite interdigitated with the tails from the adjacent row. Despite the addition of 16 methylene units in the transition from 8-8 OHSQ to 12-12 OHSQ, the adsorbate structure observed is essentially the same for both and

donor-acceptor interactions still appear to play a significant role. Figure 3.13A shows the proposed molecular model for 12-12 OHSQ single layer packing.

Polymorph (2) of 12-12 OHSQ does not follow this model. For this molecule the width of bright stripes (18 ± 2 Å) is longer than the chromophore length from nitrogen to nitrogen (15 Å). Since the alkyl tails do not contribute significantly to the tunneling current measured by STM for adsorbed squaraines, we find it plausible to attribute this increase in bright row width to multilayer imaging in which rows of molecules from two adjacent molecular layers are slightly offset from one another (~4 Å) but are not resolved by the STM. We call these proposed structures bimolecular rows. A small number of STM images were obtained which show a gradation in contrast across the width of the bright rows. The brightest portion of the width was measured to be ~14 Å wide and ~0.8 Å in relative height, as compared to the rest of the bright row, which measured 4 Å in width and ~0.5 Å in relative height. These measurements provide evidence for a multiple layer structure. These images, however, will not be presented here. Figure 3.13B shows a structure incorporating two molecular layers, both of Figure 3.13A type packing. In this structure molecules in the second layer are parallel to, but offset from, molecules in the first layer such that two separate interlayer D-A interactions are possible between each pair of molecules (one originating from the first layer and one from the second). A pair is now defined as a molecule in the first layer and the molecule in the second layer directly above it. The second layer molecule overlaps with the molecule below such that its acceptor group and one of its donor groups overlap with one

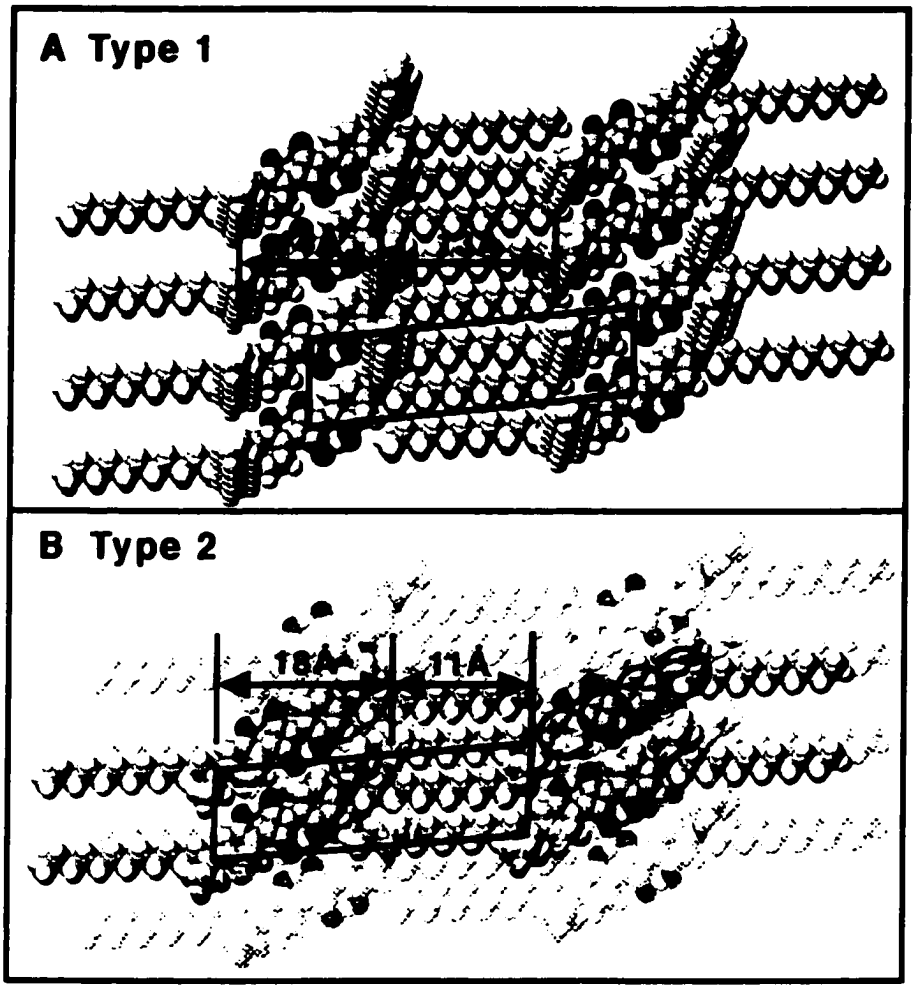

Figure 3.13: Molecular models of the proposed packing of 12-12 OHSQ on HOPG corresponding to the two types of rows observed. Model (A) shows 2 adjacent molecular rows within the same molecular layer. This structure corresponds to a bright row width of 14 Å and a dark of 13 Å (Type 1). Model (B) shows a second molecular layer (highlighted) adsorbed on the first (shadowed) which corresponds to a bright row width of 18 Å and a dark of 11 Å. The molecules in the second layer are commensurate with but offset from the positions of the molecules in the first such that the donors and acceptors within the two layers may align. If the STM tip does not distinguish between molecules in the two layers, then the bright rows may appear wider than a Type 1 bright row and the dark rows narrower. This is assuming that the chromophores alone (regardless of proximity to the tip) contribute to bright contrast and a lack of chromophore produces a dark region. The circles indicate positions of phenyl groups in both layers that may be contributing to the increased tunneling current of a bright row. Red circles correspond to the position of a phenyl group in the second (top) layer and blue to phenyl groups in the first (bottom) layer.

of the donors and the acceptor group of the molecule in the layer beneath. Due to the 4 Å offset, a 4 Å portion of the alkyl tail (or dark row) of the first layer is eclipsed by the bright chromophore of the second layer molecule. This may explain the reduction in the width of the dark rows to 11 ± 2 Å and the increase in width of the bright rows to 18 ± 2 Å, both within experimental error of the expected widths of 16 Å and 9 Å respectively.

2-18 OHSQ

2-18 OHSQ is the only squaraine represented within the series presented here that has different alkyl tail lengths within the same molecule. In addition, it has the longest alkyl tail of any squaraine within the series, its stearyl tails being six methylene units longer than a dodecyl tail, yet its ethyl tails are only one methylene unit longer than the shortest tail in the series (methyl). This difference resulted in some special characteristics of the adsorption and ordering of 2-18 OHSQ onto the HOPG surface when compared to the other squaraines. Upon deposition of 2-18 OHSQ/phenyloctane solution onto the graphite surface, ordered domains of 2-18 OHSQ were imaged almost immediately, however, almost always as isolated domains which then grew together over time and eventually formed multiple layers (see Figures 3.2A and B). The only other squaraine that was observed at submonolayer coverages was 1-1 OHSQ, although, unlike 1-1 OHSQ, adsorbed domains of 2-18 OHSQ were free of noise and easily imaged. Although domains of ordered 2-18 OHSQ consisted of alternating bright and dark stripes (as in and 8-8 OHSQ and 12-12 OHSQ), rather than being diamondlike and angular (as in 8-8 OHSQ and 12-12 OHSQ),

domains of 2-18 OHSQ instead were meandering and irregularly shaped compared to those of 12-12 OHSQ and 8-8 OHSQ. Bright stripes of adsorbed 2-18 OHSQ were often found to bend around corners and merge with other bright stripes (see Figure 3.13A). In addition, upon inspection of hundreds of 2-18 OHSQ domains, it was discovered that 2-18 OHSQ produces a wide variety of bright and dark stripe widths as listed in Table 3.3 and shown by their frequencies of observation in Figure 3.14. All the rows showed a 60° angle between the molecules within the row to the direction of the row. All bright stripes were measured to have vertical heights of 1 to 2 Å relative to the dark stripes.

The lower symmetry of the 2-18 OHSQ molecule allows for a different structural conformation than the other long-tailed squaraines that form row structures. The small size of the ethyl tails, on either side of the 2-18 OHSQ molecule, allows for the ethyls to lie coplanar with the chromophore and the stearyl tails. This is not possible for the more symmetrical long-double-tailed squaraines because, as described in the section on 8-8 OHSQ, the coplanarity of the tails would preclude the formation of the observed close-packed structure. This structure, in which all four of the alkyl tails lie flat within the same plane, alters the degree of interdigitation that is possible between the stearyl tails of molecules in adjacent rows. Because the ethyl tails are occupying space within the plane of the stearyl tails, stearyls from molecules in the adjacent row cannot interdigitate to the degree that is seen in 8-8 OHSQ and 12-12 OHSQ row structures. As a result the width of the portion of the alkyl tail rows appears larger than the actual length of the tails (see Observed Dark Row Width and Expected Dark Row Width measurements for

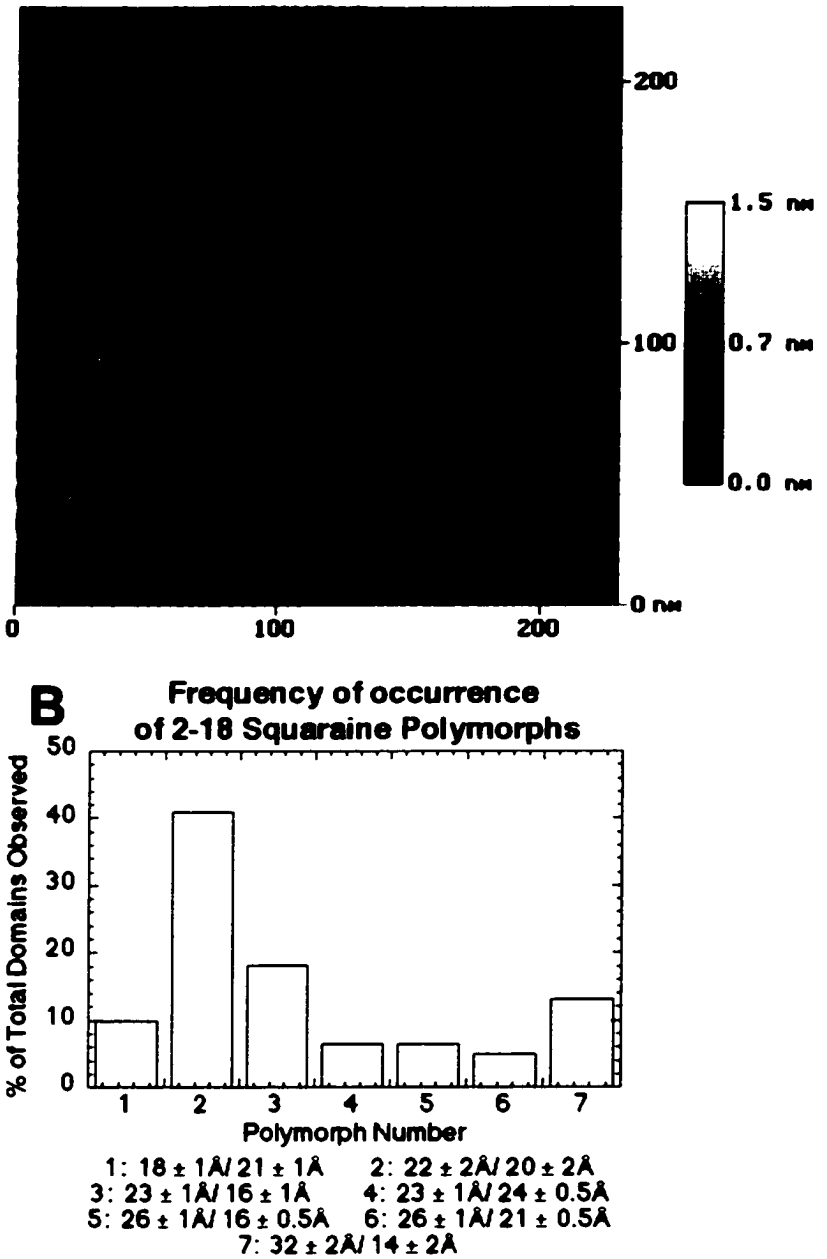

Figure 3.14: (A) 225 nm × 225 nm image showing several domains of ordered 2-18 OHSQ molecules in which various widths of bright and dark rows are exhibited. Each combination of bright and dark row width represents a different polymorph. Numbers overlaid on the domains correspond to the polymorph of that number. Polymorphs 2 and 6 show a degree of flexibility in which rows are able to bend around each other. Arrows point out smooth transformations from one structural phase to another. (B) Histogram showing the frequency of observation of the 7 different polymorphs of 2-18 OHSQ ordered adsorbate structure.

2-18 OHSQ in Table 3.3). Dark row widths of 8-8 OHSQ and 12-12 OHSQ, however, were roughly equal to the lengths of the octyl and dodecyl tails, respectively. A model representing a single layer row structure for 2-18 OHSQ was produced based on: (1) the measured angle of the long axis of squaraine chromophore to the direction of their molecular rows, (2) the measured distance between adjacent molecules within the same row, (3) the length of the chromophore, and (4) the assumption that all 4 alkyl tails are interdigitated and coplanar on the HOPG surface. This particular model structure would produce a bright row width of approximately 12 Å and a dark row width of approximately 29 Å. A model of this single layer packing is shown in the top (highlighted) layer of Figure 3.15B. However, a polymorph fitting these measurements was not observed. In fact, none of the polymorphs observed exhibited bright row widths of less than 17 Å. Again, like 12-12 OHSQ, the observation of bright row widths larger than 12 Å suggests that additional molecular layers are formed but are not molecularly resolved by the STM. Since all seven of the 2-18 OHSQ polymorphs observed exhibited bright row widths of larger than 12 Å, we assume that they are all composed of multiple layers of 2-18 OHSQ molecules with various orientations of adjacent layers. It is not clear why a single-layer 2-18 OHSQ structure was never observed. Solutions of relatively dilute concentration were used to try to prevent multiple layer adsorption, but with no success. Either multiple layer adsorption was observed or no adsorption was observed. The coplanarity of the ethyl tails with the chromophore and the stearyl tails may allow 2-18 OHSQ chromophores in adjacent layers to come closer to one another, making interlayer D-A interactions and thus multilayering more favorable than with more symmetrical long tailed squaraines. For example, one dodecyl tail from each side of 12-

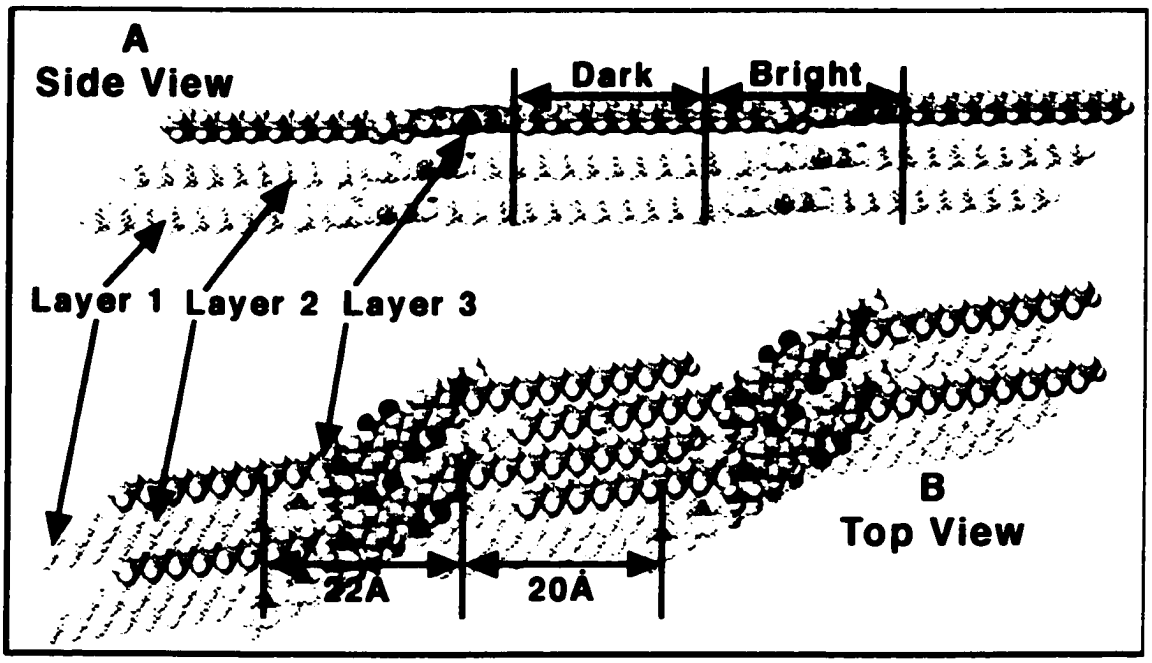

Figure 3.15: Molecular model representing a possible structure for the most commonly observed row structure polymorph of 2-18 OHSQ adsorbed on HOPG. This polymorph (#2 from Table 3.3) exhibits bright rows of 23 Å width and dark rows of 20 Å width. A possible structure corresponding to these measurements consists of three separate layers of 2-18 OHSQ ordered in rows in which each layer is commensurate with the layer below, but is offset by approximately 4 Å such that donor and acceptor moieties between the two layers may align. The bright rows correspond to the total width of the three layers of overlapping chromophores whereas the dark rows correspond to areas lacking in chromophore (areas of only alkyl tails). Other polymorphs exhibited by 2-18 OHSQ may be variations of this model in which multilayer structures are formed, but the distances between molecules in adjacent rows are either greater or lesser (alkyl tails are interdigitated to varying degrees) or the number of layers producing the polymorph is different, thus producing different bright and dark row widths as observed by STM.

12 OHSQ must lie between molecular layers since it cannot adopt a coplanar conformation. The presence of these tails may prevent molecules from getting as close to one another as is optimum for multilayering. Thus it may be that the lower symmetry of the 2-18 OHSQ molecule promotes multilayering more so than the symmetrical squaraines.

Due to the large number of polymorphs exhibited by 2-18 OHSQ and the difficulty in resolving individual molecules within molecular rows (making unambiguous assignment of structure difficult) only the major polymorph of 2-18 OHSQ will be discussed in detail. The #2 polymorph is the most frequently observed 2-18 OHSQ polymorph and exhibits a bright row width of 22 ± 2 Å and a dark row width of 20 ± 2 Å. Figure 3.15(A and B) shows a molecular model that may explain the measurements. Using the packing arrangement of the single layer structure mentioned above (which was not observed by itself) three molecular layers of this packing are adsorbed atop one another such that the second layer is parallel to but offset from the first by 4 Å and the third is parallel but offset from the second by 4 Å. This trilayer structure is analogous to the type (2) structure proposed for 12-12 OHSQ in which two donor-acceptor interactions are present between every pair of molecules, however the addition of a third layer introduces a second pair to the structure. Pair 1 is the molecule from the second layer and the molecule in the first that it is overlapping and Pair 2 is the molecule in the third layer and the molecule in the second layer of the first pair that it is overlapping. Of course, dispersion interactions between tails lying atop one another in adjacent layers are also possible. The eclipsing of a total of 8 Å of the tail length by the chromophores of the second and third layers produces a dark row of 21 Å in width

instead of the 29 Å full width. The extension in length of the chromophore by 8-9 Å produces a bright row of 21 Å width instead of the 12 Å width of the single layer structure. The observed bright and dark row widths are within experimental error to the expected row widths for this molecular model (22 ± 2 Å for bright row and 20 ± 2 Å for dark row).

The remaining six of the observed polymorphs of 2-18 OHSQ also appear to be multilayer structures. Variation in degrees of overlap between chromophores of molecules in adjacent layers may be one of the factors producing the different observed row widths. This overlap variation may also allow different interlayer interactions to occur than the donor-acceptor interaction that appears to drive the #2 polymorph. For example, an offset of ~7.5 Å between adjacent layer chromophores allows a slightly different donor-acceptor interaction to occur in which the electron-donating amino group of one of the chromophores in the pair and the electron accepting central ring of the second chromophore overlap one another. A dipole-dipole interaction may be introduced with an offset of ~12 Å, which allows the C-N bond linking the amino nitrogen and the phenyl of one molecule of a pair to overlap the same bond in the second molecule of the pair. The C-N bonds overlap each other such that the positively-polarized N of one molecule overlaps the negatively polarized C of the other molecule and vice versa.

As mentioned in the very beginning of the "Results and Discussion" section, 2-18 OHSQ adsorbed from 8CB maintained the same packing structures and unit cell dimensions as 2-18 OHSQ adsorbed from phenyloctane (this work was performed by D.L. Sampson). The major difference between the two systems is the number and size

of squaraine domains and the occurrence of diamond and triangle-shaped defects within squaraine rows (see Figure 3.16A). Both these effects can be understood when the large excess of 8CB in the binary system is considered. Although the beginnings of nucleation of squaraine domains from the 8CB melt were never directly observed with STM (the 2-18 OHSQ nucleation timescale from the 8CB melt being must faster than the timescale of imaging), it can be assumed that initially the surface is occupied by 8CB due to its great excess. 2-18 OHSQ molecules must then adsorb into 8CB voids or displace 8CB molecules (most likely two at a time). Having reached a critical diameter, 2-18 OHSQ nuclei grow and spread across the HOPG surface, replacing the adsorbed 8CB. This competitive growth process may account for the numerous small domains arising from 2-18 OHSQ adsorption from 8CB. 8CB can become trapped within the 2-18 OHSQ monolayer, causing a disruption of the local squaraine packing, and thus a defect. A single 8CB molecule trapped within a row of squaraine molecules may be the cause of the triangle-shaped defects observed. A diamond-shaped defect may be the effect of two correlated triangle defects arising from the presence of two 8CB molecules trapped directly across from each other in adjacent rows, as is illustrated in Figure 3.16B. It has been observed that when a molecule is missing from an interdigitated row structure the molecule across from it is destabilized and often leaves the row as well [63]. These two squaraine vacancies can be easily filled by 8CB molecules, resulting in a diamond-shaped defect.

Another type of defect that was observed regularly when 2-18 OHSQ was adsorbed from an 8CB melt can be seen in Figure 3.17. An isolated row within a domain whose chromophores are aligned in the opposite direction to the chromophores

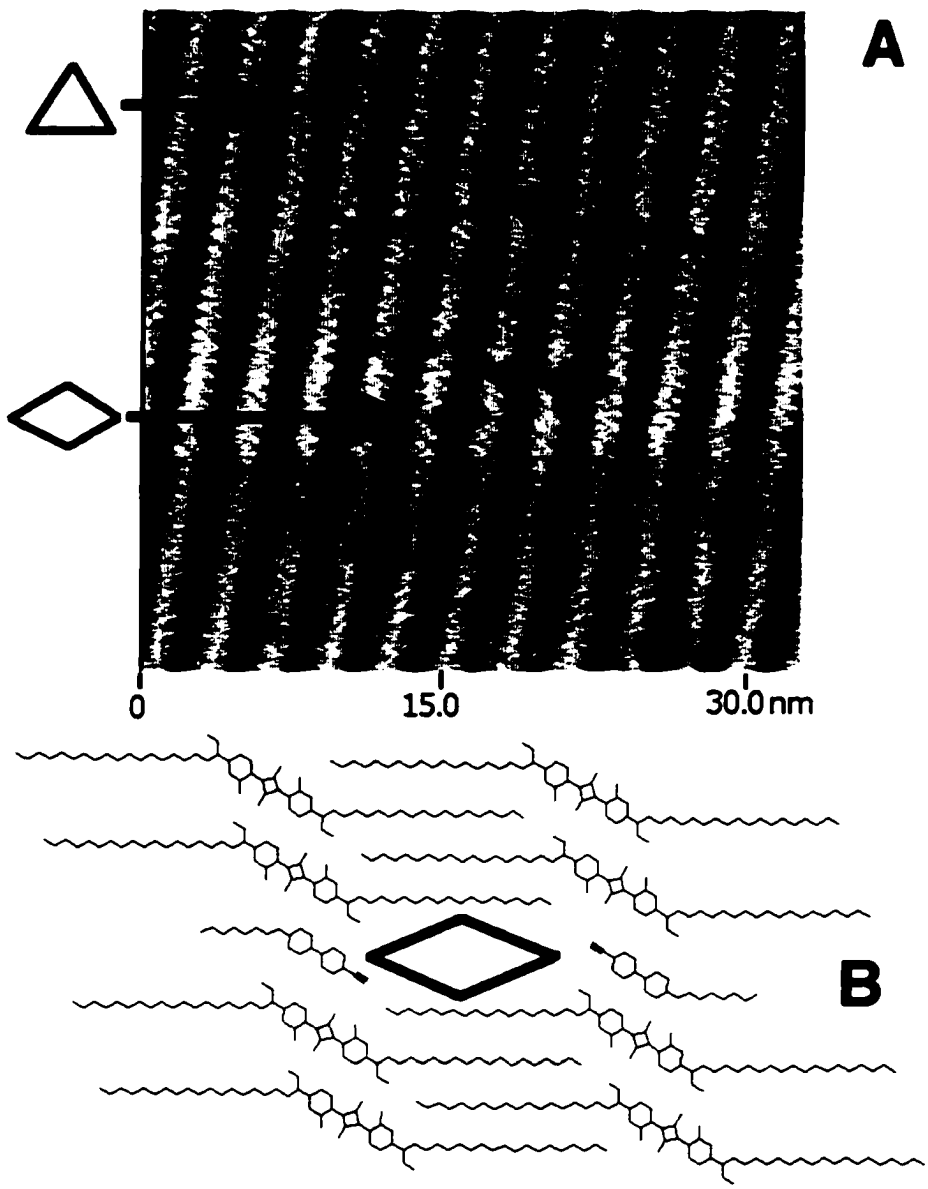

Figure 3.16: Ordered adsorption of 2-18 OHSQ on HOPG from a solution of 99% wt/wt 8CB. (A) 35 nm x 35 nm STM image of a typical domain showing numerous diamond and triangle defects. We propose that triangle defects are caused by single 8CB molecules trapped within the row structure of 2-18 OHSQ, whereas diamond defects are a pair of 8CB molecules trapped in adjacent squaraine rows. (B) Simple model showing how a pair of correlated triangle defects may form a diamond defect. A single layer 2-18 OHSQ row structure is used for the sake of simplicity.

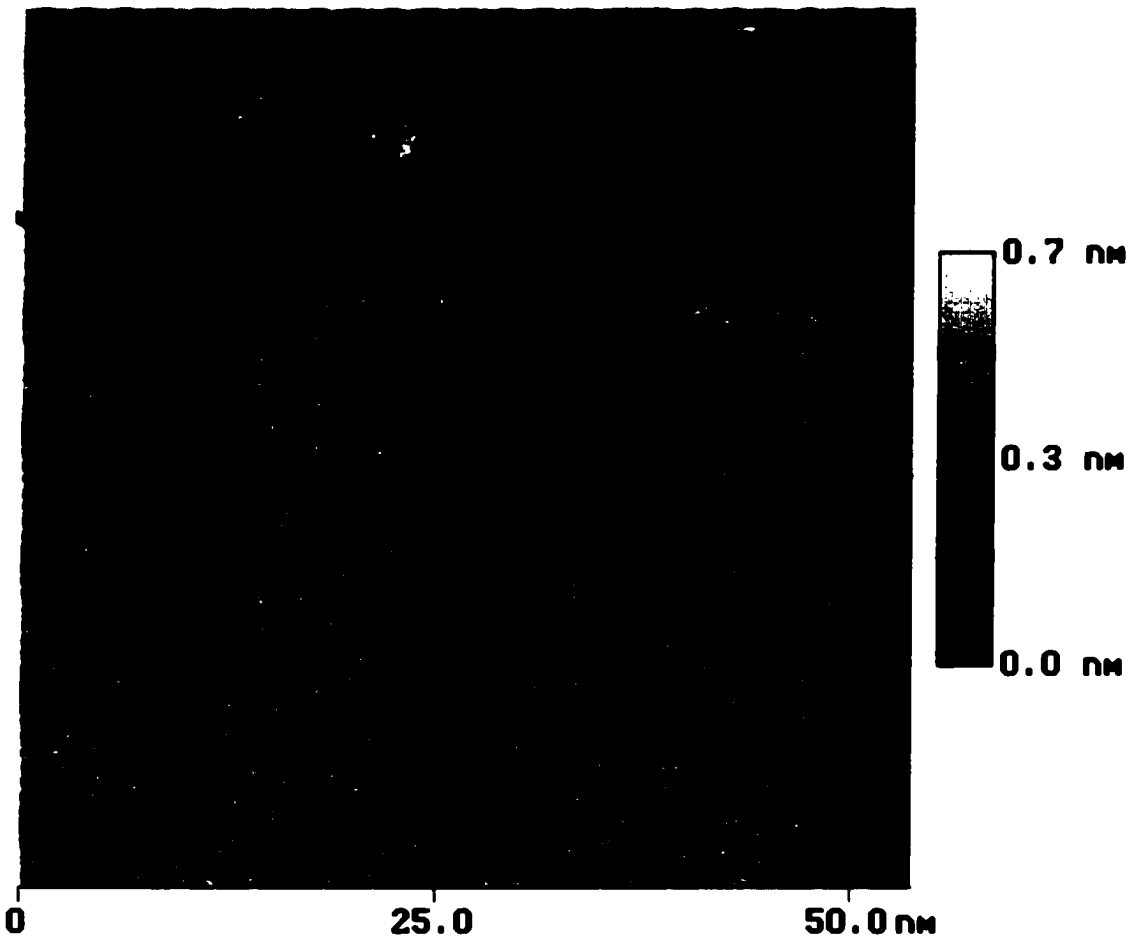

Figure 3.17: 54 nm x 54 nm STM image showing another type of defect commonly observed in images of 2-18 OHSQ adsorbed from 8CB melt: the arrow points out 2 rows within a domain whose chromophores are oriented in the opposite direction to the chromophores in adjacent rows.

in all the other rows within that domain can be seen in the figure. Such defects were also observed in layers adsorbed from squaraine/phenyloctane solution, however, less often than from squaraine/8CB melts. A molecular model for this opposite chromophore direction will be proposed in the next chapter.

Multilayers

Multiple layers of squaraine adsorption and ordering were observed consistently for every squaraine system studied except 4-4 OHSQ, as can be seen in Table 3.3. Figure 3.18A shows an image obtained from a 8-8/12-12 (10/1) OHSQ mixture where four layers of ordered molecules grown one on top of another can be seen. These multiple layers usually occurred when concentrations of squaraine in phenyloctane greater that 1.0×10^{-6} M were used. About 70 % of the overlayer domains coincided with the domain direction of the molecules directly beneath them. The remaining overlayer domains, not in registry with the domain just beneath, tended to be oriented at a 60 ° angle to the lower domain. Criss-crossing of rows in adjacent layers occurred often forming a cross-hatch pattern as can be seen in Figure 3.18B. This figure also provides a method to distinguish between a squaraine layer that is adsorbed atop a graphite terrace and squaraine multiple layering. In STM images, squaraines that are adsorbed atop a graphite terrace always show a stripe of what we think are non-ordered molecules along the edge of the graphite step, as can be clearly seen in Figure 3.18B. The relative height measured between the adsorbate and the terrace below is always within experimental error of the sum of the height of the molecular layer and a multiple of the interplane distance of graphite (~3.4 Å). As can be seen in Figure 3.18A, squaraine layers show an abrupt end to the stripes of the domains that lie at the step

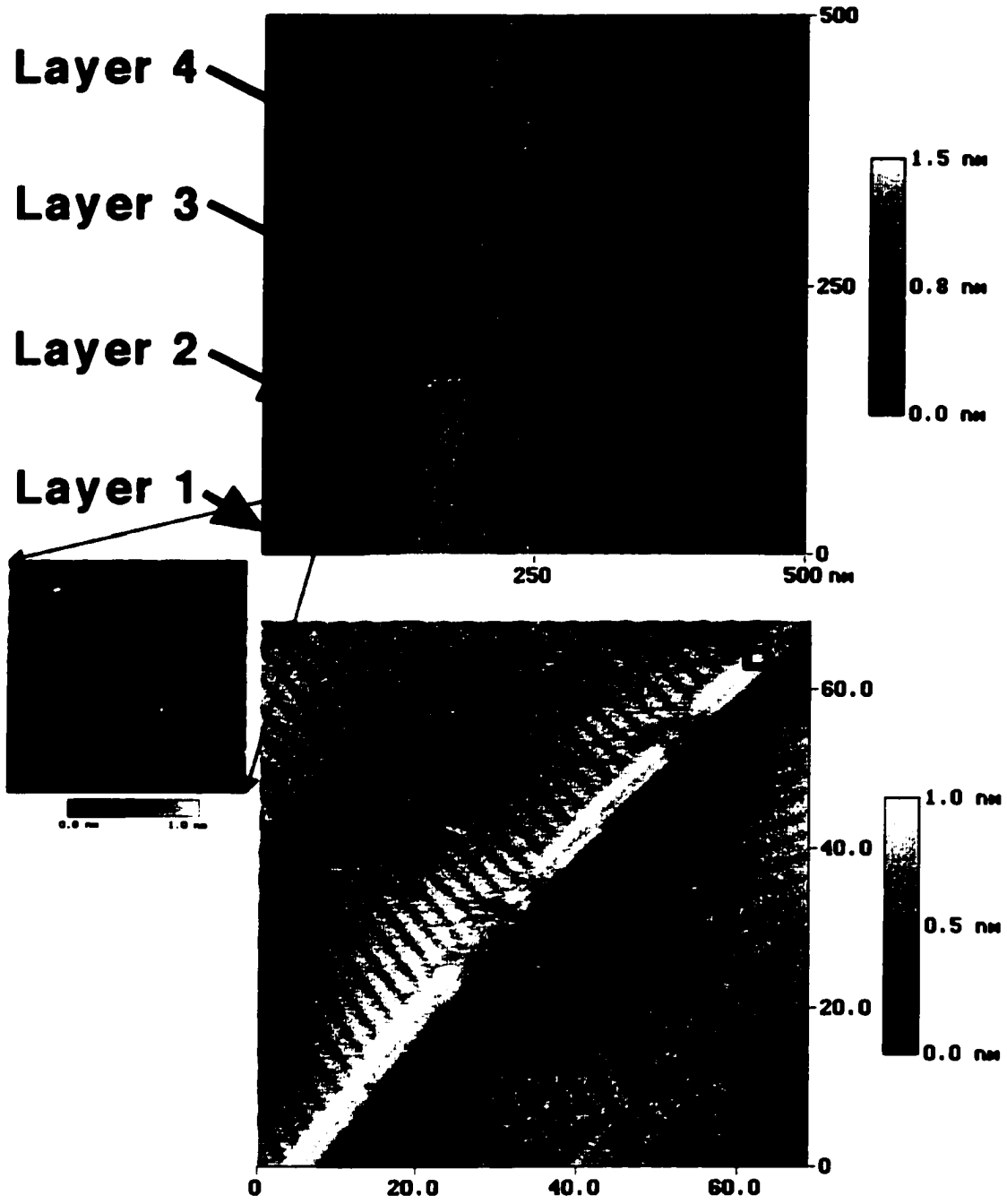

Figure 3.18: Ordered adsorption produced by the deposition of an 8-8/12-12 OHSQ mixture (10/1 ratio) on HOPG. (A) 500 nm x 500 nm STM image showing four molecular layers (from bottom left to right) adsorbed one atop the other. The inset shows the first layer and edge of the second in greater detail. (B) 70 nm x 70 nm image showing the ordered adsorption of 12-12 OHSQ at a graphite step edge. A thick bright stripe runs parallel to the step edge. The arrow points to the growth of another layer of squaraine rows oriented criss-cross to the rows below.

edge, with no border stripe. The relative height measured for the molecular terraces was always found to be 2.5 ± 0.5 Å, or some multiple of this height.

Since the first work reporting the study of molecular adsorbate systems with STM,[64-66] the generally-accepted model of STM imaging assumed that only the first layer of adsorbed molecules on a conducting/semiconducting substrate are imaged by the probing tip. In fact, there are often many layers of molecules with varying degrees of order adsorbed onto the substrate. The layer in contact with the surface is usually highly ordered due to strong molecule-substrate interactions. Subsequent layers are more and more loosely bound (due to increasing distance from the substrate surface) and may become more and more amorphous unless the surface structure is similar to a bulk crystallization plane. In order for the STM tip to reach the current setpoint value, it must push□ through many layers of loosely organized or amorphous molecules until it reaches a well-organized layer which can transport electrons/charge well enough to support the predetermined tunneling current. There are two requirements for the imaging of multiple adsorbed layers: (1) the multiple layers must be sufficiently organized and (2) these organized layers must be able to support facile charge transport to the substrate. Due to the insulating nature of the majority of the molecules investigated by STM, it was thought only the molecular layer in direct contact with the surface could be imaged. Since then there have been a number of instances demonstrating that islands adsorbed upon monolayers or second layer adsorption can be observed with the STM.[2,4,67] However, there are few reports in the literature showing STM images of multiple adsorbed layers, presumably due to a lack of molecular systems which are organized over several molecular layers and also are able to

transport charge easily over this distance of several molecular layers. Liquid crystalline molecules form many layers of organized molecules, however, they cannot transport electrons or charge easily through these layers. As a result multilayers of these molecules have not yet been imaged with molecular resolution with STM.

Many molecular systems have been reported to form organized multilayers which can be resolved via AFM but not in STM images.[61,67,68] DAPDA is one such molecule that self-organizes in three-dimensions.[61] As mentioned before, DAPDA has a dialkylamino functionality that is similar to the squaraines and forms multiple layers of ordered molecules. However, DAPDA has no D-A-D chromophore. Gorman et al demonstrated that multiple layers of DAPDA molecules can be imaged with atomic force microscopy, but only single layers are imaged with STM.[61] The inability to image multiple layers of DAPDA with STM is most likely due to DAPDA's lack of charge transferring functionality precluding any charge-transfer pathway through the multiple layers of adsorbed molecules. Without a means of transporting electrons through the thickness of the multiple layers, the STM tip must push through the insulating molecular layers until it is close enough to the substrate to support the setpoint current. Thus only the first molecular layer is imaged.

As was shown in Figure 3.18, squaraine multilayers can be imaged by STM. The difference between squaraine and other STM-investigated molecules, which form extensive 3-D networks as a result of strong intermolecular interactions, is the inherent charge-transferring ability of squaraines in the solid state. Squaraines are exploited commercially in photoreceptors because of their charge transporting ability. The D-A interactions between adjacent molecules within the same layer and between adjacent

molecules in adjacent molecular layers provide the electronic coupling needed for facile charge transport. We have shown that additional layers of squaraines tend to adsorb such that donor and acceptor moieties within the two adjacent layers align with each other. The existence of this pathway may facilitate the imaging of several molecular layers of squaraine molecules by STM. The large gap resistance that is typically used to image squaraines (on the order of 50 gigaohms) dictates a tip-sample separation where several molecular layers can exist between the tip and the substrate. Thus tunneling can be accomplished through a great tip-substrate distance in the squaraine system due to the facile transport of electrons through the squaraine layers.

Orientation with Respect to HOPG

An important distinction was made between the alignment of the long axis of the chromophore of the molecule with the graphite lattice and alignment of the alkyl tails of the molecule in order to determine the relationship of molecular adsorbate symmetry to graphite lattice symmetry. This distinction was not previously needed for studies with linear adsorbates. Thus, these two alignments of the squaraine adsorbate must be analyzed separately. It has been shown previously that long chain alkanes preferentially align along the carbon chains or $[01\bar{1}0]$ (and symmetry equivalent) directions of the graphite lattice (see Figure 3.19A).[1,12] Therefore we might expect that the longer tails in the squaraine series might align along this direction. It is not known how a squaraine chromophore aligns on the graphite surface. The most common polytype of graphite layers forms with the lattice vectors of two adjacent planes coinciding; however, the aromatic rings within adjacent planes do not. They are slipped by 1.42 Å, as seen in Figure 3.19B. We assume that a likely vector for the long axis of

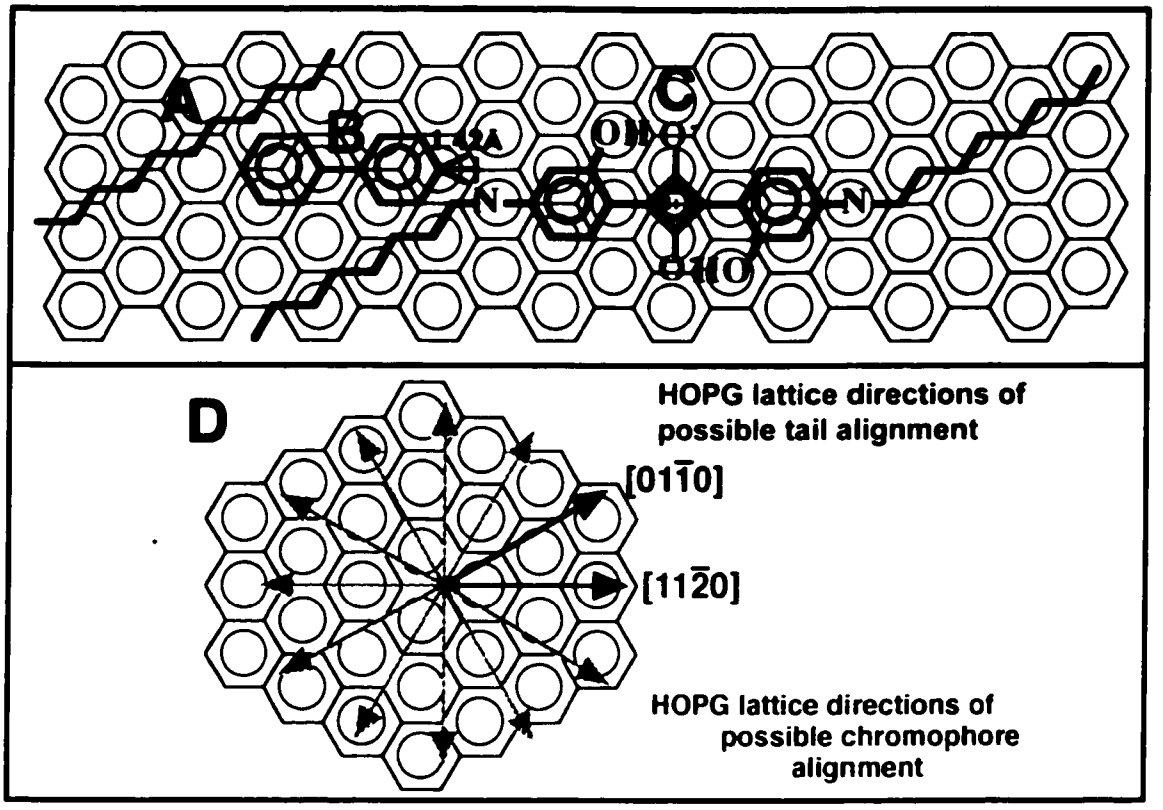

Figure 3.19: Cartoon showing the graphite lattice and the preferred orientation of several molecular adsorbates. (A) The preferred orientation of alkanes adsorbed on the graphite surface: aligned along the carbon chain backbone of the graphite lattice. (B) Biphenyl representing the position of a very small portion of a second graphite layer with respect to the orientation of the first layer. The directions of the lattice vectors for each of the layers coincide, however, the two are slipped relative to one another 1.42 Å along the chain of rings. (C) Theoretically expected position of the squaraine molecule oriented on the graphite lattice. The chromophore lies parallel to the same lattice direction as the biphenyl representation, and the alkyl tails parallel to the same lattice direction as the alkane representation. (D) Cartoon showing the graphite lattice vectors along which the squaraine chromophores and alkyl tails may be expected to align or lie parallel to. The red arrow represents one of the graphite vectors the squaraine chromophore may be expected to align along ([11$\bar{2}$0]). Other vectors symmetrically equivalent to the [11$\bar{2}$0] are shown in muted red. The blue arrow represents one of the graphite lattice vectors the squaraine alkyl tails may be expected to align along or lie parallel to [01$\bar{1}$0]. Symmetrically equivalent vectors are shown in muted blue.

a squaraine chromophore to orient, should it be aligned, would be along the $[11\bar{2}0]$ direction or symmetry related directions. Aligning the squaraine chromophore along this direction would maximize π stacking between the squaraine rings and the graphite rings. Figure 3.19C shows a cartoon representation of our expected orientation of a squaraine molecule on the graphite surface, taking into account the alignment of both the alkyl tails and the chromophore with the graphite surface.

To determine any alignment of the squaraine layers with the graphite substrate, images of graphite were used as a reference to compare the positions of adsorbed squaraine molecules. Graphite images were obtained by increasing the setpoint current and decreasing the bias voltage in the same area as submolecularly-resolved squaraine images had been obtained. The graphite lattice vectors of possible chromophore alignment and alkyl tail alignment were then determined (see Figure 3.19D). Images of molecularly-resolved squaraines provided the directions of the long axes of the squaraine chromophores which were then compared to the directions of the rings in the graphite lattice ($[11\bar{2}0]$ and related vectors in Figure 3.19D). Figure 3.20A shows a graphical compilation of the deviation of the angle of the chromophores' long axes from the expected orientation (i.e. parallel to the $[11\bar{2}0]$ or related direction in Figure 3.19D). Only the major polymorph of the five squaraines is represented in this graph.

To determine the alignment of squaraine alkyl tails we assumed that two of the alkyl tails (four for 2-18 OHSQ) adsorbed onto the surface coplanar with the chromophore and at a 30° angle to the direction of the long axis of the chromophore (as is represented in the molecular models of 8-8 OHSQ and 12-12 OHSQ). This angle of the tails to the long axis of the chromophore was determined through minimization of

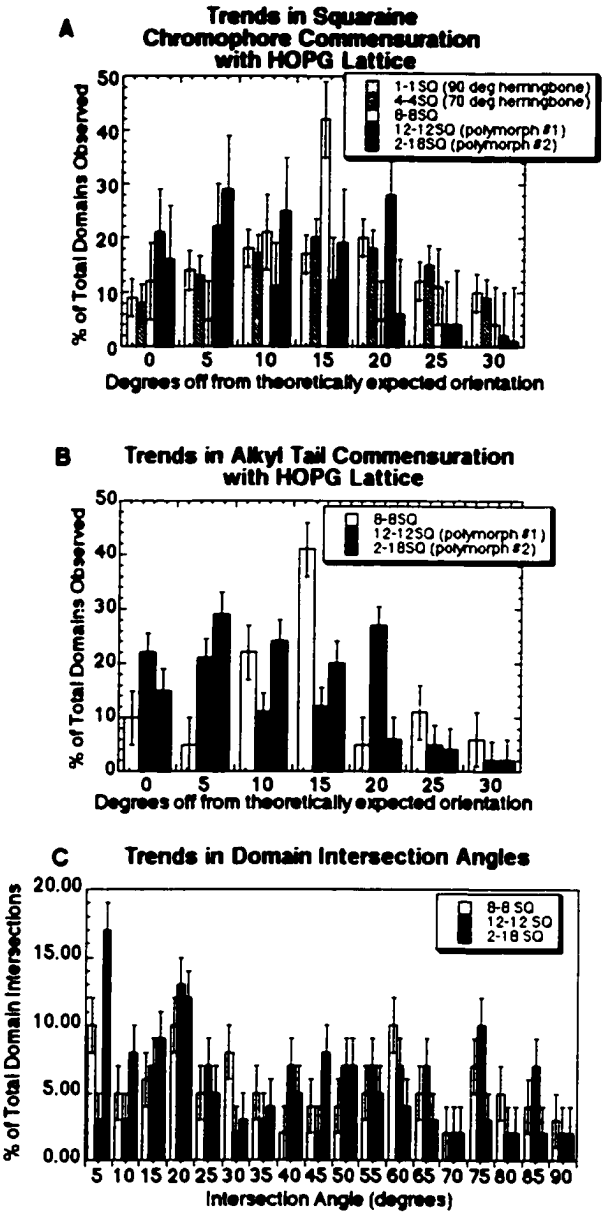

Figure 3.20: Histograms showing the trends in orientation of the major polymorphs of the OHSQs on HOPG. (A) Orientation of the chromophores in the major polymorphs of 1-1 OHSQ, 4-4 OHSQ, 8-8 OHSQ, 12-12 OHSQ, and 2-18 OHSQ and (B) the alkyl tails in the major polymorphs of 8-8 OHSQ, 12-12 OHSQ, and 2-18 OHSQ with respect to the $[11\bar{2}0]$ symmetry related and $[01\bar{1}0]$ symmetry related graphite lattice vectors, respectively. Histogram (C) shows the trends in domain intersection angle for the ordered domains of adsorbed 8-8, 12-12, and 2-18 OHSQ on HOPG. Molecular orientation and domain intersection angles are two of the characteristics useful in determination of the degree of commensuration of an adsorbed layer to its substrate. Here it can be seen that no squaraine polymorphs show true alignment with the graphite lattice.

the molecular structure and constraining it to be coplanar using the molecular modeling program Biograf. It was possible to deduce the orientation of the alkyl tails with respect to the graphite lattice from the determined direction of the long axis of the chromophore with respect to the graphite lattice (provided the assumption is valid). Determination of the orientation of the alkyl tails was not attempted for the shorter-tailed squaraines, 1-1 OHSQ and 4-4 OHSQ, since there is more ambiguity associated with the orientations of the tails in 1-1 OHSQ and 4-4 OHSQ than in the longer-tailed squaraines. Figure 3.20B shows the graphical compilation of the deviation of the assumed tail direction from the expected orientation of the 8-8, 12-12, and 2-18 OHSQ tails shown in Figure 3.19C. The same polymorphs as those sampled for the chromophore alignment histogram are represented in the alkyl tail alignment histogram. Since the angular difference between the orientation of the chromophore and the direction of the adsorbed alkyl tail is 30°, and the angular difference between the $[11\bar{2}0]$ direction and the $[01\bar{1}0]$ direction is likewise 30°, the histogram for the alignment of the tails is essentially the same as the histogram for the alignment of the chromophores.

Figures 3.20A and B show that the expected orientation of the squaraine chromophore and of the adsorbed alkyl tails is not preferred by any of the squaraines listed. The only significant spike in the histogram appears to be for 8-8 OHSQ at 15° from the expected orientation. It is not clear why this orientation is slightly preferred for 8-8 OHSQ. When the squaraine chromophore is rotated 15° from the expected direction, the tails should be 15° rotated from the direction of the preferred alkane chain alignment ($[01\bar{1}0]$ direction). The other squaraine polymorphs apparently can accommodate any position on the graphite surface, although orientations far from the

expected directions (25° and 30°) seem to be slightly disfavored among all squaraines except 1-1 OHSQ and 4-4 OHSQ. 1-1 OHSQ and 4-4 OHSQ have no preferred orientation. When the percentage of total domains oriented at the expected orientation along the $[11\bar{2}0]$ and symmetry related directions were compared between the five squaraine polymorphs listed, it was found that 12-12 OHSQ and 2-18 OHSQ exhibited the highest occurrence of domains at the expected orientation (although this orientation was not the highest occurring orientation for either of these molecules). 1-1 OHSQ and 4-4 OHSQ showed the lowest occurrence of domains at this orientation, with a very even percentage of domains across the whole range of orientations.

In addition to measuring the orientation of the individual molecules with respect to the graphite lattice, the angle formed between the directions of stripes within adjacent domains was measured and compiled for the row-forming squaraines (8-8 OHSQ, 12-12 OHSQ, and 2-18 OHSQ). This angle was termed the "domain intersection angle". A histogram relating the percentage of total domain intersections observed at various angles for each of the longer tailed squaraines is shown in Figure 3.20C. An aligned adsorbate structure should show spikes in the intersection angle histogram at angles reflecting the symmetry of the graphite lattice (30°, 60°). No strong preference for any domain intersection angles is seen with the exception of 2-18 OHSQ where there is a significant low angle domain intersection preference at about 5°.

We conclude that none of the squaraine molecules studied forms a truly aligned structure with respect to the orientation of the HOPG substrate. This result is somewhat surprising when the theoretical influence of alkyl tail length on commensuration is considered. The fact that 1-1 OHSQ and 4-4 OHSQ do not show any tendency towards

alignment with the HOPG surface can be easily understood since the donor-acceptor intermolecular charge transfer interactions (or Coulomb forces between oppositely polarized moieties of adjacent molecules) of the squaraine core are dominant. Maximizing the donor and acceptor interaction by having adjacent molecules canted towards each other results in a herringbone pattern much like that observed for perylenes on HOPG and MoS_2.[69,70] Structural differences between 1-1 OHSQ and 4-4 OHSQ are most likely due to the steric effect of the additional 12 methylene groups in 4-4 OHSQ. The existence of at least three different 1-1 OHSQ polymorphs points to the flexibility of the structure while still maintaining strong Coulomb interactions. The observed instability of the 4-4 OHSQ structures may be due to an inflexibility where slight orientational changes in molecular position may interfere with the molecule-molecule forces, causing the butyl groups to eclipse favorable interactions between adjacent oppositely polarized moieties.

The increased tail length of 8-8 OHSQ induces a structural transition in which the herringbone-like structure of 1-1 OHSQ and 4-4 OHSQ are now disfavored. Longer-tailed squaraines instead exclusively exhibit row structures. In these structures, the molecules arrange to allow the interdigitation of alkyl tails between adjacent rows. Reorienting the squaraine molecules from a herringbone to a row-structure does not preclude donor-acceptor or Coulomb interactions between adjacent squaraine chromophores within the same row. The 65 ± 5° angle between the long axis of the molecules to the direction of the molecular row results in adjacent molecules within the same row being offset from each other by about 3 Å. This allows the adjacent donor and acceptor sites to interact. It appears that the interaction between the octyl tails and

the HOPG substrate is not strong enough to overcome the molecule-molecule interactions between adsorbed squaraines resulting in no alignment with the graphite lattice. Additional evidence that an eight carbon tail is not sufficient to promote alignment is provided by an STM study of the ordered adsorption of the dialkylamine molecule, DAPDA, containing two decyl groups, as reported by Gorman et al.[61] This molecule, analogous in structure to the two dialkylamino moieties of squaraines we studied, adsorbs to produce domains of linear rows that show no strong epitaxy with the HOPG surface.[61] The interaction between 14 methylene groups (if two of the fourteen tails are lying flat) and the HOPG lattice is not sufficient to overcome the molecule-molecule interactions between squaraines and promote a commensurate structure instead.

Increasing the length of the alkyl tail to 12 carbons, as is the case for 12-12 OHSQ, results in the interaction between 22 methylene groups and the graphite surface. This increased interaction results in 12-12 OHSQ showing a slight tendency to align along the major lattice vectors of HOPG. The molecular packing within the row structure of 12-12 OHSQ, however, does not appear to change very much from that of 8-8 OHSQ as a result of the small increase in graphite interaction. The 60 ± 5° angle of the chromophore of the molecule to the direction of the row ensures the interaction of the donor and acceptor moieties of adjacent molecules within the same row. It appears that even with the greater interaction of the alkyl tail with the substrate, the strength of DA interactions and Coulomb interactions between squaraine cores is important. One might expect that with 18-carbon tails the surface structure of 2-18 OHSQ would be commensurate due to a very large interaction between its 34 methylene groups and the

HOPG lattice. This is not observed since the 2-18 OHSQ molecule within polymorph 2 actually shows less alignment with the HOPG lattice than 12-12 OHSQ. The length of the stearyl tail in 2-18 OHSQ (and the reduction in total molecular bulkiness due to the two ethyl tails) results in a flexible row structure for 2-18 OHSQ. In addition, rows of one polytype have been seen to transform smoothly into another polytype (Figure 3.2C). This structural flexibility can result in undulation of the rows, demonstrating the dominance of the molecule-molecule interactions.

Conclusions

The hydroxylated dialkylamino squaraine molecules that we studied form well-ordered two-dimensional surface structures that can be imaged with STM. Squaraines are highly surface active, forming domains of adsorbed molecules with a rich variety of 2-D structures and polymorphs from quite dilute solutions in phenyloctane or liquid crystal solvents. These properties are most likely due to their propensity for intermolecular donor-acceptor interactions. The 2D structures form domains of ordered molecules from tens of nanometers to a micron in size and tend not to be commensurate with the HOPG substrate. A definite change in the type of adsorbate structure was observed to occur with increasing alkyl tail length. At tail lengths of 1 and 4 carbons, various polytypes of herringbone packings were observed arising from the strong D-A interactions and Coulomb forces between oppositely-polarized areas of adjacent squaraine molecules. At alkyl tail lengths of 8 carbons and above, despite their non-linear molecular geometry, qualitatively similar row structures were formed with slight variations in the angle between the long axis of the chromophore and the row

direction in the various polytypes. The strong intermolecular donor-acceptor interactions and the charge transport ability of the squaraine molecules allowed the most extensive STM imaging of multiple molecular layers yet reported.

Acknowledgements

The authors gratefully acknowledge Dr. P.M. Kazmaier of the Xerox Research Centre of Canada for providing the 4-4, 8-8, and 12-12 squaraine dyes and Dr. Gregg Haggquist of Lexmark for providing the 1-1 squaraine dye. Brenda Randall is thanked for her assistance as a summer REU student. The US Department of Energy, Division of Chemical Sciences is acknowledged for financial support through contract DE-G03-96ER14625.

REFERENCES

(1) McGonigal, G. C.; Bernhardt, R. H.; Thomson, D. J., *Appl. Phys. Lett.* **1990**, *57*, 28-30.
(2) Thibaudau, F.; Watel, G.; Cousty, J., *Surf. Sci. Lett.* **1993**, *281*, L303-L307.
(3) Watel, G.; Thibaudau, F.; Cousty, J., *Surf. Sci. Lett.* **1993**, *281*, L297-L302.
(4) Wawkuschewski, A.; Cantow, H.-J.; Magonov, S. N., *Langmuir* **1993**, *9*, 2778-2781.
(5) Askadskaya, L.; Rabe, J. P., *Phys. Rev. Lett.* **1992**, *69*, 1395-1398.
(6) Cincotti, S.; Rabe, J. P., *Supramol. Sci.* **1994**, *1*, 7-10.
(7) Claypool, C. L.; Faglioni, F.; III, W. A. G.; Gray, H. B.; Lewis, N. S.; Marcus, R. A., *J. Phys. Chem. B* **1997**, *101*, 5978-5995.
(8) Giancarlo, L.; Cyr, D.; Muyskens, K.; Flynn, G. W., *Langmuir* **1998**, *14*, 1465-1471.
(9) Groszek, A. J., *Proc. Roy. Soc. Lond. A.* **1970**, *314*, 473-498.
(10) Habenschuss, A.; Narten, A. H., *J. Chem. Phys.* **1990**, *92*, 5692-5699.
(11) Peters, G. H., *Surface Science* **1996**, *347*, 169-181.
(12) Rabe, J. P.; Buchholtz, S., *Science* **1991**, *253*, 424-427.
(13) Rabe, J. P.; Buchholz, S.; Askadskaya, L., *Phys. Scr.* **1993**, *T49*, 260-263.
(14) Segerman, E., *Acta Crystallographica* **1965**, *19*, 789-796.
(15) Venkataraman, B.; Breen, J. J.; Flynn, G. W., *J. Phys. Chem.* **1995**, *99*, 6608-6619.
(16) Cyr, D. M.; Venkataraman, B.; Flynn, G. W., *Chem. Mater.* **1996**, *8*, 1600-1615.
(17) Hentschke, R.; Schurmann, B. L.; Rabe, J. P., *J. Chem. Phys.* **1992**, *96*, 6213-6221.
(18) Cincotti, S.; Rabe, J. P., *Appl. Phys. Lett.* **1993**, *62*, 3531-3533.
(19) Stevens, F.; Dyer, D. J.; Walba, D. M., *Langmuir* **1996**, *12*, 436-440.
(20) Stevens, F.; Dyer, D. J.; Walba, D. M.; Shao, R.; Clark, N. A., *Liq. Cryst.* **1997**, *22*, 531-534.
(21) Palermo, V.; Biscarini, F.; Zannoni, C., *Phys. Rev. E* **1998**, *57*, R2519-R2522.
(22) Stevens, F.; Patrick, D. L.; Cee, V. J.; Purcell, T. J.; T.P. Beebe, J., *Langmuir* **1998**, *14*, 2396-2401.
(23) Spong, J. K.; Mizes, H. A.; L.J. LaComb, J.; Dovek, M. M.; Frommer, J. E.; Foster, J. S., *Nature* **1989**, *338*, 137-139.
(24) Patrick, D. L.; Cee, V. J.; Purcell, T. J.; T.P. Beebe, J., *Langmuir* **1996**, *12*, 1830-1835.
(25) Patrick, D. L.; Cee, V. J.; T.P. Beebe, J., *Science* **1994**, *265*, 231-234.
(26) Cleaver, D. J.; Callaway, M. J.; Forester, T.; Smith, W.; Tildesley, D. J., *Mol. Phys.* **1995**, *86*, 613-636.
(27) Smith, D. P. E.; Heckl, W. M.; Klagges, H. A., *Surf. Sci.* **1992**, *278*, 166-174.

(28) Lacaze, E.; Barois, P.; Lacaze, R., *J. Phys. I* **1997**, *7*, 1645-1664.
(29) Smith, D. P. E.; Horber, H.; Gerber, C.; Binng, G., *Science* **1989**, *245*, R43-R45.
(30) Hara, M.; Iwakabe, Y.; Tochigi, K.; Sasabe, H.; Garito, A. F.; Yamada, A., *Nature* **1990**, *244*, 228-230.
(31) Smith, D. P. E.; Horber, J. K. H.; Binnig, G.; Nejoh, H., *Nature* **1990**, *244*, 641.
(32) Iwakabe, Y.; Hara, M.; Kondo, K.; Oh-Hara, S.; Mukoh, A.; Sasabe, H., *Jpn. J. Appl. Phys.* **1992**, *31*, L1771-L1774.
(33) Smith, D. P. E., *J. Vac. Sci. Technol. B* **1991**, *9*, 1119-1125.
(34) Patrick, D. L.; Cee, V. J.; T.P. Beebe, J., *J. Phys. Chem.* **1996**, *100*, 8478-8481.
(35) Iwakabe, Y.; Hara, M.; Kondo, K.; Tochigi, K.; Mukoh, M.; Yamada, A.; Carito, A. F.; Sasabe, H., *Jpn. J. Appl. Phys.* **1991**, *30*, 2542-2546.
(36) Allen, M. J.; Balooch, M.; Subbiah, S.; Tench, R. J.; Balhorn, R.; Siekhaus, W., *Ultramicroscopy* **1992**, *42-44*, 1049-1053.
(37) Tanaka, H.; Yoshinobu, J.; Kawai, M., *Jpn. J. Appl. Phys., Part 2* **1996**, *35*, L244-L246.
(38) Kasaya, M.; Tabata, H.; Kawai, T., *Surf. Sci.* **1996**, *357-358*, 195-201.
(39) Furukawa, M.; Tanaka, H.; Kawai, T., *Surf. Sci.* **1997**, *392*, L33-L39.
(40) Freund, J. E.; Edelwirth, M.; Krobel, P.; Heckl, W. M., *Phys. Rev. B* **1997**, *55*, 5394-5397.
(41) Kawai, T.; Tanaka, H.; Nakagawa, T., *Surf. Sci.* **1997**, *386*, 124-136.
(42) Sowerby, S. J.; Edelwirth, M.; Reiter, M.; Heckl, W. M., *Langmuir* **1998**, *14*, 5195-5202.
(43) Schmidt, A. H. In *Oxocarbons*; R. West, Ed.; Academic Press: New York, 1980; pp 185.
(44) Bigelow, R. W.; Freund, H. J., *Chem. Phys.* **1986**, *107*, 159-174.
(45) Law, K. Y., *Chem. Rev.* **1993**, *93*, 449-486.
(46) Tristani-Kendra, M.; Eckhardt, C. J.; Bernstein, J.; Goldstein, E., *Chem. Phys. Lett.* **1983**, *98*, 57-61.
(47) Tristani-Kendra, M.; Eckhardt, C. J., *J. Chem. Phys.* **1984**, *81*, 1160.
(48) Loutfy, R. O.; Hsiao, C. K.; Kazmaier, P. M., *Photogr. Sci. Eng.* **1983**, *27*, 5-9.
(49) Law, K. Y., *J. Phys. Chem.* **1987**, *91*, 5184-5193.
(50) Law, K. Y.; Bailey, F. C., *J. Imaging Sci.* **1987**, *31*, 83-93.
(51) Melz, R. J.; Champ, R. B.; Chang, L. S.; Chiou, C.; Keller, G. S.; Liclican, L. C.; Neiman, R. B.; Shattuck, M. D.; Weiche, W. J., *Photogr. Sci. Eng.* **1977**, *21*, 73-78.
(52) Gravesteijn, D. J.; Steenbergen, C.; Veen, J. v. d., *Proc. SPIE* **1983**, *420*, 327.
(53) Jipson, V. B.; Jones, C. R., *J. Vac. Sci. Technol.* **1981**, *18*, 105-109.
(54) Jipson, V. P.; Jones, C. R., *IBM Tech. Discl. Bull.* **1981**, *24*, 298.
(55) Morel, D. L.; Stogryn, E. L.; Ghosh, A. K.; Feng, T.; Purwin, P. E.; Shaw, R. F.; Fishman, C.; Bird, G. R.; Piechowski, A. P., *J. Phys. Chem.* **1984**, *88*, 923-933.

(56) Piechowski, A. P.; Bird, G. R.; Morel, D. L.; Stogryn, E. L., *J. Phys. Chem.* **1984**, *88*, 934-950.
(57) Merritt, V. Y.; Hovel, H. J., *App. Phys. Lett.* **1976**, *29*, 414.
(58) Law, K. Y.; Facci, J. S.; Bailey, F. C.; Yanus, J. F., *J. Imaging Sci.* **1990**, *34*, 31-38.
(59) Sampson, D. L. Ph.D. Thesis, Colorado State University, 1997.
(60) Takeda, N.; Stawasz, M. E.; Parkinson, B. A., *J. Electroanalytical Chem.* **2001**, *498*, 19-33.
(61) Gorman, C. B.; Touzov, I.; Miller, R., *Langmuir* **1998**, *14*, 3052-3061.
(62) Law, K. Y., *J. Phys. Chem.* **1988**, *92*, 4226-4231.
(63) Stevens, F. Thesis, University of Colorado, 1996.
(64) Ohtani, H.; Wilson, R. J.; Chiang, S.; Mate, C. M., *Phys. Rev. Lett.* **1988**, *60*, 2398.
(65) Chiang, S.; Wilson, R. J.; Mate, C. M.; Ohtani, H., *J. Microsc.* **1988**, *2*, 567.
(66) Foster, J. S.; Frommer, J. E., *Nature* **1988**, *333*, 542-544.
(67) Eng, L. M.; Fuchs, H.; Buchholz, S.; Rabe, J. P., *Ultramicroscopy* **1992**, *42-44*, 1059-1066.
(68) Schwinn, T.; Gaub, H. E.; Rabe, J. P., *Supramol. Sci.* **1994**, *1*, 85-90.
(69) Ludwig, C.; Gompf, B.; Glatz, W.; Petersen, J.; Eisenmenger, W.; Mobus, M.; Zimmermann, U.; Karl, N., *J. Phys.: Condens. Matter* **1992**, *86*, 397-404.
(70) Hoshino, A.; Isoda, S.; Kurata, H.; Kobayashi, T., *J. Appl. Phys.* **1994**, *76*, 4113-4120.

CHAPTER FOUR

STM Investigation of the Ordered Structures of Non-Hydroxylated Dialkylamino Squaraines Adsorbed on HOPG

To be submitted to Langmuir, 2001.

Abstract:

We report the ordered structures of five bis(4-dialkylamino-phenyl) squaraines (both symmetric and asymmetric) of varying tail lengths, adsorbed on the (0001) surface of HOPG from phenyloctane solution, with scanning tunneling microscopy (STM). Like their hydroxylated counterparts (OHSQs), non-hydroxylated squaraines (HSQs) were found to be highly surface active, forming monolayer and multiple layer ordered films. Molecules that were non-hydroxylated analogues to hydroxylated molecules studied previously[1] exhibited structures that were within experimental error of those exhibited by the equivalent OHSQ. This suggests that intermolecular hydrogen bonding does not drive the ordered structures observed for OHSQs. The stability and STM image quality of the HSQ adsorbate structures was poorer than that of OHSQs, however, suggesting that H-bonding affects these characteristics. Some molecules exhibited several polymorphs, a few of which were 2-dimensionally chiral.

Introduction:

In the last chapter, the ordered adsorption of a series of hydroxylated squaraines of varying tail length on HOPG was presented. Although it appeared that donor-acceptor interactions between adjacent molecules are a significant driving force for chromophore-chromophore alignment, the role of intermolecular hydrogen bonding in influencing the 2D adsorbate structure was unclear. In this chapter, a series of non-hydroxylated squaraines is presented, some of which have the same alkyl tail lengths as squaraines presented in Chapter 3. The ordered adsorbate structure of these analogous squaraines on HOPG can be directly compared to their hydroxylated counterparts. Differences in the adsorbed structures of hydroxylated and non-hydroxylated squaraine analogs can shed light on the influence of intermolecular hydrogen bonding on the squaraine structures presented in the last chapter.

In addition to studying the influence of hydrogen bonding, the effect of alkyl tail asymmetry is further investigated. In Chapter 3, a single molecule with unequal R_1 and R_2 tail lengths (2-18 OHSQ) was investigated. Similarly, in this chapter, non-hydroxylated molecules with two short alkyl tails as well as two intermediate length tails are investigated. Utilizing these less-symmetric molecules, the effect of the reduction of interactions between carbon tails on the molecular row structure was probed.

Finally, the tail lengths of symmetrical non-hydroxylated molecules are varied from relatively short lengths to intermediate tail lengths. In Chapter 3, a transition in molecular packing was observed from herringbone structures to row

structures. Herringbone structures were observed only for shorter tail lengths, whereas only row structures were observed for longer tail lengths. This transition was observed to occur between tail lengths of 4 and 8 carbons. In this chapter, non-hydroxylated squaraines with tail lengths of 3 carbons, 4 carbons, and 6 carbons, are studied to determine whether such a transition in packing structure occurs for non-hydroxylated squaraines.

Experimental:

Experiments were performed with a Digital Instruments Nanoscope III STM under ambient conditions. Vibration isolation was provided by a bungee system enclosed in an environmental chamber. Four different squaraine molecules were obtained from Marina Stanescu of the Whitten group at the University of Rochester. They were bis(4-dipropylamino-phenyl) squaraine (3-3 HSQ), bis(4-dibutylamino-phenyl)squaraine (4-4 HSQ), bis(4-dioctylamino-phenyl)squaraine (8-8 HSQ), and bis(4-methyloctylamino-phenyl)squaraine (1-8 HSQ). Bis(4-methyl-hexylamino-phenyl)squaraine (1-6 HSQ) was generously donated by the Ashwell group of Cranfield University. Table 4.1 shows the structure of the five squaraine molecules studied and the abbreviations used in the rest of this paper. Solutions of each of the squaraines were prepared in concentrations of approximately 10^{-4} to 10^{-6} M in phenyloctane (Aldrich). STM tips were cut to a sharp point mechanically from (80:20) Platinum/Iridium 0.2mm diameter wire (Alpha Aesar). Samples were prepared by applying a drop of squaraine solution onto a freshly cleaved piece of highly ordered pyrolytic graphite (HOPG). Tunneling occurred with the tip immersed into the layer of

Table 4.1

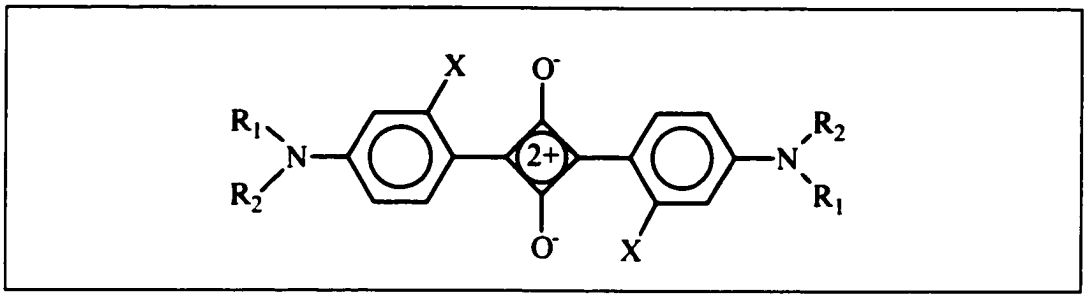

3-3 HSQ	X = H	$R_1 = R_2 = C_3H_7$
4-4 HSQ	X = H	$R_1 = R_2 = C_4H_9$
8-8 HSQ	X = H	$R_1 = R_2 = C_8H_{17}$
1-8 HSQ	X = H	$R_1 = CH3;\ R_2 = C_8H_{17}$
1-6 HSQ	X = H	$R_1 = CH_3;\ R_2 = C_6H_{13}$

TABLE 4.1: Structure of a generic squaraine molecule and list of HSQs studied.

solution using typical tunneling parameters of –1.6 V to –0.8 V (sample negative) and 30 to 40 pA with the STM operating in constant current mode. After a series of squaraine images were obtained, the tunneling gap resistance was lowered in order to characterize the HOPG surface in the exact same spot. Images were obtained with different tips and several different series of solutions to test for reproducibility and ensure that data was free of tip and sample artifacts. All images presented here have been flattened by software routines.

Results and Discussion:

Previous studies with bis(4-dialkylamino-2-hydroxyphenyl)squaraines[1] showed that squaraine molecules appear in most STM images as football-shaped areas of bright contrast measuring 15.0 ± 1.5 Å in length, 2.5 ± 1.5 Å in width, and from 0.7 Å to 1.5 Å in relative height. Images of particularly good resolution show two bright spots within the elliptical region each measuring ~3 A in length. In the present study, it was found that STM images of non-hydroxylated dialkylamino squaraines were similar. For both types of squaraines the length of the football shape corresponds well with the length of the chromophore of the molecule (from the nitrogen at one end of the molecule to the nitrogen at the other end) with the spots assigned to the phenyl rings. The width of the elipse corresponds well with the width of a phenyl group, not including the oxygens, hydroxyls or hydrogens. As described previously[1], the aromatic chromophore of the squaraine molecule should be imaged as an area of bright contrast since this moiety is where the majority of the electron density is located

in the molecule. In addition, this moiety is highly polarizable in contrast to the rather insulating alkyl tails. The difference in exhibited contrast between the oxygens (dark) and the nitrogens (bright), is explained by the theory, proposed by Claypool et al, relating ionization potential to STM contrast.[2] The lack of resolution of the alkyl tails of these squaraine molecules may be attributed to the tunneling conditions necessary for imaging of squaraines on graphite. Alkanes and other adsorbate molecules in which the alkyl portions of the molecule are resolved with STM (on HOPG) are usually imaged with tunneling currents of several hundred picoamperes up to a few nanoamps.[2-7] Squaraines are not clearly imaged at tunneling currents of more than 50 pA. The length, width, and relative height of the bright elliptical areas correspond well with a model of the molecule lying with its chromophore flat on the HOPG surface. Measured relative heights of 1 to 2 Å are typical for π systems adsorbed lying flat on the substrate surface, as measured by STM.[8] Since the alkyl tails are not resolved, packing of the bright chromophores must be examined quantitatively to deduce the orientation of the tails.

Like hydroxylated squaraines[1], non-hydroxylated dialkylamino squaraines were found to be highly surface active. Pure solutions of non-hydroxylated squaraine in phenyloctane (with concentrations within the range described above) formed ordered layers that could be observed with STM shortly after deposition. In general, ordered domains of squaraine molecules were visible with the STM within ten minutes of solution deposition. Nucleation and growth of domains was often observed using more dilute squaraine solutions as small,

isolated domains grew to completely cover the substrate surface. More concentrated solutions tended to form complete monolayers and even multilayers immediately upon deposition. Typical domains sizes ranged from tens of nanometers to almost a micron depending upon the identity of the squaraine. In general, squaraines which produced row structures (3-3 HSQ, 8-8 HSQ, and 1-8 HSQ) exhibited smaller domains than those which did not (4-4 HSQ).

STM images of ordered layers of non-hydroxylated squaraines were not as stable as those of their hydroxylated counterparts. Ordered layers of non-hydroxylated molecules could not be imaged with the STM after approximately 12 hours unless the solution was redeposited onto the surface. In contrast, hydroxylated squaraines could be imaged continuously over the course of several days. In addition, solutions of non-hydroxylated squaraines in phenyloctane decomposed as evidenced by a color change from a bright blue, teal, or purple color to yellow within several days. Decomposition of hydroxylated squaraine solutions generally occurred only after several months, and sometimes not until a year, after the preparation of the solution. Decomposition of the squaraine chromophore in different solutions has been reported in the literature and has been attributed to the attack of ^{-}OH on the squaric oxygens.[9-11]

STM images of non-hydroxylated squaraines tended to be noisier than those of hydroxylated squaraines. Bright streaks in the fast scan direction and general "fuzziness" of features in the image were common. It was found that by using biases less negative than the –1.6 to –2.0 V range necessary for

hydroxylated squaraine imaging, molecular order could still be imaged with reduced noise.

Unit cell parameters for each of the packing structures observed for the ordered adsorption of the non-hydroxylated squaraines on HOPG studied by STM are shown in Table 4.2.

3-3 HSQ

3-3 HSQ is a molecule without a previously studied hydroxylated analog. Because of the similar tail length of 3-3 HSQ to that of 4-4 OHSQ, it was expected that it would exhibit a herringbone packing similar to that produced by the ordered adsorption of 4-4 OHSQ on HOPG. Although it was discovered previously with 1-1 OHSQ that short-tailed squaraines may adopt a row configuration even though the tail-length is too short to allow substantial interdigitation or interaction with the HOPG lattice, we expected a herringbone packing. We found, however, that 3-3 HSQ exhibits row packing that is characteristic of the longer-tailed squaraines. Figure 4.1 shows a 209 nm x 209 nm STM image of an ordered domain of 3-3 HSQ adsorbed on HOPG. This image is typical of those taken immediately after deposition of the 3-3 HSQ/phenyloctane solution onto the graphite surface. It shows a monolayer composed of multiple domains with a few defects (lower right). Although somewhat faint, bright rows can be seen within the domains, especially towards the bottom of the image. Domains tended to be elongated in one direction, with typical lengths of several hundred nm and widths of only 50 – 100 nm. The

Table 4.2

Squaraine	Packing Structure	Unit Cell α (°)	Unit Cell a (Å)	Unit Cell b (Å)	Packing Density (molecules /nm^2)	Molecular Area (Å^2 /molecule)
3-3 HSQ	Type 1 Row Type 2 Row	55±4 40±4	21±1 ?	9±1 9±1	0.53±0.06 ?	189±23 ?
4-4 HSQ	Herringbone*	85±2	17±2	19.5±1.5	0.60±0.08	166±23
8-8 HSQ	Type 1 Row Type 2 Row*	58±5 100±5	27.5±1.5 50±1.5	9.0±1.5 9.0±1.5	0.40±0.07 0.44±0.08	247±33 225±38
1-6 HSQ	Row	50±2	24±1.5	9±1	0.46±0.06	216±28
1-8 HSQ	Type 1 Row Type 2 Row*	50±4 100±5	27±1.5 49±2	8.5±1.5 9.0±1.5	0.44±0.08 0.45±0.08	230±43 221±38

TABLE 4.2: Unit cell data for the major polymorphs of the five HSQs studied. Question marks represent a lack of data due to insufficient molecular STM resolution. Asterisks represent packing structures with two molecules per unit cell. All others have one molecule per unit cell.

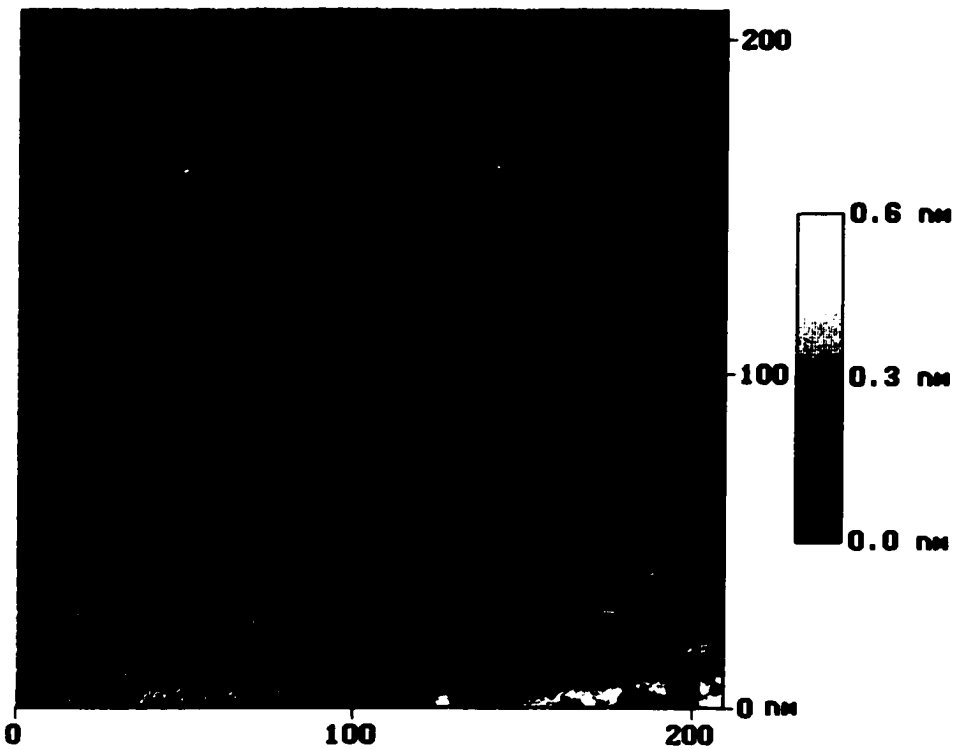

Figure 4.1: 209 nm x 209 nm STM image of the ordered adsorption of 3-3 HSQ on HOPG. Several domains are shown composed of faint rows. A defect in the monolayer is shown at the bottom right of the image.

direction of the domain elongation tended to correspond to the direction of the *a* unit cell vector.

Zooming-in on the domains further revealed the row structure. However, as can be seen in Figure 4.2, several different molecular contrasts were observed. These patterns were obtained in separate experiments, sometimes with the same tip, sometimes with a freshly cut tip. It is not clear whether these changes in contrast are due to changes in tip shape, or due to differences in molecular conformation, unit cell structure, or interaction with the graphite lattice. The pattern shown in Figure 4.2a was observed most often. It features a central round bright region 5 - 7 Å in diameter and ~1 Å in apparent height, flanked on either side by faint "wings". As mentioned earlier, the squaraine chromophore is usually imaged as an elliptical shape with a length of ~15 Å and width of ~5Å. The diameter of the round feature shown in Figure 4.2a is too small to account for the entire length of the squaraine chromophore and slightly too big to account for the width. It is possible that the pattern observed in Figure 4.2a is due to a change in conformation of the chromophore from one that is planar to one in which the square core is rotated out of the plane of the phenyl groups. In this conformation, the phenyls would lie approximately flat on the HOPG surface and the square core would protrude from the surface. If this is the case, the central bright round region is the square core, which is topographically higher than the rest of the molecule, and the faint wings are the phenyl groups. The wings, measured from tip to tip, are ~14 Å in length, thus supporting this hypothesis. It may be argued that the phenyl rings, not the square core, are rotated out of the

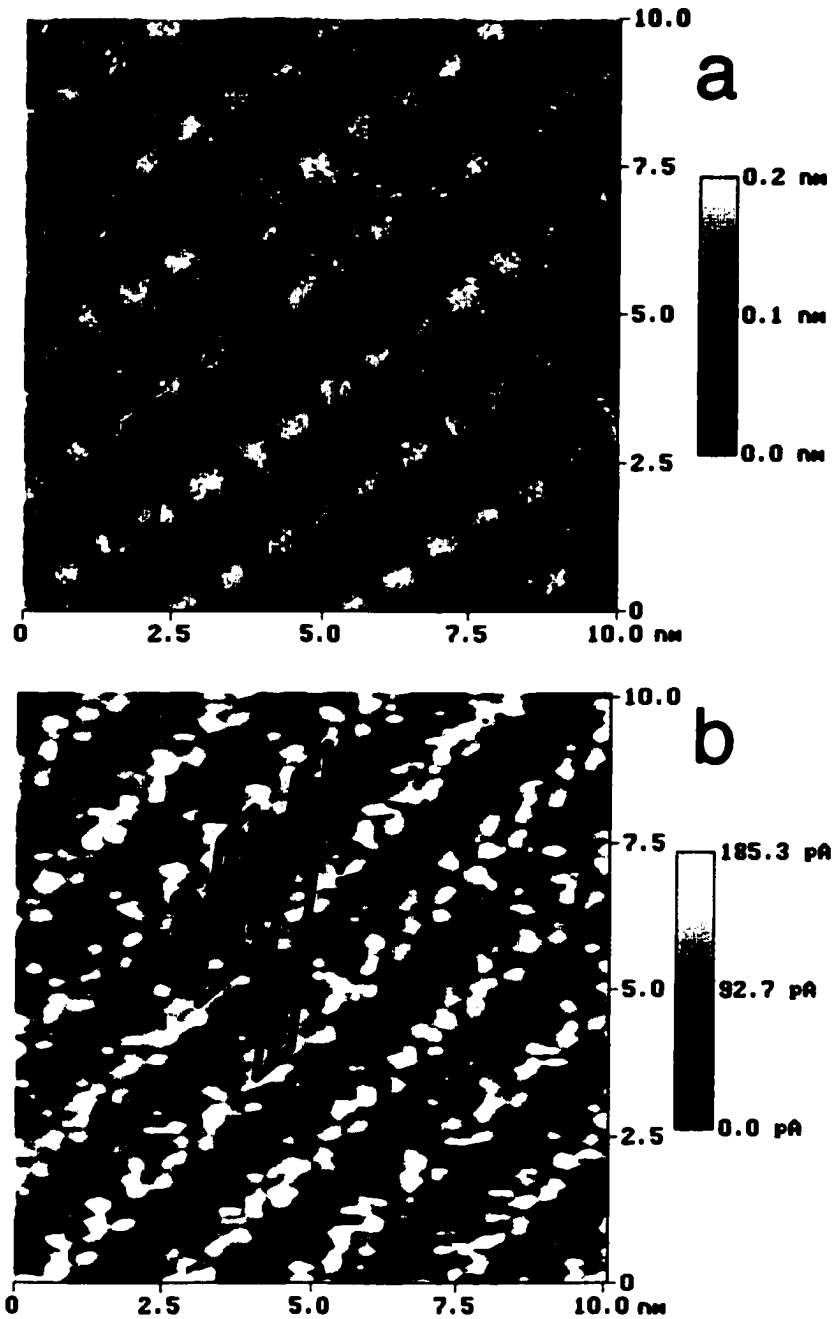

Figure 4.2: Two high resolution images of 3-3 HSQ on HOPG showing two different contrasts. Image (a) shows individual molecules appearing as a bright circle with bright "wings" on either side. Image (b) shows individual molecules as a series of bright spots. Black boxes overlaid on the images represent the unit cells. The unit cell of image (b) is ambiguous due to the irregular contrast of every other row, which obscures the orientation of chromophores within those rows.

plane of the molecule, thus making them appear "thinner". This conformation seems unlikely, however, due to the larger overall interaction of the two phenyl groups with the HOPG surface than that of the square core.

Assuming that the "wings" are the phenyl groups, the orientation of the molecules with respect to the direction of the row can be determined. This angle was measured to be ~50 °. The distance from each molecule to its nearest neighbor in the adjacent molecular row is ~16 Å. The distance from each molecule to its nearest neighbor within the same molecular row was measured to be ~9 Å, a typical molecule-molecule distance observed in OHSQs forming row structures[1]. The width of the dark trough between bright "wings" (measured perpendicular to the edge of the molecular row) was found to be ~2 Å, corresponding to a structure in which the propyl tails of adjacent molecules in neighboring molecular rows are fully interdigitated. A molecular model illustrating this structure is shown in Figure 4.3a. In this model, the square cores are shown slightly tilted. There is no way, however, for us to determine with surety how much the rings are tilted, given the images and resolution we have obtained. We will refer to this row structure as Type 1.

Figure 4.2b shows a second observed molecular contrast, exhibiting rows of molecules appearing as linear groups of 2 or 3 bright spots. The orientation of these lines of spots is apparent in every other row. However, those rows in between show ambiguous orientation due to smearing of adjacent molecular contrasts. It is possible that the molecules in these smeared rows are oriented differently than those in the relatively clear rows, and that their orientation

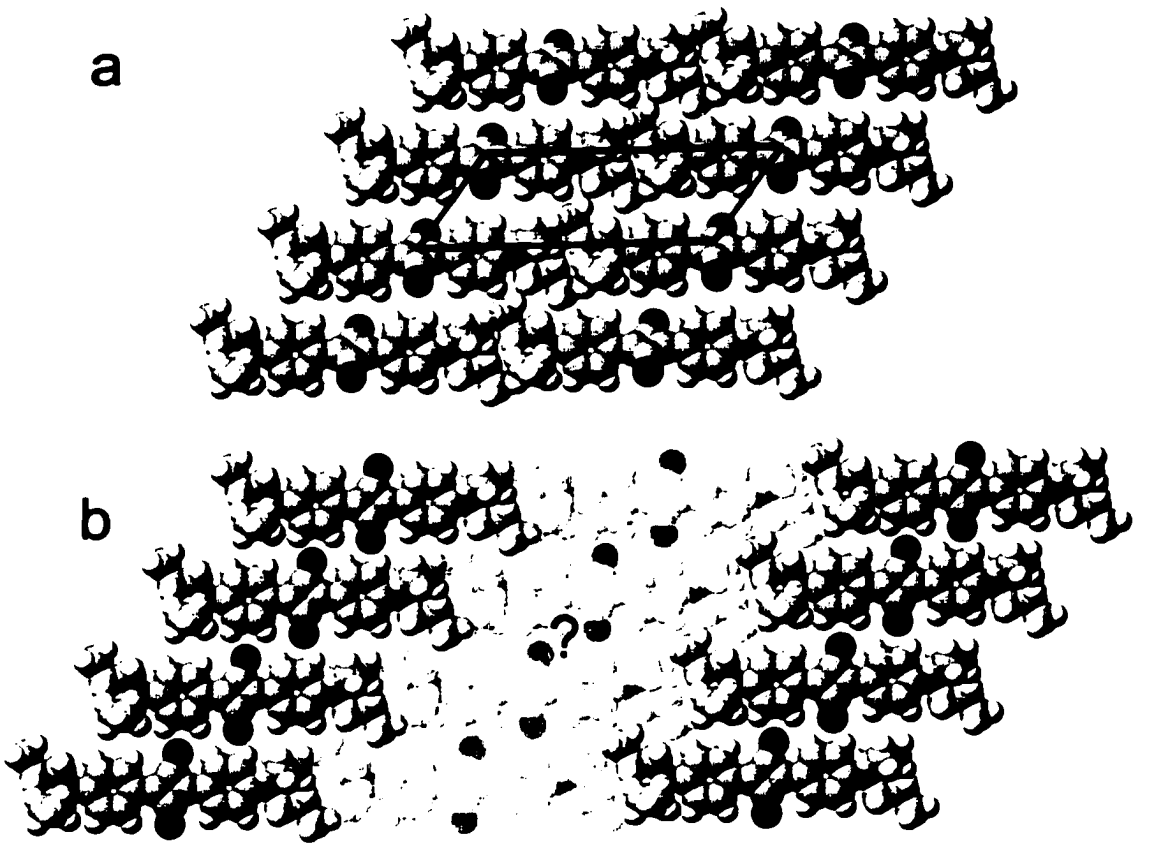

Figure 4.3: Molecular models corresponding to the adsorbed structures shown in Figures 4.2a (a) and b (b). Model (a) represents the Type 1 polymorph and (b) the Type 2 polymorph. The center row of molecules in (b) is muted to represent the ambiguity of some of the molecular rows in Figure 4.2b. In every other row, the orientation of the chromophores within the row is unclear.

resulted in an unfavorable interaction with the tip which decreased resolution. Analysis of the clear rows shows that the molecules are oriented at ~40 ° to the direction of the row, and that the distance between adjacent molecules in the same row is ~9 Å, as is usual for squaraines ordered in rows. Despite the lack of resolution in smeared rows, a periodicity of ~9 Å was determined along their length as well. Thus we can be fairly certain that the unit cell parameter *a* for this image is ~9 Å. However, the lack of resolution in the smeared rows prevents us from confidently reporting the unit cell parameter *b*. Since it is unclear if the smeared rows are oriented in the same direction as the clearly resolved rows, we cannot know whether the unit cell is one or two rows in length. We will refer to this structure as Type 2. These two possible unit cells are shown overlaid on Figure 4.2b. Figure 4.3b shows a molecular model of the identified structure of the clearly resolved rows. A third row is included in between to more easily visualize the distance measured between consecutive clearly resolved rows (~46 Å), but is dimmed to denote uncertainty in its molecular orientation.

Another series of unique molecular images, that were observed to evolve from one another, is shown in Figure 4.4. Figure 4.4 features three STM images of 3-3 HSQ adsorbed on HOPG that were taken within minutes of one another. Figure 4.4a shows a 100 nm x 100 nm image exhibiting bright rows of 3-3 HSQ molecules. These rows had the same unit cell distances as those in Figure 4.2a. Figure 4.4b, taken 3 minutes later, is a zoomed-in area from Figure 4.4a. The same single row pattern apparent in Figure 4.4a is not observed in 4.4b. Instead, two different patterns are observed within this image. The center of the image

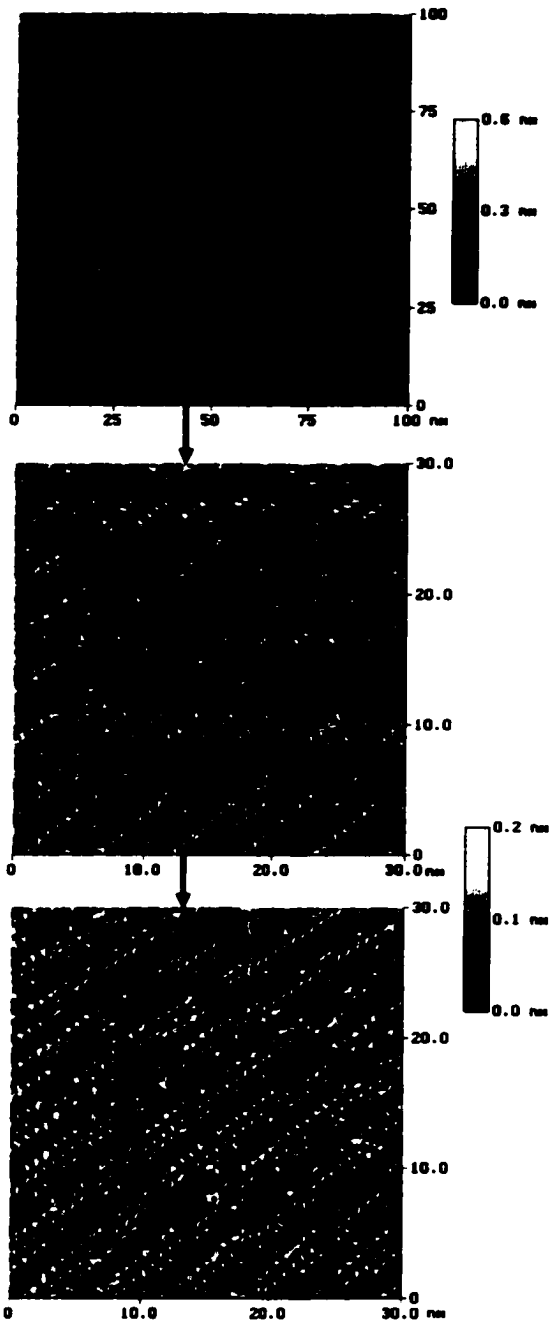

Figure 4.4: Three images showing the evolution in contrast of an area of ordered 3-3 HSQ on HOPG over the period of several minutes of scanning. (b) is a zoomed-in area of (a) and (c) is the same scan area as (b), taken a minute later. The ordered rows in (a) correspond to Type 1, whereas (b) and (c) are more ambiguous. Similarities in distances between common features in the images, however, are evidence that they are all of the same polymorph type.

exhibits pairs of bright rows. These pairs appear to be morphing into single, wide rows at the bottom of the image. The pairs of rows exhibit the same *b* and α unit cell parameters as in 4.4a, but the *a* parameter is almost exactly doubled (~42 Å). In Figure 4.4c, taken 4 minutes after 4.4b, all of the rows have transformed into the wide rows. The bright wide rows consist of 3 bright spots. The width of the bright rows, measured along the direction of the lines of spots (~52 ° to the edge of the molecular row), was found to be ~35 Å. This width is the same as the distance measured from the outside edge of a 3-3 HSQ chromophore in the single row structure shown in Figure 4.4a with the outside edge of the chromophore in the adjacent row. It is also the same distance as that measured between the outside edges of a single pair of bright rows shown in Figure 4.4b. Double-headed arrows overlaid on the images in Figures 4.4b and c show these distances. The width of the dark rows separating pairs of rows in Figure 4.4b, again measured at an angle of ~52 ° from the edge of the molecular row, was measured to be ~7 Å. This width is approximately the same as that found for the dark row width in Figure 4.4a, as well as for the dark rows in Figure 4.4c. Thus, it appears that the images shown in Figures 4.4a, 4.4b, and 4.4c are all due to the same monomolecular Type 1 row structure.

Figures 4.5a, b, and c show molecular models constructed to illustrate the changes in the molecular images observed in Figure 4.4. Model 4.5a corresponds to the pattern observed in Figure 4.4a, model 4.5b to Figure 4.4b, and model 4.5c to Figure 4.4c. All three are based upon the same row structure as that shown in Figure 4.3a. The dimmed areas of the models correspond to

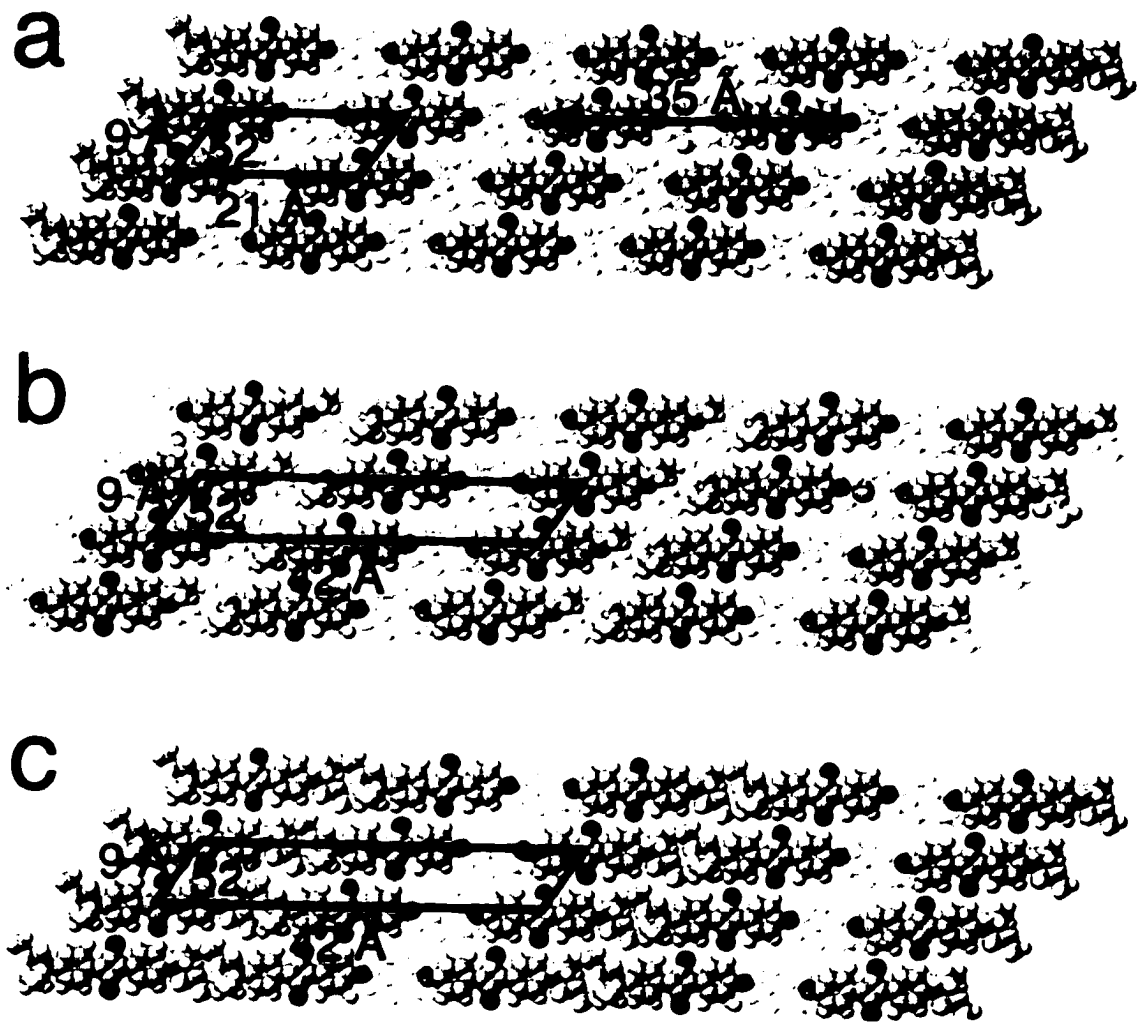

Figure 4.5: Molecular models corresponding to the images in Figure 4.4. Model (a) corresponds to Figure 4.4a, (b) to 4.4b, and (c) to 4.4c. All three models have the same Type 1 structure. The dimmed areas in each model correspond to the dark rows exhibited by each image in Figure 4.4.

the width and positions of the dark rows for each of the contrasts. We propose that the differences in the images for this structure are due to tip changes.

4-4 HSQ

4-4 HSQ is a direct analog to a hydroxylated squaraine molecule which has already been investigated with STM.[1] 4-4 HSQ and 4-4 OHSQ differ only in the presence or absence of two hydroxyl groups. As reported previously, it was found that deposition of 4-4 OHSQ solution onto the graphite surface produces somewhat noisy STM images of quasi-stable layers of adsorbed molecules ordered in relatively large (500 nm to several μm in diameter) domains exhibiting a herringbone pattern. The non-hydroxylated 4-4 SQ produced similar results. Immediately upon deposition of 4-4 HSQ solution onto the graphite surface, isolated ordered domains were observed in the STM images which then grew across the scanned area of the graphite surface to form monolayer coverage (see Figure 4.6). When the deposited solution was allowed to equilibrate before scanning was commenced, it was often observed that a single domain comprised the entire scan area, even at the maximum scan area of the STM head (2 μm × 2 μm). Thus, what may be thermodynamically stable domain shapes were not observed due to the limits in size of the scan head. When multiple domains were observed within a scan area, they were generally oblong in shape, with one set of parallel sides being much shorter (100 to 300 nm in length) than the second (500 nm to several μm). Figure 4.6 shows a portion of such a domain, with a herringbone pattern faintly visible.

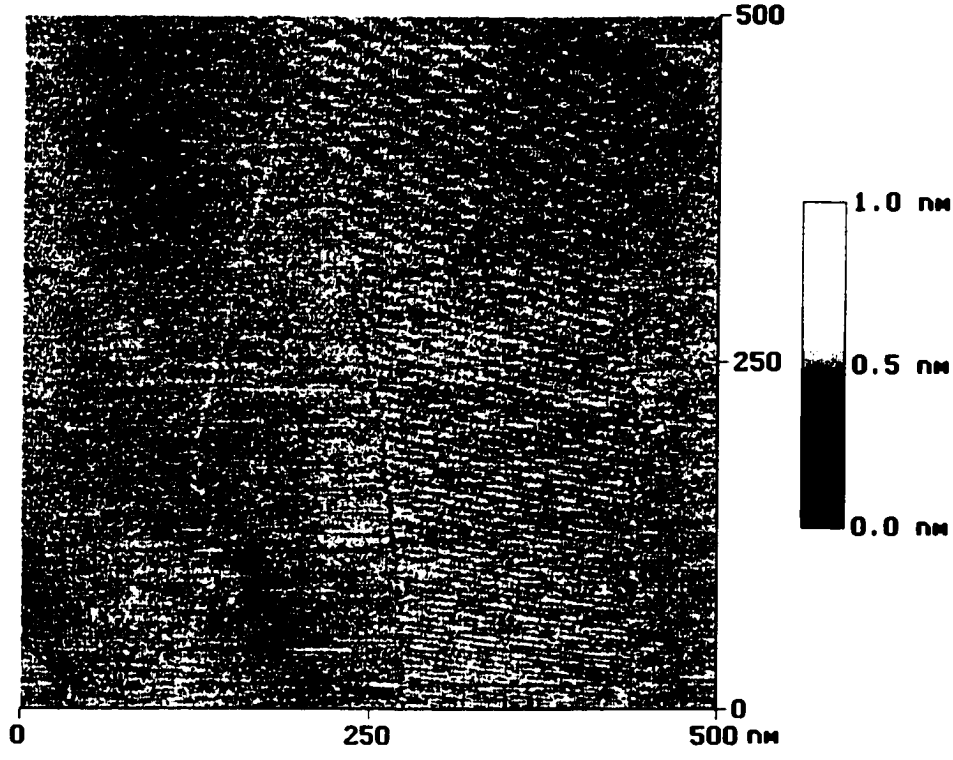

Figure 4.6: 500 nm × 500 nm image of several domains of ordered 4-4 HSQ molecules on HOPG

Figure 4.7 shows two higher magnification images of an ordered domain of 4-4 HSQ. The 20 nm x 20 nm image was zoomed-in from the 50 nm x 50 nm image in an attempt to obtain a molecularly-resolved image that clearly shows molecular orientation. From these images it is clear that the molecules are NOT ordered in a row structure. However, it is not especially clear how the molecules do orient with respect to one another. 4-4 OHSQ orders in a herringbone pattern, with donor and acceptor regions of neighboring molecules oriented towards one another. Images of 4-4 OHSQ clearly exhibit such orientation (see Figure 3.7).[1] Images of 4-4 HSQ, as typified in Figure 4.7, however, are not as clear. Glimpses of herringbone-like ordering are often observed, as can be see in the bottom portion of Figure 4.7a, but when the scan size is reduced, as in Figure 4.7b, most often only the unit cell pattern is clear. It appears that the tip images one of the two possible orientations of the adsorbed molecules easily, but has difficulty imaging the other. This could be a result of the lack of intramolecular hydrogen bonding among the molecules within ordered layers of 4-4 HSQ. As can be seen in Figure 4.8, hydrogen bonding between the hydroxyl groups located at the C-2 positions of the phenyl rings of hydroxylated-phenyl squaraine and the squaric oxygens on the molecule's central four-membered ring force the molecule into a rigid planar configuration. Lack of these hydroxyl groups, and subsequently of the hydrogen bonding, allows the phenyl moieties to rotate in solution.[12] Although interaction with the graphite surface causes the 4-4 HSQ molecules to lie flat, thus forcing a more rigid and planar configuration onto

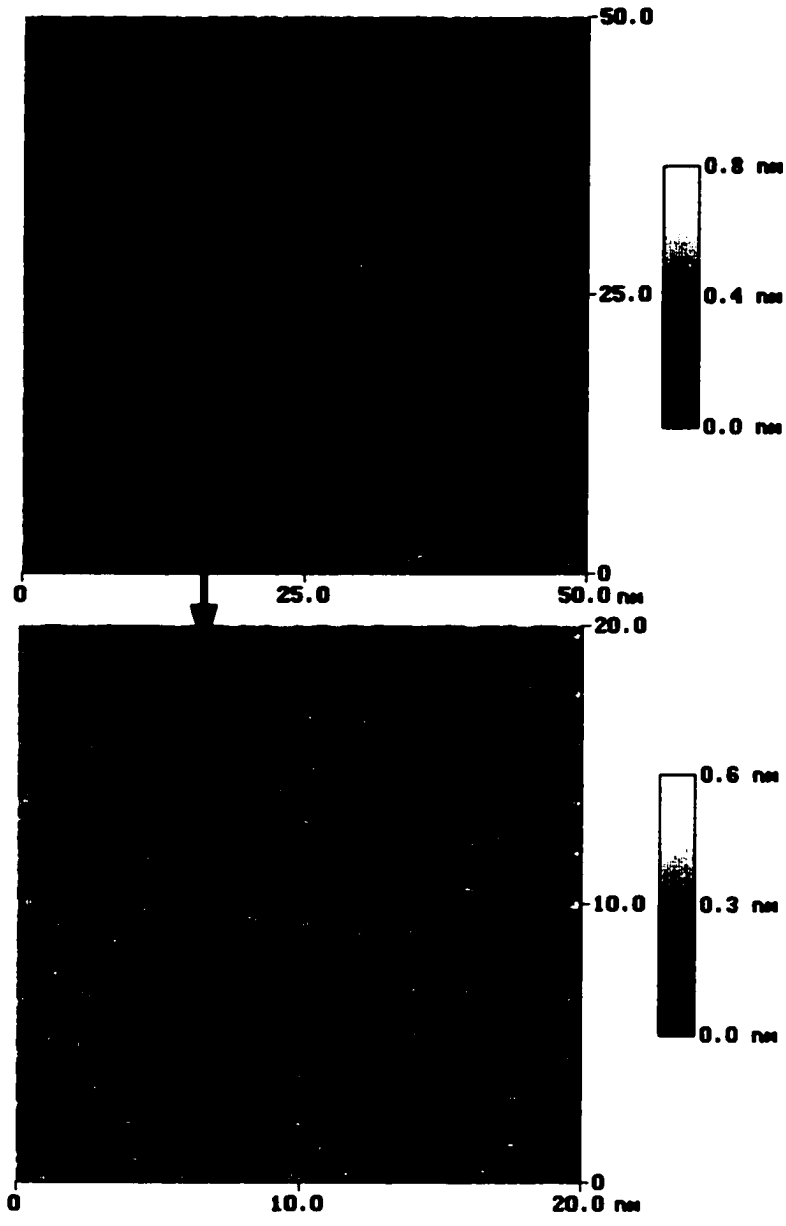

Figure 4.7: Two zoomed-in portions of an ordered 4-4 HSQ domain on HOPG. (a) 50 nm x 50 nm image showing a herringbone pattern. (b) 20 nm x 20 nm image zoomed-in from (a). The black box indicates the unit cell.

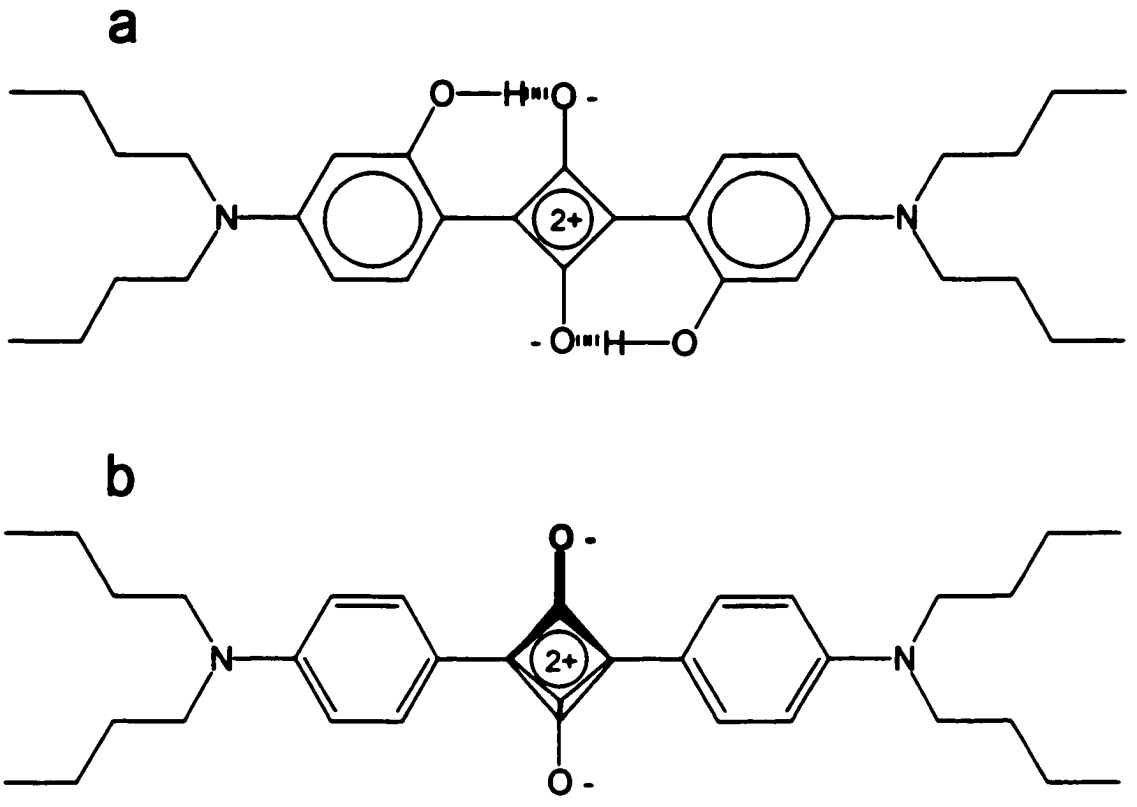

Figure 4.8: Schematics of (a) hydroxylated and (b) non-hydroxylated squaraine structures. Intra-molecular hydrogen bonding in the hydroxylated molecule holds the chromophore rigid and planar. The non-hydroxylated molecule may have a non-planar conformation, as represented by the canted C_4O_2 group.

the adsorbed molecule, there may still be some slight motion around the C-C bond connecting a phenyl ring to the square core. Because the phenyls should have a stronger interaction with the surface than that of the square core, making desorption of the phenyls unlikely, it is probably the square core that tilts out of planarity. Non-planarity of the 4-4 HSQ molecules while adsorbed on the surface makes them vulnerable to increased interaction with the scanning tip. This interaction may cause molecules that are oriented in a particular direction with respect to the direction of scanning of the tip to appear as blurs, or otherwise to decrease their image contrast. An asymmetric tip may also be responsible for selectively resolving a particular molecular orientation over another. The tips used in this study were mechanically cut. Either of these scenarios may be the cause of the loss in resolution of half of the molecules adsorbed on the surface in the majority of the small scan size images. In some rare cases, however, a distinct herringbone pattern was observed at small scan sizes, but only in small portions of the images. This is typified in Figure 4.9a. The length, width, and apparent height of the bright oblong shapes were measured to be ~ 14 Å, 5 Å, and 1-2 Å, respectively. These measurements correspond to the chromophore area of the 4-4 HSQ molecules lying flat on the graphite surface. Adjacent molecules were measured to form a 70 ± 5 ° angle to one another. This orientation allows the donor and acceptor moieties of adjacent molecules to interact. However, the proximity of molecules to one another in this orientation precludes the entire length of each of the butyl tails from lying flat on the graphite surface. In other words, each of the butyl tails is either partially or fully desorbed

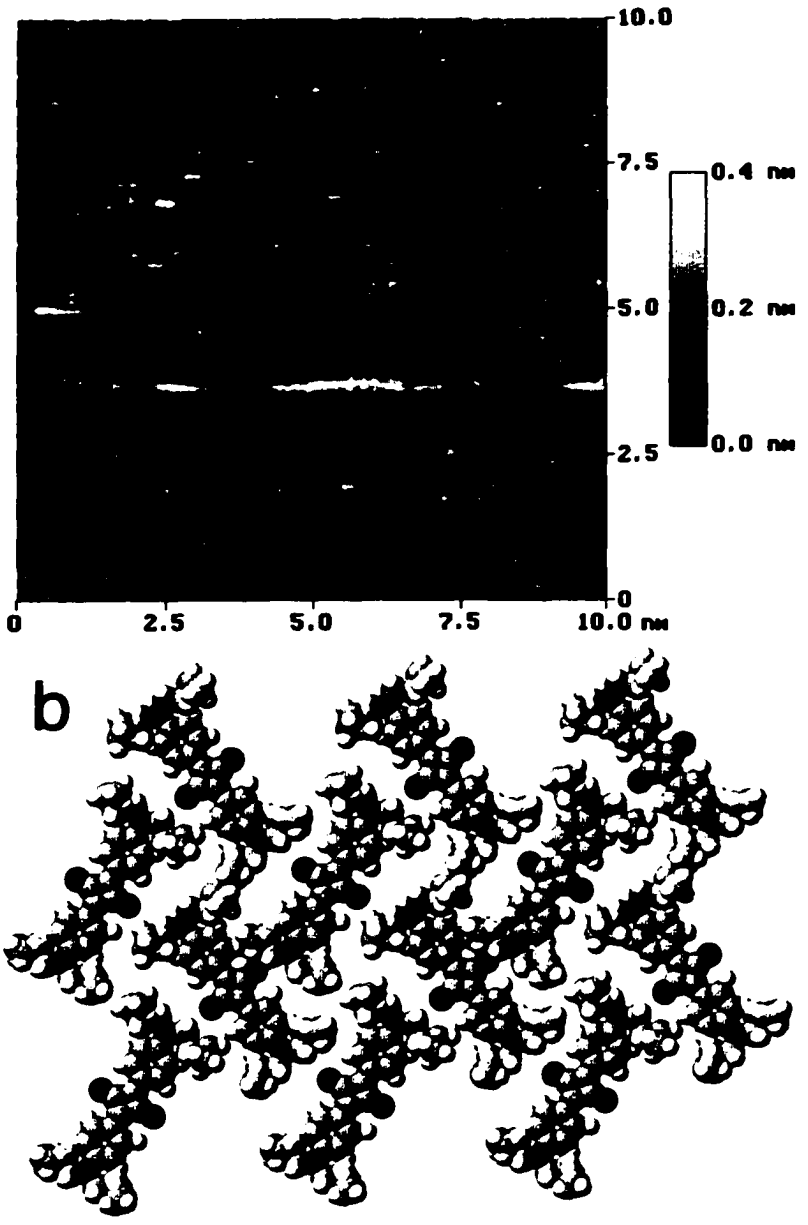

Figure 4.9: Typical partial image of 70° herringbone pattern (a) exhibited by 4-4 HSQ on HOPG and its corresponding molecular model (b).

from the surface. This tail desorption may also act to expose the donor moiety for increased interaction with the neighboring molecule's acceptor. A model of this observed herringbone structure is shown in Figure 4.9b. Images in which the herringbone pattern was resolved (Figure 4.9a, for example) produced the same unit cell parameters as those measured from images in which the herringbone pattern was not. The unit cell parameters for 4-4 HSQ on graphite are listed in Table 4.2. It is unlikely that the different images are the result of a change in polymorph. With the unit cell distances of 29 Å (*a*), 25 Å (*b*), and 85 ° (α), there is no other way for the 4-4 HSQ molecules to pack while lying flat on the surface without overlapping, and at the same time maintaining attractive intermolecular interactions. This packing structure is essentially the same for that observed with 4-4 OHSQ adsorbed on graphite.[1] The 80° and 90° herringbone structures observed for 4-4 OHSQ on HOPG were not observed for 4-4 HSQ, however. This does not necessarily mean that they are not formed for 4-4 HSQ. Rather, the transition from 90° to 80° to 70° herringbone structures may have occurred on a faster timescale than that observable by STM.

8-8 HSQ

Like 4-4 HSQ, 8-8 HSQ is an analog to a hydroxylated squaraine molecule that has already been investigated with STM. 8-8 HSQ and 8-8 OHSQ differ only in the presence or absence of two hydroxyl groups. As reported previously[1], it was found that deposition of 8-8 OHSQ solution onto the graphite surface produces clear STM images of stable layers of adsorbed molecules ordered in domains composed of alternating bright and dark rows. The non-hydroxylated

8-8 SQ produced similar results. Immediately upon deposition of 8-8 HSQ solution onto the graphite surface monolayer and sometimes multilayer coverage of ordered domains were observed in the STM images (see Figure 4.10). Domains were typically about 500 nm x 500 nm in size of irregular shape with jagged edges. In contrast, 8-8 OHSQ typically produced much smaller domains on the order of 50 nm x 50 nm which were rhomboid in shape with faceted domain boundaries. As can be seen in Figure 4.11, domains of 8-8 HSQ also exhibited a high density of missing-molecule defects that ranged in size from about 2 nm x 3 nm (spanning across one molecular row) to 50 nm x 75 nm (spanning tens of rows). Such defects were not observed in domains of 8-8 OHSQ, however.

Closer investigation of these domains showed that two types of row polymorph are exhibited by 8-8 HSQ. The first type produced bright rows measuring 13.7 ± 1.6 Å in width and dark rows of 8.9 ± 1.6 Å (both measured perpendicular to the edge of the row). These measurements correspond well with the length of a squaraine chromophore (~14 Å) and the length of an octyl tail (~10 Å). The height of the bright rows relative to the dark rows (1 ± 0.5 Å) is within the range of relative heights typically measured for π systems adsorbed lying flat on the graphite surface[8] suggesting that the squaraine chromophore is likewise lying flat on the graphite surface. At small scan sizes it was possible to discern individual phenyl rings within the bright rows (seen as a pair of bright spots). An example of sub-molecular resolution of the Type 1 polymorph can be seen in Figure 4.12. The distance between chromophores within the same

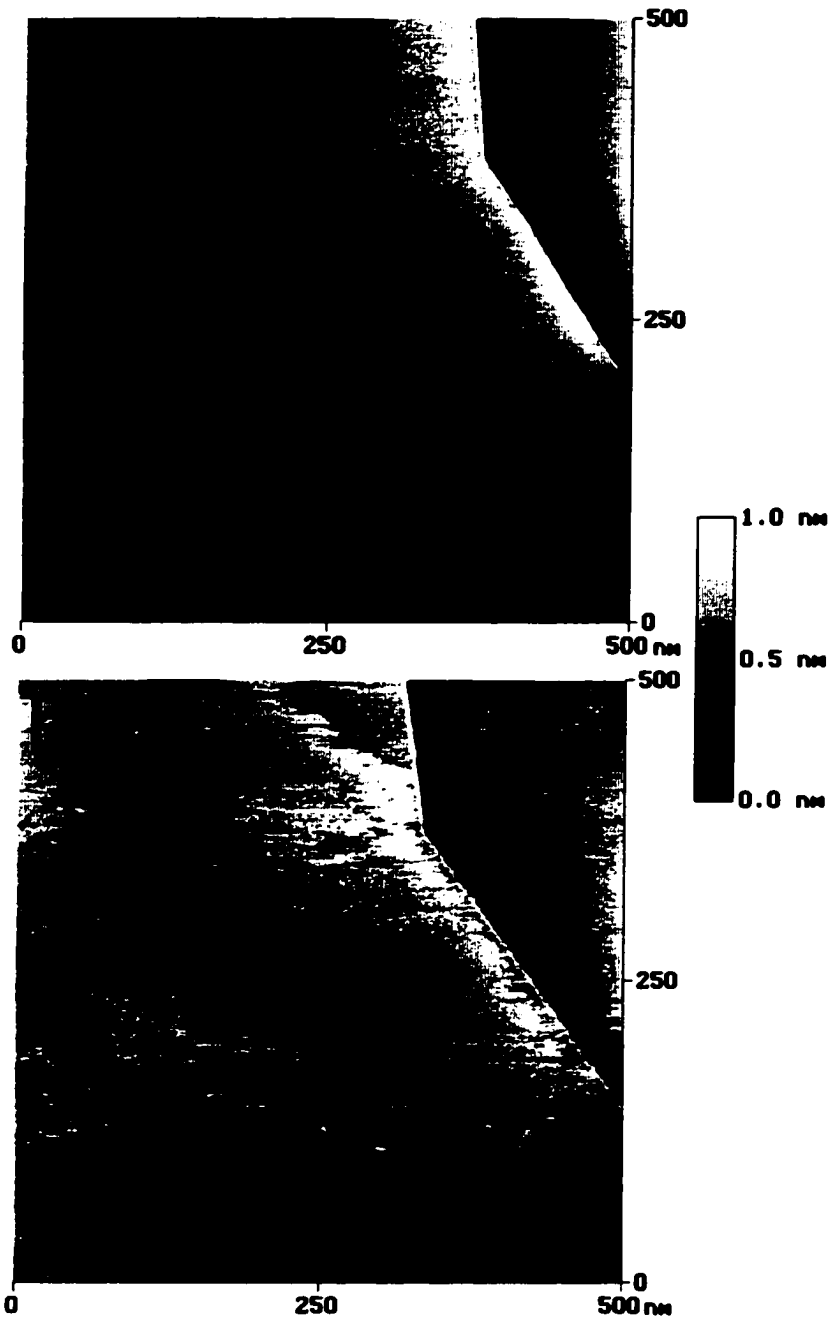

Figure 4.10: 500 nm × 500 nm STM images showing the timelapsed adsorption of 8-8 HSQ onto HOPG. (a) Image showing a bare HOPG surface just before solution deposition. (b) Image obtained a few minutes after solution deposition showing the adsorption of ordered domains of 8-8 HSQ.

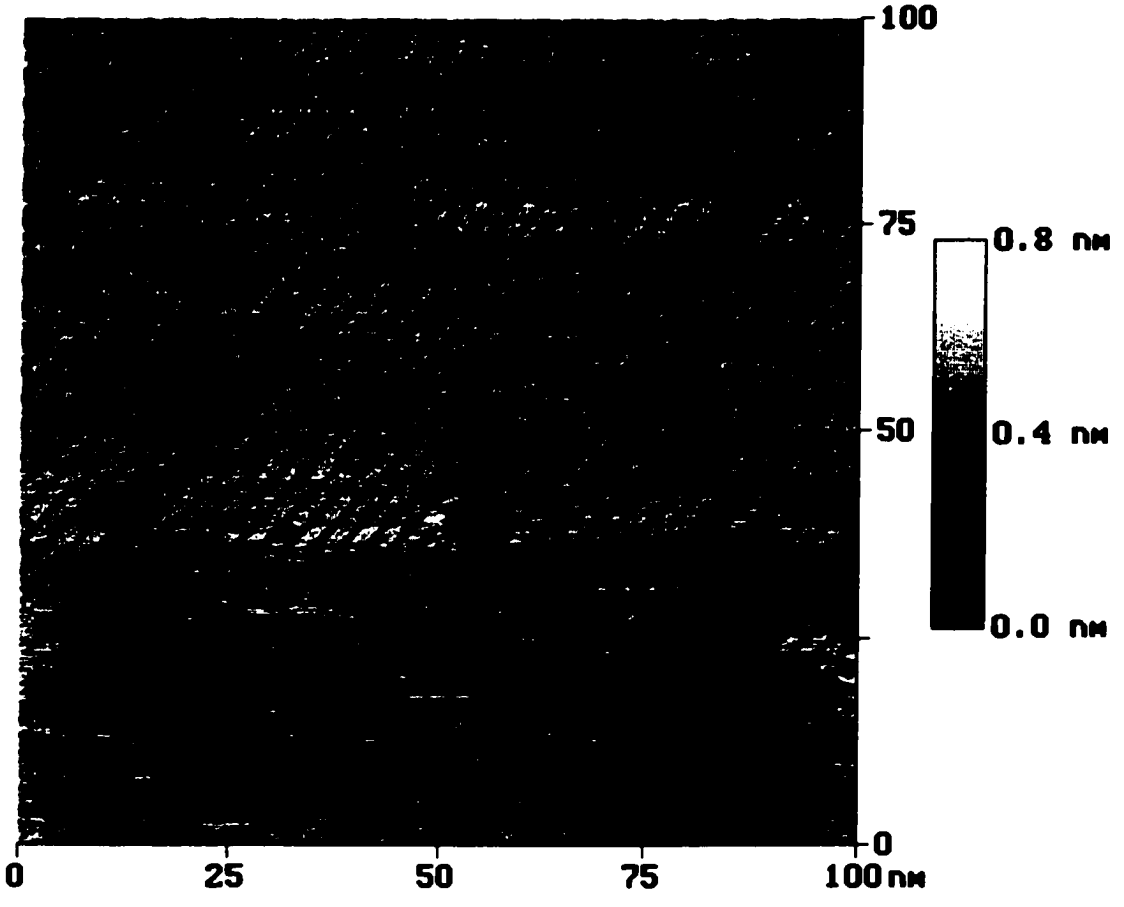

Figure 4.11: 100 nm × 100 nm STM image showing several missing-molecule defects within a domain of ordered 8-8 HSQ. The bottom of the image shows a change in contrast probably due to tip changes. It is also possible that the domain is multilayered, and the top layer of molecules has been stripped away, revealing a lower layer in the bottom portion of the image.

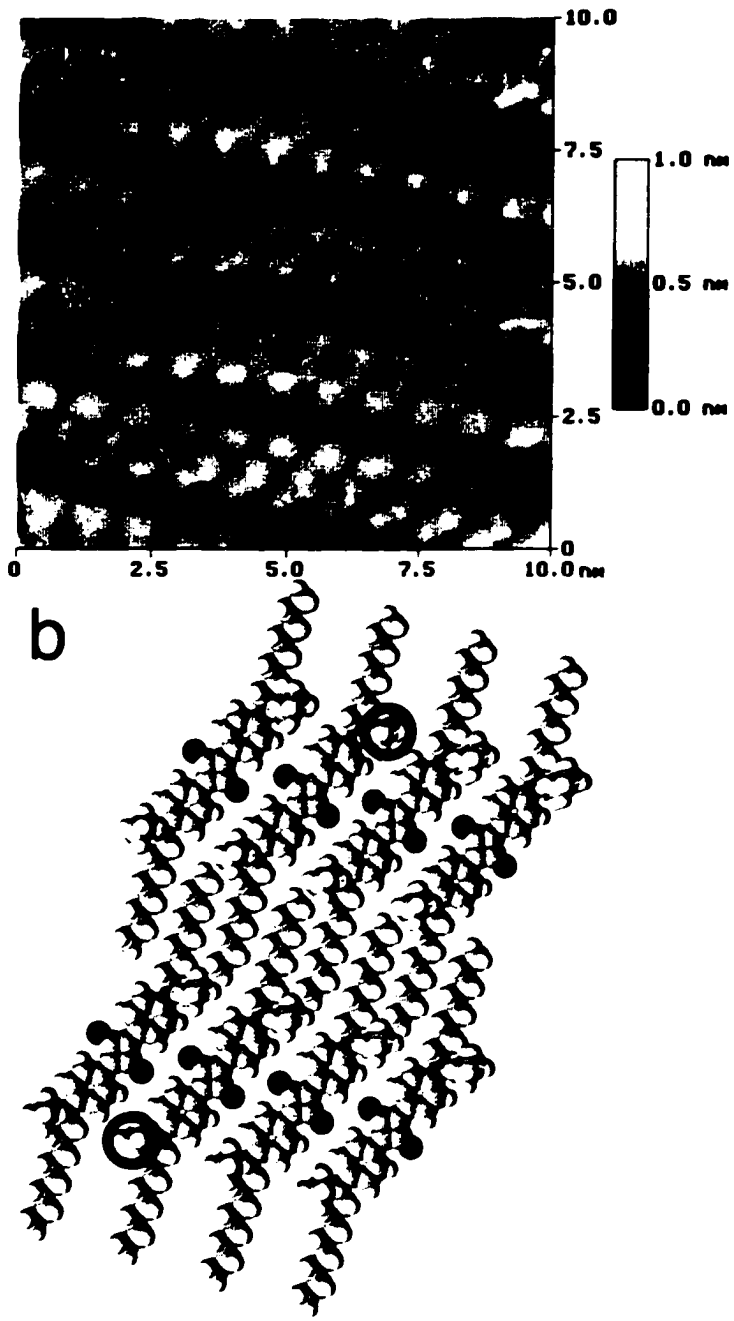

Figure 4.12: High resolution STM image (a) and model (b) of the Type 1 row structure of 8-8 HSQ adsorbed on HOPG. Circles overlaid on the image may correspond to the octyl tails protruding from the surface (elucidated by circles on the model).

molecular row was measured to be 3.1 ± 0.5 Å. Thus, we assume that only two of the octyl tails (one from each dialkylamino group) can be adsorbed onto the surface in this row structure. The ~9 Å width of the dark rows further prescribes that the adsorbed alkyl tails from adjacent molecular rows must be interdigitated, thus introducing attractive alkyl-alkyl dispersion interactions as well as alkyl-graphite dispersion interactions to the ordered structure. The remaining alkyl tails may lie on top of the adsorbed alkyl tail, on top of the chromophore, or extend up from the surface where it is solvated by the phenyloctane. Evidence of the latter three-dimensional adsorbate structure may be present in Figure 4.12a. In some molecular rows of 8-8 HSQ in Figure 4.12a, a small bright spot (indicated by arrows) exists to the outer side of one or both of the phenyl rings in the squaraine chromophore. These spots add 2 to 3 Å per spot to the length of the chromophore, producing a total length of 18 to 21 Å (for a chromophore exhibiting 2 spots). It is possible that these spots are the desorbed octyl tails acting as antennae to the scanning tip. The resolution of these spots provides the best evidence thus far that the desorbed alkyl tails most likely orient perpendicular to the plane of the chromophore, being partially solvated by the phenyloctane solvent. The fact that these spots are observed in only a small percentage of the total experiments points to the reality that tip-molecule interaction can change molecular contrast in STM images, and parameters like scan angle, rate, and tip shape can affect this interaction.

By measuring the angle between the direction of the bright stripe and the long axis of the bright football shapes within the stripe, it was found that the 8-8

HSQ molecules within a row orient 65 ± 6° to the direction of the row. This angle results in an offset between adjacent molecules of ~ 3 Å, allowing alignment of their respective donor and acceptor moieties. The proposed model of this molecular packing is shown in Figure 4.12b. This structure is very similar to the "slipped-stack variant structure" proposed by Law et al for 1-1 HSQ solution aggregates.[13] Hence the D-A interaction between adsorbate molecules is preserved in the row structure despite the introduction of dispersion interactions between akyl tails with other alkyl tails and the substrate.

A second type of row polymorph was observed in domains of adsorbed 8-8 HSQ. The measurements for this polymorph were within experimental error of the type 1 polymorph just described in all respects except one. In Figure 4.12 it is clear that all of the chromophores in adjacent bright rows of the type 1 polymorph are oriented in the same direction. As can be seen in Figure 4.13, however, chromophores in adjacent rows of polymorph type 2 are not oriented in the same direction. Rather, they alternate direction from one row to the next in an A, B, A, B pattern. Thus, if the angle of the chromophores to the left edge of row A was measured to be ~115°, the same angle measured for row B would be~65°, and the next row A ~115° again. The angle between chromophores of adjacent rows is ~130°. As a result of this alternating pattern, polymorph two has an *a* unit cell parameter that is twice as long as that for the unit cell of polymorph 1 (see Table 4.2). The packing densities and molecular areas measured for both polymorphs 1 and 2 are the same, however. The structure of polymorph 2 arises from the fact that there are four different geometries possible for a squaraine

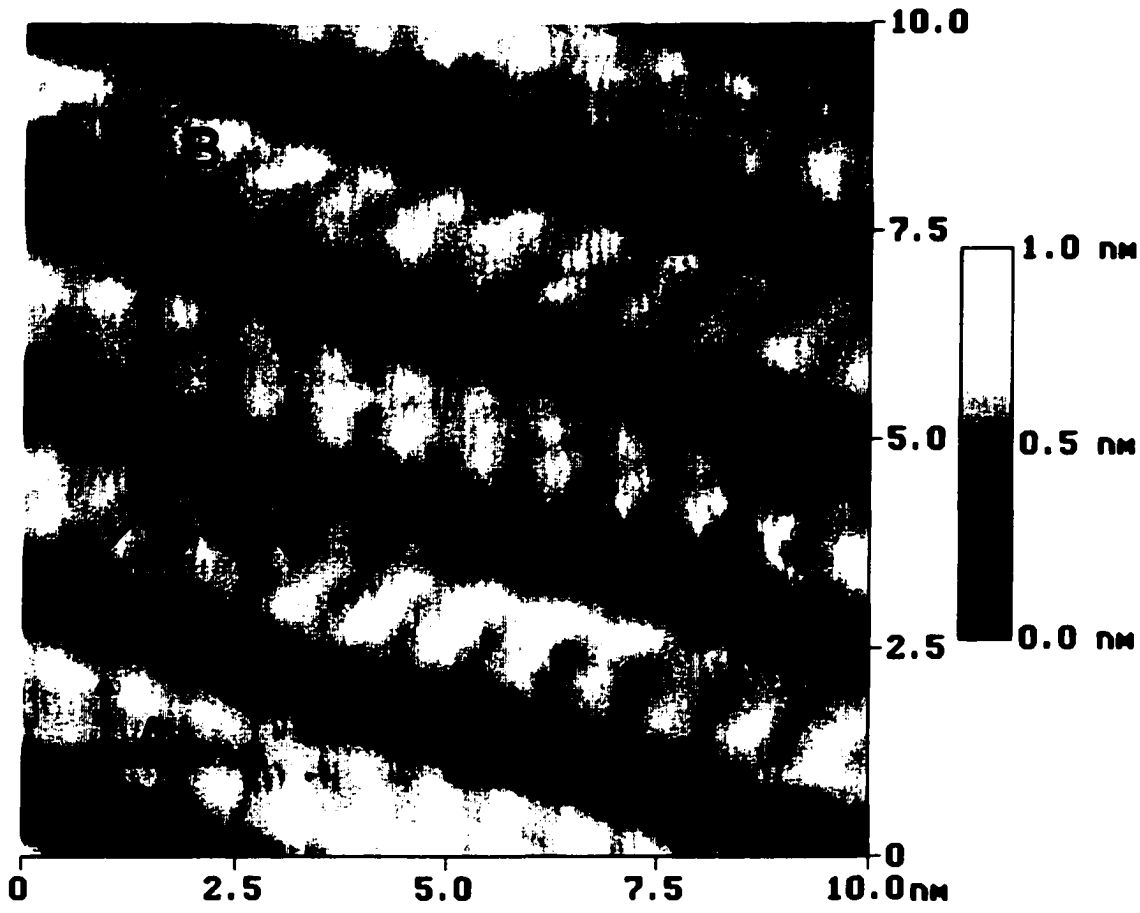

Figure 4.13: High resolution STM image showing the Type 2 row structure. It can be clearly seen that the orientation of the chromophores within the molecular rows alternates from row to row.

molecule which is ordered in an interdigitated-tail row structure. Two of the alkyl tails (one from each dialkylamino group) must lie adsorbed on the surface and two must be desorbed. The two cis and two trans alkyl tails configurations that are possible for squaraine molecules, that are under these constraints, are shown in Figure 4.14. It should be noticed that there is no structural difference between between cis 1 and 2 geometries. Cis 2 may be obtained by a simple 180° (C_2) rotation of cis 1 along the axis normal to the molecular plane. Trans 3 and 4 geometries, however, are structurally different from one another. Trans 4 is a mirror plane reflection of trans 3; thus they are enantiomers of one another. Although polymorph 2 utilizes the same packing scheme (same intermolecular distances, angles, and intermolecular forces) as polymorph 1, type 1 is composed only of rows of trans 3 or 4 geometries, whereas type 2 is composed of alternating rows of trans 3 and 4. It is important to note that trans 3 and 4 do not coexist in the same row. Thus, the populations of trans 3 and trans 4 squaraine geometries are different between the two types. Domains of the type 1 polymorph are composed entirely of squaraine molecules configured in one of the trans geometries, whereas domains of type 2 polymorph have roughly equal populations of both trans geometries. Hence, it appears that squaraines of different geometries can coexist within the same domain, however, they segregate at the level of rows. In addition, it has been shown that the 2 enantiomers (trans 3 and 4) are distinguished from one another within polymorph 2, but not within polymorph 1 (since it is either all trans 3 or all trans 4).

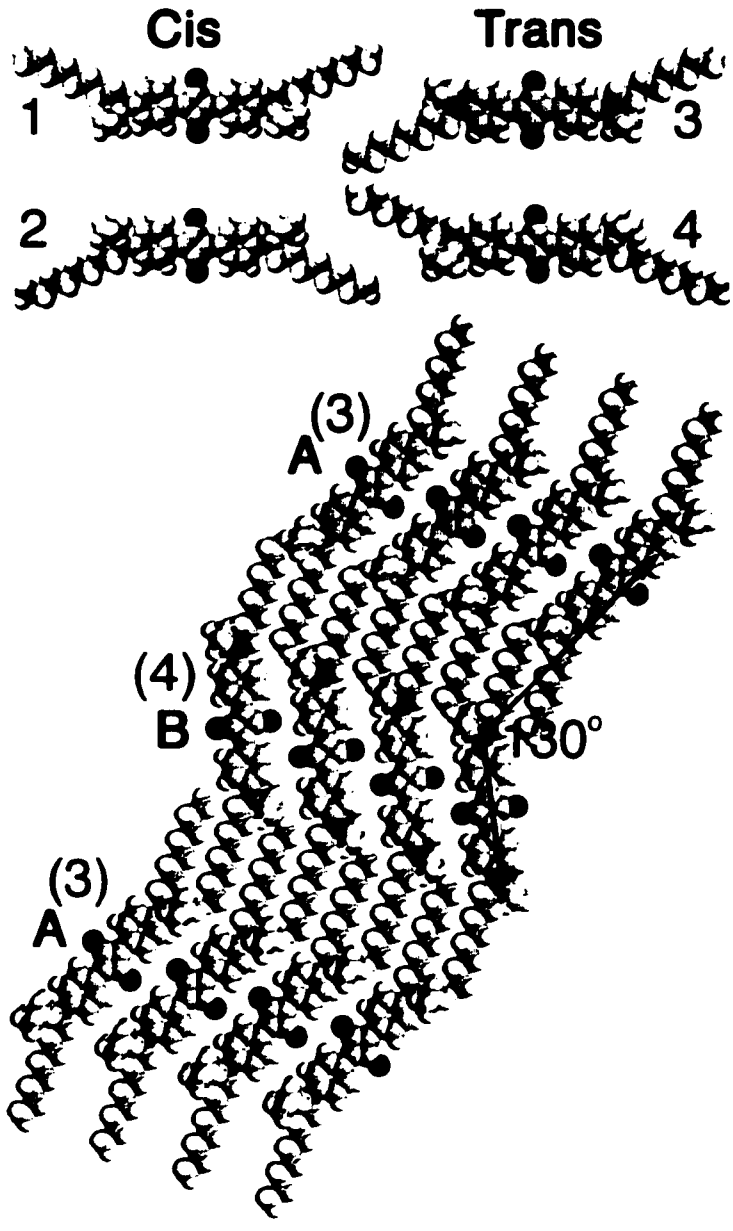

Figure 4.14: Models showing the four different geometries possible for a squaraine molecule adsorbed in a row structure. The conformations differ in the geometry of the tails, being either Cis (1 and 2) or Trans (3 and 4). The model below illustrates the Type 2 row structure observed for 8-8 HSQ. The chromophore orientation switching from row to row can be explained by alternating rows of Trans 3 and Trans 4 geometry squaraines.

It is not clear as to whether adsorbed molecules in the trans 3 or 4 conformations may switch back and forth between conformations, or whether a single conformation is permanently adopted by an adsorbed molecule. A squaraine molecule adsorbed onto the substrate surface transitioning from the trans 3 conformation to the trans 4, or vice versa, must overcome several potential barriers. Firstly, the 2 alkyl tails of the squaraine molecule that are adsorbed onto the substrate surface must desorb and the molecule's chromophore must rotate on the surface to adopt an orientation which provides adequate surface area for the solvated tails to adsorb. Then the solvated tails must break free of the dispersion interactions with the solvent and overcome any steric interactions with molecules/tails adsorbed on the surface that lie in the way of its optimum orientation with the substrate atoms. If such a transition from one adsorbed conformation to another were to occur it would most likely be a concerted effort on the part of entire ensembles of molecules, rather than one molecule at a time. The individual transformation of molecules within an assembly would require the separate reorganization of each of the molecules surrounding the transitioning molecule with each transition event, thus making the occurrence of transitions less likely. It is not known whether the trans 3 and 4 populations of these 2 observed polymorphs are a direct result of the composition of squaraine aggregates in the solution above the surface, or of the local surface environment. If the structure of solution aggregates plays a dominant role in the structure of adsorbed domains, then it is likely that the

conformation of the molecule within the aggregate is maintained on the surface and retained over time, thus keeping trans 3 and 4 populations constant. Conversely, if the adsorbed molecules are sensitive to changes in local environment, it is conceivable that populations of trans 3 and 4 may change over time through conformational transformations. Thus far there has been no evidence that adsorbed domains undergo interconversion between polymorphs 1 and 2, thus it does not appear that squaraine molecules transform from one conformation to another, changing the local populations of trans 3 and 4.

1-8H Squaraine

Although not a direct analog of any of the molecules in the hydroxylated squaraine series presented previously[1], 1-8 HSQ represents a less symmetric squaraine molecule, akin to 2-18 OHSQ. With 2 octyl tails and 2 methyl tails 1-8 HSQ is similar to an 8-8 HSQ molecule that is adsorbed onto the surface with 2 of its tails adsorbed on the surface and 2 solvated. Thus it is not surprising that 1-8 HSQ and 8-8 HSQ showed essentially the same ordering characteristics when investigated with STM. Like 8-8 HSQ, monolayers and sometimes multiple layers of ordered domains of 1-8 HSQ were observed immediately upon solution deposition. As can be seen in Figure 4.15, these domains are similar to those produced by 8-8 HSQ. Dimensions for domains of 1-8 HSQ ranged from 100 nm x 50 nm to micron sized. Like 3-3 HSQ and 4-4 HSQ, it was not possible to observe these domains with normal squaraine parameters (–2.0 V, 40 pA) due to substantial noise. Lowering the sample voltage to –1.0 V and the setpoint current to ~30 pA reduced the noise and allowed the domains to be imaged.

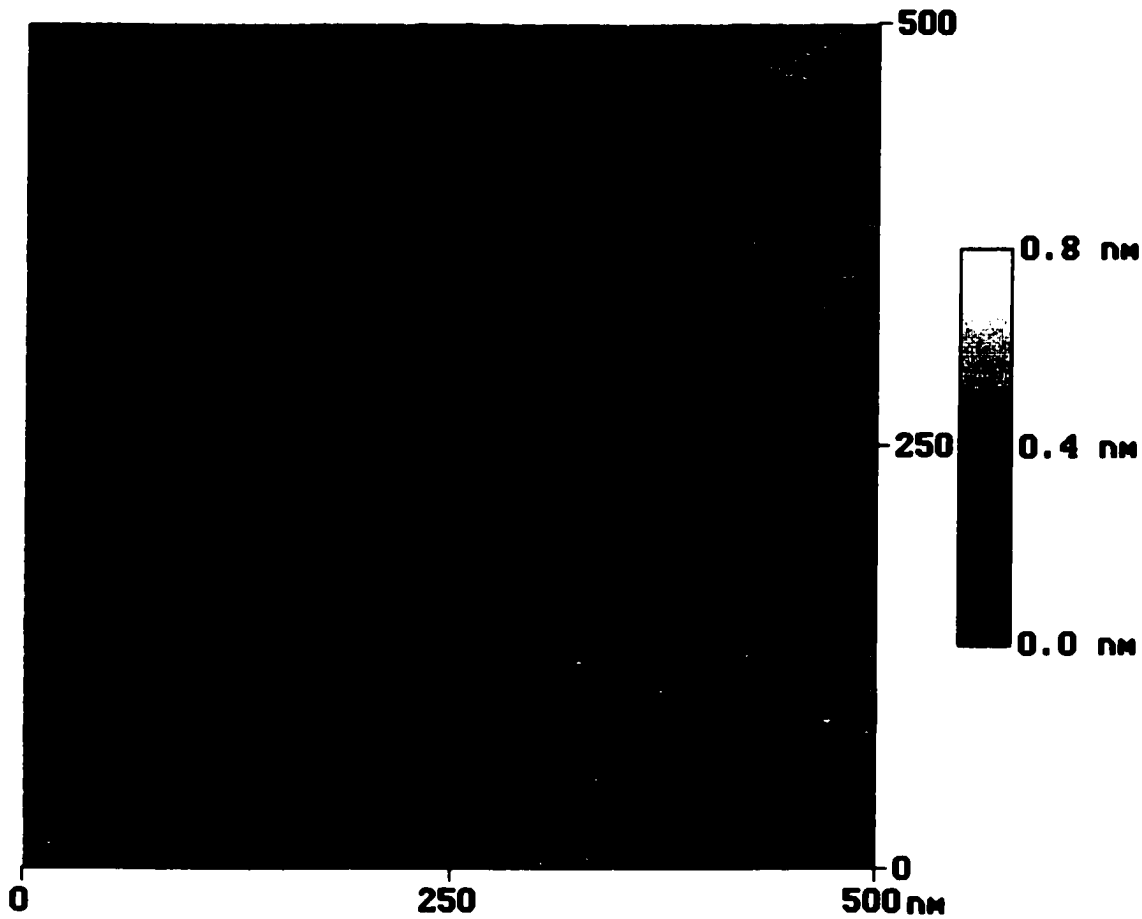

Figure 4.15: 500 nm × 500 nm image of several domains of ordered 1-8 HSQ molecules on the HOPG surface.

Investigation of these domains showed that at least two types of row polymorph of the same type as those exhibited by 8-8 HSQ are exhibited by 1-8 HSQ. The first type, as can be seen in Figure 4.16a, produced bright rows measuring 12.8 ± 1.3 Å in width and dark rows of 9.0 ± 1.6 Å (both measured perpendicular to the edge of the row). Both the measurements of the bright and dark rows correspond well with the length of the chromophore (14-15 Å) and an octyl tail (~10 Å). The relative height of the bright rows as compared to the dark rows (1.2 ± 0.2 Å) is within the range of relative heights typically measured for π systems adsorbed lying flat on the graphite surface[8] suggesting that the squaraine chromophore is likewise lying flat on the graphite surface. The angle of the 1-8 HSQ chromophore with respect to the edge of the molecular row was measured to be 50 ± 4°. This angle is within experimental error of that of the 8-8 HSQ type 1 polymorph. The distance between chromophores within the same row was measured to be 3.1 ± 0.5 Å. As we have seen already in the symmetrical row-forming squaraines, such a small distance between adjacent molecules within the same row precludes the adsorption of all 4 alkyl tails onto the HOPG surface, and necessitates the desorption of one alkyl tail from each side of the chromophore. The 1-8 HSQ molecule, due to its lower symmetry and the small size of the methyl groups, does not need to desorb one tail from each end of the molecules to accommodate the strong intermolecular interaction between adjacent squaraine chromophores within the same molecular row. The

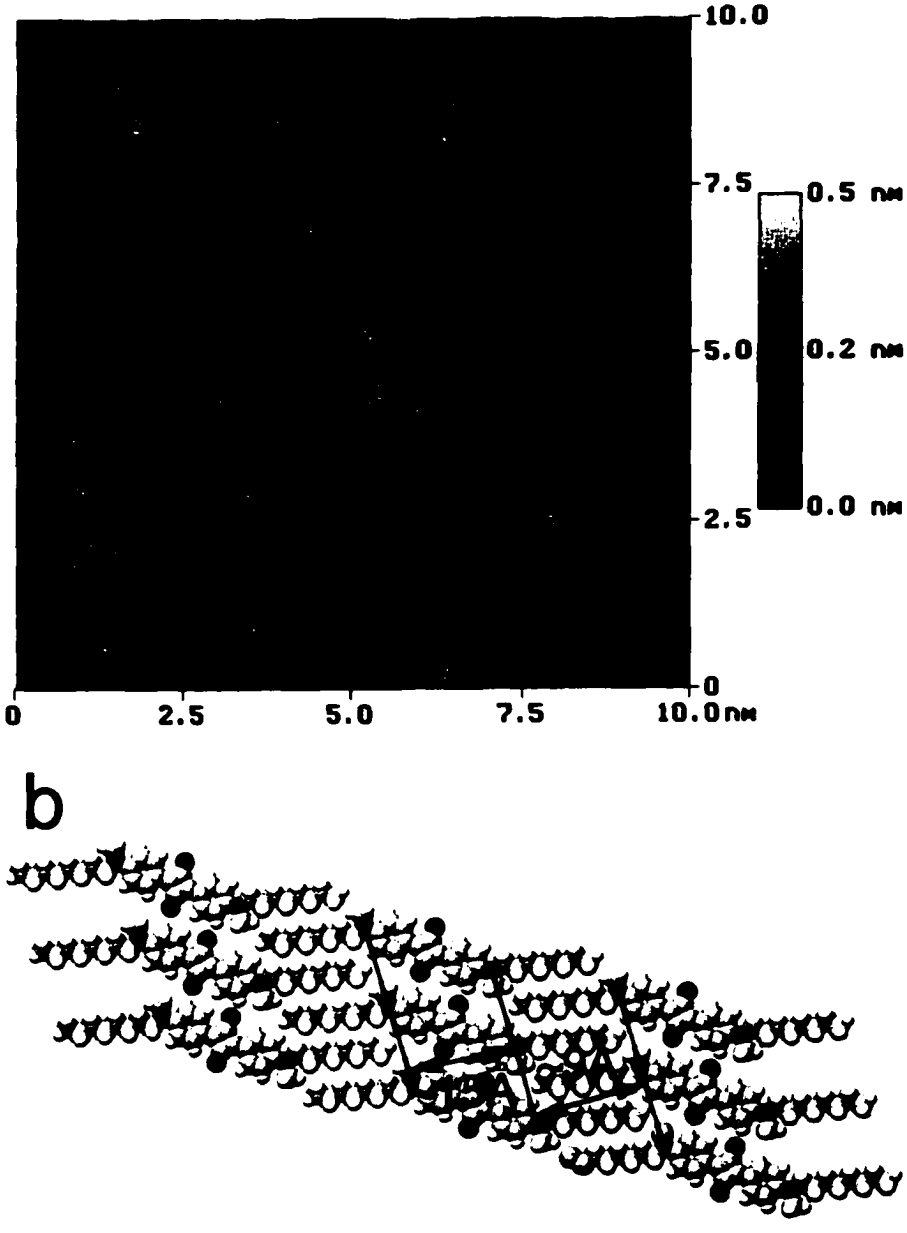

Figure 4.16: 10 nm x 10 nm high resolution STM image (a) and molecular model (b) showing the Type 1 polymorph structure of 1-8 HSQ adsorbed on HOPG.

2 methyl tails of 1-8 HSQ are short enough that all 4 alkyl tails may lie on the HOPG surface at once. Thus like 8-8 HSQ and 8-8 OHSQ, the octyl tails of 1-8 HSQ lie on the HOPG surface, forming a dark trench in the STM image, and interdigitate with the octyl tails from the molecules in the adjacent molecular row. The methyl tails lie within the trenches as well, but because of their small size, do not sterically interfere with the interdigitated tails of the molecules in the next row. A model for this proposed mode of packing is shown in Figure 4.16b. Although the presence of the methyl tails adsorbed on the surface adds to the dispersion interaction between the adsorbed molecule and the HOPG lattice, the 50 ° angle of the molecule to the edge of its rows allows it to maintain a strong donor-acceptor intermolecular interaction.

As mentioned, the second type of row packing observed for 1-8 HSQ is of the same type as the second exhibited by 8-8 HSQ. Although not as clear as in the 8-8 HSQ image, with the aid of arrows in Figure 4.17a, the orientation of rows chromophores can be seen alternating within the same domain. The angle of the molecule to the edge of the row alternated from 65° to 115°, with a 130° angle between molecules in adjacent rows. As with 8-8 HSQ, molecules were not observed to transform between the two trans forms. A 3 Å distance was measured between adjacent 1-8 HSQ molecules within the same row. This factor and the 65 ° angle of the molecules to the edge of the row allowed for maximum donor-acceptor intermolecular interaction. A molecular model for this row type is shown in Figure 4.17b.

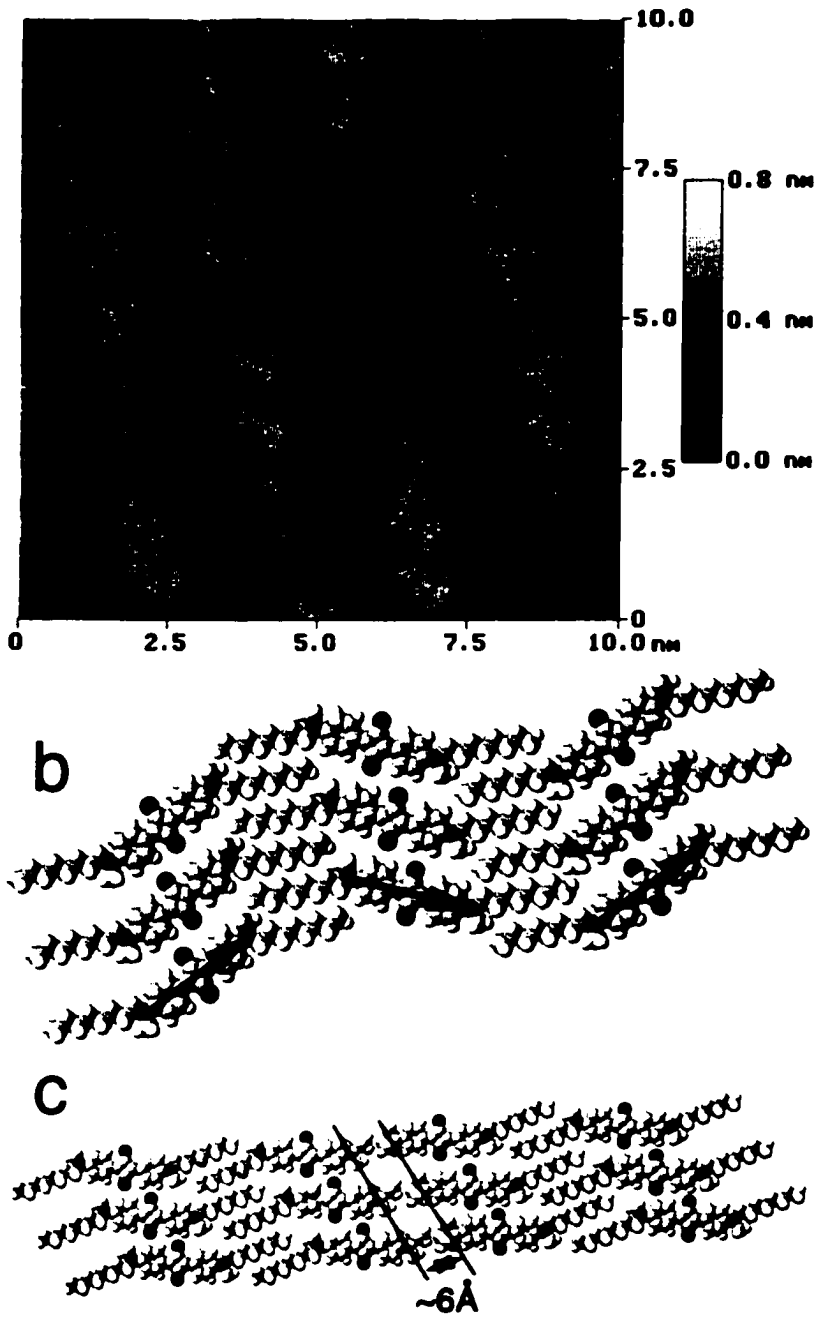

Figure 4.17: 10 nm × 10 nm STM image (a) and molecular model (b) showing the Type 2 polymorph structure of 1-8 HSQ adsorbed on HOPG. A third conceivable polymorph (Type 3) is shown in the model in (c). This polymorph was not experimentally observed.

Looking at Table 4.2 it can be seen that the unit cell parameters of both 1-8 HSQ type 1 and type 2 polymorphs are within experimental error of those of the 8-8 HSQ polymorphs. Because only 2 tails (1 from each side of the molecule) are involved in the surface packing of 8-8 HSQ and because of the sterically-insignificant size of the methyl tails in the 1-8 HSQ molecule, on the surface these molecules are effectively the same in two dimensions. One might even assume that other asymmetric analogs of the 8-8 HSQ molecule (up to 7-8 HSQ) would likewise exhibit the same molecular packing on HOPG. Since the designation of which tail ends up adsorbed to the surface is probably determined by length of the tail, with the longer tail achieving a larger dispersion interaction with HOPG, and thus preference for adsorption, any tail longer than 8 would probably cause an increase in the unit cell *a* parameter. Thus, it makes sense that 1-8 HSQ would exhibit the same unit cell distances as 8-8 HSQ for the types 1 and 2 polymorphs. A third polymorph is conceivable for the 1-8 HSQ molecule, in which the octyl tails desorb from the surface and the methyl groups remain, thus producing a much smaller in length *a* parameter. A molecular model for this polymorph is shown in Figure 4.17c. Such a polymorph is highly improbable, however, following the argument above that when it is not possible for all 4 alkyl tails to adsorb at once (due to sterics) the one alkyl tail from each dialkylamino moiety with the larger dispersion interaction with HOPG will preferentially adsorb. Furthermore, in the case where it *is* possible for all for alkyl tails to adsorb (as with 1-8 HSQ), it is unlikely that any tails would desorb, as this would decrease the overall interaction of the adsorbate with the substrate, with seemingly no gain

in intermolecular interaction. Expectedly, this third polymorph was not observed in our investigation of 1-8 HSQ.

1-6 HSQ

1-6 HSQ does not have a previously-studied analog, neither a hydroxylated 1-6 HSQ molecule nor a symmetric 6-6 HSQ or 6-6 OHSQ. The fact that the 1-8 HSQ molecule exhibited the same structures as 8-8 HSQ, suggests that 1-6 HSQ would likewise exhibit the same structures as a 6-6 HSQ.

1-6 HSQ produced very large (several μm in diameter) domains. These domains were often multiple layer, with non-uniform pits extending through the depth of the layers. Figure 4.18a shows a 3 μm x 3μm image with such pits. Figure 4.18b is a 1 μm x 1μm zoomed-in area of 4.18a which more clearly shows the 2 molecular layers that the pits extend through. Pits such as these have not been observed for any of the previously investigated squaraines except 1-1 OHSQ deposited on HOPG via CH_2Cl_2 solution deposition (with tapping mode AFM)[14]. Smaller scan sizes reveal that the domains are composed of the familiar molecular lamella. An 8 nm x 8 nm molecular-resolution image of a single layer of rows is shown in Figure 4.19a. Bright rows measure 10.0 ± 0.8 Å in width (measured perpendicular to the edge of the row), and dark 8.0 ± 0.8 Å. These distances correspond well to the length of a squaraine chromophore oriented at an angle to the row, and to a fully-interdigitated hexyl tail, respectively. As is common with most of the row forming squaraines, the chromophores orient at an ~50° angle to the edge of the row, allowing donor-acceptor interactions between adjacent chromophores in the same molecular row. A model for this observed

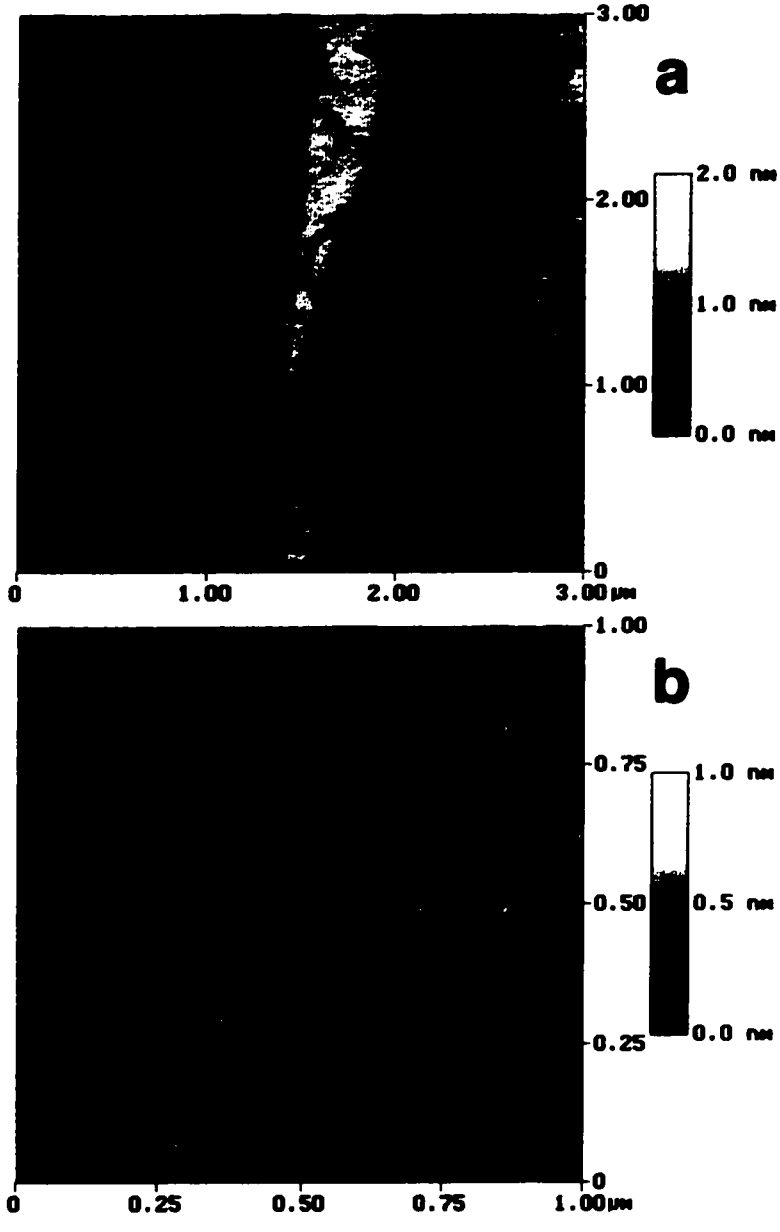

Figure 4.18: Two STM images showing the multiple layer adsorption of 1-6 HSQ on HOPG. (a) 3 μm x 3μm image exhibiting smooth molecular layers devoid of domain boundaries, but spattered with irregularly shaped pits. (b) 1 μm × 1 μm image zoomed-in from (a) showing the multiple-layer nature of these pits.

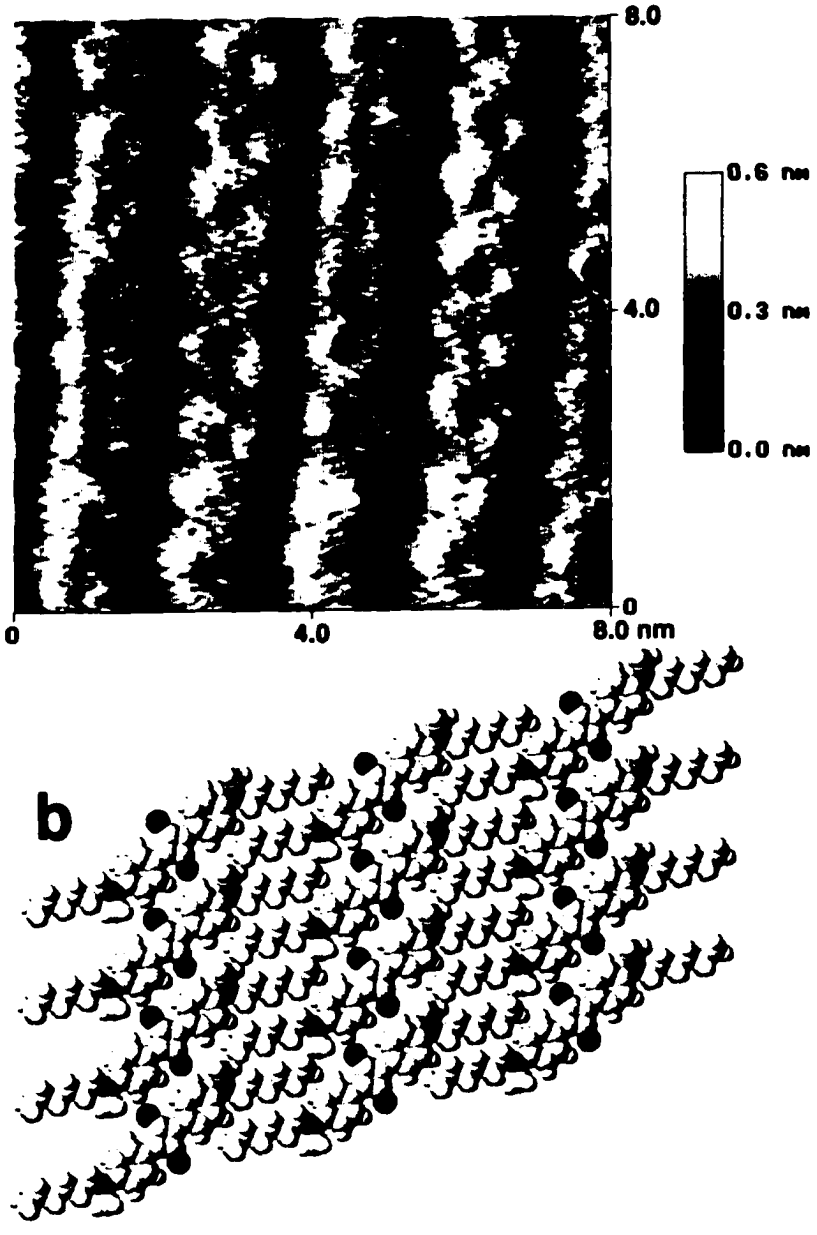

Figure 4.19: (a) 8 nm × 8 nm STM image of ordered rows of 1-6 HSQ on HOPG. (b) Molecular model of the observed 1-6 HSQ row structure.

row structure is shown in Figure 4.19b. As with 1-8 HSQ, the methyl tails are short enough to lie on the HOPG surface in the plane of the molecule and not interfere with the interdigitation of the two longer hexyl tails. The 50° orientation of the long axis of the molecules to the edge of their molecular rows allows the adjacent chromophores within the same row to offset from one another such that the donors and acceptors are aligned.

The relationship of the additionally adsorbed layers to the first layer (in contact with the HOPG surface) has not yet been resolved. Rather, the additional layers appear fuzzy. This is contrary to other squaraines which clearly show multiple layer rows in cases where the second layer is adsorbed directly atop the first layer and at the same orientation.[15] In cases where the second layer does not adsorb in the same orientation as the first, other squaraines commonly show cross-hatching of one layer atop the other.[1,15] It is unclear why multiple layer characteristics such as these were not observed for 1-6 HSQ.

HSQ'S vs. OHSQ's

Comparison of the observed ordered structures of homologous hydroxylated and non-hydroxylated bis(dialkylamino-phenyl) squaraines adsorbed on HOPG has shed light on the interadsorbate interactions driving the observed structures. The homologous pairs 4-4 HSQ and 4-4 OHSQ, and 8-8 HSQ and 8-8 OHSQ both exhibited equivalent structures. Interadsorbate distances and orientations, as well as unit cell parameters, were within experimental error of one another for the HSQ/OHSQ pairs. This equivalence tells us that interadsorbate H-bonding does not appear to play an important role

in the ordering of dialkylamino-phenyl squaraines on HOPG. Inter-adsorbate H-bonding may be present in the 2D structures of OHSQs, but it does not appear to be the primary interaction that drives the observed packing structure. As a result, it appears that donor-acceptor interactions are, in fact, the dominating interadsorbate chromophore-chromophore interaction in the ordered adsorption of these molecules on HOPG.

The absence of hydrogen bonding in the non-hydroxylated molecules does appear to have an effect on the STM imaging of squaraines on HOPG, however. STM imaging of the ordered films of 4-4 HSQ and 8-8 HSQ, as compared to that of their hydroxylated counterparts of the same solution concentration, was much noisier. It is conceivable that this noise is due to the instability of the HSQ molecules on the HOPG surface, as was mentioned in the section on 4-4 HSQ. Without these H-bonds, the phenyl groups of the HSQ molecules in solution have been shown to rotate about the C–C bond between the phenyl ring and the four-membered ring in polar solvents.[12,16] Despite the fact that the solvent used in our experiments was non-polar and aromatic (characteristics which have been shown to planarize non-hydroxylated squaraines[12]) we expect that some adventitious water is present at the solid/liquid interface. Water molecules present at this interface may interact with the polarized charges in the C_4O_2 moiety of the squaraine molecule, causing it to twist from planarity due to steric repulsion.[12] Although interaction with the HOPG surface should contribute to the planarity of the adsorbed HSQ molecules, the high local field of the scanning tip may exert enough force to destabilize the

adsorbed HSQ molecules and cause them to partially or fully desorb. Partial desorption could introduce fuzziness into the image due to rapid movement of the molecule on the surface. Complete desorption could result in the molecule(s) becoming trapped between the scanning tip and the adsorbate film, thus interfering with tunneling and introducing noise. It is also possible that intermolecular H-bonding, although not influential in driving adsorbate packing-structure, has an influence on the stability of the ordered squaraine film. Whether due to inter- or intra-molecular H-bonding, films of OHSQs were much less noisy and much more stable to the rastering motion of the tip than films of HSQs, allowing for crisp images a majority of the time.

Figure 4.20 shows the relationship between alkyl tail length and unit cell parameter (*a* or *b*) for each of the HSQ molecules forming Type 1 row structures. The alkyl tail length is represented by the number of carbons in the tails (R_2 for HSQs with $R_1 < R_2$, since the longer of the tails determines row structure). It can be seen that the *a* unit cell parameter (red circles), which includes the region of interdigitated tails, increases approximately linearly with increasing carbon tail length. The interdigitated tail region increases ~1.3 Å per additional methylene unit. The y-intercept of the line for these points (17 ± 2 Å) is only slightly larger than that expected for the length of the chromophore region (~14 Å). The *b* unit cell parameter remains approximately constant with a value of ~9.2 Å, corresponding the to distance between adjacent chromophores within the same molecular row. The constant distance of *b* suggests that increasing tail length does not alter intra-row chromophore-chromophore interactions.

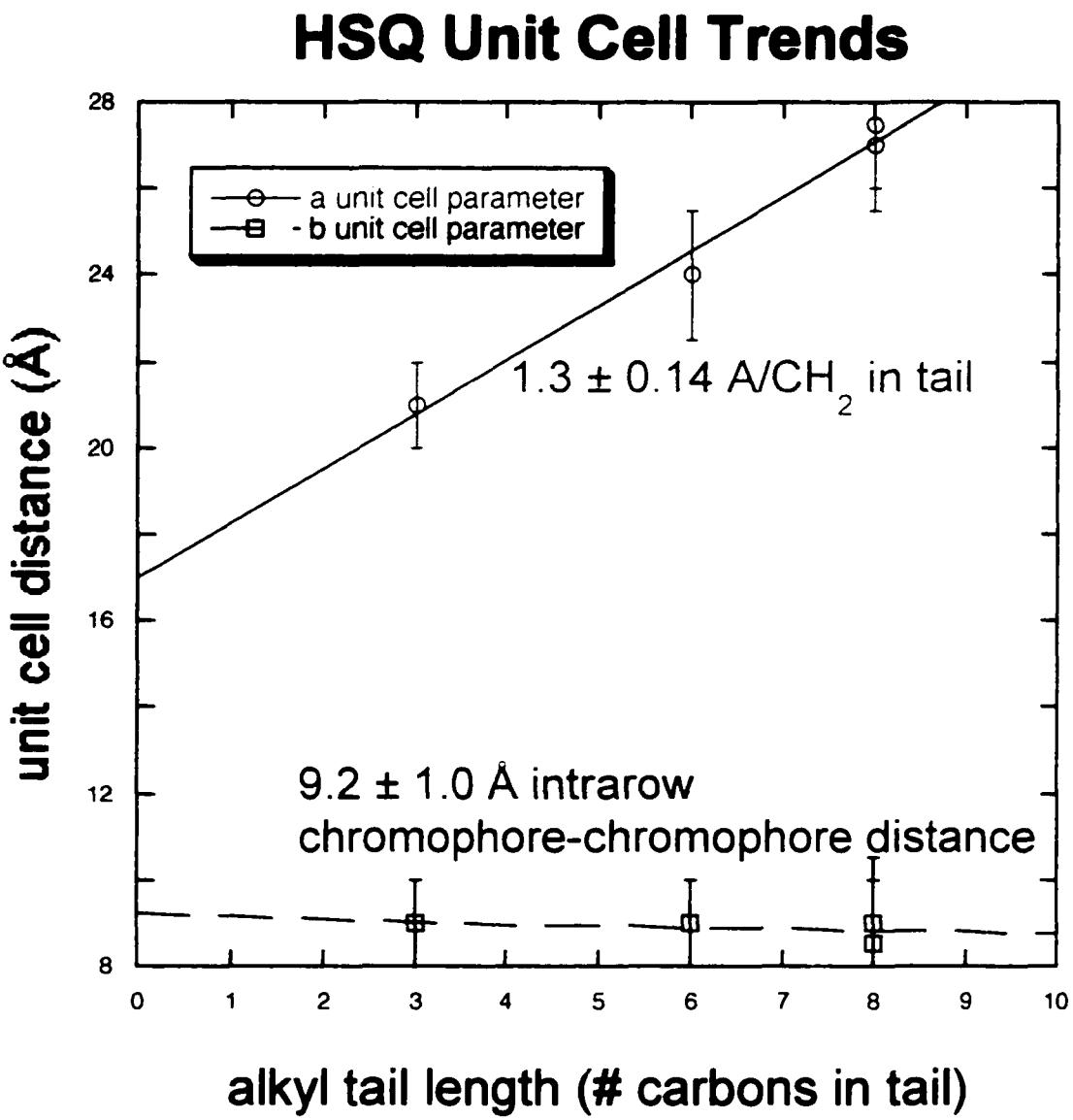

Figure 4.20: Plot showing the relationship between *a* and *b* unit cell parameters and alkyl tail length for the HSQs exhibiting Type 1 row structures. An approximately linear increase in *a* unit cell parameter with number of carbons was observed. The b parameter remains approximately constant with increasing number of alkyl tail carbons.

Conclusions

Non-hydroxylated squaraines, like their hydroxylated counterparts, were found to be highly surface active, forming well-ordered monolayer or multilayer films on the HOPG surface. Row structures were found to be the predominant packing structure formed, even among shorter tails, although a herringbone structure was observed for 4-4 HSQ. An approximately-linear increase in dark row width and in *a* unit cell parameter was observed for row structures as the length of the alkyl tails was increased.

It was found that less-symmetric molecules, molecules in which $R_1 = CH_3 \neq R_2$, tend to form the same structures as their symmetrical analogs. The methyl tail is small enough to lie on the HOPG surface without sterically interfering with tail interdigitation between the longer tails.

Non-hydroxylated analogs of the OHSQs studied in Chapter 3 exhibited the same ordered structure as their OHSQ counterparts. This suggests that H-bonding does not have a significant effect on the packing structure observed. Lack of H-bonding, both inter- and intra-molecular, however, does appear to have an effect on film stability and image noise. Lowering of the electric field at the tip (lowering bias V) appeared to reduce the noise.

REFERENCES

(1) Stawasz, M. E.; Sampson, D. L.; Parkinson, B. A., *Langmuir* **2000**, *16*, 2326-2342.
(2) Claypool, C. L.; Faglioni, F.; III, W. A. G.; Gray, H. B.; Lewis, N. S.; Marcus, R. A., *J. Phys. Chem. B* **1997**, *101*, 5978-5995.
(3) McGonigal, G. C.; Bernhardt, R. H.; Thomson, D. J., *Appl. Phys. Lett.* **1990**, *57*, 28-30.
(4) Eng, L. M.; Fuchs, H.; Buchholz, S.; Rabe, J. P., *Ultramicroscopy* **1992**, *42-44*, 1059-1066.
(5) Giancarlo, L.; Cyr, D.; Muyskens, K.; Flynn, G. W., *Langmuir* **1998**, *14*, 1465-1471.
(6) DeFeyter, S.; Grim, P. C. M.; Esch, J. v.; Kellogg, R. M.; Feringa, B. L.; DeSchryver, F. C., *J. Phys. Chem. B* **1998**, *102*, 8981-8987.
(7) Qiu, X.; Wang, C.; Yin, S.; Zheng, Q.; Xu, B.; Bai, C., *J. Phys. Chem. B* **2000**, *104*, 3570-3574.
(8) Kawai, T.; Tanaka, H.; Nakagawa, T., *Surf. Sci.* **1997**, *386*, 124-136.
(9) Forster, M.; Hester, R. E., *J. Chem. Soc. Faraday Trans. 1* **1982**, *78*, 1847-1866.
(10) Law, K. Y.; Bailey, F. C., *J. Org. Chem.* **1992**, *57*, 3278-.
(11) McKerrow, A. J.; Buncel, E.; Kazmaier, P. M., *Can. J. Chem.* **1995**, *73*, 1605-1615.
(12) Law, K. Y., *J. Phys. Chem.* **1989**, *93*, 5925-5930.
(13) Law, K. Y., *J. Phys. Chem.* **1988**, *92*, 4226-4231.
(14) Stawasz, M. E.; Takeda, N., **unpublished results**,
(15) Stawasz, M. E.; Parkinson, B. A., **in prep**,
(16) Law, K. Y., *J. Phys. Chem.* **1987**, *91*, 5184-5193.

CHAPTER FIVE

STM Investigation of the Ordered Thin Films of Bis(4-Dioctadecylamino-phenyl) Squaraine on HOPG

Abstract:

We report the ordered structures of the long-chain non-hydroxylated squaraine, bis(4-dioctadecylamino-phenyl)squaraine, adsorbed on the (0001) surface of HOPG. Scanning tunneling microscopy (STM) investigations of this molecule (referred to as 18-18 HSQ) were performed at both low and high phenyloctane solution concentrations. Nucleation and growth events were observed at lower concentrations. Multiple layer structures were present at both low and high deposition solution concentrations, but single layer structures were observed only at low concentrations. A number of polymorphs were observed within both concentration ranges, some quite remarkable. Although an achiral molecule, 2-dimensionally chiral polymorphs were observed. The adsorbed structures of 18-18 HSQ appeared to be coincident with the HOPG lattice.

Introduction:

In Chapter 4 the ordered adsorption of a series of five non-hydroxylated squaraines on HOPG was described. A sixth non-hydroxylated molecule was also studied, bis(4-dioctadecylamino-phenyl) squaraine (18-18 HSQ). This molecular system was found to be so rich in its number of observed polymorphs and in the remarkable features that it produces on the HOPG surface, that it was not included with the other HSQs, but was given its own chapter.

As described in Chapter 3, the 2D ordering on HOPG of the long-chained molecule 2-18 OHSQ exhibited an unexpected and intriguing effect. Despite the similarity in angle and distances of the HOPG backbone ($[0\bar{1}\bar{1}0]$ and equivalent lattice vectors) to those of hydrocarbon chains,[1] and the observed tendency towards coincidence of squaraine adsorbate structures at tail lengths of 12 carbons (12-12 OHSQ), 2-18 OHSQ displayed no coincidence with the HOPG lattice. Instead, rows that curved and meandered freely across the surface, exhibiting no strict relationship to graphite lattice directions whatsoever, were observed. It was hypothesized that the existence of the two short tails (one ethyl on either side of the molecule), instead of four total long and bulky octadecyl tails, allowed the 2-18 molecule some flexibility in its adsorption and ability to orient with respect to its neighbors. 18-18 HSQ was studied in an effort to discern whether the incommensurate structures exhibited by 2-18 OHSQ were, in fact, due to the asymmetry of the molecule, or due to the large number of low energy conformations that a tail of 18 carbons may take on. The ordered adsorbate structures of the symmetrical, long-tailed 18-18 HSQ molecule on

HOPG were expected to answer this question. They are presented in this chapter.

Experimental:

Experiments were performed with a Digital Instruments Nanoscope III STM under ambient conditions. Vibration isolation was provided by a bungee system enclosed in an environmental chamber. Bis(4-dioctadecylamino-phenyl)squaraine (18-18HSQ) was obtained from Dr. Marina Stanescu of the Whitten group at the University of Rochester. Table 5.1 shows the structure of 18-18HSQ.

Solutions of 18-18HSQ were prepared in concentrations of approximately 10^{-4} to 10^{-6} M in phenyloctane (Aldrich). Experiments were performed with solutions in either the low concentration range (low 10^{-5} to low 10^{-6}) or the high range (high 10^{-4} to high 10^{-5}) to observe differences in nucleation. STM tips were cut to a sharp point mechanically from (80:20) Platinum/Iridium 0.2mm diameter wire (Alpha Aesar). Samples were prepared by applying a drop of squaraine solution onto a freshly cleaved piece of highly ordered pyrolytic graphite (HOPG). Tunneling occurred with the tip immersed into the layer of solution using typical tunneling parameters of –1.6V to –0.8V (sample negative) and 30 to 45pA with the STM operating in constant current mode. After a series of squaraine images were obtained, the tunneling gap resistance was lowered in order to characterize the HOPG surface in the exact same spot. Images were obtained with different Pt/Ir tips and several different solutions to test for reproducibility and ensure that data was free of tip and sample artifacts. All images presented here have been flattened by software routines.

Table 5.1

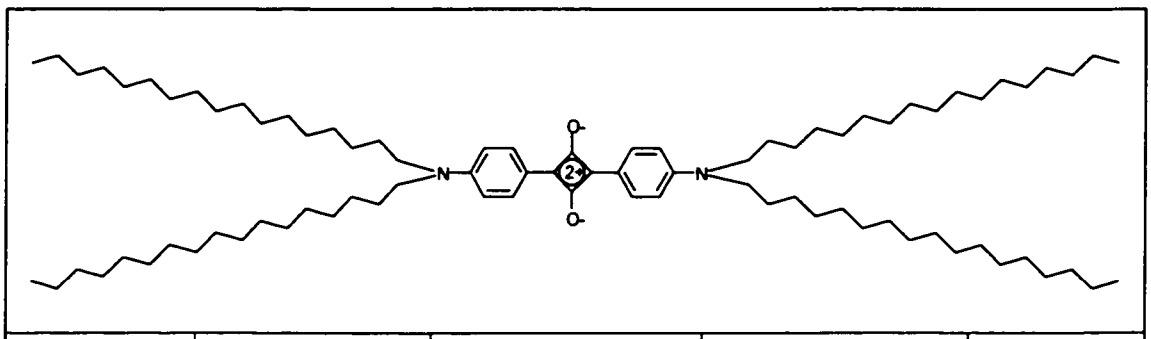

18-18HSQ polymorph	# layers in structure	Bright row width (Å)	Dark row width (Å)	*a* unit cell parameter (Å)
1	2	19 ± 2	13.5 ± 2.5	32 ± 2
2	2	16.5 ± 1.5	34 ± 3	50 ± 2
3	1 or 2	13 ± 1	12 ± 3	25 ± 1
4	1	13 ± 2	26 ± 3	39 ± 1

Table 5.1: Structure of 18-18HSQ and distance parameters for the four main polymorphs exhibited by 18-18HSQ under phenyloctane on HOPG as measured with STM.

Results and Discussion:

Low Concentration Range Studies

Two concentration ranges of 18-18HSQ in phenyloctane were investigated: high (~10^{-4} to 10^{-2} M) and low (~10^{-7} to 10^{-5} M). Previous studies demonstrated that longer-tailed squaraines tend to form multiple-layers of molecules on the HOPG surface.[2] Therefore, STM experiments were performed at low concentrations in an effort to observe nucleation and growth events and the formation of multiple layer structures from single layer structures. In these experiments, STM imaging of the surface commenced within seconds of solution deposition. An image obtained early in such an experiment, showing 18-18HSQ nuclei scattered about the bare HOPG surface, can be seen in Figure 5.1a. A subsequent image, taken 9 minutes later, shows these nuclei growing into domains that eventually cover the surface. These domains are composed of alternating bright and dark lamella or rows. Previous studies[2] of hydroxylated squaraines showed that the chromophore area (anilines and four-membered ring) of each adsorbed squaraine molecule is commonly resolved by STM as an oval or "football" shape of bright contrast. The alkyl tails are not resolved, however, and appear as dark areas in the image. Thus the bright and dark rows shown in Figure 5.1 correspond to different areas of the squaraine molecule. For hydroxylated squaraines on HOPG, it was found that the bright rows designated j-like aggregates of squaraine chromophores and the dark, interdigitated alkyl tails belonging to the molecules ordered in two adjacent bright rows.[2] Measurement of the row spacings of the bright and dark rows shown in Figure

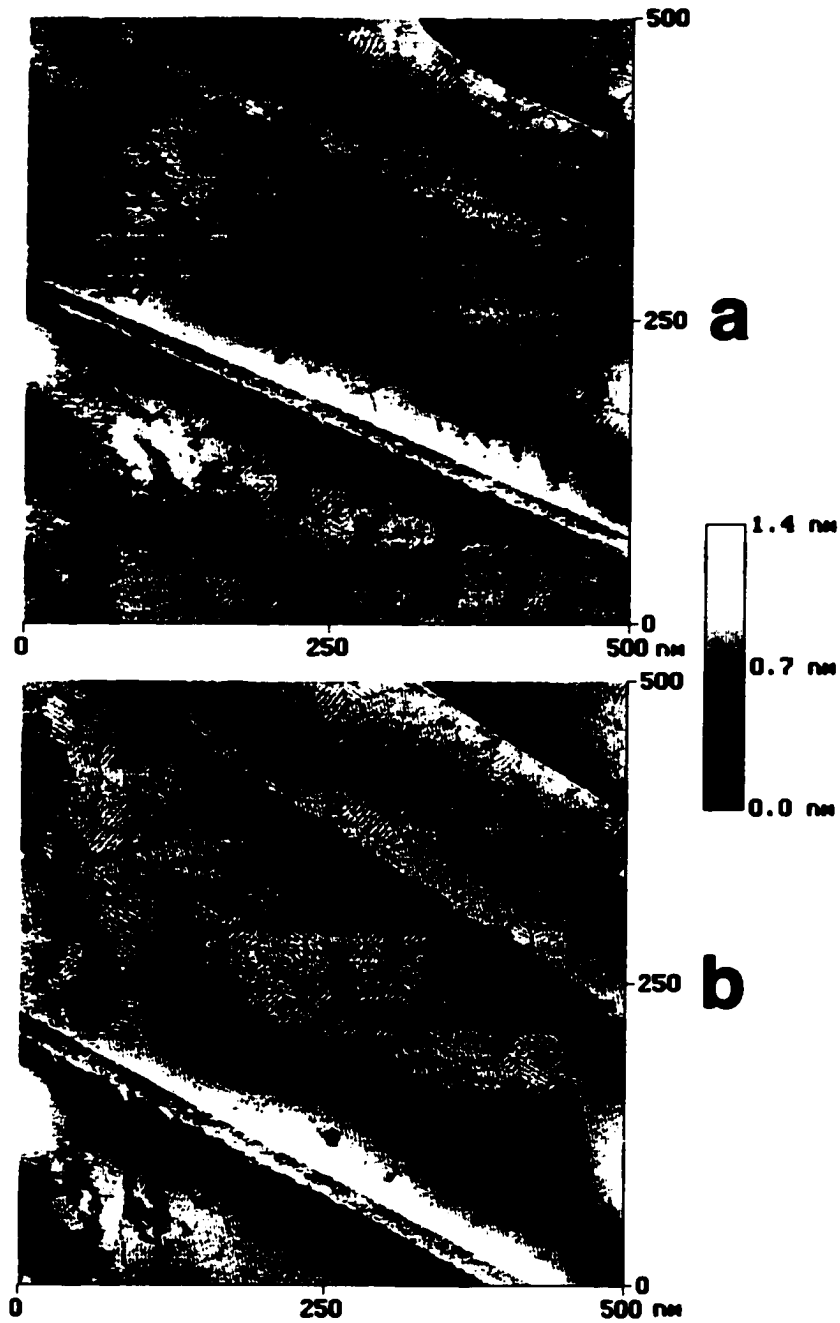

Figure 5.1: Two sequential 500 nm × 500 nm images showing the ordered adsorption of 18-18HSQ at low deposition solution concentrations. (a) Image captured within seconds of solution deposition. (b) Image captured captured 9 minutes after image (a).

5.1 reveals that the domains are composed of only one polymorph, designated polymorph 1. This polymorph was observed most frequently in the several experiments conducted. The width of the bright rows (measured perpendicular to the edge of the bright row) exhibited by polymorph 1 is ~19 Å, a distance that is wider than the length of one 18-18HSQ chromophore measuring from N to N (~14 Å). This suggests that, as was often seen in polymorphs formed by other long tailed squaraines[2], polymorph 1 consists of multiple layers of chromophores. The dark row width for polymorph 1 is ~14 Å. This is shorter than the length of an all-trans octadecyl tail (~21 Å). These measurements support the model where multiple layers are formed. In the models proposed for other multiple layer squaraine polymorphs, the second layer of molecules lies on top of the first layer such that the donor and acceptor groups of the bottom and top molecules are aligned. This alignment requires that the top molecule be offset from the end of the bottom molecule (thus, the top molecule cannot completely eclipse the bottom molecule). The total length of the chromophore region, from the exposed edge of the bottom layer chromophore to the opposite edge of the top chromophore corresponds to the observed width of the bright row in this polymorph. Because a portion of the tail region of the bottom layer molecules is eclipsed by the top layer chromophores, the dark row width is observed to be shorter than the actual width occupied by the 18 carbon tails. This configuration is shown in Figure 5.2. Alternate explanations for the unexpected short dark row regions involve coiling or stacking of the 18 carbon tails, thus decreasing the observed length of the tail. This is unlikely, at least in the bottom layer of

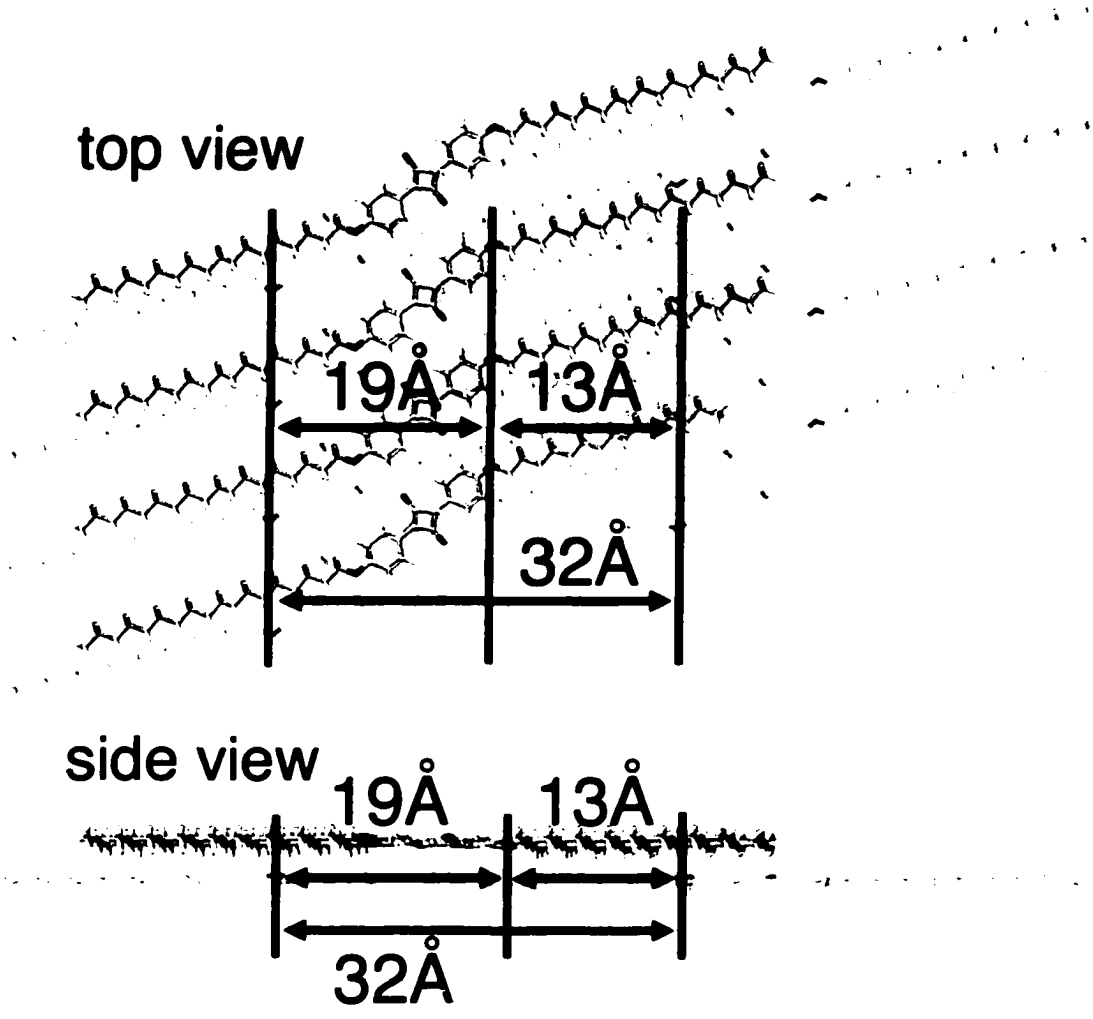

Figure 5.2: Top and side views of the proposed two-layer molecular model for polymorph 1. The bottom (first) layer is shown shadowed, and the top (second) layer is shown highlighted. The bright row area corresponds to regions occupied by chromophores, whereas the dark row area corresponds to regions occupied by only tails. Arrows indicate the distances corresponding to the *a* unit cell parameter (32 Å), bright row width (19 Å), and dark row width (13 Å).

molecules, because of the energetic gain in the attractive interaction of the tails with the HOPG substrate and has not been observed with other molecules containing long chain alkyl tails, such as alkylated-perylenes[3], -phthalocyanines[4,5], and –porphyrins[5]. The orientation of the chromophores to the edge of the bright molecular rows of polymorph 1 has not been experimentally determined due to insufficient resolution of the images. The model shown in Figure 5.2 was constructed taking into consideration the average angular orientation of the chromophores of other long tailed squaraines that form rows (~50 °).[2] Likewise, the distance between adjacent chromophores within the same molecular row was not determined. Again, due to the consistency of the ~8 Å distance between adjacent chromophores in all row-forming squaraine systems studied thus far[2], this distance was used to construct the model shown in Figure 5.2.

Figure 5.3a shows a 200 nm by 200 nm STM image of a surface displaying several domains. Measurement of the rows within these domains has shown that they consist of polymorph 1, just described, and another polymorph (polymorph 2), the second most frequently observed polymorph in these studies. Compared to polymorph 1, polymorph 2 has wider dark rows (~33 Å for polymorph 2 vs ~13 Å for polymorph 1) and a larger *a* unit cell parameter (~50 Å vs ~32 Å). The large dark row width exhibited by polymorph 2 is ~12 Å longer than the length of an all-trans octadecyl tail. We ascribe this to an adsorbed structure with incomplete interdigitation of the octadecyl tails between adjacent molecular rows. The molecular model in Figure 5.3b shows that the ~33 Å dark

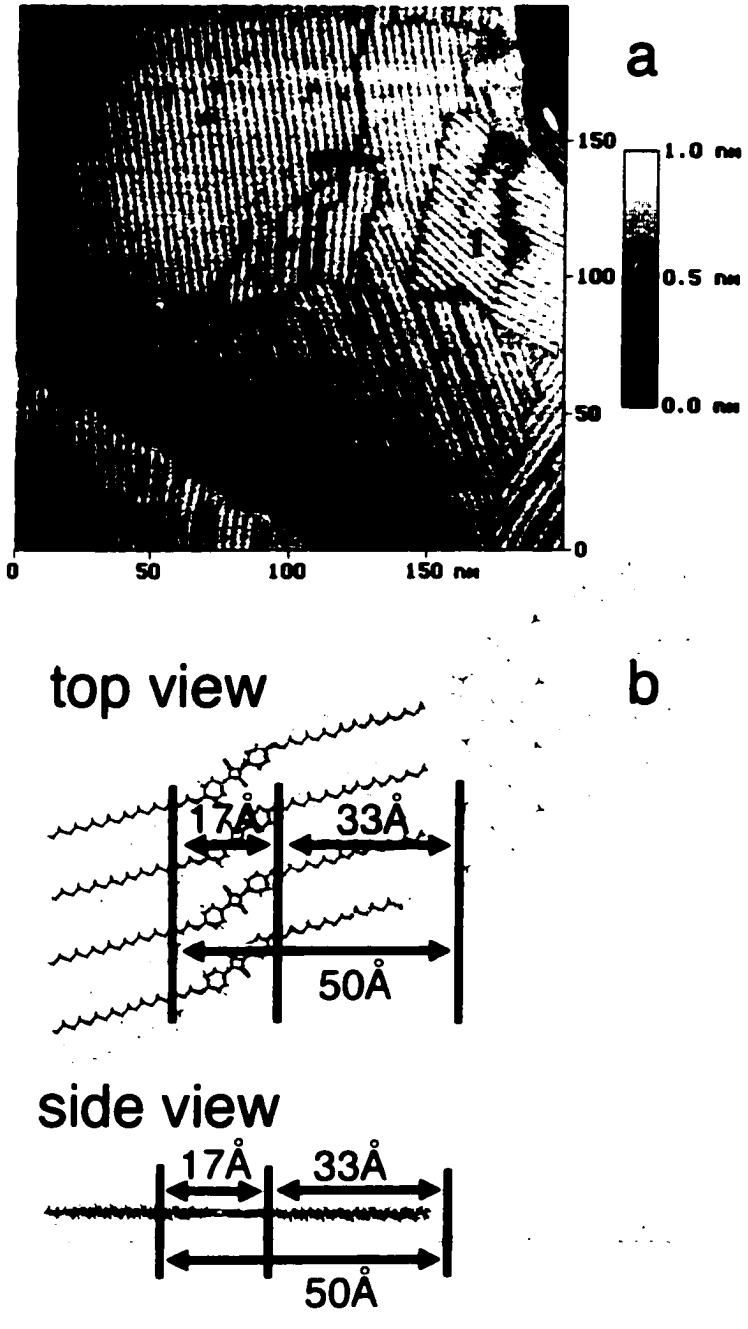

Figure 5.3: (a) 200 nm × 200 nm image showing various domains of polymorphs 1 and 2. Numbers overlaid on the domains show each polymorph. Asterisks denote areas of polymorph 1 coexisting with areas of polymorph 2. (b) Top and side views of the proposed two-layer molecular model for polymorph 2.

row width corresponds to an overlap of ~6 carbon atoms. The bare areas of graphite created by this incomplete interdigitation are occupied by the remaining two alkyl tails of each molecule, provided that they incorporate several gauche defects, decreasing the tail's observed length. The model in Figure 5.3b shows that gauche defects result in the tails twisting out of the plane of the chromophore but then returning to the surface, fitting into the space between interdigitated tails. Although this structure has decreased dispersion interactions between tails in adjacent rows, relative to fully interdigitated structures, it has increased overall attractive dispersion interaction due to the adsorption of the two usually surface-excluded tails onto the HOPG surface. The energetic cost[‡] of the incorporation of gauche defects (~5 × 0.8 kcal mol^{-1} ≈4 kcal mol^{-1}) into the tails to allow this structure is outweighed by the larger number of attractive methylene-HOPG interactions now possible (1.5[1,8] kcal mol^{-1} CH_2^{-1} × ~12 CH_2 $tail^{-1}$ ≈18 kcal mol^{-1} $tail^{-1}$). There is also an additional attractive lateral dispersion interaction between the 2 tails on each side of every adsorbed chromophore. The bright row width of polymorph 2 (~17 Å), is within experimental error of that of polymorph 1, and like polymorph 1, hypothetically consists of two chromophores (oriented at ~50° to the direction of the molecular row) layered atop one another in a way that allows for donor-acceptor interactions.

The asterisks on the image in Figure 5.3a point out areas where polymorphs 1 and 2 coexist. This coexistence can be easily understood by

[‡]The energy difference between the anti and gauche conformations of n-butane is ~0.8 kcal/mol.[6,7]

comparing the dimensions of polymorphs 1 and 2. The *a* unit cell parameter of polymorph 1 (~32 Å) is within experimental error of the dark row width of polymorph 2 (~33 Å). Thus, the whole structure of polymorph 1 can fit nicely into the area occupied by the tails in polymorph 2. Rather than lying on top of the tails, however, the polymorph 1 structure can incorporate into the tail region. This is shown in the model in Figure 5.4. There are two requirements of this coexistence of polymorph 1 and 2 within the same domain, each illustrated in Figure 5.4. The first is that the tails adsorbed on the left side of the polymorph 2 row model (16 Å wide bright row), which normally incorporate gauche defects to fit onto the surface, must desorb to allow the more extensive interdigitation of tails within a polymorph 1 13 Å wide dark row. The second is that the tails on the right side of the polymorph 1 row (19 Å wide bright row), which are normally desorbed, must adsorb onto the surface to make up the energetic loss from decreased tail interdigitation within a 34 Å wide dark row. As a result of these alterations, as illustrated by asterisks in Figure 5.3a, a 13 Å polymorph 1 dark row can exist within a domain of polymorph 2 rows.

Figure 5.5a shows a second type of nucleation observed at low concentrations within one minute after applying the squaraine-containing solution to the freshly-cleaved HOPG surface. The image shows isolated domains of ordered 18-18HSQ molecules. However, the area surrounding the domains appears to be occupied by an amorphous layer of adsorbed molecules rather than bare graphite, as was observed in Figure 5.1. In addition, the size of the domains (~150 nm in diameter) is considerably larger than those observed in

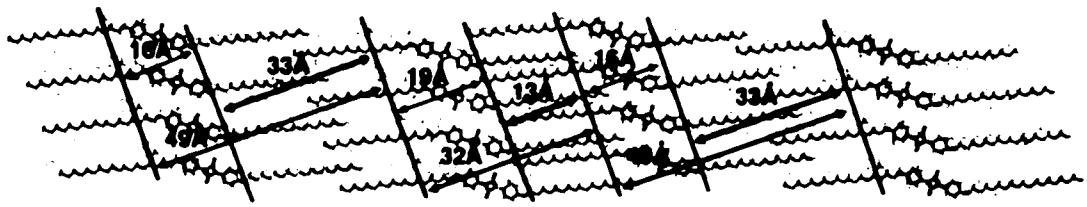

Figure 5.4: Proposed molecular model for incorporation of polymorph 1 into 2. The bottom (first) layer is shown shadowed and the second layer is shown highlighted. Bright and dark row widths for both polymorphs 1 and 2 are illustrated by green and black double-headed arrows, respectively. The *a* unit cell parameter is designated by a red double-headed arrow for polymorph 1 and blue for polymorph 2.

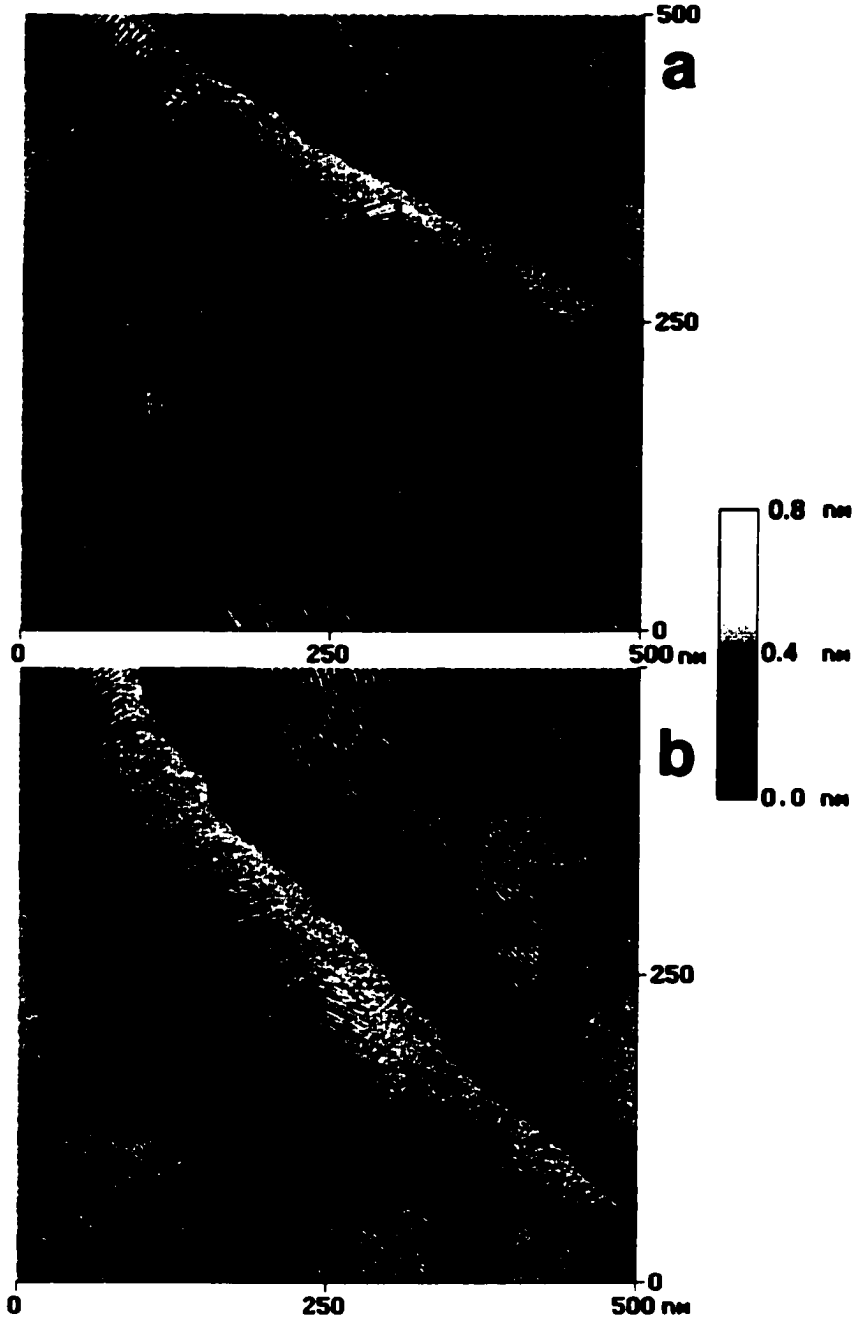

Figure 5.5: (a) 500 nm × 500 nm image showing nucleation of isolated ordered domains of 18-18HSQ amidst amorphous adsorbate taken within one minute of low concentration solution deposition. (b) Image of same area of surface taken 4 minutes later.

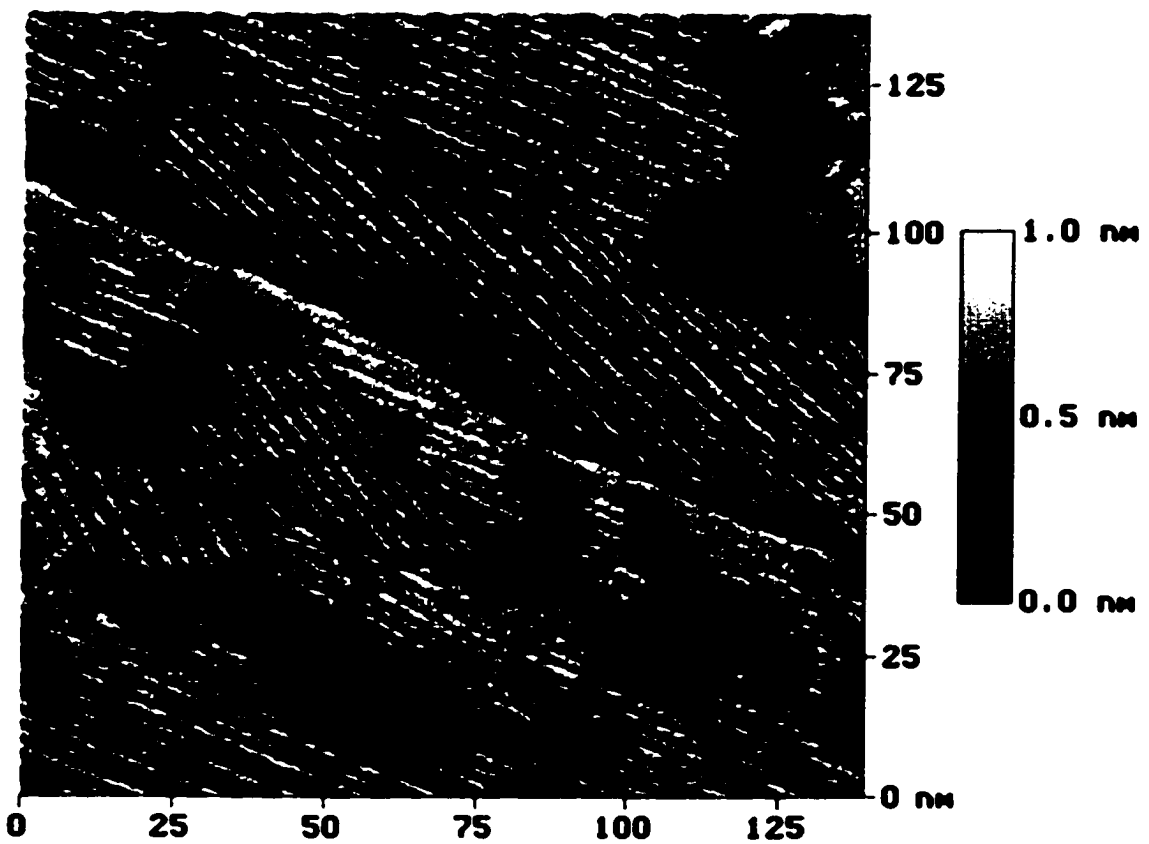

Figure 5.5(c): 135 nm × 135 nm image zoomed-in from (b) showing domains of polymorphs 3 and 4. Amorphous material and pinhole defects are visible between the domains.

Figure 5.1a (~40 nm). Figure 5.5b shows an image obtained ~4 minutes after 5.5a where the domains have grown. Zooming in on an area from Figure 5.5b (Figure 5.5c) reveals that the area between ordered domains is definitely composed of amorphously adsorbed molecules and that the domains consist of at least 2 different polymorphs. These polymorphs are distinct from 1 and 2 and are labeled 3 and 4 on the image. Holes in the amorphous material reveal the HOPG surface. It appears that the ordered domains incorporate the amorphous material as they grow. Growth subsided when the amorphous areas had been consumed. Table 5.1 summarizes all the measurements obtained for the four polymorphs.

Higher resolution images (Figure 5.6a) where chromophores are resolved were obtained by zooming-in on a polymorph 4 domain. The distance measured from the right edge of one row of chromophores to the right edge of the next row of chromophores (the *a* unit cell parameter) is 39 ± 1 Å. The measured width of the dark and bright rows is 26 ± 3 Å and 13 ± 2 Å, respectively. These measurements were taken perpendicular to the edges of the rows. The fuzzy stripe appearing to the left of most of the rows of chromophores is possibly a second layer of non-localized chromophores in the process of adsorbing atop the single-layer polymorph 4 rows. The fuzzy stripe did not appear in all of the high resolution images of polymorph 4. The ~13 Å bright row width, and the ~15 Å length from end to end of the bright ovals composing the bright rows, correspond well with the length of a single squaraine chromophore. The distance between chromophores adjacent to one another in the same row is ~9 Å. The ~26 Å dark

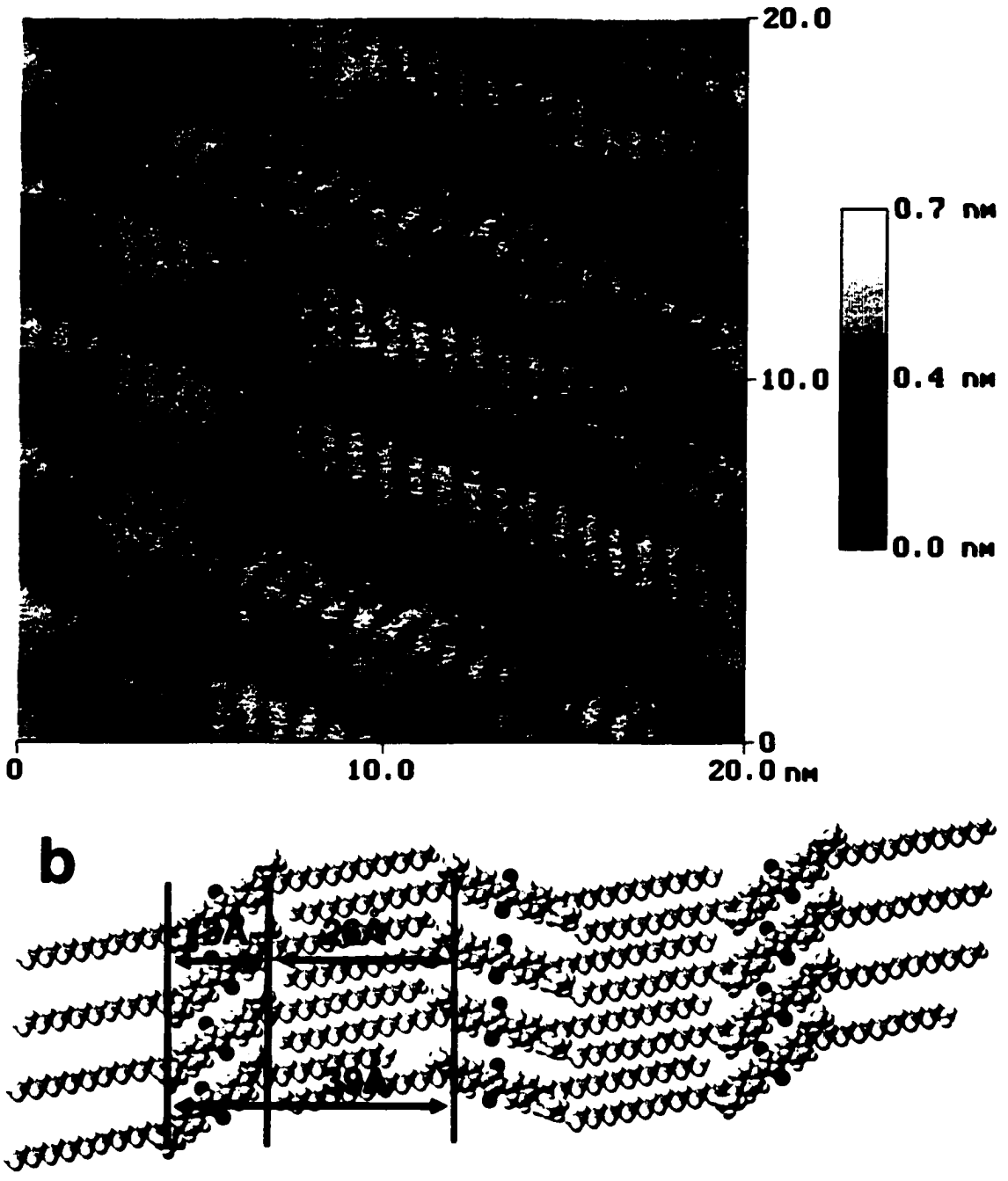

Figure 5.6: (a) 20 nm × 20 nm STM image of polymorph 4. Arrows overlaid on the image indicate the orientation of the chromophores within molecular rows. (b) Proposed single-layer molecular model of polymorph 4.

row width corresponds to a structure where two of the octadecyl tails (one from each side of the molecule) are adsorbed on the surface interdigitated with the alkyl tails of the molecules in the row adjacent to it. This interdigitation is not complete, however. The dark rows are 5-6 Å longer than a single octadecyl tail (~20 Å) meaning that ~3 of the methylene groups from each adsorbed tail are not interdigitated. The molecular model shown in Figure 5.6b illustrates this 2D single layer structure. The incomplete interdigitation increases the effective width of the area occupied by tails beyond the ~20 Å length of an all-trans octadecyl tail. Unlike polymorph 2, however, the interdigitation is complete enough to preclude the adsorption of the remaining two octadecyl tails. For this reason, the remaining tails are shown protruding from the plane of the molecule in the model in Figure 5.6. Since we never resolve the alkyl tails, it is also possible that the remaining tails are lying on top of the adsorbed tails. Black arrows overlaid on the image point out one more intriguing characteristic of this polymorph: the ability of the chromophores within a row to switch direction from one row to the next (~60° to the direction of the row to ~120° in the next row, or vice versa), a signature of 2-dimensional chirality. Two-dimensional chirality results when a molecule cannot be superimposed on itself when rotated in 2 dimensions. Because the molecules are restricted to the surface, they cannot rotate in 3 dimensions without desorbing. STM images have previously resolved 2D enantiomers of several achiral molecules adsorbed on surfaces.[9-12] As illustrated in the molecular model in Figure 5.6b, the difference between 18-18HSQ molecules in rows with different chromophore orientation is which pair of tails is

adsorbed on the surface. When chromophore direction switches from one row to the next, the 18-18HSQ chromophores of one row cannot be rotated within the plane of the layer so as to superimpose upon the chromophores in the next row. Thus, it is the non-superimposability of the adsorbed and desorbed tails that qualifies them as two-dimensional enantiomers of one another.

Polymorph 3 has a bright row width of 13 ± 1 Å, and a dark row width of 12 ± 3 Å. As discussed, 13 Å is a reasonable length for a single 18-18HSQ chromophore, however 12 Å is just over half the length of an octadecyl tail. If the 18-18HSQ molecules were to lie flat on the HOPG surface (as is observed for all other squaraines studied thus far on HOPG)[2,12], this would require that the tails either fold over on themselves (resulting in an apparent length halve of the all-trans length), or that they lie across the top of the chromophores in the bright row region. Another possible explanation, that would allow the majority of the methylene units in the dodecyl tails to lie flat on the surface, is that the chromophores stand on-edge, perpendicular to the HOPG surface, in a face-to-face card-stack fashion. This packing model is shown in Figure 5.7. Figure 5.7a presents a top view of the structure, showing the face-to-face donor-acceptor interaction between adjacent chromophores laterally offset from one another (~4 Å) within a card-stack aggregate. As was mentioned earlier, no solid-state crystal structures for 18-18HSQ have been reported. However, a solid-state structure similar to this card-stack model was reported by Wingard for bis(4-dimethylamino-2-methylphenyl)squaraine.[13] He found an ~3.5 Å interplanar distance between adjacent face-on chromophores. In a review of the solid-state

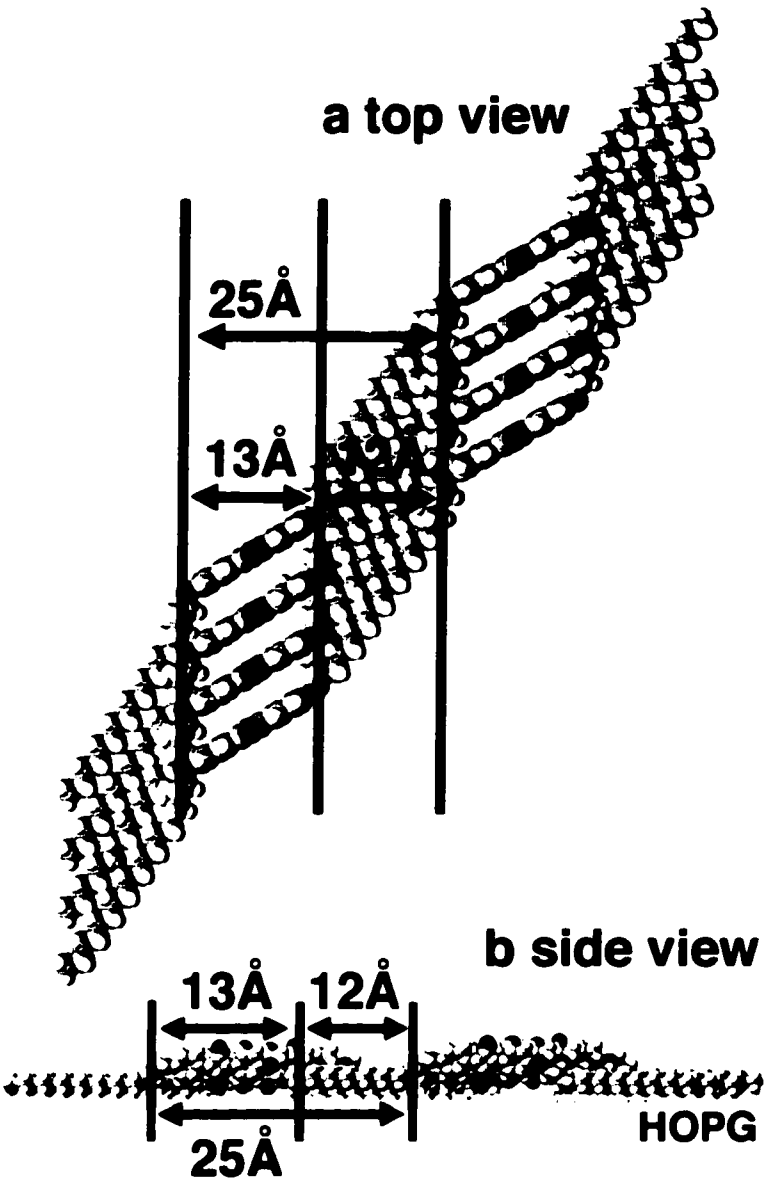

Figure 5.7: Top and side view of the proposed single-layer card stack conformation molecular model of polymorph 3.

structures of several short-tailed, aminophenyl squaraines, Law summarized that the C2 substituent in the phenyl ring has very little effect on the intermolecular CT.[14] As a result of the energetic driving force provided by the tails maintaining a majority of interaction with the HOPG surface, it is therefore reasonable to assume that 18-18HSQ might exhibit the same chromophore-chromophore relationship as that of bis(4-dimethylamino-2-methylphenyl)SQ despite the large difference in tail lengths and the differing phenyl functionalities. The side view of the model (Figure 5.7b) shows the relationships of the 18-18HSQ chromophore and tails to the HOPG surface. Two tails from each molecule (as is usual for row structures) are shown in direct contact with the HOPG surface. In order to allow the chromophore to stand perpendicular to the graphite, the methylene units closest to the chromophore act as supports, propping the chromophore above the surface and also decreasing the effective lateral length of the dodecyl tail. A few gauche defects in the first few carbons are necessary to allow this tail conformation. The rest of the tail may lie flat and attractively interact with the surface. As shown in Figure 5.7a, the ends of the tails may interdigitate with the edge-on chromophores in the ~3.5 Å of space between chromophores. In this way, all of the tail (excepting the first few methylene units) may adsorb and interact with the surface. The two tails not in contact with the HOPG may interact with the tails on the surface by lying on top of them (again necessitating the incorporation of a few gauche defects). The resulting structure has the possibility of enjoying a strong chromophore-chromophore interaction as well as significant tail-graphite and tail-tail interactions. If the molecules are indeed adsorbed in a

perpendicular card-stack, then high resolution images should reveal the chromophores as thin lines 1-2 Å in width and ~15 Å in length, with intra-lamellar chromophore distances of 3-4 Å. Rather, if they are adsorbed flat on the HOPG surface, then high resolution images should reveal the chromophores as bright ellipses 4-5 Å in width. Adequate resolution to validate either of these models was not achieved, however.

High concentration range studies

Figure 5.8 shows two 500 nm × 500nm STM images of the ordered adsorption of 18-18 HSQ onto the graphite surface from higher concentrations in phenyloctane. The image in Figure 5.8a was taken a few seconds after solution deposition. It shows a myriad of small (10s of nm to 100 nm in length or width) domains oriented predominantly at angles of 30 ° or multiples of 30 ° from one another. Figure 5.8b shows an image taken within the same experiment (but in a different location on the graphite surface) a few hours after deposition. It is clear that the domains are much larger now, with the longer axis of many of the domains measuring several hundred nm in length. The high aspect ratio of the domains in Figure 5.8b indicates that for most of the nuclei, growth has occurred along the row direction. Again, most of the domains are oriented at multiples of 30 ° from one another. This angular dependence suggests a strong orientational interaction with the graphite surface.

A 100 nm x 100 nm zoomed-in portion of Figure 5.8a, taken 5 minutes after the image in Figure 5.8a, is shown in Figure 5.9. Several domains oriented close to 90° angles to one another are observed. Within these domains an

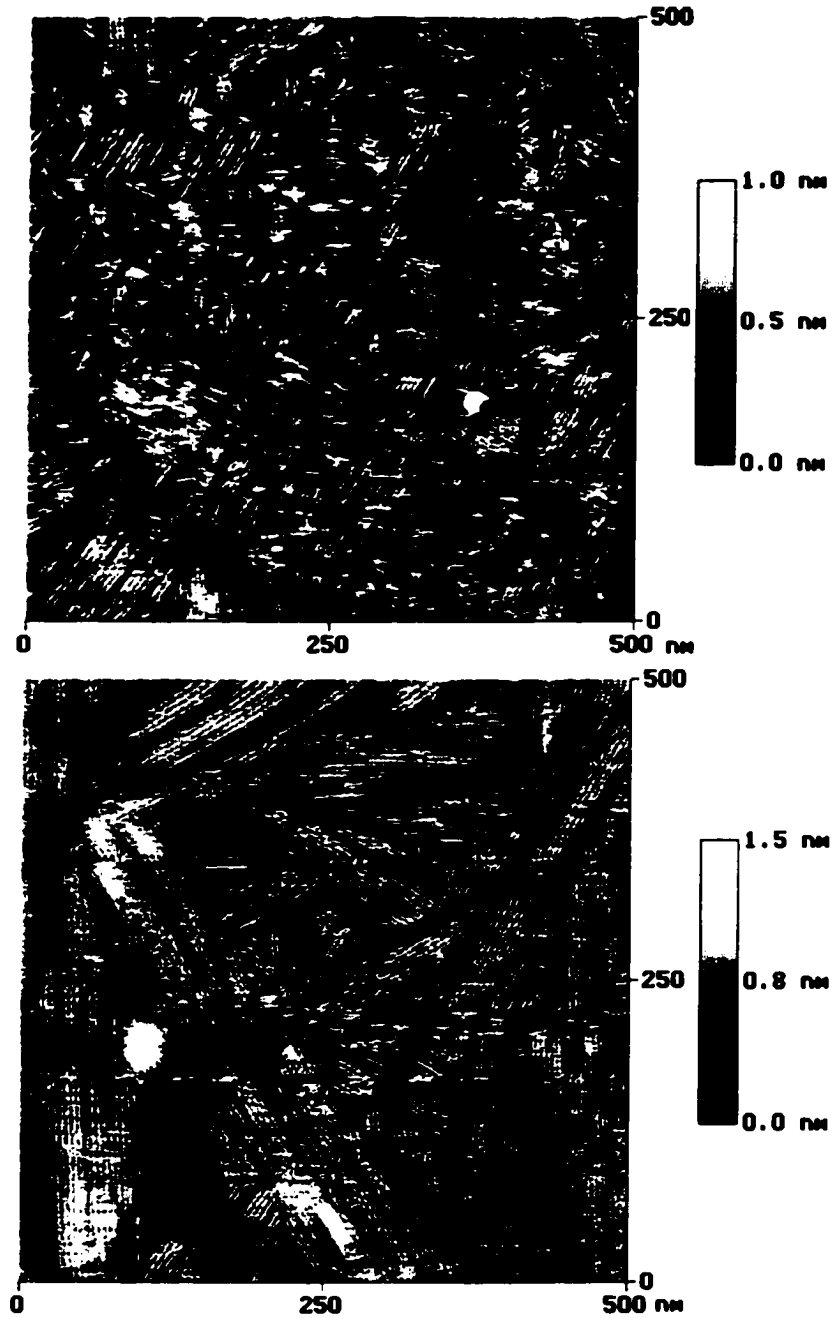

Figure 5.8: (a) 500 nm × 500 nm image taken a few seconds after deposition of a high concentration 18-18HSQ solution onto the HOPG surface. Many small domains are shown covering the surface, oriented at predominantly 30° angles to one another. (b) 500 nm × 500 nm image taken 4 hours after (a) on a different area of the same surface.

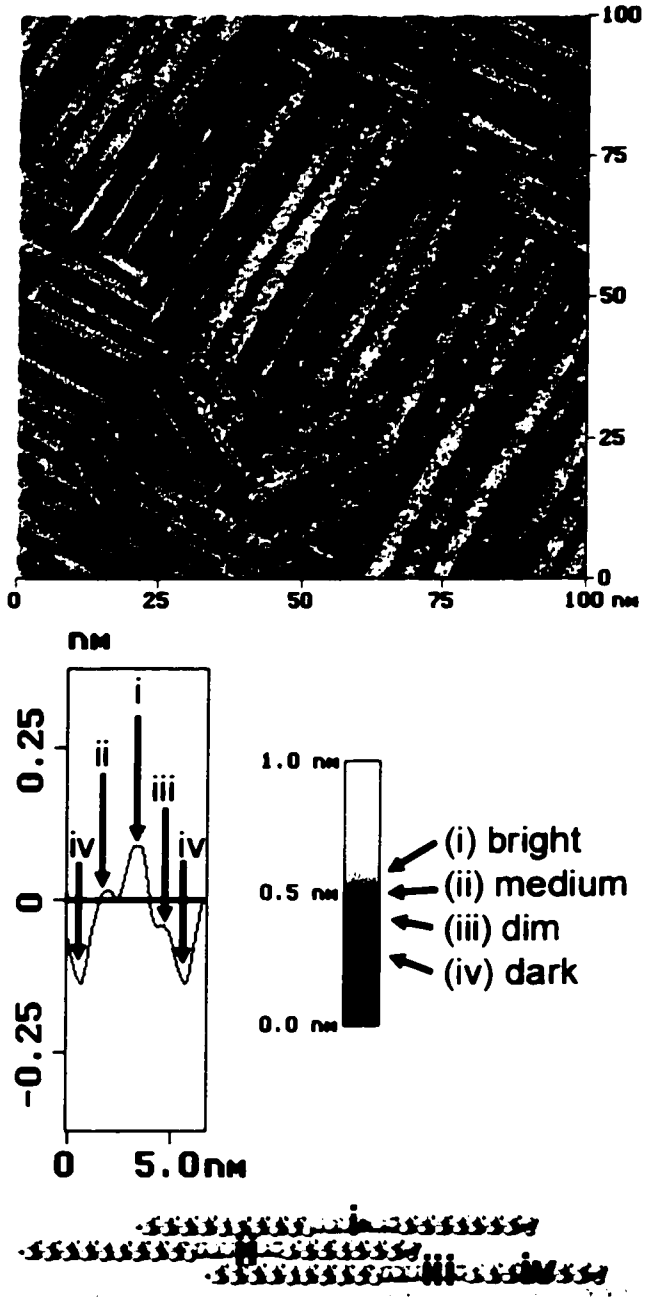

Figure 5.9: (Top) 100 nm × 100 nm image showing several domains at 90° or 120° to one another, displaying rows of four different contrasts: (i) bright, (ii) medium, (iii) dim, and (iv) dark. These contrast designations can be related to different apparent heights, illustrated by the scale bar and the image cross-section. The red line overlaid on the image indicates the cluster of rows from which the section is taken. A molecular model of this cross section appears below. The observed image contrasts (i), (ii), (iii), and (iv) are overlaid on their corresponding areas within the model. Chromophores are highlighted in yellow. Letters overlaid on the image illustrate the four variations of row clusters: A (i)/(i)/(i), B (i)/(i)/(iii), C (ii)/(i)/(iii), and D (ii)/(ii)/(iii).

incredibly rich system of rows with varying apparent heights[†] is shown. Careful inspection reveals that there are four row apparent row heights exhibited within this image: (i) bright, (ii) medium, (iii) dim, and (iv) dark. These designations can be related to the z-scale bar, with (i) occurring highest on the bar, (iv) lowest, and (ii) and (iii) in between. This point is further illustrated by taking a cross-section of a cluster of rows within the image (designated by a red line in Figure 5.9) that exhibits all four apparent row heights. It can clearly be seen that the bright row (i) has the largest apparent height, the medium contrast row (ii) has the next largest height, the dim row (iii) has the third largest height, and the dark row (iv) appears as a trough. The difference between the apparent heights of the bright and medium (i and ii), medium and dim (ii and iii), and dim and dark contrast rows (iii and iv) is ~1 Å for each pairing (within error of the measured height of a squaraine chromophore in previous STM studies[2,12,15]). The width of each of the rows (measured perpendicular to the edge of the row) was also consistently 12 ± 1 Å for (i), (ii), and (iii). The ~12 Å width corresponds well with the length of a squaraine chromophore. Dark rows (iv) were slightly narrower at 8.5 ± 1.5 Å. The similarity of the measured row widths to the squaraine chromophore length, and the consistent differences in apparent heights between the rows of differing contrast, lead us to believe that each of the different heights (except the dark rows) corresponds to a different layer of chromophores in a multilayer adsorbate film. The film shown in Figure 5.9 then consists of at least 3 layers of 18-18HSQ

[†]This may not be a true topographical height, but a convolution of electronic and topographical effects complicated by different possible electron paths through chromophores. The true topographical height is expected to be larger since it would be the thickness of a squaraine molecule.

molecules. The dim rows (iii) correspond to chromophores that are in contact with the HOPG surface (the bottom or first layer); the medium height rows (ii) are adsorbed atop the first layer (the middle or second layer); and the bright rows (i) are the top (or third) layer.

Assuming an adsorbate-mediated tunneling mechanism[‡‡], this particular designation of image contrast with layer identity (i.e. bright contrast with the layer furthest from the HOPG surface) seems counterintuitive. Adsorbate-mediated tunneling (a tunneling mechanism involving alteration of the surface electronic states by an adsorbate), would necessitate that the adsorbate being imaged be in close proximity to the surface. Since tunneling current decays exponentially with distance, one may expect that adsorbate layers closest to the substrate surface exhibit the highest tunneling current, and thus brightest image contrast. Likewise, the greatest adsorbate-substrate electronic state mixing would occur between the substrate and the molecules adsorbed in the proximal layer. We presume, however, that the molecular contrast of the squaraine system occurs by another tunneling mechanism which likely incorporates their ability to undergo intermolecular charge transfer.[13,14,16-22] The details of this mechanism will not be presented here.

Closer examination of the varying apparent heights (i, ii, iii, iv) exhibited by the rows in Figure 5.9 reveals several patterns. Dark rows, or troughs, (iv) occur approximately every fourth row. Thus, (i), (ii), and (iii) rows appear to cluster in groups of three. The contrast sequences within these clusters displays four

[‡‡] resonant tunneling from the tip into an adsorbate state with subsequent resonant tunneling into a substrate state.

different combinations: (A) (i)/(i)/(i); (B) (i)/(i)/(iii); (C) (ii)/(i)/(iii); and (D) (ii)/(ii)/(iii). To facilitate recognition of each type of cluster within the image, the letter of each of the four cluster types is overlaid on the image in Figure 5.9 in a region displaying each type. Figure 5.10 shows a zoomed-in portion of Figure 5.9 and cross sections of each of the four cluster types. The red and blue lines overlaid on the image show where the cross-sections were taken. Again, the letter of each of the clusters is overlaid on both the image (where the cross sections were taken) and the cross-sections themselves. In addition, the apparent height of each of the rows within each cluster is designated by (i), (ii), (iii), or (iv) in the cross-section. As was mentioned earlier, the consistency in the differences in apparent height (~1 Å), combined with the similarity in size of the widths of the (i),(ii), and (iii) rows (~12 Å) with the length of a squaraine chromophore, lead us to believe that the (i),(ii), and (iii) rows are lamella of squaraine chromophores in the bottom (iii), middle (ii), and top (i) layers of a three-layer film.

The following analysis attempts to discern the polytype of the ordered structures in each of the layers. The distance between the left edge of a cluster of rows to the left edge of the nearest cluster is consistently ~50 Å, regardless of the contrast sequences of the neighboring clusters. The same is true for the distance between the second row of a 3-row cluster to the second row of its neighboring 3-row cluster, and from the right edge to the next cluster's right edge. Thus it appears that the single layer structure of each of the 3 layers has the same *a* unit cell parameter of 50 Å. Recall that polymorph 2 of the low

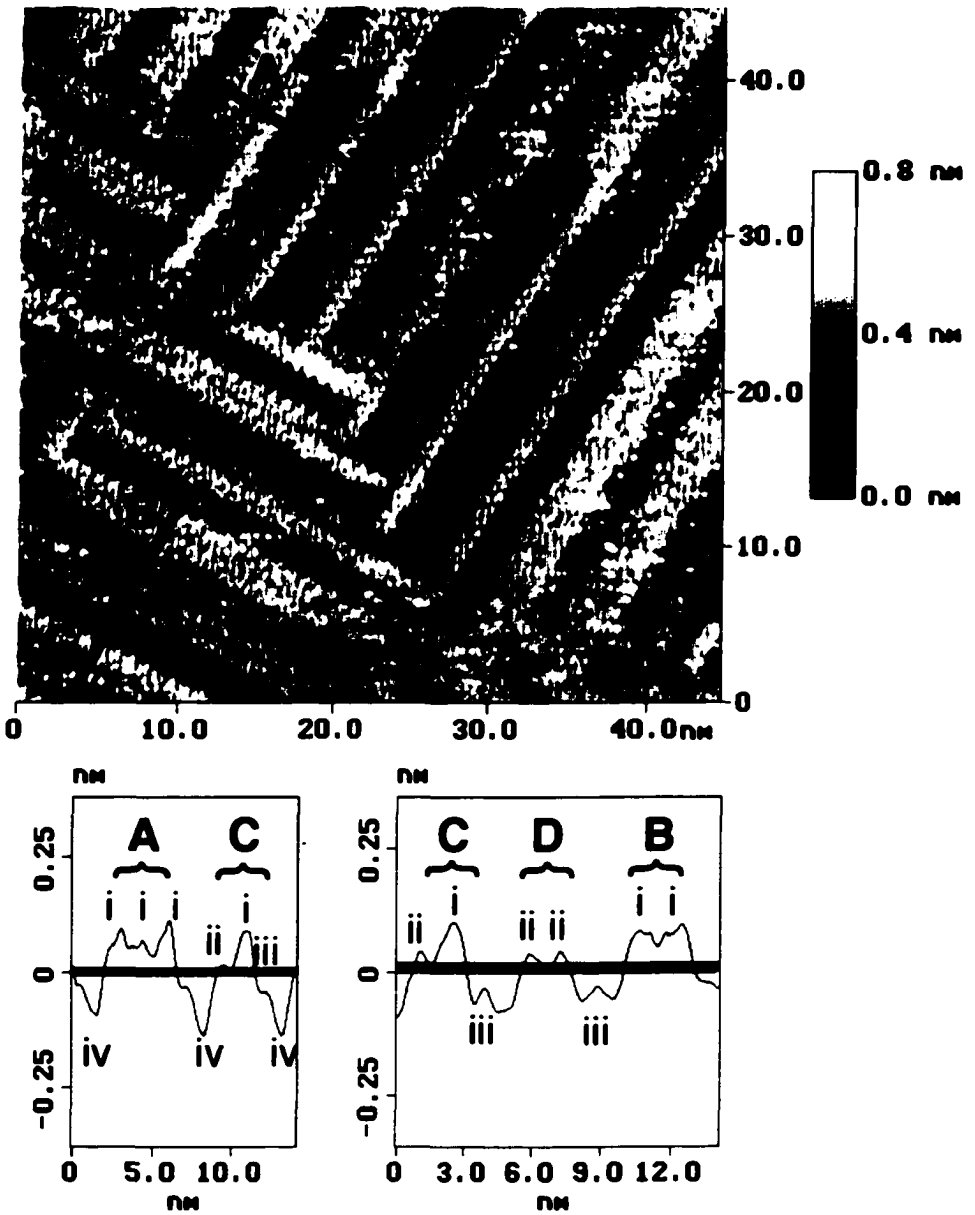

Figure 5.10: 45 nm x 45 nm image zoomed-in from Figure 5.9 exhibiting the 4 cluster types, A (i)/(i)/(i); B (i)/(i)/(iii); C (ii)/(i)/(iii); and D (ii)/(ii)/(iii). Red and blue lines overlaid on the image correspond to the cross-sections of the same color below. Letters overlaid on the image and on the cross-sections designate the cluster type shown. The cross sections illustrate the differences in apparent height between the bright (i), medium (ii), dim (iii), and dark (iv) contrast rows and the sequences of these row heights for each cluster.

concentration solution structures presented earlier also exhibits a 50 Å *a* unit cell parameter. Polymorph 2, however, exhibits a bright row width of ~17 Å and consists of a two-layer structure in which the chromophores in adjacent layers overlap by ~7Å. It is clear in the clusters shown in Figure 5.10 that the chromophores of adjacent layers do not overlap: they appear distinctly and separately as ~12 Å wide rows. Although the *combined* 2 layer structure of polymorph 2 is not the same as that observed here, it is likely that the *single layer* structure of polymorph 2 (its first layer) and the thin films shown here are similar, if not the same.

As mentioned earlier, the chromophores in polymorph 2 were not able to be resolved and thus the actual angle of the chromophores within a molecular row to the direction of the row was not determined. As a result, the model for polymorph 2 was constructed using a molecular angle that had been found to be common for other long-tailed squaraine systems (50°). Unlike the low concentration studies, however, single molecule resolution was achieved in Figure 5.10 in some of the bright (i) and medium (ii) apparent height rows and allowed measurement of the angle of the chromophores to the direction of their molecular row. It was found to be ~50° for both row apparent heights ((i) and (ii)) in this system. Although it could not be resolved, it is assumed that a similar angle exists in the dim (iii) apparent height rows. As a result of this common molecular angle and *a* unit cell parameter, the single layer structure used to construct the models of the multiple layer films observed here was the same as that used in the low concentration polymorph 2.

Figure 5.11 shows top and side views of the proposed models for the (a) Type C (ii)/(i)/(iii), (b) Type D (ii)/(ii)/(iii), (c) Type B (i)/(i)/(iii), and (d) Type A (i)/(i)/(i) row clusters. To facilitate recognition of the three-row cluster region in the models, red vertical lines are used to enclose the cluster region. In the side views of the models, the rows of chromophores within the cluster region are highlighted in yellow. They are further labeled with their observed STM image contrast, (i), (ii), (iii), or (iv). As mentioned above, each of the molecular layers within each cluster type is assumed to have the same or similar structure as that represented by the first layer of the polymorph 2 structure. This structure is shown in its entirety as the bottom (shadowed) layer in the top view of each of the models. Excepting model in Figure 5.11b, only the chromophore region of the molecules is shown in the subsequent layers. The tails are left out of the top view of these multilayer models for two reasons: (1) to facilitate viewing of the interlayer relationship of the chromophores, and (2) because the tails do not contribute to the tunneling contrast in the STM images of these cluster structures. As can be seen in the top view, the chromophores of subsequent layers do not overlap in any of the cluster types- they are either separate and discreet or they are totally eclipsed by the chromophore of a subsequent layer. This is surprising considering that the low concentration multilayer polymorphs (and multilayer polymorphs of other squaraines) each included substantial donor-acceptor interactions between molecules in adjacent layers.[2] Instead, in these cluster models the chromophores of each subsequent layer adsorb atop the tail region of

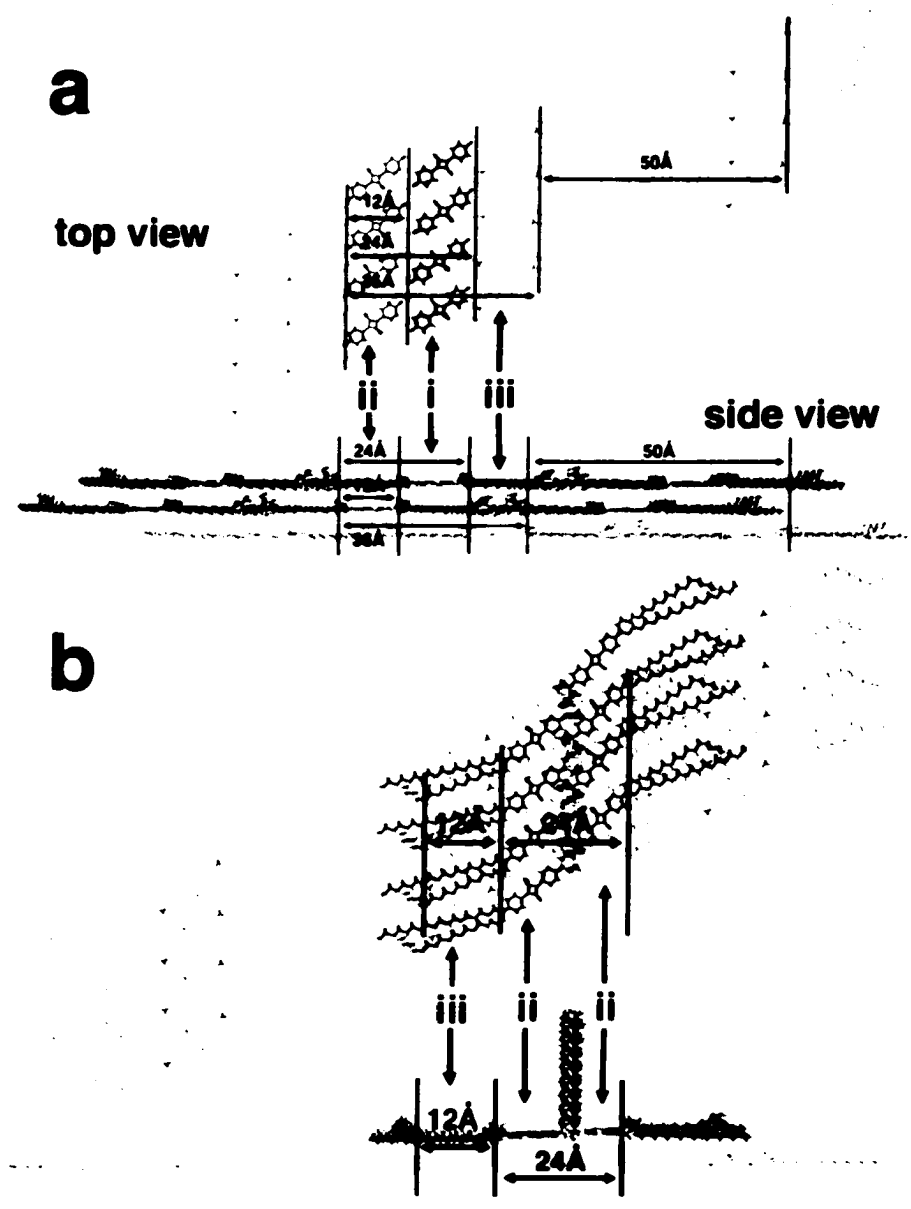

Figure 5.11: Top and side views of the proposed 3-layer molecular models of the (a) C and (b) D cluster types. The layers for each cluster have the same polymorph 2 structure, however, the tails are left out of the models of the second (middle) and third (top) layers in the three-layer models for simplicity. The first (bottom) layer is shown in its entirety in the top view in muted contrast. The middle layer is shown as medium contrast while the top layer is the darkest row of chromophores. The side view shows the entire structure of all two (Figure 5.11 b) or three (5.11 a, c, d) of the layers. The chromophores are highlighted in yellow to facilitate recognition. Chromophore regions in both the top and side views of the cluster models are labeled with their observed STM image contrast. The regions of the models that correspond to the clusters observed in Figures 5.9 and 5.10 are bracketed by red lines.

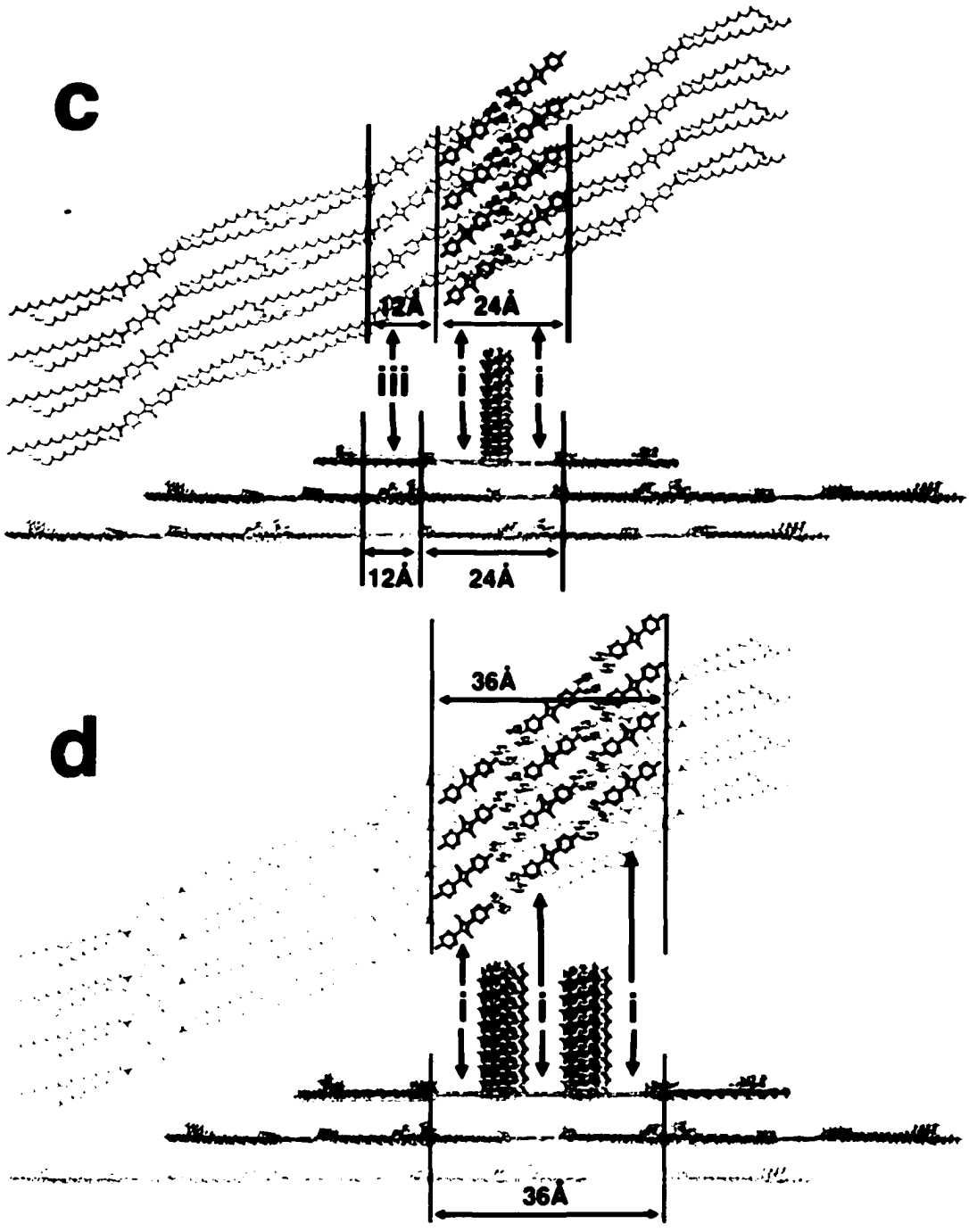

Figure 5.11: continued.

the layer beneath it. This can be seen in the side views of the models, which include the tails for all the molecular layers in each of the cluster types.

The Type C cluster of rows ((ii),(i), (iii)), shown in Figure 5.11a, is the only cluster in which all three of the molecular layers is resolved. Each row in the STM image (Figure 5.10) appears to be adjacent to a row of another apparent height. Since the adjacent rows have differing apparent heights, the chromophores of each of the rows are actually in different layers. As a result, there is no steric hindrance between the adjacent (i) and (ii) and (i) and (iii) rows, and the tails of the molecules within each of the layers may lie flat and interact with the adjacent tails both within their own layer and in the adjacent layer(s).

The remaining cluster types (D (ii)/(ii)/iii), B (i)/(i)/(iii), and A (i)/(i)/(i)) involve adjacent rows of the same contrast. Molecular rows of the same image contrast have the same apparent height and are thus in the same layer. The proximity of adjacent molecular rows of the same apparent height complicates the cluster structure. This proximity precludes the inclusion of the alkyl tails in the plane of the molecule in the region between adjacent chromophores of the same apparent height. As a result, we have modeled the tails in this intermolecular region as oriented perpendicular to the plane of the chromophore. This can be seen in Figure 5.11b in the model for the Type D cluster ((ii)/(ii)/(iii)), where a single row[‡] of perpendicular tails can be seen. This tail orientation allows the chromophores in adjacent rows to get close enough together to

[‡] Perpendicular tails in this inter-row region are referred to as a single "row" of tails despite the fact that the tails are actually from two different molecular rows. The singularity in the term "row" comes from the single inter-row region that all of the tails occupy. Two rows would then indicate two inter-row regions of perpendicularly oriented tails.

achieve the 24 Å total (ii)/(ii) row distance measured. In addition, as can be seen in the side view of the model, this orientation allows attractive dispersion interaction between the vertically-oriented tails. The total attractive interaction between the tails may mitigate any molecule-molecule repulsion between the amino groups of adjacent molecules, thus allowing chromophores to orient end to end. Also, adventitious water may exist in some structures and contribute to H-bonding between molecules. Figure 5.11c shows the model for the Type B, (i)/(i)/(iii), row cluster. From the top the (i)/(i)/(iii) model looks the same as the (ii)/(ii)/(iii), Type D, model. However, as can be seen in the side view, it is actually composed of 3 layers, the second layer of which is eclipsed by the third (top) layer. Chromophores in the top layer appear as bright (i) apparent height rows, those in the bottom layer appear as dim (iii) rows, and the middle layer chromophores do not appear at all because they are eclipsed by the top layer. Like the (ii)/(ii)/(iii) clusters, the tails in rows adjacent to another row of the same contrast are shown oriented perpendicularly to the molecular plane, thus forming a row of perpendicular tails. The (i)/(i)/(i) row cluster structure (Type A) is similar to that of the (i)/(i)/(iii) Type B cluster. Figure 5.11d shows the proposed model for the (i)/(i)/(i) structure, which is identical to that in 5.11c with the addition of a third consecutive row in the topmost (third) layer, producing a total of two rows of perpendicular tails. The models shown in Figures 5.11a, b, c, and d are our best guesses for the row cluster structures.

In addition to exhibiting the remarkable multiple-layer row clusters mentioned above, the film shown in Figure 5.9 also reveals intriguing 90° angles

between adjacent domains that at first seems incompatible with a substrate having trigonal symmetry. At least three types of 90° intersections can be observed in the image shown in Figure 5.12. Each type is illustrated with a different color ring. The first type, indicated by a red ring, exhibits a row of a particular apparent height suddenly taking a 90° turn, merging into a row of the same apparent height in an adjacent domain oriented 90° to the first domain. As shown in the model in Figure 5.12a, if the chromophores within a row are oriented ~45° to the edge of the row, then the orientation of a chromophore in a row 90° to the first is practically indistinguishable from the chromophores in the first row. Thus, essentially the same intermolecular interaction is possible between two adjacent chromophores in rows oriented 90° to one another compared to that between two chromophores in the same row. As a result, a row (or pair of rows) may make a 90° turn. This is exemplified by the frequent occurrence of 90° turns in rows of both medium (ii) and bright (i) contrast. A second type of 90° intersection, indicated in Figure 5.12 by a blue ring, resembles a "T". In this type, a row of a particular contrast appears to be capped or abruptly interrupted by a row of the same contrast oriented 90° to it. Close inspection of these areas shows that a slight gap exists between most 90° rows involved in "T" intersections. Thus, unlike the 90° turn, the perpendicular molecular rows do not actually blend together. We interpret this gap to signify that there is no chromophore-chromophore interaction between the rows at 90° to one another in this "T" conformation. A model of this structure is shown in Figure 5.12b. If the rows comprising the "T" intersection actually met one

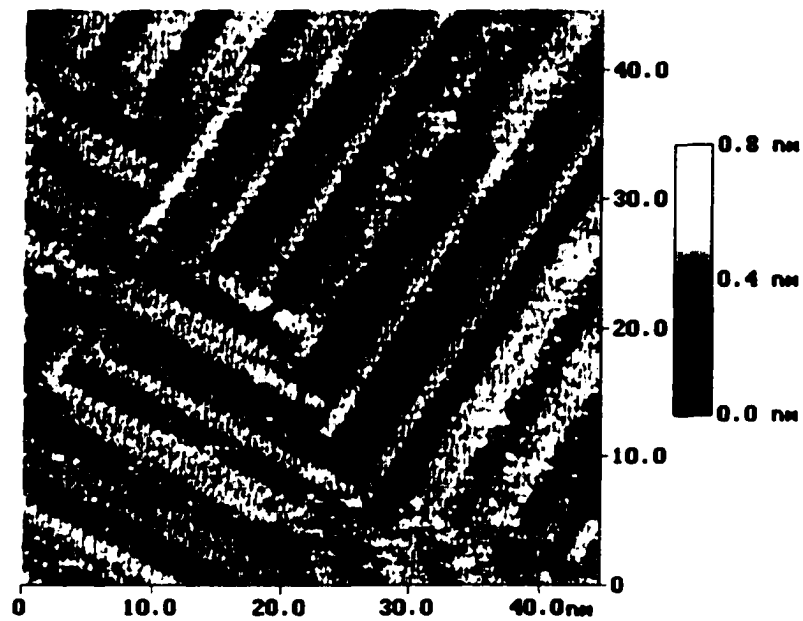

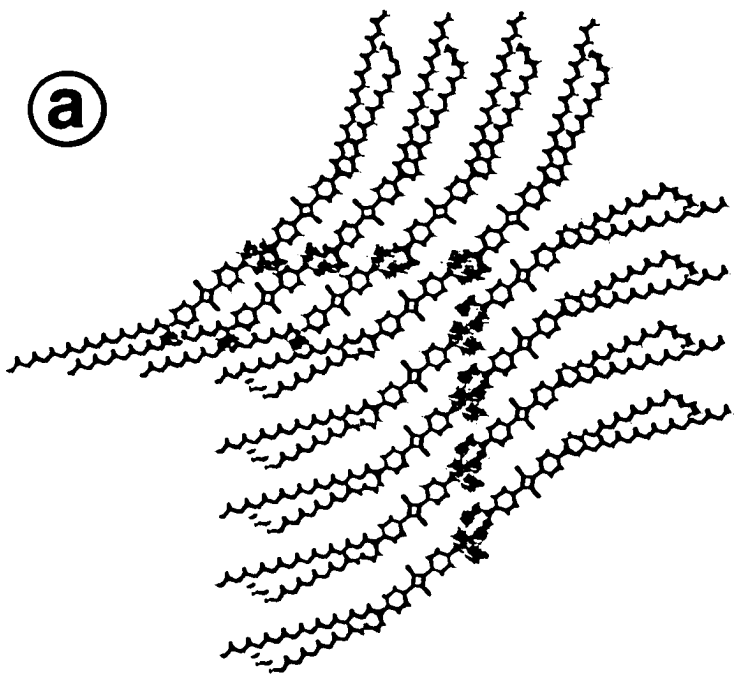

Figure 5.12: 45 nm x 45 nm image illustrating the three types of 90° row intersections. The red ring designates a 90° turn; the blue ring, a "T" intersection; and the green ring, a false "T" intersection. Models of the 90° turn (a) and "T" intersection (b) shown below.

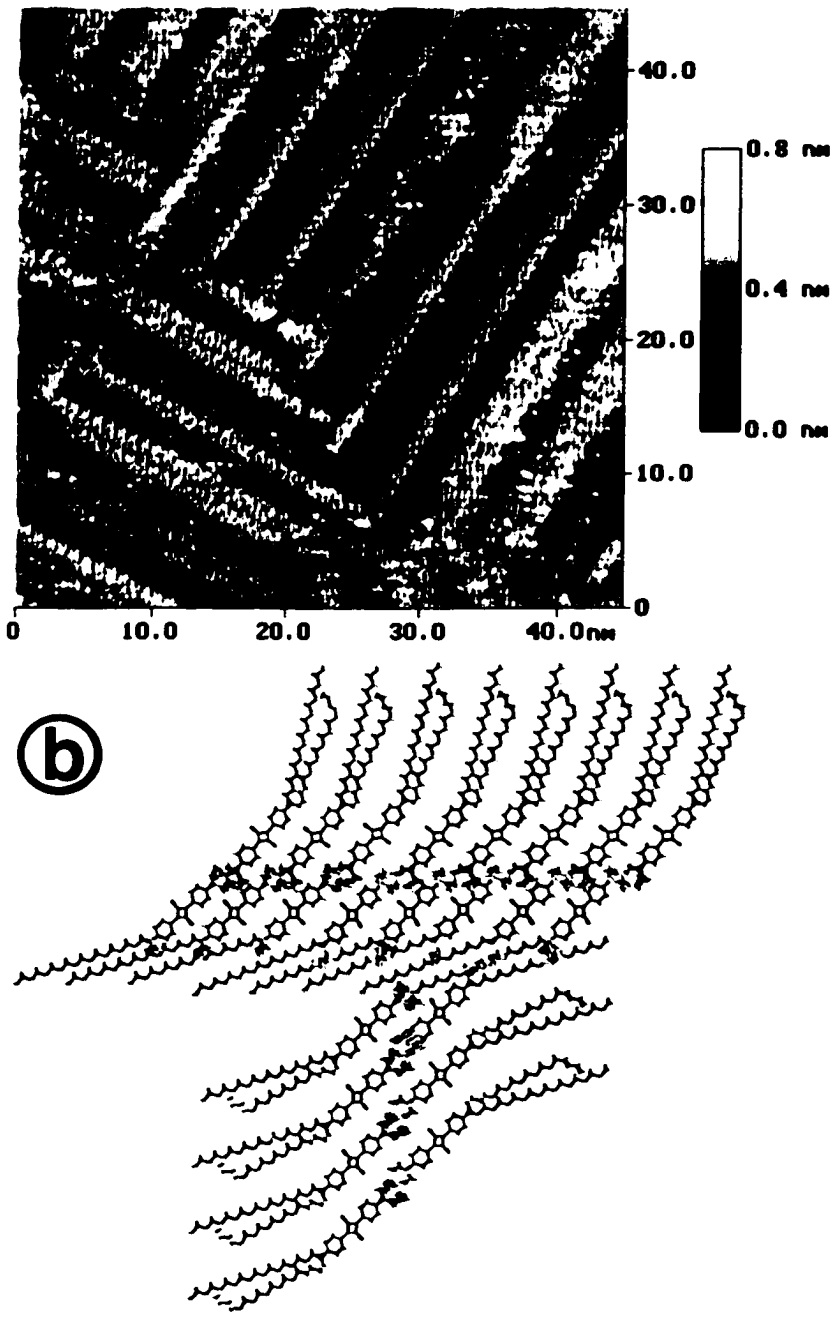

Figure 5.12: continued.

another, as they do in the 90° turn, the intersection area would result in a large amount of steric hindrance due to the abundance of tails in this intersection region. In addition, the chromophores at this intersection would have to overlap, thus creating a difference in apparent height between the overlapping chromophores. The two intersection types just described occur between rows of the same apparent height that intersect at 90° angles. A third type of 90° intersection (indicated in Figure 5.12 by a green ring) can be observed between rows of differing contrast (medium and bright rows) oriented perpendicular to one another. This type of intersection is always located next to a 90° turn or "T" intersection. In this intersection, one of the rows appears to be abruptly ended by the perpendicular row. With the exception that the intersecting rows differ in apparent height, it appears to be a "T" intersection. But the fact that the intersecting rows *are* of different contrasts, assumedly signifying that they are in different layers, indicates that the rows do not intersect in the same plane, but are only overlapping at 90°. Thus, it is not a true intersection.

Other high concentration experiments did not produce the row clusters or the 90° intersections just described. Rather they produced small domains similar to that in Figure 5.8a, composed primarily of polymorph 1. These domains then grew across the surface, completely covering the HOPG. When the HOPG was covered, growth continued in a layer by layer fashion (although not in the layered structures just discussed). An example of the layer by layer growth observed is shown in the timelapse sequence of images in Figure 5.13. The image in Figure 5.13a was captured 12 minutes after solution deposition. It shows a fairly

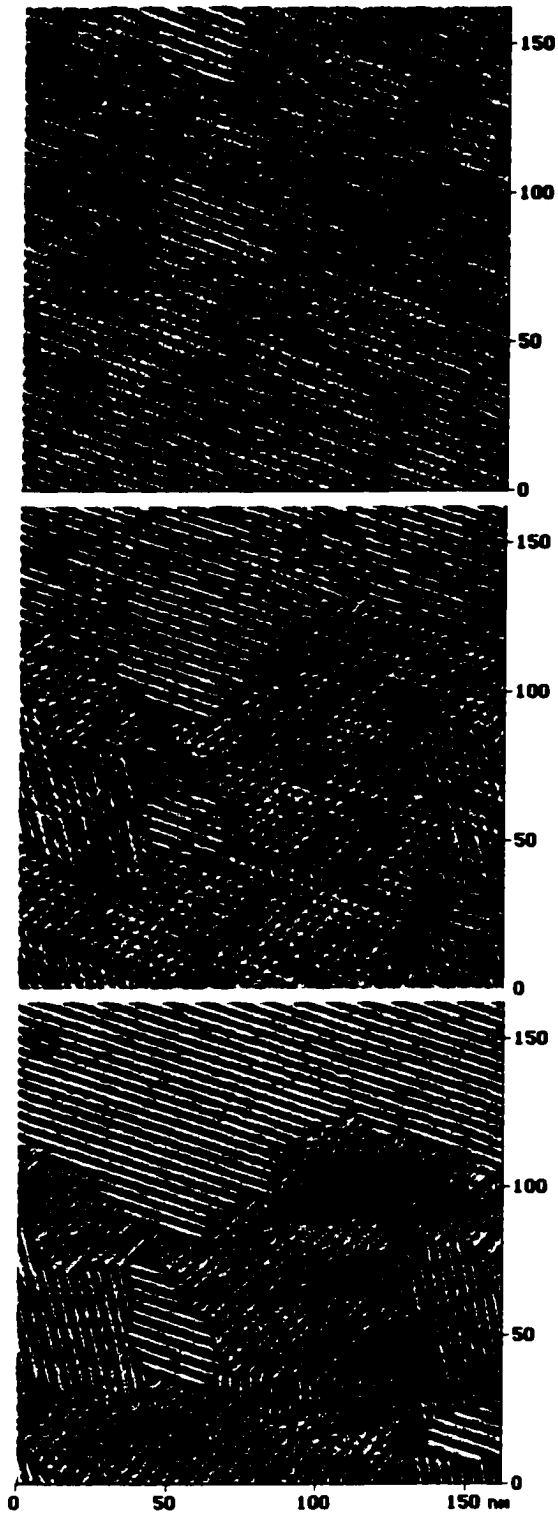

Figure 5.13: Three 160 nm × 160 nm images showing the same area of adsorbed 18-18HSQ, taken over a period of 32 minutes, showing the growth of multiple layers. Image (a) was taken 12 minutes after solution deposition, (b) 23 minutes after (a), and (c) 9 minutes after (b).

complete adsorbed layer of polymorph 1 with rows oriented ~110° from the left edge of the image. Faintly visible rows of differing orientation are seen growing in atop this layer. Image b was captured 23 minutes after a. The growing second layer is more visible now, forming a cross-hatch pattern over the still visible first layer. The predominant orientation of the second layer domains is 60 ° to the orientation of the first layer, although it is clear that some adsorption is occurring also directly atop the first layer in the same orientation as the first layer. Figure 5.13c, captured 9 minutes after b, shows a more complete second layer, the first layer now being visible only in small patches.

Epitaxial Relationship of 18-18HSQ with HOPG

As mentioned in previous sections, domains of 18-18HSQ tend to orient with respect to one another at angles of 30° or 60° multiples. These orientations signify an epitaxial relationship of the domains with the underlying HOPG substrate. When domain directions were compared to the directions of the underlying HOPG, a 30° difference was often found between the orientations of the domains (row directions) and the orientation of the HOPG lattice. This is illustrated in Figure 5.14, which shows the 2D spectra of an 18-18HSQ polymorph 1 layer and HOPG overlaid on one another. The 18-18HSQ image from which one of the 2D spectra was taken, shown in Figure 5.14, is composed of several domains of polymorph 1. The image of the HOPG surface from which the other spectrum was taken (not shown) was captured 5 minutes after the squaraine image was taken from within the same area of the surface. The 2 spectra were normalized in both intensity and magnification. The angular

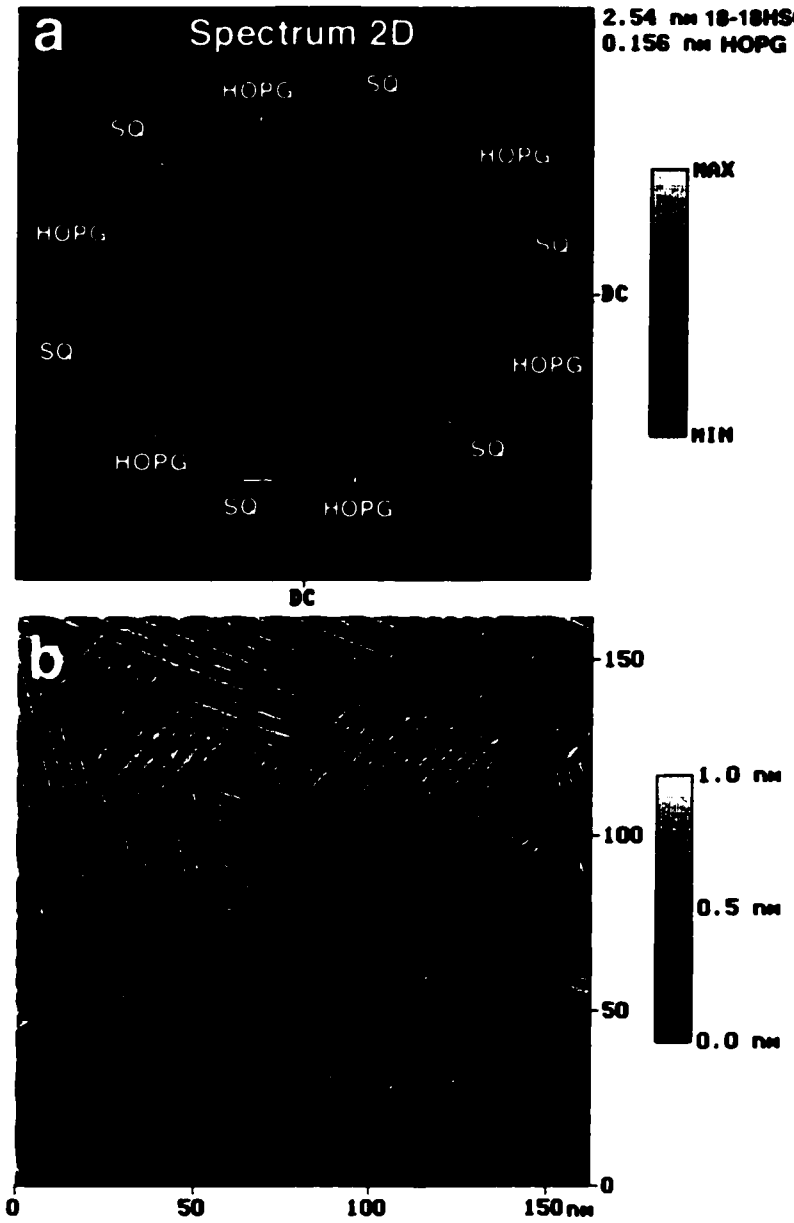

Figure 5.14: (a) 2D spectra of HOPG and the 18-18HSQ overlayer shown in (b) overlaid on one another. Spots corresponding to the overlayer and the substrate lattices are labeled by either HOPG or SQ. The spectra are normalized in intensity and distance, but the angular relationship has not been altered. 18-18HSQ spots appear 30° from the HOPG spots, illustrating a distinct relationship between the overlayer and the substrate.

orientation of the spectra, however, were not changed. The spots for HOPG and 18-18HSQ within the spectrum are labeled to distinguish the two. It can be clearly seen that both the HOPG and the domains in the SQ overlayer have 3-fold symmetry. It is also clear that the SQ spots occur 30° from the HOPG spots. Thus, the squaraine overlayer has a coincident relationship to the HOPG lattice. The comparison of spectra for 18-18HSQ overlayers and HOPG was not possible for all polymorphs, however, it can be said that (except for the predominantly 90° films illustrated by Figure 5.9) domains exhibited orientations that varied by 30° or 60° multiples from one another, a relationship that reflects the symmetry of the HOPG lattice. Even within Figure 5.9, however, it can be seen that some 120° relationships exist. Thus, the polymorphs observed for 18-18HSQ on HOPG appear to have a stronger epitaxial relationship to HOPG than any of the squaraines studied on HOPG thus far.[2,12]

Mechanism of Nucleation and Growth

The three nucleation and growth scenarios for 18-18HSQ presented in the previous sections suggest the involvement of at least two separate nucleation mechanisms. Since 18-18HSQ is not very soluble in phenyloctane, it is reasonable to assume that there are aggregates even in the low concentration solutions used in these experiments. The aggregate structure of long-chain bis[4-(dialkylamino)phenyl]squaraines (such as 18-18HSQ) has not been determined. However, recent electrospray ionization mass spectrometry studies by Ashwell et al on the solution aggregation of 2,4-bis[4-(N-methyl-N-alkylamino)phenyl]squaraines where the alkyl group varies from butyl to dodecyl

have found that these long-tailed molecules readily form dimers.[23] Extensive studies of short-tailed bis(dialkylamino-hydroxyphenyl)squaraines show that face-to-face aggregates appear to form in solvents in which they are reasonably soluble.[24] We will assume that similar face-to-face or card-stack structure dimers or higher order aggregates exist in the solutions of these longer-tailed molecules in phenyloctane. The presence of small domains of multiple-layer structures at the onset of nucleation (see Figures 5.1 and 5.8) supports a scheme involving such solution aggregates as domain nuclei. The manner in which these aggregates adsorb onto the surface can influence the kind of structures that develop. These variations in aggregate adsorption are the subject of the following discussion.

We will focus on the adsorption of a stacked dimer aggregate with the long axis of the squaraine molecules oriented parallel to the plane of the HOPG surface. In this general classification, the plane of the aromatic rings of the squaraines within the aggregate may adsorb either parallel to the HOPG surface or perpendicular to the surface. We will refer to the adsorption of the squaraine aggregate with the aromatic rings oriented either parallel or perpendicular to the plane of the surface as *parallel* and *perpendicular* adsorption, respectively. In the case of the *parallel* adsorption of the squaraine aggregate, shown in Figure 5.15a, only one of the molecules is in contact with the graphite, since the second molecule lies on top of the first. Thus, the face-to-face structure of the aggregate is maintained due to the strong donor-acceptor, or dipole-dipole, interaction between the chromophores. Aggregates adsorbed in this manner may be the

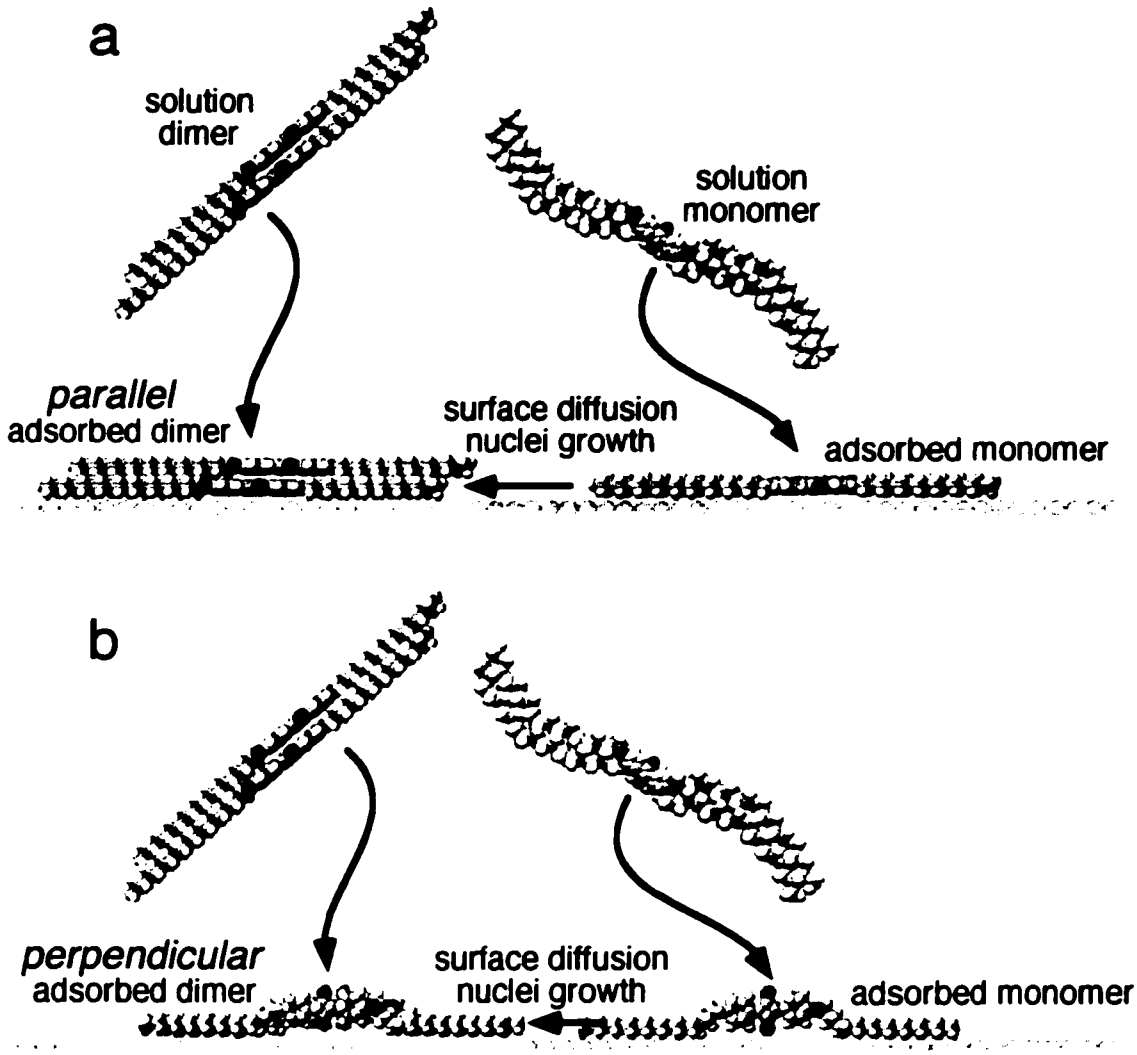

Figure 5.15: Schematics showing two mechanisms proposed for the nucleation and growth of 18-18HSQ on HOPG in the low and high deposition solution concentration regimes. (a) *Parallel* adsorption of 18-18HSQ dimers onto the HOPG surface and subsequent lateral growth to produce the 2-layer structures observed (polymorphs 1 and 2). (b) *Perpendicular* adsorption of 18-18HSQ dimers onto the HOPG surface and subsequent lateral growth to produce the single-layer card-stack structure observed (polymorph 3).

nuclei of the multiple layer structures that appeared almost immediately upon solution deposition in Figures 5.1 and 5.2 (polymorphs 1 and 2). Lateral growth of these nuclei across a surface may occur either from incorporation of monomers or other aggregates at the edges of the nuclei. This first mechanism of nucleation and growth is shown schematically in Figure 5.15a.

A dimer or trimer that adsorbs onto the graphite surface with the plane of the squaraine chromophores oriented perpendicular to the HOPG plane forms the basis for the second mechanism of nucleation. *Perpendicular* adsorption of a card-stack aggregate causes the stack to lie on it side. In this orientation, each of the molecules contacts the surface on one edge while still maintaining a close (~4 Å) face-on donor-acceptor interaction between the adjacent molecules. Assuming that a few gauche defects are incorporated into the tail, two of the octadecyl tails per molecule may adsorb and attractively interact with the HOPG lattice. This second mechanism is shown in Figure 5.15b. Again, monomers or additional aggregates add to the card-stack to lengthen the rows. Clearly this mechanism can explain the polymorph 3 single-layer card stack structure shown in Figure 5.7.

Polymorph 4 (Figure 5.6) is most easily explained by 18-18HSQ monomers that have partitioned to the HOPG surface and lie flat, whereas the structures shown in Figure 5.9 are too complex and were not observed early in their growth and so our understanding of this type of nucleation is incomplete.

The large number of polymorphs observed in the investigation of the ordered adsorption of this molecule on HOPG is common for long-tailed

squaraines. As reported previously,[2] a total of seven polymorphs were observed for the ordered adsorption of 2-18OHSQ on HOPG from phenyloctane solution. These polymorphs were also complex multiple-layer structures. The increase in the number of observed polymorphs in these combined (2-18OHSQ and 18-18HSQ) studies of long-tailed squaraines, as compared to shorter-tailed squaraines,[2,12] is in part due to the large number of attractive methylene-methylene dispersion interactions possible between octadecyl tails and the variety of ways that these interactions may occur. Attractive tail-tail interactions may arise between (1) the alkyl tails of molecules in adjacent rows within the same molecular layer through interdigitation; (2) the alkyl tails of molecules in adjacent layers, through stacking; (3) the two alkyl tails on the same side of a single molecule through gauche defects that allow both of the tails to reside in the molecular plane. Additionally, the large sum of attractive methylene-methylene interactions allows for small variations in the extent of these interactions. For example, as was seen in polymorph 2, the extent of intra-layer interdigitation between tails in adjacent molecular rows is dramatically reduced compared to that of polymorph 4. However, this reduction in interdigitation allows all four of the 18-18HSQ octadecyl tails to fit into the same plane. Attractive interaction between the adjacent dialkylamino tails within the same molecule is thereby introduced, and compensates for the energetic loss caused by decreased interdigitation. Further compensation occurs when subsequent molecular layers are incorporated into the structure such that the tail regions of adjacent layers overlap. As a result of the variety of ways that the four octadecyl

tails per 18-18HSQ molecule can interact, and the large number of low energy conformations that the tails can take on, numerous structures may be formed with similar energies- hence the large number of polymorphs observed in this study. One of these polymorphs is probably the thermodynamically most stable structure, but without performing extended timescale or temperature studies, it cannot be known which, if any of the observed polymorphs, it is.

Conclusions:

In this chapter the nucleation and growth of ordered layers of 18-18HSQ onto the basal plane of HOPG from both low and high concentration phenyloctane solutions has been reported. It has been shown that adsorbed 18-18HSQ forms at least four polymorphs, three of which are multiple layer structures. Single layer polymorphs were observed only at low concentrations, however, small multiple layer domains were observed at both low and high concentrations immediately following solution deposition. Nucleation mechanisms incorporating aggregate adsorption from solution were proposed to explain the observation of the many multiple layer polymorphs.

The balance between attractive intermolecular chromophore-chromophore interactions and attractive tail-tail or tail-HOPG interactions in the various structures was discussed. Although it was observed that many of the polymorphs exhibited a coincident relationship to the surface, intra-layer chromophore-chromophore interactions (similar to those exhibited by other squaraines adsorbed on HOPG) were still present in all of the ordered structures.

Inter-layer chromophore-chromophore interactions were sometimes compromised, however, as in the observed multiple layer row clusters. Nevertheless, it did not appear that the ordered structures reported here were being driven by one interaction over the other.

Finally, a few intriguing characteristics of this system have been presented: remarkable multiple layer films may be formed from the layering of 2-layer polymorphs onto one another; and although achiral, 2D chiral assemblies of these molecules were observed in one of the single layer polymorphs.

References

(1) Groszek, A. J., *Proc. Roy. Soc. Lond. A.* **1970**, *314*, 473-498.
(2) Stawasz, M. E.; Sampson, D. L.; Parkinson, B. A., *Langmuir* **2000**, *16*, 2326-2342.
(3) Kaneda, Y.; Stawasz, M. E.; Sampson, D. L.; Parkinson, B. A., *Langmuir* **2001**, *17*, 6185-6195.
(4) Qiu, X.; Wang, C.; Yin, S.; Zheng, Q.; Xu, B.; Bai, C., *J. Phys. Chem. B* **2000**, *104*, 3570-3574.
(5) Qiu, X. H.; Wang, C.; Zeng, Q. D.; Xu, B.; Yin, S. X.; Wang, H. N.; Xu, S. D.; Bai, C. L., *JACS* **2000**, *122*, 5550-5556.
(6) Szasz, G. J.; Sheppard, N.; Rank, D. H., *J. Chem. Phys.* **1948**, *16*, 704-711.
(7) Woller, P. B.; E.W. Garbisch, J., *JACS* **1972**, *94*, 5310.
(8) Kiselev, A., *Russ. J. Phys. Chem.* **1961**, *35*, 111.
(9) DeFeyter, S.; Grim, P. C. M.; Rucker, M.; Vanoppen, P.; Meiners, C.; Sieffert, M.; Valiyaveettil, S.; Mullen, K.; DeSchryver, F. C., *Angew.Chem.Int.Ed.* **1998**, *37*, 1223-1226.
(10) Yablon, D. G.; Giancarlo, L. C.; Flynn, G. W., *J.Phys.Chem.B* **2000**, *104*, 7627-7635.
(11) DeFeyter, S.; Gesquiere, A.; Wurst, K.; Amabilino, D.; Veciana, J.; DeSchryver, F., *Angew.Chem.Int.Ed.* **2001**, *40*, 3217-3220.
(12) Stawasz, M. E.; Parkinson, B. A., **manuscript in preparation**,
(13) Wingard, R. E., *IEEE Trans. Ind. Appl.* **1982**, 1251-1254.
(14) Law, K. Y., *Chem. Rev.* **1993**, *93*, 449-486.
(15) Takeda, N.; Stawasz, M. E.; Parkinson, B. A., *J. Electroanalytical Chem.* **2001**, *498*, 19-33.
(16) Loutfy, R. O.; Hsiao, C. K.; Kazmaier, P. M., *Photogr. Sci. Eng.* **1983**, *27*, 5-9.
(17) Bernstein, J.; Tristani-Kendra, M.; Eckhardt, C. J., *J. Phys. Chem.* **1986**, *90*, 1069-1073.
(18) Tristani-Kendra, M.; Eckhardt, C. J.; Bernstein, J.; Goldstein, E., *Chem. Phys. Lett.* **1983**, *98*, 57-61.
(19) Tristani-Kendra, M.; Eckhardt, C. J., *J. Chem. Phys.* **1984**, *81*, 1160.
(20) Law, K. Y., *J. Phys. Chem.* **1987**, *91*, 5184-5193.
(21) Law, K. Y., *J. Phys. Chem.* **1988**, *92*, 4226-4231.
(22) Law, K. Y.; Facci, J. S.; Bailey, F. C.; Yanus, J. F., *J. Imaging Sci.* **1990**, *34*, 31-38.
(23) Ashwell, G. J.; Roberts, M. P. S.; Rees, N. D.; Bahra, G. S.; Brown, C. R., *Langmuir* **1998**, *14*, 5279-5284.
(24) McKerrow, A. J.; Buncel, E.; Kazmaier, P. M., *Can. J. Chem.* **1995**, *73*, 1605-1615.

CHAPTER SIX

Conclusions and Future Work

This Dissertation has described the systematic study of the ordered adsorption of twelve different squaraine molecules on the HOPG surface. These molecules were varied in the lengths of their alkyl tails (from CH_3 to $C_{18}H_{37}$), the identity of their C2 phenyl ring substituent (OH or H), and the degree of symmetry within the molecule ($R_1 = R_2$, or $R_1 \neq R_2$). It was found that when deposited onto the HOPG surface from phenyloctane solution, all of these squaraines were highly surface active, forming sometimes remarkable monolayer and multiple layer ordered structures.

By comparing the ordered structures exhibited by these systematically varied squaraines, the major intermolecular forces influencing the molecular order observed via STM were determined. They were chromophore-chromophore interactions, tail-tail interactions, and tail-HOPG interactions. The balance between these interactions in driving the ordered structure observed was dependent upon the molecular structure of the squaraine. In all the squaraines studied, the donor-acceptor-donor structure of the molecule contributed significantly to the orientation of adsorbate molecules with respect to one another both in 2 dimensions (monolayer) and in 3 (multiple layers). In addition to single layer structures, multiple layer structures were often observed in which a distinct relationship between the donor and acceptor moieties of molecules within the adjacent layers was present. Two general structures were observed in ordered

squaraine adsorbates: herringbone and row structures. In both structures, the chromophores of adjacent molecules orient with respect to one another such that donor-acceptor (or Coulomb) interactions between the aniline moieties (donor) and central C_4O_2 rings (acceptor) of adjacent molecules are possible. In herringbone structures, adjacent molecules orient with their long molecular axes at 70 - 90° angles to one another such that donor and acceptor moieties of adjacent molecules point towards one another. A total of four donor-acceptor chromophore-chromophore interactions are possible between a single molecule and its nearest neighbors (one for each neighbor). In row structures, chromophores within the same row are oriented with their long molecular axes parallel to one another. Adjacent molecules within the same row are offset from one another by ~4 Å, allowing the donor and acceptor moieties of adjacent molecules to align. In this structure, a total of 4 donor-acceptor interactions are possible with its nearest neighbors (two for each nearest neighbor within the same row, but none with neighbors in adjacent rows). Both herringbone and row structures were observed for shorter-tailed squaraine molecules ($\leq$ 4 carbons). Only row structures were observed for longer-tailed molecules ($\geq$ 6 carbons). This adsorbate structure transition indicates a corresponding transition in the influence of the alkyl tails on the observed adsorbate structure. The close proximity of the molecules in herringbone structures prevents more than a few methylene units from contacting the HOPG surface. In addition, in the small intermolecular region of a herringbone structure, steric repulsion between tails can become significant. Between 4 and 6 carbons, the herringbone structure

appears to become energetically unfavorable. Row structures, however, minimize tail-tail repulsion and maximize tail-tail attraction by allowing interdigitation of every other adjacent tail (the other tails are necessarily desorbed from the HOPG surface). Squaraines with medium length tails ($6 \leq C_n < 12$) did not show any coincidence with the HOPG lattice, indicating that tail-HOPG interaction is not significant enough to template the squaraine adsorbate structure. Longer-tailed squaraines ($C_{12}H_{25}$ and $C_{18}H_{37}$, but not for 2-18 OHSQ) tended to show a stronger orientational relationship to the HOPG lattice, indicating an increased influence of tail-HOPG interaction.

Squaraines with long alkyl tails (2-18 OHSQ and 18-18 HSQ) exhibited many row polymorphs relative to shorter-tailed squaraines. This is most likely due to the large number of possible nearly-all-trans (low energy) tail conformations that have nearly equivalent energies.

Comparison of the ordered structures of hydroxylated and non-hydroxylated squaraines shed light on the influence of hydrogen bonding on squaraine adsorbate order. It was found that hydroxyl substitution at the C2 position of the phenyl ring does not influence squaraine molecular order on HOPG. The same ordered structures were observed for hydroxylated and non-hydroxylated squaraines of the same tail length. However, it was observed that the lack of inter- and intra-molecular H-bonding caused these orientationally-equivalent non-hydroxylated squaraine adsorbate structures to be less stable, and for the STM images of these molecules to be more noisy.

By decreasing the symmetry of the squaraine molecule in introducing $R_1 \neq R_2$ a number of tail-related factors effecting the ordering of squaraine molecules in row structures were elucidated. Squaraines having $R_1 = CH_3$ and R_2 = the length of a more symmetrical squaraine (1-8 HSQ and 8-8 HSQ) have exhibited the same ordered structures as the more symmetrical squaraine. This proves that the two alkyl tails not involved in the adsorbed interdigitating tail structure have no influence on the adsorbed structure at all. In addition, it suggests that the desorbed tails in the symmetrical squaraine row structure occupy an area on the HOPG surface similar to that of a methyl group. The ordered adsorbate characteristics of 2-18 HSQ suggest that when a short R_1 tail is paired with a long R_2 tail, a degree of flexibility is somehow introduced into the row structure, allowing the row to depart from its usual rigidly linear form. This meandering row characteristic was not observed for 18-18 HSQ.

Of course, there are still many questions remaining to be answered concerning the ordered adsorption of sqaraines on HOPG. Molecular mechanics has not been a part of this dissertation. One of the questions that remains unanswered is why are both herringbone and row structures observed for 1-1 OHSQ, only row structures for 3-3 HSQ, and only herringbone for 4-4 OHSQ/4-4HSQ? What are the relative energies of these two structures at each of these tail lengths? Future experiments would include the use of a mechanics program such as Cerius to determine the relative energies of the herringbone and row structures at these short tail lengths. Additionally, the interaction energy of the chromophore-chromophore interactions in both row and herringbone structures

are presently unknown. By modeling dimers of squaraines without alkyl tails and without the HOPG substrate present (in both row and herringbone orientations), the approximate energies of these chromophore-chromophore interactions could be determined.

A rigorous classification of the adsorbate structures observed in terms of their epitaxial relationship to the HOPG lattice has not been performed. Future work would utilize the epitaxial calculation program EpiCalc[1] to determine if any supercell structures (see Appendix A) exist for the squaraine adsorbate structures observed. The presence (or absence) of supercells, as well as the size of the supercell, can aid in providing an epitaxial classification (commensurate, coincident, or incommensurate) for the adsorbate structures observed.

An investigation that would be of interest to industrial users of squaraine films is the effect of substrate roughness on squaraine interfacial (film/substrate) ordering. The basal plane surface of HOPG can easily and controllably be roughened through its controlled oxidation in air at ~ 500° C temperatures.[2-4] The result is single layer deep circular pits in the HOPG surface. The diameter, density and depth of the pits can be controlled by varying the temperature and time duration of the oxidation, and by varying the quality of the original HOPG sample. By systematically increasing the pit depth and pit density, the effect of HOPG roughness on the number and type of ordered structures exhibited by adsorbed squaraines as well as their domain size and stability can be probed. This same oxidation procedure can be used to determine the lower size limit of

squaraine aggregates that can nucleate ordered domains. Due to the relatively fast timescale (compared to that of STM imaging) of ordered squaraine nucleation on the HOPG surface, this limit has not been determined thus far. However, it is possible to use single layer circular pits in the HOPG surface as "molecule corrals".[5-8] For some molecular systems, it has been shown that domain nucleation inside the graphite pits occurs independently of nucleation on the HOPG terrace. In this way, a domain nucleus can be isolated (or "corralled") and studied inside the pit independent of the nucleation and growth occurring on the HOPG terrace. By varying the diameter of the pit from large to small sizes, the smallest ordered domain nuclei can be determined. Pits that are too small for nucleation will contain either amorphously-adsorbed squaraines, or no squaraines at all.

Structural variation of the squaraine molecule can be continued. Within the original hydroxylated and non-hydroxylated series, alkyl tail length can be further probed. Strange ordering effects have been observed for other molecules incorporating alkane chains with odd numbers of carbon atoms on HOPG.[9] The only odd-tailed molecule investigated in this Dissertation is 3-3 HSQ. It was expected that this molecule would exhibit a herringbone pattern since 4-4 HSQ, 4-4 OHSQ, and 1-1 OHSQ did. Rather, it was the only short-tailed squaraine not to exhibit a herringbone structure. Will 3-3 OHSQ or 5-5 OHSQ/HSQ produce herringbone structures? Will further strange effects be observed for 7-7 OHSQ/HSQ, 9-9 OHSQ/HSQ, 11-11 OHSQ/HSQ, or 13-13 OHSQ/HSQ?

Another aspect of squaraine order that remains unknown is whether there is an alkyl tail length at which tail interaction with the HOPG surface unambiguously templates squaraine order. Studying very long-tailed squaraines such as 30-30 or 36-36 (or 1-30 and 1-36) OHSQ/HSQ should provide insight into this question. It would be intriguing to see whether the alkyl tails orient along the HOPG lattice directions typical for alkane registry. Furthermore, if they do, are chromophore-chromophore interactions still maintained? Is there a point of transition to tail-HOPG interaction dominance in driving the squaraine adsorbate structure?

Thus far, only three asymmetric ($R_1 \neq R_2$) squaraines have been studied, with $R_1 \ll R_2$. As mentioned earlier, this was illustrative in determining the role of the desorbed tails in row structures. It would be interesting to study squaraines with R_1 closer in length to R_2, such as C_6H_{13} and C_8H_{17}, or $C_{10}H_{21}$ and $C_{12}H_{25}$. Tail lengths such as these are close enough that the energetic difference between the adsorption of ± two methylene units may be small. It this case, it may be possible for either the R_1 or R_2 tails to adsorb, thus allowing for multiple adsorbate polymorphs of similar energy. Another variation on asymmetry is the study of squaraines that have two short tails (same number of carbons) on one aniline and two long tails (same number of carbons) on the other.

Several variations in chromophore structure are possible. Changing the identity of the X substituent at C2 position on phenyls could change the planarity of the molecule, affecting its adsorbate order. It has been shown that squaraines with CH_3 or F at the C2 position are not planar. These substituents cause a

tilting of the C_4O_2 ring out of planarity with the phenyls.[10] What changes in adsorbate order will this non-planarity cause? Changes in the adsorbate structure as a result of a change in the position of the phenyl substituent from C2 to C3/C5 would also be instructive.

My final proposed change in squaraine structure is directed not at changes in adsorbate structure, but at changes in STM image contrast. In the experiments reported here, it was not possible to resolve the C_4O_2 oxygens or the phenyl hydroxyl groups. This is typical for the STM image contrast of molecular adsorbates containing oxygens. It has been shown that sulfurs and thiols, however, appear as bright areas in STM images of molecular adsorbates. This has been proposed to be due to the lower ionization potential of S relative to O, thus making it easier to tunnel through than O. Sulfur and oxygen have very similar electronic structures and both can form hydrogen bonds. Therefore, if the oxygen atoms present in OHSQs were replaced with sulfurs, the intra- and intermolecular interactions would not be expected to change significantly from those present in OHSQs, but the sulfurs would be resolved in the STM image contrast. This would aid in more precisely determining the relationship of donor and acceptor moieties in adjacent molecules within an adsorbate structure.

My final suggestion for future work involving this molecular system on HOPG involves temperature studies. By raising the temperature of the ordered squaraine films by a few degrees while imaging, the thermodynamic polymorphs can be determined. If a number of polymorphs are observed to coexist within an

ordered thin film at room temperature, then raising the temperature will cause conversion of these polymorphs to more thermodynamically-stable structures.

REFERENCES

(1) Yip, C.; Ward, M. D., *http://www.wardgroup.umn.edu/software.html*
(2) Evans, E. L.; Griffiths, R. J. M.; Thomas, J. M., *Science* **1971**, *171*, 174-175.
(3) Chang, H.; Bard, A. J., *J. Am. Chem. Soc.* **1990**, *112*, 4598-4599.
(4) Chu, X.; Schmidt, L. D., *Carbon* **1991**, *29*, 1251-1255.
(5) Patrick, D. L.; Cee, V. J.; T.P. Beebe, J., *Science* **1994**, *265*, 231-234.
(6) Patrick, D. L.; Cee, V. J.; T.P. Beebe, J., *J. Phys. Chem.* **1996**, *100*, 8478-8481.
(7) Patrick, D. L.; Cee, V. J.; Purcell, T. J.; T.P. Beebe, J., *Langmuir* **1996**, *12*, 1830-1835.
(8) Stevens, F.; Buehner, D.; T.P. Beebe, J., *J. Phys. Chem.* **1997**, *101*, 6491-6496.
(9) Hibino, M.; Sumi, A.; Tsuchiya, H.; Hatta, I., *J. Phys. Chem. B* **1998**, *102*, 4544-4547.
(10) Law, K. Y., *J. Phys. Chem.* **1989**, *93*, 5925-5930.

APPENDIX A

Commensuration

The concept of epitaxy has been firmly established through the development and study of inorganic systems in which a monolayer, film, or crystal of a material is grown atop a substrate of the same or a different material. In these systems, covalent bonds are often formed between the overlayer species and the substrate surface. Adsorbate-adsorbate interactions are small compared to the adsorbate-substrate binding forces. As a result, adsorbate locations on the substrate surface are determined by the optimum adsorbate-substrate bonding, which is directly related to the substrate lattice spacing and symmetry. From the study of such systems, a rigid definition for the term epitaxy has been developed: epitaxy is a strict relationship between the overlayer and the substrate in which the overlayer exhibits the same crystal structure, orientation, and lattice parameter as the substrate.[1]

The role of epitaxy in physisorbed molecular overlayers requires special attention, however, because they often depend upon a delicate balance of noncovalent interactions between the adsorbate molecules within the layer (intralayer interactions) and the adsorbate molecules and the substrate. In addition, the size and symmetry of the unit cells of molecular overlayers typically differ from those of common substrates, arguing against epitaxial lattices in the absence of severe distortions of a "native" close-packed overlayer structure.[2] As a result, these adsorbate overlayer structures are rarely epitaxial by this rigid

definition. But this does not mean that such adsorption is not influenced by the substrate lattice. Rather, less obvious modes of epitaxy come to play. A looser definition of epitaxy, that is more suitably applied to the study of physisorbed overlayers, is the following: "epitaxy is the relationship of an overlayer to its substrate such that the substrate acts as a template and has significant influence on the mode of growth of the overlayer".[1] The relationship of the size of the this template to that of the substrate unit cell and the subsequent extent to which the substrate influences the growth of the overlayer is described as the *mode of epitaxy*. The purpose of this appendix is to describe and define the modes of epitaxy that are possible between a physisorbed molecular overlayer lattice and the substrate lattice.

Before listing the different modes of epitaxy and their definitions, the terms that are used to describe an epitaxial interface must be presented. The two most important concepts in fully describing epitaxy are those of the *primitive unit cell* and the *supercell*. The primitive unit cell is what is commonly conceived of as the *unit cell* of a crystal lattice: the most primitive unit of the crystal lattice that can reproduce the lattice by repeated translations. Figure A1.1a shows a cartoon of the primitive unit cell of a generic overlayer (in blue) with its unit cell parameters b_1, b_2, and β (also in blue). Likewise, the primitive unit cell of the substrate and its parameters a_1, a_2, and α are shown in red. The angle θ between the vectors a_1 and b_1 defines the azimuthal orientation of the overlayer with respect to the substrate. The supercell, shown in green, is the integer multiple of primitive overlayer unit cells such that the corners of the supercell all reside on equivalent

substrate lattice sites. In other words, the overlayer supercell corners reside on the corners of an integer multiple of primitive substrate unit cells. The substrate

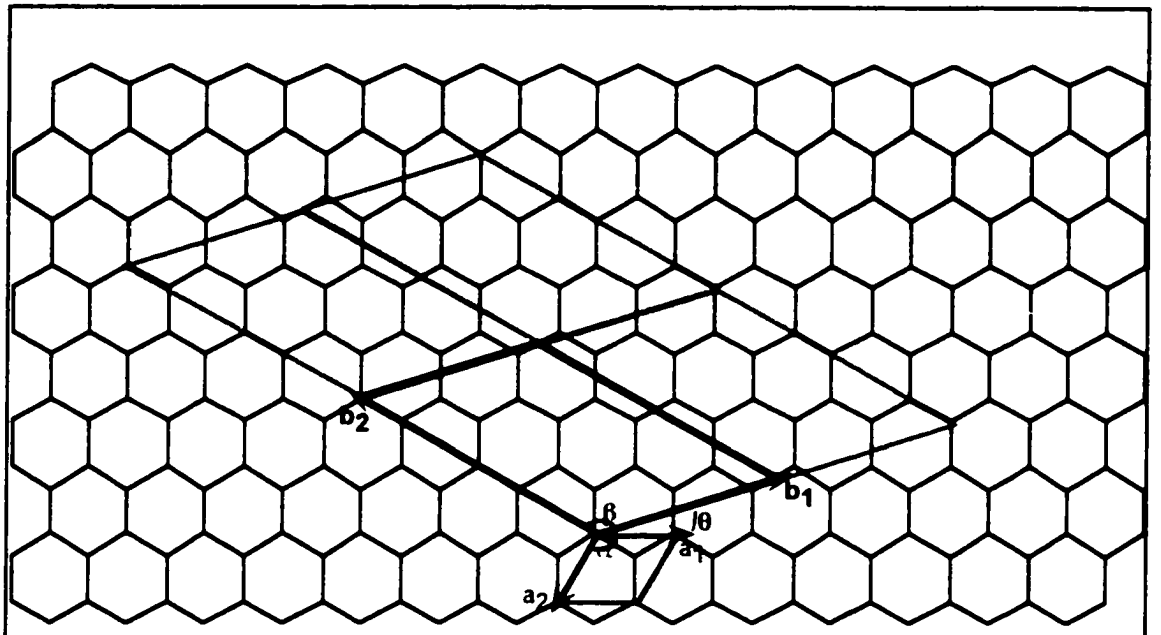

Figure A1.1: Schematic representation of a generic physisorbed molecular overlayer on a HOPG substrate. The red and blue boxes represent the primitive unit cells of the substrate and overlayer, respectively. The green box denotes the overlayer supercell, which has dimensions of 2 × 2 ($b_1 \times b_2$). Based upon Last et al, (Figure 1).

and overlayer primitive unit cell parameters (a_1, a_2, α, b_1, b_2, and β), along with the azimuthal angle, can be used to describe the mode of epitaxy mathematically through the transformation matrix [**C**] in equation (1).[2-4] The matrix coefficients are defined by equations (2) – (5).[2-4]

$$\begin{bmatrix}\vec{b}_1\\ \vec{b}_2\end{bmatrix} = [\mathrm{C}]\begin{bmatrix}\vec{a}_1\\ \vec{a}_2\end{bmatrix} = \begin{bmatrix}p & q\\ r & s\end{bmatrix}\begin{bmatrix}\vec{a}_1\\ \vec{a}_2\end{bmatrix} \qquad (1)$$

$$p = \frac{b_1 \sin(\alpha - \theta)}{a_1 \sin(\alpha)} \qquad (2)$$

$$q = \frac{b_1 \sin(\theta)}{a_2 \sin(\alpha)} \quad (3)$$

$$r = \frac{b_2 \sin(\alpha - \theta - \beta)}{a_1 \sin(\alpha)} \quad (4)$$

$$s = \frac{b_2 \sin(\theta + \beta)}{a_2 \sin(\alpha)} \quad (5)$$

The overlayer lattice vectors can likewise be expressed in terms of the substrate lattice vectors by equations (6) and (7).[2,4]

$$\vec{b}_1 = p\vec{a}_1 + q\vec{a}_2 \quad (6)$$

$$\vec{b}_2 = r\vec{a}_1 + s\vec{a}_2 \quad (7)$$

Using equation (1), three general categories of epitaxy can be described: commensuration, coincidence, and incommensuration. These categories will be described in the following sections.

Commensuration

The mode of epitaxy referred to as commensuration occurs when the periodicities of the overlayer and substrate are related by integer multiples along two lattice vectors such that each overlayer lattice point can be placed on equivalent substrate lattice points. In other words, the primitive overlayer unit cell can be described by a minimum integral number of substrate primitive unit cells at some rotation angle.[3] Using the mathematical model in equation (1), the designation of an overlayer structure as commensurate applies when det(C), *p*, *q*, *r and s* are all integers.[3,4] Figure A1.2a shows a schematic of a generic overlayer lattice (designated by filled circles) that is commensurate with the substrate lattice (designated by open circles). The corners of the overlayer unit

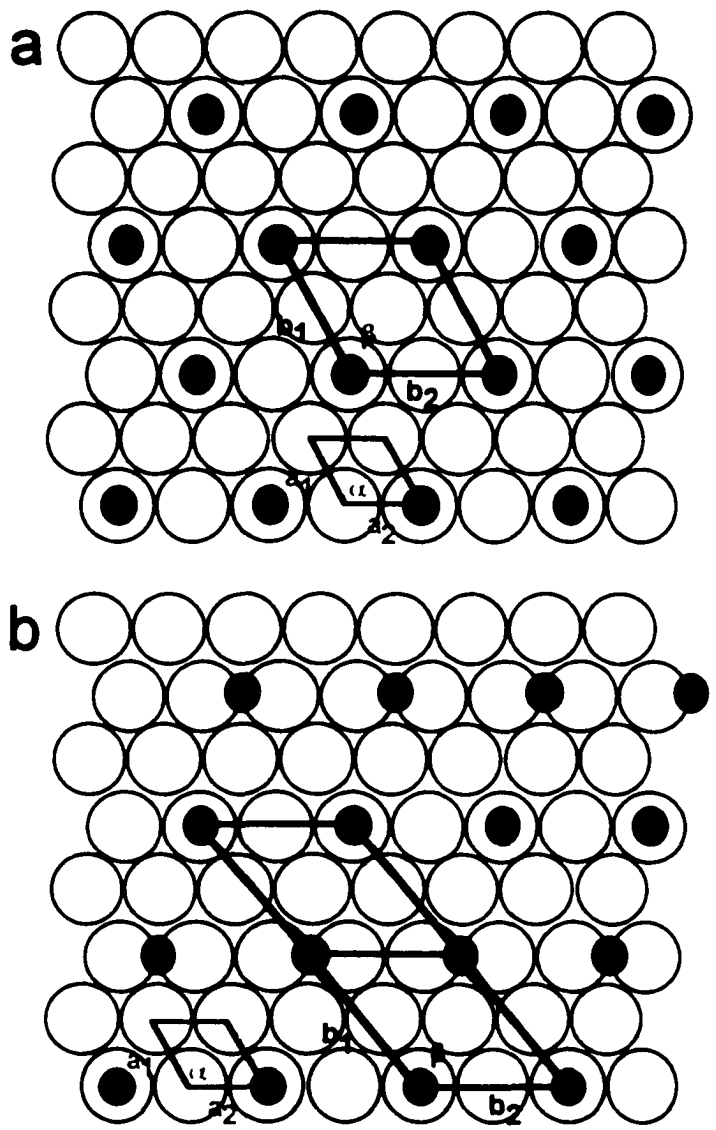

Figure A1.2: Schematic representations of generic overlayer structures that are (a) commensurate and (b) coincident with the substrate lattice. Open and filled circles represent the substrate and overlayer lattices, respectively. Based upon Last et al (figure 1).

cell coincide with equivalent substrate lattice points. Specifically, the overlayer primitive unit cell in this figure has dimensions of four substrate primitive unit cells. Thus, the template for overlayer growth, referred to earlier in this appendix, is 2 × 2 ($a_1 \times a_2$) for this particular example. It should be noted that in this schematic, $\theta = 0$ for ease of visualization. Likewise, the overlayer lattice points are shown to coincide with those of the substrate simply for ease of visualization. The actual positions of the overlayer lattice points are dictated by energetics.[2] The categorization of an overlayer/substrate system as commensurate is evidence of strong adsorbate-substrate forces relative to the adsorbate-adsorbate interactions present within the overlayer. As a result of this adsorbate-substrate interaction dominance, commensurate overlayer structures tend to be perturbed from their bulk crystal order.

Coincidence

Coincidence is a weaker mode of epitaxy than that of commensuration. In coincidence, the corners of the overlayer supercell coincide with the substrate lattice points at periodic intervals, while the overlayer lattice points within the supercell do not coincide with the substrate lattice points. Thus the overlayer supercell itself is commensurate with the substrate lattice, whereas the primitive overlayer unit cell is not. This is represented schematically in Figure A1.2b, in which the substrate and overlayer lattice points are represented by open and filled circles, respectively, as in A1.2a. The primitive overlayer unit cell, shown in blue, does not reside on equivalent substrate lattice sites no matter what the azimuthal angle, θ. The overlayer supercell, shown in green and consisting of 4

primitive cells, does reside on equivalent substrate lattice sites. Thus the substrate template size is eight primitive unit cells, or 4 × 2 ($a_1 \times a_2$). The angle θ is shown in this figure as 0 for ease of visualization. Using the mathematical model in equation (1), the designation of an overlayer structure as coincident applies when among *p, q, r and s*, there exist two integers confined to a single column of the matrix and det(C) is a simple fraction.[3,4] In other words, if *p and r* or *q and s* are integers, then every lattice point of the overlayer resides on at least one primitive lattice line of the substrate at some angle θ. This is also referred to as "point-on-line" coincidence.[5] The categorization of an overlayer/substrate system as coincident is evidence of the delicate balance between adsorbate-substrate forces and adsorbate-adsorbate interactions within the overlayer. The strengths of these interactions are similar and thus one does not obviously dominate the other. As a result of this balance, coincident overlayer structures tend to be only slightly perturbed from their bulk crystal order.

Incomensuration

An incommensurate overlayer structure has no distinctive registry between the overlayer lattice and the substrate lattice: a commensurate supercell cannot be constructed no matter what the value of θ, and thus, the substrate does not template the growth of the overlayer. Utilizing the mathematical model, incommensurate structures have at least one irrational number among *p, q, r, and s*, and neither of the columns of the matrix contains integers.[4] Incommensurate structures indicate strong intralayer interactions relative to the

adsorbate-substrate interactions. As a result, incommensurate overlayer structures tend not to deviate from the molecular bulk structure.

REFERENCES

(1) Somorjai, G. A. *Introduction to Surface Chemistry and Catalysis*; John Wiley & Sons, Inc.: New York, 1994, pp 667.

(2) Last, J. A.; Hooks, D. E.; Hillier, A. C.; Ward, M. D., *J. Phys. Chem. B* **1999**, *103*, 6723-6733.

(3) Hillier, A. C.; Ward, M. D., *Phys. Rev. B* **1996**, *54*, 14037-14050.

(4) Hooks, D. E.; Fritz, T.; Ward, M. D., *Advanced Materials* **2001**,

(5) Hoshino, A.; Isoda, S.; Kurata, H.; Kobayashi, T., *J. Appl. Phys.* **1994**, *76*, 4113-4120.

APPENDIX B

Independent Research Proposal:

Template Synthesis of Size-controlled Transition Metal Dichalcogenide Inorganic Fullerene-like Nested-shell Nanoparticles

Abstract:

A simple method for the production of inorganic fullerene-like (*IF*) particles with controlled shape, size, and size distribution that does not require subsequent purification or separation is currently lacking. Described herein is a template method that utilizes a high temperature-resistant material with uniform (both in size and shape) spherical pores within which IF nanoparticles may be synthesized. The template is constructed by making a "mold" of a three-dimensional crystal of highly-ordered monodisperse spherical latex particles. Solution phase precursors of the inorganic material may be loaded into the template pores for subsequent firing and gas-phase reaction to produce *IF* nanoparticles that retain the size and shape of the template pores. The *IF* material may then be isolated by dissolution of the template material. Detailed procedures and considerations for the synthesis of MoS_2 and WS_2 *IF* nanoparticles by this method are described.

Background:

Friction is an interfacial phenomenon that is ubiquitous in everyday life. In many cases it is desired, as in the friction between brake pads and a wheel drum and between sandpaper and a rough piece of wood. However, there are innumerable instances in which friction is unwanted, such as between an ice skate blade and ice, and between pistons and their housing walls. Liquids, particularly oils, have long been known to decrease friction and increase sliding when placed between 2 surfaces. In addition, the presence of the liquid media between the 2 solid surfaces helps to prevent local asperities on either surface from contacting each other, thereby reducing wear.

However, there are many scenarios in which the use of liquid lubricants is impractical or impossible. High temperatures above the boiling point or low temperatures below the melting point cause traditional liquid lubricants to either evaporate from the interface or freeze, thus destroying the facile liquid sheering that decreases friction. In addition vacuum applications, such as lubrication in space technology, preclude the use of liquids. In these applications, solid lubricants are used, the most common of which are graphite and the transition metal dichalcogenides (MX_2). These materials consist of planes of covalently-bound atoms which are held together by weak van der Waals interactions. The mechanism by which these solid lubricants work is one of intracrystalline slip, in which the mechanically weak interplanar regions undergo separation under the influence of a shear force. The planes separate from one another, forming new

relatively inert interfaces, which slide across one another easily thereby providing lubrication (see Figure A2.1 A).

The sheet-like structure of the transition metal dichalcogenides also poses a tribological problem, however. The bonds at the edges of the sheets are unsaturated. These dangling bonds are reactive sites susceptible to oxidation in humid air. Oxidation severely decreases the efficiency of these materials as lubricants. In addition, defect sites such as missing atom sites and fractures occur naturally within the sheets. These defects can be exacerbated and propagated through the sliding process, thereby creating more reactive sites. Thus, conditions in which oxygen and water vapor are present causes the friction coefficient of the metal dichalcogenide to increase and the wear life to decrease, significantly degrading the ability of the material to lubricate. Graphite will also undergo oxidation at higher temperatures (~500 °C), although its oxidation products are volatile at these temperatures. This has the effect of very slowly disintegrating the graphite based lubricant. This situation is not nearly as problematic as that posed in vacuum, however. Adsorbed vapors between the graphite planes facilitate their shearing at ambient gas pressures. In the absence of these vapors, graphite resists shearing, and thus loses its ability to lubricate.

A material that can lubricate at high or low temperatures, in vacuum, and in humid conditions would be highly desirable. Inorganic fullerene-like (*IF*)

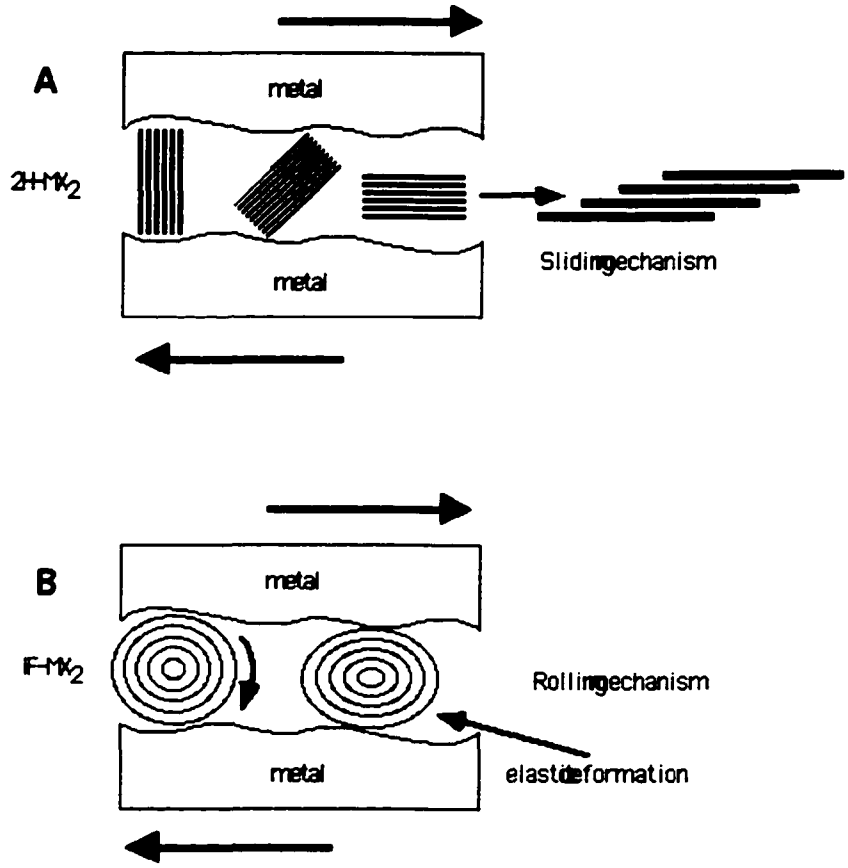

Figure A2.1: (A) Schematic showing the sliding mechanism responsible for lubrication by graphite or transition metal dichalcogenide nanoparticles. (B) Shematic showing the rolling mechanism responsible for lubrication by inorganic fullerene-like (IF) nanoparticles. Schematic adapted from R. Tenne, M. Homyonfer, Y. Feldman Chemistry of Materials, 1998, 10(11), 3236.

structures*, consisting of onion-like layers of closed nested-shells (~10 nm to 500 nm in diameter), (see Figure A2.2 A for a transmission electron micrograph of a WS_2 *IF* particle) have been observed to exhibit superior lubrication and wear properties (when added to oil) compared to graphite and metal dichalcogenides in their sheet-like 2H–MX_2 form.[2] Because they are closed shell structures, they exhibit no dangling bonds. As a result, their seamless and chemically inert structures do not react in humid air and resist sticking to surfaces or one another, regardless of the friction conditions. This onion-like structure also prevents shear between the layers, precluding an intracrystalline slip mechanism for lubrication. Instead, it has been shown that *IF* metal dichalcogenides lubricate interfaces via a mechanism of rolling rather than sliding,[3] making them analogous to nano-ball bearings (see Figure A2.1 B). This mechanism is unhindered either in vacuum or at high or low temperatures. In addition, because they are still essentially layered materials, when used under very high stress conditions that cause breakdown of the nested shell structure, *IF* nanoparticles will shear and maintain lubrication with the same sliding mechanism that layered solids utilize. Because of their small sizes, they are able to fit into small valleys between asperities on opposite sides of the interface and prevent their contact even under heavy loads

---

* Inorganic fullerene-**like** (*IF*) materials are so called for several reasons: (1) they display closed-shell cage-like structures similar to that exhibited by carbon fullerenes, but (2) unlike carbon fullerenes, *IF*s do not favor forming particular size cages like C_{60} or C_{70}, so it is improper to call them fullerenes. Rather, non-uniform size cages tend to be formed. MoS_2 nano-octahedra of dicreet sizes have been produced and are being called the first true inorganic fullerenes,[1] however, they are not the norm among synthesized inorganic nested shell structures. The inorganic fullerene-like nanoparticles discussed in this proposal are not true fullerenes of discrete size and polyhedra, but rather are nested shell structures composed of non-carbonaceous material that vary non-systematically in size and shape.

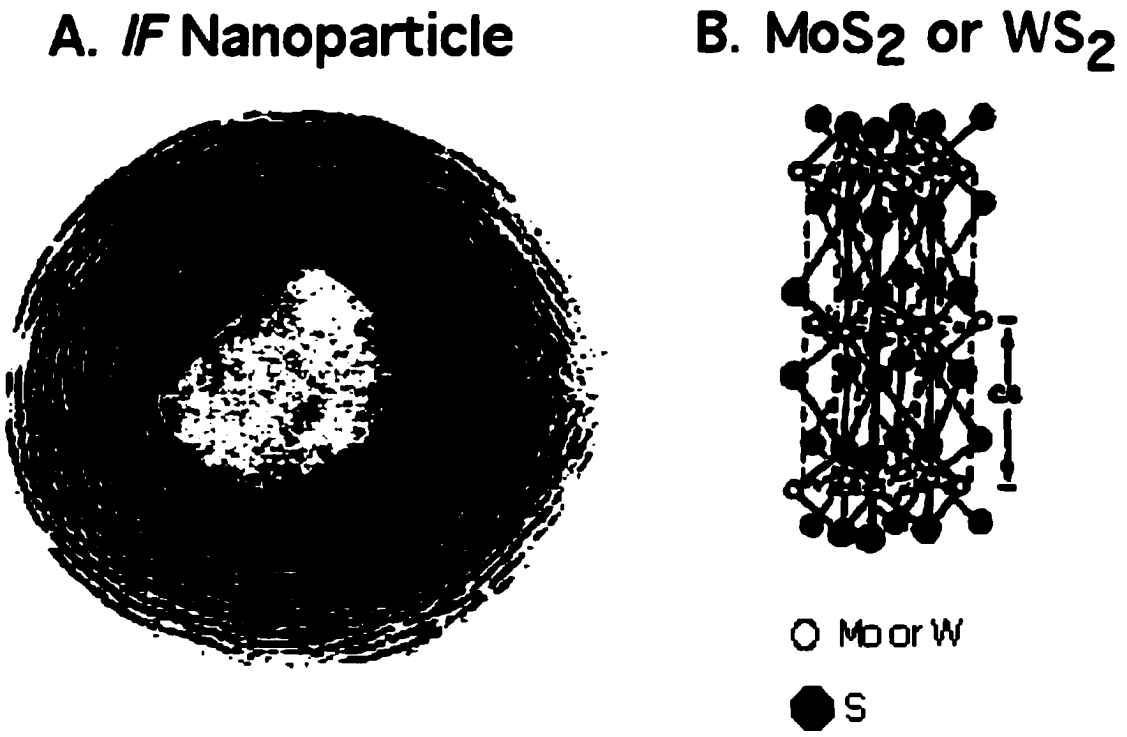

Figure A2.2: (A) TEM of an ~40 nm diameter WS2 *IF* nested-shell nanoparticle. Image taken from R. Tenne, L. Margulis, G. Hodes Advanced Materials, 1993, 5(5), 387. (B) Structure of the bulk platelet phase of MoS2 or WS2. Structure taken from R. Tenne, M. Homyonter, Y. Feldman Chemistry of Materials, 1998, 10(11), 3227.

that would usually squeeze out liquids.[4] They are also highly elastic, enabling dissipation of frictional energy to be decreased. This is a quality that increases with increasing size of the particle. It has been proposed that the more evenly spherical the *IF* nanoparticle structure, the better its rolling ability, and subsequent lubrication qualities.[4] It has also been proposed that larger diameter *IF* particles will have superior lubrication qualities.[5]

Current methods of synthesizing *IF* metal dichalcogenides (including laser ablation, electron-beam bombardment, gas phase reactions, gas-solid reactions, and electrical arc methods) lack definitive control over size or shape distribution. In addition, the difficulty of synthesizing particles with diameters >200nm has been pointed out.[5] The most successful (in terms of purity, reaction yield, and size distribution control) method thus far, developed by Feldman and Tenne *et al*, utilizes a solid-gas phase reaction to synthesize WS_2.[5] They have reported that the two most important parameters in producing size-controlled *IF* WS_2 are (1) the size of the solid WO_3 precursor particle, and (2) preventing contact between individual WO_3 particles during the gas reaction. The precursor WO_3 reacts with H_2S gas to convert its outermost layer into a completely closed layer of WS_2. The reaction then proceeds inward to convert the rest of the oxide precursor. Thus, the size of the precursor particle dictates the size of the *IF* WS_2. If the precursor particles contact one another during the reaction, however, they will aggregate to form the 2H–WS_2 platelet phase rather than an *IF* structure. To enforce these conditions, however, Feldman *et al* had to (1) sort WO_3 nanoparticles to ensure their size and distribution, and (2) develop a relatively

elaborate reactor which prevented contact between the WO_3 precursor particles.[5] Herein, I propose a new technique of WS_2 and MoS_2 *IF* synthesis which can be applied to other transition metal dichalcogenides in which particle size, shape, and size distribution can be quite easily controlled through the use of a template containing spherical pores with controllable pore size.

Description of colloidal crystal template

It has been demonstrated that monolithic structures containing interconnected spherical pores of tunable size can be produced from three-dimensional colloidal crystals.[6-13] These structures are produced by a "lost wax"[9] method in which a mold is created from an original 3D structure. The original structure is removed by dissolution, melting or evaporation and the mold remains. A replica of the original structure can be made by filling the mold with the material of choice, setting it chemically or physically, and then melting, dissolving, or evaporating the mold. The original 3D colloidal crystal is an approximately mm sized highly ordered aggregate of monodisperse polymer or silica beads. The beads are arranged in a hexagonally close-packed or cubic crystal (See Figure A2.3 A) and are held together by attractive capillary interactions. A material of interest is diffused into the voids in the colloidal crystal and is set. The beads are then dissolved away, leaving a monolithic structure that is a negative of the colloidal crystal. Spherical pores of approximately the same diameter and shape, free from defects, remain where the beads were. In addition, open "windows" exist where the beads were touching (See Figure A2.3 B). Thus the entire void volume of the mold is interconnected via these windows,

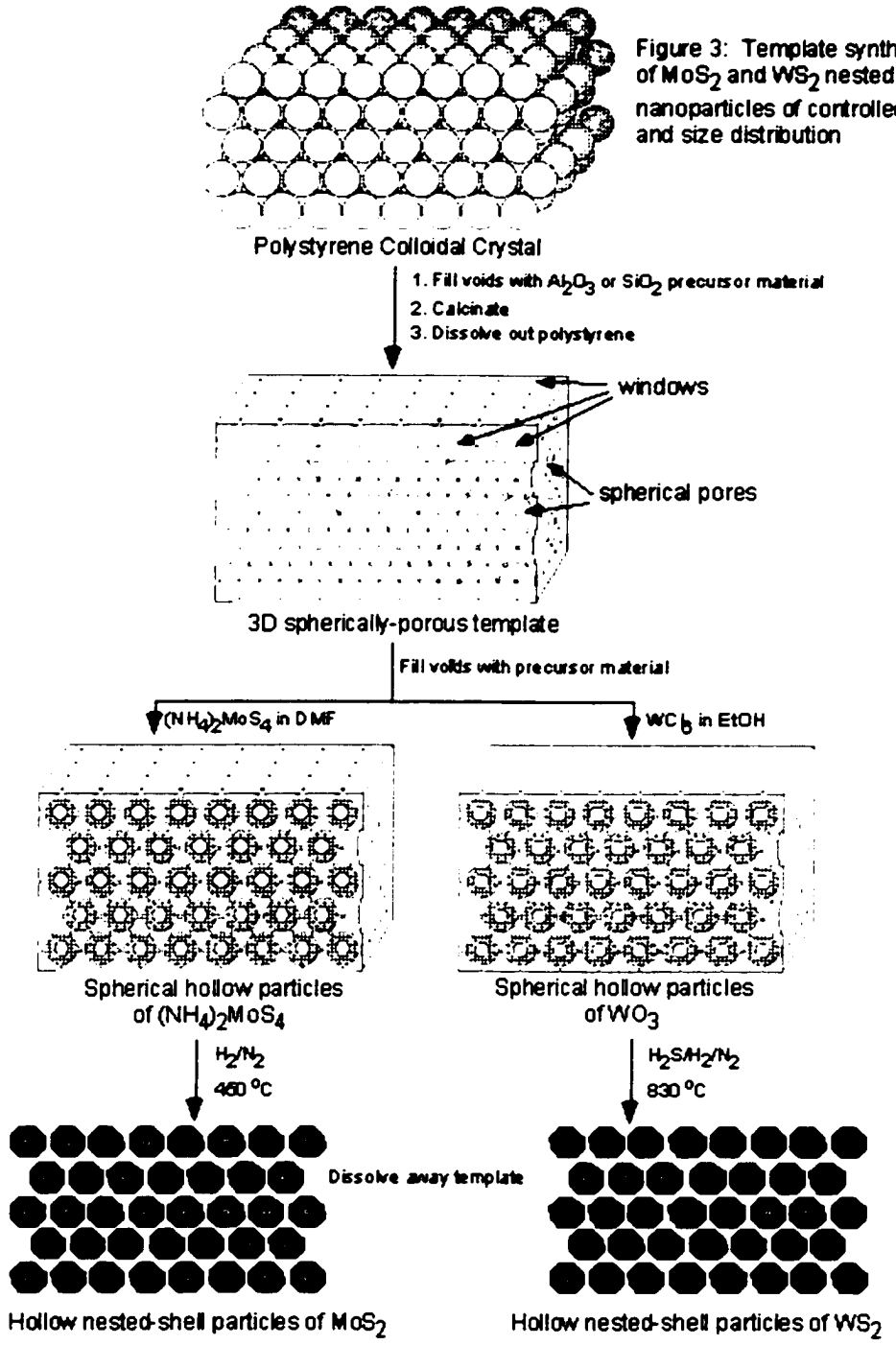

Figure A2.3: Template synthesis of MoS_2 and WS_2 nested shell nanoparticles of controlled size and size distribution.

allowing gas or solution-phase material to diffuse throughout the interior of the template. However, the windows can be made small enough to restrict the growth of material between two adjacent pores. Nanoparticles of a variety of materials, including oxides, have been produced successfully by this method and have been found to be spherical and discreet.

This spherically-porous structure will be used as a template for formation of size-controlled *IF* nanoparticles. *IF* precursor material will be diffused into the pores through the interconnecting network of windows. The spherical pores will be utilized as nano-reactors in which *IF* nanoparticles may be grown within the pore. In addition to providing a void in which the material may be grown, the pore also templates its size and shape onto the material. Because the windows are small enough to ensure discreet particle formation, *IF* precursor material that has been deposited within the pores will not aggregate with material in an adjacent connected pore. In addition, the size of the interconnecting windows may be controlled by changing the viscosity of the mold material.[9] Thus, one of the paramount conditions outlined by Feldman for *IF* formation, that *IF* precursor particles do not come in contact with one another, will be ensured. The size of the nanoparticle will be templated by the pore volume*, which may be controlled by changing the diameter of the beads used to make the colloidal crystal (see Figure A2.3 C). Synthesis of *IF* nanoparticles by traditional methods is poor for producing particles of diameters larger than 100 nm, sizes that are of interest to tribological studies. This template method would be ideal for the production of

these larger *IF* diameter nanoparticles, for uniformly spherical latex beads in this size regime (hundreds of nm) are easily produced and readily available commercially. The amount of *IF* product produced can be varied by controlling the number of layers of beads in the original colloidal crystal. If the porous template is constructed of a material able to withstand high temperatures (~400 to 1000 °C), then the loaded template could be fired to allow conversion of the precursor to *IF* material. The templated *IF* nanoparticles could be isolated by dissolution of the template.

Indeed, a similar method of template synthesis has been performed by Zelenski and Dorhout[14] to produce size- and shape-controlled MoS_2 nanotubules and nanofibers via solution deposition of thiomolybdate precursor and subsequent firing. They found that by changing the pore diameter of a cylindrically-pored alumina template, they could control the diameter of the nanotubules/nanofibers, up to a limit where the MoS_2 sheets no longer formed fused cylinders, but rather elongated platelets. By varying the precursor solution concentration, they were able to control the thickness and density of the tubules and fibers. Solvent identity likewise affected the morphology of the MoS_2. By analogy, it should be possible to synthesize MoS_2 *IF* nanoparticles of controlled size and shape utilizing the same solution deposition methods within an alumina template produced by the lost-wax method described above. Zelenski *et al* hypothesized that the unique shapes obtained by their template synthesis were a result of the shape of the thiomolybdate precursor left in the template pores after

---

• up to a limit where the radius of curvature of the pore is too large to maintain the surface tension of the liquid precursor. At this point the liquid precursor will no longer coat the surface of the

solvent evaporation. It is likely that capillary forces within the pores during evaporation caused coating of the precursor material on the inside walls of the cylindrical pores. Firing caused subsequent conversion to MoS_2, retaining the shape of the pore walls. Variation in the concentration of the precursor solution led to variation in the density of the nanotubules and fibers. If this hypothesis holds true, then by the method of solution precursor deposition and subsequent firing within a sphere-shaped pore, a spherical particle, in which growth of the basal plane of the particle occurs parallel to the plane of the pore surface, should be produced. Assuming that the pores are relatively defect-free and spherical, it is unlikely that more than one particle would form within each pore due to the capillary force that is enacted on the precursor material by the shape of the pore walls. Subsequent growth of the MoS_2 material should produce a nested-shell *IF* particle. Indeed, Zelenski *et al* reported the formation of nested-shell MoS_2 in their template synthesis of MoS_2 nanotubules and fibers, although at lower concentration than the tubules. This shows that it is possible to produce fullerene-like MoS_2 particles with solution-deposited thiomolybdate precursors. With the added influence of the spherical geometry of the template pores, it is likely that formation of *IF* MoS_2 particles will be possible and even favored. As mentioned above, by controlling the size of the template pore the size of the *IF* particle may be controlled. Control of the concentration of the precursor solution should produce *IF* particles with a specified thickness (number of shells nested within the particle). Finally, the shape of the pores themselves will control the shape of the *IF* nanoparticle.

---

template pore, but will be dominated by gravity, and non-uniform shapes will result.

Some possible difficulties for the MoS_2 synthesis should be noted. Zelenski *et al* demonstrated difficulty in using amorphous alumina templates as a sample holder during firing. They reported that upon firing, crystalline Al_2O_3 formed, thus destroying the structural integrity of the nanotubes and fibers. As a result, they dissolved the alumina template prior to firing, and allowed the precursor nanostructures to contact one another during conversion to MoS_2. This would be a problem for synthesis of nested-shell MoS_2 nanoparticles, for they must not contact one another significantly during conversion else they form the 2H-MoS_2 structure rather than the *IF* structure. I do not foresee formation of crystalline Al_2O_3 in the spherical pore alumina template, however. The synthesis of this template requires firing to undergo calcination. It has been reported by Holland *et al*[6] that these spherical porous templates produced via replication of colloidal crystals actually undergo shrinkage during the firing process (25 – 35 %) with pore shape remaining intact throughout the process. It seems unlikely that a second firing at temperatures and time durations lower than the original should cause crystallization of the alumina template and subsequent destruction of the spherical pores. Thus, the alumina template produced by the colloidal crystal replication process should pose no problem in its use during the firing process as a sample holder which additionally prevents contact between the precursor particles during firing, thus favoring the production of nested-shell *IF* particles. In the event that crystallization of alumina does occur during firing, silica is another material which can endure the temperatures required for firing, being well below

its glass transition temperature, and may be used alternatively as a porous template material.[7]

WS_2 *IF* nanoparticles may also be produced by adapting Feldman *et al*'s solid-gas phase synthesis to this template method. Again, using a solution phase precursor (although technically a sol), the template can be loaded with *IF* precursor material, in this case WO_3. The oxide can then be heated to relatively high temperatures (~800 °C) in the presence of $H_2S/H_2/N_2$ gases to convert the WO_3 to WS_2. Like in the Zelenski et al thiomolybdate precursor deposition method, the shape of the precursor solid (and ultimately the *IF* nanoparticle) is dictated by the capillary-induced coating of the inner surface of the capillary pores. Thus, this sol deposition method should succeed in producing WO_3 (and thus WS_2) with a negative structure to the template pore shape. *IF* shell thickness should be controllable by variation of precursor concentration, and product yield should be adjustable by varying the number of layers of beads in the original 3D colloidal crystal. This method appears to be ideal for the size and shape-controlled synthesis of transition metal dichalcogenide *IF* nanoparticles.

Experimental Procedure

The formation of three-dimensional monolithic colloidal crystal can be accomplished by at least 2 published methods:

Method 1[8]*:* Clean, monodisperse (< 8% size distribution*) polystyrene latex spheres of specified diameter are added to ethanol to produce a sample with a

* Size distributions of > 8% (Jiang et al, Nagayama et al) produce colloidal crystals exhibiting grain boundaries in the plane parallel to the substrate.

volume fraction in the range of 0.1% to 3.0%[**]. For the same volume fraction, a solution of larger particles yields fewer layers. More concentrated colloidal solutions leave thicker multilayer deposits. Thus, by varying the diameter of the latex spheres and the volume fraction of spheres in ethanol the thickness of the colloidal crystal may be tailored. Larger particles create a template with larger pores and windows connecting the pores. A clean microslide is then placed into 15 mL of colloidal solution in a clean scintillation vial. The vial is covered to keep out external airflow and contamination. The ethanol is allowed to evaporate naturally at room temperature for at least 24 hours. Thicker films are produced by successive dipping and evaporation cycles using the same size latex spheres. Film thickness in number of bead layers deposited (for a single dipping and drying cycle) plotted as a function of sphere diameter and volume fractions is shown in Figure A2.4. An upper limit for film thickness formed by this method has not been reported.

Method 2[6,12,15]*:* Clean, monodisperse* polystyrene latex spheres of specified diameter are added to ethanol at the same volume fraction range as in method 1. The colloidal solution is sonicated to produce a suspension, and is poured onto a smooth narrow-pore filter loaded into a Buchner funnel under vacuum. The latex particles accumulate slowly on the membrane surface, building up hexagonally

[**] Volume fractions of > 4% produce films with degraded uniformity.

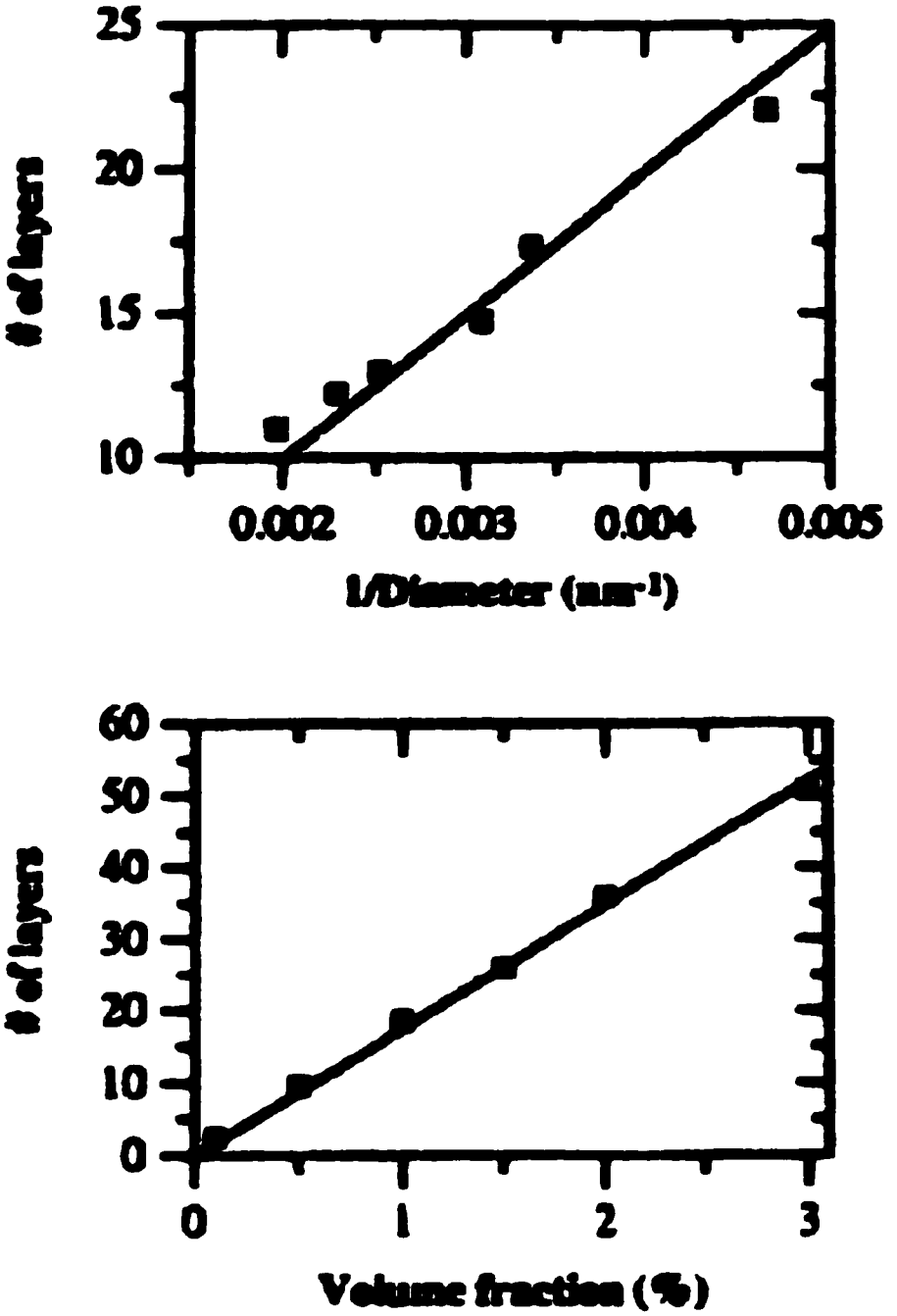

Figure A2.4: Plots illustrating the relationship between (A) bead size, (B) volume fraction and the number of layers produced in a single deposition cycle for the formation of a monolithic three-dimensional colloidal crystal produced by Method 1.

closely-packed or cubic ordered layers up to a few mm thick. The deposited crystal layer can be washed with ethanol and detached from the membrane.

Characterization of colloidal crystal films:

Scanning electron microscopy (SEM) can be used to determine film integrity and thickness. An edge suitable for cross-sectional analysis can be formed by scraping the end of the sample against a sharp razor blade.[8] A thin layer of gold must be sputtered onto the sample prior to imaging.

Synthesis of the silica or nanoporous template via published methods:

Material 1- Alumina[6]*:* The colloidal crystal is soaked, *in situ*[***], with 2-butanol. Aluminum tri-*sec*-butoxide (diluted 50/50 wt/wt with 2-butanol) is added drop-wise to cover the latex spheres completely while suction is applied. Mass ratios of alkoxide to latex of 1.4 to 3 can be used. The composite is then dried in a vacuum desiccator for 3 to 24 hours. The latex spheres are removed by heating the composite in flowing air at 575 °C for 7 to 12 hours. Comparison between the original latex spheres and the baked alumina template has shown that the alumina shrinks by 26-32 %. Window size may be controlled by varying the wt/wt ratio of aluminum tri-*sec*-butoxide/2-butanol, thus altering the viscosity of the alumina precursor. Thus, the nanoporous alumina template can be made with desirable pore and window sizes by refining the mass ratio of alkoxide to latex, the identity of the solvent, the calcination conditions and times, and the wt/wt ratio of the precursor/solvent solution.

[***] Within the Buchner funnel (i.e. without removing the colloidal crystal from the filter membrane or the vacuum).

Material 2- Silica[12]*:* To induce silica "polymerization" by this method, the polystyrene latex spheres must be functionalized *in situ* by adsorption of the surfactant hexadecyltrimethyl ammonium bromide (HTAB). The colloidal crystal is soaked with 0.2 M HTAB solution for 20 minutes. The excess, unabsorbed surfactant is removed by washing briefly with de-ionized water. The void space within the crystal is mineralized by passing 0.5 M silica sol through the latex covered filter while suction is applied. As the mineralization proceeds, the permeability of the colloidal crystal decreases until flow-through of the liquid stops (< 1 minute). The silica solution within the colloidal crystal then gels naturally. When this occurs, the excess solution is removed and the latex/silica composite is dried under vacuum. The latex within the composite may then be removed by heating at 450 °C for 4 hours. Comparison between the original latex spheres and the baked silica template has shown that the silica shrinks by 20-35 %, thus producing smaller pores than the original latex bead diameter. This value is comparable to that in M41S mesoporous silicas[16]. Shrinking is uniform throughout the template, however. The solvent of the silica solution may be altered to fine-tune the size of the windows connecting the pores within the template (more viscous solutions create larger windows). Further experiments for both the silica and alumina templates would include determination of the largest size colloidal template that can be produced while maintaining interconnectedness throughout its void volume.

Characterization of porous templates:

SEM and TEM can be used to determine pore size, integrity, and order. Determination of crystallinity can be accomplished by powder x-ray diffraction of the crushed sample.

Synthesis of inorganic fullerene-like nanoparticles:

MoS_2 (solution deposition of precursors and subsequent firing): This method is based upon the template synthesis of MoS_2 nanofibers and nanotubules method of Zelenski and Dorhout[14]. $(NH_4)_2MoS_4$ is dissolved in a suitable solvent (DMF or DMSO, for example) to create a solution of approximately 0.1 M (as a concentration starting point). This solution is filtered to ensure that all solids are dissolved. The alumina or silica template is then dipped into the precursor solution and the solvent is allowed to dry, either naturally under a crystallizing dish or on a ~70 °C hotplate in air. Several variables will affect the transport of solution throughout the template (for example overall template size, the dimensions of the template's pores and windows, solution viscosity, etc), thus the dipping time as well as solution solvent identity and concentration must be refined to ensure that precursor material deposits throughout the entirety of the template interior in as uniform a fashion as possible. After drying the loaded template is then placed on a stage in a fused silica flow-through tube and placed in a tube furnace. An atmosphere of 10 % H_2/N_2 is introduced into the tube flowing at a rate of 20 mL/min while the template is heated at a rate of 10 °C/min to 450 °C. The furnace is held at this temperature for 1 hour before step cooling to room temperature. Obviously, these conditions of gas ratio and flow rate,

temperature ramping rate, final temperature and duration, and cooling rates act as a starting point for further refinement in its application to *IF*-template synthesis. To isolate the MoS_2 nanoparticles the alumina template is dissolved away by soaking in a 1 M NaOH solution undisturbed for approximately 30 minutes. The silica template is removed by dissolution in aqueous HF. The liquid is carefully removed via filter syringe and replaced with distilled water to rinse the product. Rinsing is repeated a few more times. Material trapped in the filter syringe is saved for analysis along with the bulk product. Other inorganic fullerenes may be synthesized by this method utilizing the proper solution deposition conditions, gas ratios and firing temperatures.

WS_2 (solid-gas phase reaction): This method is based upon the solid-gas phase reaction of WO_3 with H_2S of Feldman *et al* with the modification that the WO_3 nanoparticles be grown inside the spherical template to ensure shape and size uniformity (Feldman *et al* used presorted WO_3 nanoparticles in their synthesis[5]). WCl_6 is reacted with anhydrous ethanol and stirred for several hours, forming a sol. Optimum ratios of WCl_6 to ethanol will have to be determined to produce a sol with an appropriate viscosity to completely coat the pores within the template. The sol is filtered and the alumina or silica template is dipped into it. As with the MoS_2 synthesis, the dipping process must be optimized. The solvent is allowed to dry naturally in air for one hour and then on a hot plate at ~ 40 °C until fully dry. The loaded template is then placed on a stage in a fused silica flow-through tube and placed in a tube furnace. An atmosphere of H_2/N_2 and H_2S is introduced into

[*] Solutions of approximately 0.05 M $(NH_4)_2Mo_3S_{13}$ have also been used as a MoS_2 precursor. These solutions did not produce a morphology significantly different from that of the $(NH_4)_2MoS_4$

the tube. The optimum ratio of gases and flow rate will have to be determined. For initial experiments, the template should be heated to ~ 830 °C.[5] Ramping rate, duration of heating time at ~ 830 °C, and cooling rate will have to be optimized. To isolate the WS_2 nanoparticles the alumina template is dissolved away by soaking in a 1 M NaOH solution undisturbed for approximately 30 minutes. The silica template is removed by dissolution in aqueous HF. The liquid is carefully removed via filter syringe and replaced with distilled water to rinse the product. Rinsing is repeated a few more times. Material trapped in the filter syringe is saved for analysis along with the bulk product.

Characterization of *IF*-loaded templates:

Before the templates are removed, SEM may be used to determine whether precursor material has accumulated on the surface of the template, or has blocked the template pores. Breaking apart the templates reveals the inner pores. EDS (energy dispersive spectroscopy) can be used to determine the elements present within the loaded templates, including contaminants, although it cannot determine the stoichiometry in the case of MoS_2 (Mo and S produce the same X-ray energies). Optical absorption can determine the identity of the nanoparticles (MoS_2 as opposed to MoS_3 or MoO_3) while they are still contained within the alumina or silica template. The spectral response of the unloaded templates will have to be determined previously to ascertain whether spectral effects of these 3D dielectric composites (with lattice spacings on the order of UV up to ~ blue light) will interfere with the optical nanoparticle analysis.

---

precursor.

Characterization of *IF* nanoparticles:

After removal of the template, the nanoparticle product may be characterized using HRTEM, EDS, EELS, XPS, and XRD. High resolution TEM will reveal the morphology of the nanoparticles (hollow or filled, nested-shell or platelet-like, tetrahedral or octahedral or neither) as well as size distribution of the particles and the diameter of the hollow region in the *IF* nanoparticles. EDS will reveal the elemental composition of the nanoparticles (as mentioned in the above section), EELS (electron energy loss spectroscopy) may also be used to determine elemental composition. Ultrahigh vacuum XPS (x-ray photoelectron spectroscopy) is yet a third way to determine elemental composition. Powder XRD may determine the structure of the nanoparticles (amorphous, 2H–MX_2, or IF–MX_2), if there is enough material present. 2H–MX_2 yields smaller interlayer spacings than IF–MX_2, presumably due to the curvature of the *IF* material[17], although sorption of H_2 cannot be ruled out as a possible cause[14]. If there is not enough material to perform powder XRD and long x-ray exposure times appear to change the morphology of the nanoparticles, electron diffraction may substitute to determine the structural nature of the particles, using the method of comparative *d* spacings[14].

In addition, the lubrication qualities of the *IF* nanoparticles produced may be determined by measuring friction coefficients and wear properties by standard tribological methods[18] alone and also in a small amount of oil. These properties should be measured in diverse environmental conditions such as at varying loads, humidities, gas pressures, and temperatures. *IF* nanoparticles of different

compositions as well as sizes and shapes should be studied for comparison and to determine the characteristics responsible for increased lubricant performance.

Future experiments:

Further experiments would focus on the development of optimum growth conditions for *IF* particles. Pore, window and template sizes; precursor species identities; solution viscosities using different solvents and concentrations; firing temperatures and durations (particularly lower temperatures and longer durations); solution deposition methods; and template material could all be varied to achieve optimum IF size, shape and density (extent of shell layering). In addition, this method should be further developed for application to other *IF* nanoparticle materials. *IF* nanoparticle synthesis have been reported for substances such as $MoSe_2$[19], WSe_2[20], BN[21], $TlCl_3$[22], ReS_2[23], $NiCl_2$[24]. The methods described above could be adapted for template synthesis of size and shape controlled *IF* structures for these reported materials, which have applications besides tribology (magnetic, optical, catalytic, etc). In addition, it is foreseeable that the described template method could also be applied to gas-phase reactions, the oxide synthesis of MoS_2 being the primary candidate[25]. For this case, however, it is not clear that single particle formation per pore volume would be favored in gas-phase deposition. Finally, assuming that IF particles with the attractive features described thus far can be produced by this method, efforts to attempt to scale-up the application for increased mass yield could be made. It is understood by the author that this may be difficult, but it is

foreseeable that large numbers of these templates could be produced and utilized in parallel.

In conclusion, this proposal presents a new template synthetic method for production of MoS_2 and WS_2 IF particles with controlled particle size, size distribution, and extent of layering of nested-shells, with possible application to the synthesis of other *IF* materials.

References

(1) Parilla, P. A.; Dillon, A. C.; Jones, K. M.; Riker, G.; Schulz, D. L.; Ginley, D. S.; Heben, M. J., "The first true inorganic fulerenes?,"Nature, 397 (1999) : 114.

(2) Rapoport, L.; Bilik, Y.; Feldman, Y.; Homyonfer, M.; Cohen, S. R.; Tenne, R., "Hollow nanoparticles of WS2 as potential solid-state lubricants,"Nature, 387 (1997) : 791-793.

(3) Prasad, S.; Zabinski, J., "Super slippery solids,"Nature, 387 (1997) : 761-762.

(4) Tenne, R.; Homyonter, M.; Feldman, Y., "Nanoparticles of layered compounds of hollow cage structures (inorganic fullerene-like structures),"Chem. Mater., 10 (1998) : 3225-3238.

(5) Feldman, Y.; Zak, A.; Popovitz-Biro, R.; Tenne, R., "New reactor for production of tungsten disulfide hollow onion-like (inorganic fullerene-like) nanoparticles,"Solid State Sciences, 2 (2000) : 663-672.

(6) Holland, B. T.; Blanford, C. F.; Stein, A., "Synthesis of macroporous minerals with highly ordered 3D arrays of spheroidal voids,"Science, 281 (1998) : 538-540.

(7) Imhof, A.; Pine, D. J., "Ordered macroporous materials by emulsion templating,"Nature, 389 (1997) : 948-951.

(8) Jiang, P.; Bertone, J. F.; Hwang, K. S.; Colvin, V. L., "Single-crystal colloidal multilayers of controlled thickness,"Chem. Mater., 11 (1999) : 2132-2140.

(9) Jiang, P.; Bertone, J. F.; Colvin, V. L., "A lost-wax approach to monodisperse colloids and their crystals,"Science, 291 (2001) : 453-457.

(10) Johnson, S. A.; Ollivier, P. J.; Mallouk, T. E., "Ordered mesoporous polymers of tunable pore size from colloidal silica templates,"Science, 283 (1999) : 963-965.

(11) Park, S. H.; Xia, Y., "Macroporous membranes with highly ordered and three-dimensionally interconnected spherical pores,"Advanced Materials, 10 (1998) : 1045-1048.

(12) Velev, O. D.; Jede, T. A.; Lobo, R. F.; Lenhoff, A. M., "Porous silica via colloidal crystallization,"Nature, 389 (1997) : 447-448.

(13) Wijnhoven, J. E. G. J.; Vos, W. L., "Preparation of photonic crystals made of air spheres in titania,"Science, 281 (1998) : 802-804.

(14) Zelenski, C. M.; Dorhout, P. K., "Template Synthesis of Near-Monodisperse Microscale Nanofibers and Nanotubules of MoS2,"J. Am. Chem. Soc., 120 (1998) : 734-742.

(15) Hoyer, P.; Masuda, H., "Electrodeposited nanoporous TiO2 film by a two-step process from anodic porous alumina,"J. Mater. Sci. Lett., 15 (1996) : 1228-1230.

(16) Raman, N. K.; Anderson, M. T.; Brinker, C. J., "Template-based approaches to the preparation of amorphous, nanoporous silicas,"Chem. Mater., 8 (1996) : 1682-1701.

(17) Feldman, Y.; Wasserman, E.; Srolovitz, D. J.; Tenne, R., "High-rate, gas-phase growth of MoS2 nested inorganic fullerenes and nanotubes,"Science, 267 (1995) : 222-225.
(18) Chhowalla, M.; Amaratunga, G. A. J., "Thin films of fullerene-like MoS2 nanoparticles with ultra-low friction and wear,"Nature, 407 (2000) : 164-167.
(19) Tenne, R., "Fullerene-like structures and nanotubes from inorganic compounds,"Endeavor, 20 (1996) : 97-104.
(20) Tsirlina, T.; Feldman, Y.; Homyonfer, M.; Sloan, J.; Hutchison, J. L.; Tenne, R., "Synthesis and characterization of inorganic fullerene-like WSe2 material,"Fullerene Sci. Technol., 6 (1998) : 157-165.
(21) Stephan, O.; Bando, Y.; Loiseau, A.; Willaime, F.; Shramchenko, N.; Tamiya, T.; Sato, T., "Formation of small single-layer and nested BN cages under electron irradiation of nanotubes and bulk material,"Appl. Phys. A, 67 (1998) : 107-111.
(22) Avivi, S.; Mastai, Y.; Gedanken, A., "A new fullerene-like inorganic compound fabricated by the sonolysis of an aqueous solution of TICl3,"J. Am. Chem. Soc., 122 (2000) : 4331-4334.
(23) Chianelli, R. R.; Kelty, S. P.; Persans, P. D.; Yacaman, M. J., "Synthesis and fundamental properties of nanocrystals, sheets, and fullerenes based on layered transition metal chalcogenides,"Congr. Iberoam. Quim. Inorg., 6th, (1997) : 326.
(24) Hacohen, Y. R.; Grunbaum, E.; Tenne, R.; Sloan, J.; Hutchison, J. L., "Cage structures and nantubes of NiCl2,"Nature, 395 (1998) : 336-337.
(25) Zak, A.; Feldman, Y.; Alperovich, V.; Rosentsveig, R.; Tenne, R., "Growth mechanism of MoS2 fullerene-like nanoparticles by gas-phase synthesis,"J. Am. Chem. Soc., 122 (2000) : 11108-11116.